NEUROPROSTHETICS EDITOR'S PICK 2021

EDITED BY: Michela Chiappalone

PUBLISHED IN: Frontiers in Neuroscience

frontiers Research Topics

frontiers

ISSN 1664-8714
ISBN 978-2-88971-642-5
DOI 10.3389/978-2-88971-642-5

About Frontiers

Frontiers is more than just an open-access publisher of scholarly articles: it is a pioneering approach to the world of academia, radically improving the way scholarly research is managed. The grand vision of Frontiers is a world where all people have an equal opportunity to seek, share and generate knowledge. Frontiers provides immediate and permanent online open access to all its publications, but this alone is not enough to realize our grand goals.

Frontiers Journal Series

The Frontiers Journal Series is a multi-tier and interdisciplinary set of open-access, online journals, promising a paradigm shift from the current review, selection and dissemination processes in academic publishing. All Frontiers journals are driven by researchers for researchers; therefore, they constitute a service to the scholarly community. At the same time, the Frontiers Journal Series operates on a revolutionary invention, the tiered publishing system, initially addressing specific communities of scholars, and gradually climbing up to broader public understanding, thus serving the interests of the lay society, too.

Dedication to Quality

Each Frontiers article is a landmark of the highest quality, thanks to genuinely collaborative interactions between authors and review editors, who include some of the world's best academicians. Research must be certified by peers before entering a stream of knowledge that may eventually reach the public - and shape society; therefore, Frontiers only applies the most rigorous and unbiased reviews.
Frontiers revolutionizes research publishing by freely delivering the most outstanding research, evaluated with no bias from both the academic and social point of view. By applying the most advanced information technologies, Frontiers is catapulting scholarly publishing into a new generation.

What are Frontiers Research Topics?

Frontiers Research Topics are very popular trademarks of the Frontiers Journals Series: they are collections of at least ten articles, all centered on a particular subject. With their unique mix of varied contributions from Original Research to Review Articles, Frontiers Research Topics unify the most influential researchers, the latest key findings and historical advances in a hot research area! Find out more on how to host your own Frontiers Research Topic or contribute to one as an author by contacting the Frontiers Editorial Office: frontiersin.org/about/contact

NEUROPROSTHETICS EDITOR'S PICK 2021

Topic Editor:
Michela Chiappalone, Italian Institute of Technology (IIT), Italy

Citation: Chiappalone, M., ed. (2021). Neuroprosthetics Editor's Pick 2021. Lausanne: Frontiers Media SA. doi: 10.3389/978-2-88971-642-5

Table of Contents

frontiers in Neuroscience

ORIGINAL RESEARCH
published: 15 January 2019
doi: 10.3389/fnins.2018.01048

Exploiting Routine Clinical Measures to Inform Strategies for Better Hearing Performance in Cochlear Implant Users

Alan P. Sanderson[1], Edward T. F. Rogers[2], Carl A. Verschuur[3†] and Tracey A. Newman[4†]*

[1] Institute of Sound and Vibration Research, Faculty of Engineering and the Environment, University of Southampton, Southampton, United Kingdom, [2] Institute for Life Sciences and Optoelectronics Research Centre, University of Southampton, Southampton, United Kingdom, [3] Auditory Implant Service, Faculty of Engineering and the Environment, University of Southampton, Southampton, United Kingdom, [4] Clinical Neurosciences, Institute for Life Sciences, Faculty of Medicine, University of Southampton, Southampton, United Kingdom

OPEN ACCESS

Edited by:
Mikhail Lebedev, Duke University, United States

Reviewed by:
Etienne Gaudrain, Center for the National Scientific Research (CNRS), France
Kazutaka Takahashi, University of Chicago, United States

***Correspondence:**
Alan P. Sanderson
a.sanderson@soton.ac.uk

† These authors have contributed equally to this work

Specialty section:
This article was submitted to Neuroprosthetics, a section of the journal Frontiers in Neuroscience

Received: *03 September 2018*
Accepted: *24 December 2018*
Published: *15 January 2019*

Citation:
Sanderson AP, Rogers ETF, Verschuur CA and Newman TA (2019) Exploiting Routine Clinical Measures to Inform Strategies for Better Hearing Performance in Cochlear Implant Users. Front. Neurosci. 12:1048. doi: 10.3389/fnins.2018.01048

Neuroprostheses designed to interface with the nervous system to replace injured or missing senses can significantly improve a patient's quality of life. The challenge remains to provide implants that operate optimally over several decades. Changes in the implant-tissue interface may precede performance problems. Tools to identify and characterize such changes using existing clinical measures would be highly valuable. Modern cochlear implant (CI) systems allow easy and regular measurements of electrode impedance (EI). This measure is routinely performed as a hardware integrity test, but it also allows a level of insight into the immune-mediated response to the implant, which is associated with performance outcomes. This study is a 5-year retrospective investigation of MED-EL CI users at the University of Southampton Auditory Implant Service including 176 adult ears (18–91) and 74 pediatric ears (1–17). The trend in EI in adults showed a decrease at apical electrodes. An increase was seen at the basal electrodes which are closest to the surgery site. The trend in the pediatric cohort was increasing EI over time for nearly all electrode positions, although this group showed greater variability and had a smaller sample size. We applied an outlier-labeling rule to statistically identify individuals that exhibit raised impedance. This highlighted 14 adult ears (8%) and 3 pediatric ears (5%) with impedance levels that deviated from the group distribution. The slow development of EI suggests intra-cochlear fibrosis and/or osteogenesis as the underlying mechanism. The usual clinical intervention for extreme impedance readings is to deactivate the relevant electrode. Our findings highlight some interesting clinical contradictions: some cases with raised (but not extreme) impedance had not prompted an electrode deactivation; and many cases of electrode deactivation had been informed by subjective patient reports. This emphasizes the need for improved objective evidence to inform electrode deactivations in borderline cases, for which our outlier-labeling approach is a promising candidate. A data extraction and analysis

protocol that allows ongoing and automated statistical analysis of routinely collected data could benefit both the CI and wider neuroprosthetics communities. Our approach provides new tools to inform practice and to improve the function and longevity of neuroprosthetic devices.

Keywords: cochlear implant – neuroprosthesis, clinical monitoring and alerting, foreign body response, cochlear implant – impedance telemetry, hearing impairment

INTRODUCTION

Neuroprosthetics is a rapidly developing and profoundly important area of medical science and engineering. Substantial progress in this field, owing to improvements in biomaterials, electronics and computer science, presents opportunities to manage sensory and motor deficits that were previously untreatable. Neuroprosthetic interfaces of the central or peripheral nervous system share three common design objectives; selectivity of stimulation/recording to supplement function, biocompatibility, and long-term reliability. Despite their differences in target tissue, size and function they all face the same challenges of longevity. Device wear and tear and the biological response to the device such as fibrosis are currently major limiting factors of efficacy in neuroprosthetics (Adewole et al., 2017). Although the micro-environments of the central and peripheral nervous system exhibit specific chemical and cellular profiles, the broad challenges are universal and are driving the need for improved understanding of the tissue-implant interactions.

Cochlear implants (CIs) are the most common and successful sensory neuroprosthetic device with almost 600,000 recipients worldwide (Ear Foundation, 2016). They enable people with severe and profound deafness to hear speech, music and environmental sound (Wilson and Dorman, 2008). They make ideal models for neuroprosthetic research because their performance can be measured both subjectively and objectively: CI users can describe their hearing experience to clinicians and researchers who can then remotely measure hardware performance *in-situ*. The most common cause of deafness is loss or damage to the hair cells in the cochlea, meaning that they cannot convert vibrations in the air into electrical signals for the brain to process. CIs collect sound through an external microphone, convert it to electrical signals, and directly stimulate the auditory nerve with these signals, bypassing the normal hearing mechanism within the outer, middle and inner ear. The device delivers a sequence of current pulses, similar to those generated by the biological hearing apparatus, through a platinum multi-electrode array positioned in the cochlea. The signals from the auditory nerve are then interpreted as for normal biological hearing, by processing in the central auditory pathways of the brain. In many cases this affords 100% speech recognition for the implant user when listening in favorable acoustic conditions (Gifford et al., 2008).

The cochlea consists of a bone encased membranous spiral containing the sensory apparatus of hearing and its supporting structures, which are essential for sensory transduction and homeostasis. The scalae of the cochlea are three tube-like chambers projecting through the spiral: the scala tympani, the scala media and scala vestibuli. The electrode is usually surgically inserted into the scala tympani, in close proximity to the spiral ganglion neurons (SGNs). The average total length of the cochlear spiral is 42 mm and the total length of the first complete turn is 22.6 mm (Rask-Andersen et al., 2011). The majority of human cochleae have between 2.5 and 2.75 turns (Biedron et al., 2009). For ease of reference, these turns are conventionally denoted base, middle and apex, from the largest to the smallest (Rask-Andersen et al., 2012) (**Figure 1A**).

Since the widespread introduction of CIs in the 1980s, there have been several refinements to the technology and related health policy. Improvements in hardware manufacture, signal processing strategies, surgical techniques and the relaxation of CI candidacy criteria have all contributed to better clinical outcomes, including preservation of residual hearing (Nguyen et al., 2016), improved speech recognition (Wilson and Dorman, 2008) and fewer device related adverse events (Causon et al., 2013). Despite these improvements, however, some users still experience poor or declining speech recognition, poor sound quality and stimulation of non-auditory sensations. In around 2% of cases, additional surgery is needed to explant and replace the CI. The explanted device is tested, and if hardware failure and surgical complications are excluded, a "soft failure" is diagnosed (Balkany et al., 2005). As hardware has improved, these soft failures, or idiopathic cases, have become relatively more common (Causon et al., 2013), and research is clearly needed to better understand how individual biology, and in particular the immune system, interacts with the neuroprosthesis to drive these adverse events. Conventional counts of soft failures only record those devices which perform badly enough to need surgical removal and not those that underperform, and so will necessarily under-estimate the influence of these biological factors.

Cochlear implants, like any bio-implant, stimulate an inflammatory response, which culminates in the encapsulation of the prostheses, in a sheath of fibrotic or scar tissue (Anderson et al., 2008). Currently, CIs are constructed from a silicone carrier and platinum electrodes. A common type of medical grade silicone, polydimethylsiloxane (PDMS) is quite well understood and is used in many bio-implants including breast implants (Hillard et al., 2017), cardiac pacemakers and spinal cord stimulators which help patients with chronic pain and to manage incontinence (Hassler et al., 2011). As well as the materials themselves, though, the tissue response is modulated by electrode microscopic surface topography and chemical composition (Christo et al., 2015). It seems that tissue growth in response to CI is inevitable (Li et al., 2007) although the nature and extent of the response is somewhat variable across individuals (Fayad et al., 2009).

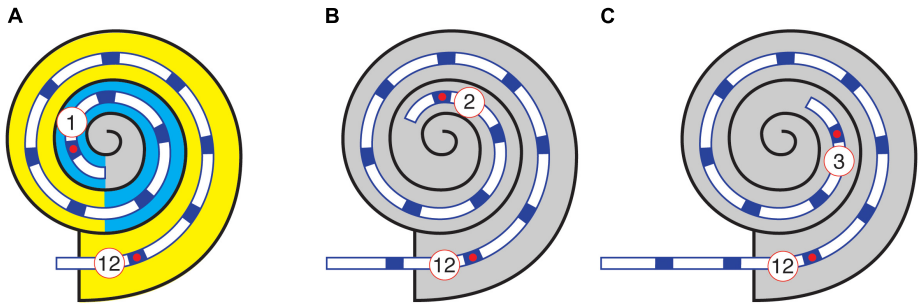

FIGURE 1 | Example corrections of electrode number to account for extra-cochlear electrodes. Schematic represents the MED-EL Standard electrode array. **(A)** Full insertion (720°). **(B)** 1 extra-cochlear electrode. **(C)** 2 extra-cochlear electrodes. In **(A)**, the three turns of the cochlea are indicated by color: yellow, base; cyan, middle; gray, apex.

Although fibrosis can foul the implant and impair its function, it is also beneficial in mechanically fixing the array within the cochlea. This helps create a seal to prevent both loss of perilymph and infiltration of bacteria from the middle ear (Stöver and Lenarz, 2009). A healthy inflammatory response to an injury comprises successive waves of pro- and anti-inflammatory chemokines and cytokines, controlled cellular migration to the wound site, with eventual resolution of inflammation and controlled apoptosis of recruited cells accompanied by wound repair and remodeling. In the case of implanted biodevices, the immune system reacts to the acute surgical trauma as well as the protracted exposure to the implanted biomaterials. Initially, the inflammatory response is characterized by exudation of fluid and plasma proteins from the circulation together with active infiltration of neutrophils to the surgical wound site. Proteins including fibrin are rapidly adsorbed onto the implanted biomaterial to form a provisional matrix that attracts macrophages, which can fuse to form multi-nucleated giant cells. Macrophages contribute to the fibrotic capsule by releasing cytokines that attract fibroblasts and stimulate them to secrete collagen.

The inflammatory process leads to the commonly described tissue reaction to a CI: a tightly packed layer of fibroblasts and collagen with occasional macrophages surrounding the electrode array (Grill and Thomas Mortimer, 1994). In the majority of cases, this tissue state remains stable over time. However, in some instances there is tissue hypertrophy, or extensive fibrosis and bone formation, which hinders the function of the electrode. Lim et al. (2011) found that pathological foreign body reactions (FBR) requiring revision surgery are rare. However, evidence from post-mortem temporal bones suggests that the characteristic indicators of FBR such as foreign body giant cells are more common than expected (Nadol et al., 2014; Seyyedi and Nadol, 2014). This highlights the potential for sub-clinical FBR, which does not reach soft-failure but is clearly detectable to post-mortem histological analysis. The complex reaction to CI often also includes new bone formation (osteogenesis) (Somdas et al., 2007). Osteogenesis appears more detrimental to implant performance than fibrosis and is associated with reduced speech discrimination scores, (Kamakura and Nadol, 2016) and an effective reduction in dynamic range of stimulus current (Kawano et al., 1998). It is therefore crucial to understand the transition from a healthy short-lived tissue response to a chronic or spontaneous over-exuberant response.

Studies of donated temporal bones from CI users have shown that intra-cochlear location can significantly affect tissue development after CI implantation. The basal, high-frequency region of the cochlea exhibits significantly greater fibrosis and osteogenesis, and poorer survival of both hair cells and peripheral projections of SGNs (Fayad et al., 2009). Histological analysis identifies greater numbers of giant cells and lymphocytes at the cochleostomy site than at the mid and apical regions of the cochlea (Seyyedi and Nadol, 2014). In addition to the consistent pattern of basal tissue hypertrophy, some individuals also exhibit fibrosis that extends along the full length of the electrode array and beyond (Somdas et al., 2007). There is evidence that the volume of new tissue correlates with the level of damage to the lateral wall (Li et al., 2007) and other structures including the basilar membrane (Kamakura and Nadol, 2016). While this data is intriguing, and clearly points to the importance of the biological response to the implant, it is limited to post-mortem studies, meaning that the majority of the data is collected after long-term implantation. This means it cannot be used to interpret performance fluctuations, and does not give us the early warning of soft failure that would be so useful in the clinic.

A readily available, non-invasive, clinical measure from a CI is electrode impedance (EI) telemetry (Hughes et al., 2001). EI describes the ease with which electrical current flows through and between implanted electrodes. The CI stimulator delivers a current pulse that flows through the platinum electrodes of the CI and into the ionic environment of the cochlear tissue. This pulse must be calibrated so that it delivers sufficient of charge to stimulate the SGN, without damaging the tissue. High EI means the implant must deliver a higher voltage to maintain the delivered charge. This has two undesirable effects: it drains the battery of the device faster and, more importantly, it spreads the excitation across more SGN reducing frequency resolution, and in turn the quality of the perceived sound. In general, therefore, low EI makes it more likely that an implant performs well.

The EI is determined by delivering a low-level current pulse through the relevant electrode inputs on the CI and

measuring the resulting voltage across the associated electrodes. It can be performed quickly in the clinic using a hardware interface that connects the implant to a computer via a transcutaneous link. In the clinic, EI telemetry is primarily used as an electrode integrity test. Open or short circuit faults (very high or very low impedances, respectively) can easily be diagnosed, which is useful to clinicians in deciding whether a given electrode should be activated. These faults are relatively common: Carlson et al. (2010) showed a 9% chance of either at least one open- or short-circuit fault in an implanted device.

Despite its primary role as an integrity check, EI is a continuous measure, which can provide much more information on the biology around the implant. A major factor in determining EI is the volume and composition of bulk tissue surrounding the implanted electrode array (Tykocinski et al., 2001). Clark (2003) recommends that EI levels should be monitored routinely as an indicator of cochlear tissue changes such as fibrosis and electrode surface roughening. In a study of chronic high-rate stimulation using cats, Xu et al. (1997) demonstrated that levels of fibrosis and presence of inflammatory cells were greatest in the cochleae that exhibited the greatest EI levels. Clark et al. (1995) found that EI was significantly correlated with the amount of tissue around the electrode contacts and cases where inflammatory cells were found in the tissue showed particularly high levels of EI.

The studies above show the value of EI as an indicator of tissue status, but initial studies also show that it may be useful for predicting patient outcomes. Electrodes that exhibit high impedance levels are associated with raised thresholds of auditory sensation and reduced dynamic range (Busby et al., 2002) which can be associated with poorer performance outcomes (Wolfe et al., 2013). EI increase and/or fluctuation are recognized as clinical indicators of soft-failure (Balkany et al., 2005). The onset of sudden changes in EI over time are correlated with marked loss of residual hearing in CI users (Choi et al., 2017).

Considering the potential value of monitoring and interpreting EI fluctuations, there is a surprising lack of consensus guidance on clinical utility of impedance telemetry, especially in light of its proven association with the immune-mediated tissue response. A number of authors have shown greater EI levels in the basal region of the cochlea compared to more apical locations. Jia et al. (2011) analyzed EI from 20 adult CI users and found higher levels at the basal position after 3 months that were maintained for the 36-month study duration. The pattern of raised EI at basal electrodes has been observed in other clinical CI studies (Hughes et al., 2001; Busby et al., 2002; Leone et al., 2017) and supports the temporal bone histology studies showing greater tissue growth in this region. These studies, which draw from cohort sizes ranging from 19 to 35 individuals, have generated useful preliminary evidence. However, a lack of larger study groups—ideally complete clinical caseloads—combined with the known inter-patient variability, is a major factor in the lack of clinical consensus. To date there is no published evidence of a clinical platform for systematic analysis of EI to produce normative models, against which individuals can be compared.

There is evidence that change in EI over time can serve as an indicator of the immune-mediated tissue response. Following surgical implantation of the CI electrode array, the tissue undergoes rapid changes attributable to the acute inflammatory response (Shepherd et al., 1994). This change manifests in a measurable increase in EI between implantation and the date of activation (Busby et al., 2002; Saunders et al., 2002). Several studies report a significant reduction in EI following commencement of electrical stimulation, which often plateaus over 1–3 months (Hughes et al., 2001; Henkin et al., 2006; Jia et al., 2011). After the initial stimulation-induced reduction, EI usually remains at a stable level in actively stimulated electrodes for several months (Henkin et al., 2003, 2006), while inactive electrodes show a steady increase over time (Dorman et al., 1992; Hughes et al., 2001).

The present study is a retrospective investigation of clinical data from an auditory implant service and demonstrates the untapped value in clinical recordings taken from neuroprostheses—in our case, CIs. As shown above, there is a pressing need to reduce the wide variance of outcomes and improve implant longevity, which will be substantially helped by improving observations of the CI-tissue interface. We describe sample-wide variability over 5 years. This view is not available through the clinical software, which prevents clinicians from easily identifying deviations from normal. We asked the question: what is the general trend of impedance change over time for different electrode positions? Based on previous evidence of tissue proliferation around the round window and hook region we predicted that the electrodes furthest from the base would show lower impedance with a downward trend over time. Next, we applied an upper threshold to identify individuals with raised impedance, statistically outside the main distribution but below the manufacturer's "high impedance" warning level. We asked the questions: how many individuals exhibit significantly raised impedance levels? Of these, how many were identified with raised impedance at electrodes away from the base? These are particularly interesting cases to consider because no mechanism has been proposed for localized tissue proliferation away from the site of array insertion, i.e., cochleostomy or round window. This information could be used as early detection of unwanted inflammatory responses caused by the implant and its function rather than the surgery, which may go on to affect the CI interface and therefore longer-term performance. Clinical data review, like that proposed here, incurs a negligible burden on the CI user and minimal cost in both money and time.

MATERIALS AND METHODS

Ethics Statement

This study was carried out in accordance with the recommendations of the University of Southampton Ethics Committee (UEC) and Faculty of Engineering and the Environment Ethics Committee (FEC). The protocol was

approved by the FEC. All subjects gave written informed consent in accordance with the Declaration of Helsinki. [UEC Ethics ID: 17430].

Participants

The study included 172 adult (176 adult ears) and 47 children (74 ears). Mean adult age was 58 years (18–91) and mean child age was 4.5 years (1–17). The patients included were implanted using either cochleostomy (approximately one third) or round window insertion (approximately two thirds). Data were collected from two sources within the University of Southampton Auditory Implant Service (USAIS); the clinical software database MED-EL Maestro and the local patient database.

Electrode Characteristics

Study participants had previously received MED-EL Standard (n = 131), Flex-28 (96), Flex-24 (7), Flex-Soft (2), or Form24 (1) CI arrays. These are relatively long arrays enabling EI measures to be taken at a wide range of physical positions in the cochlea. For example, the Standard array has an active stimulation range of 26.4 mm, which is equivalent to two turns of the cochlea or an insertion angle of 720°. Each array carries 12 electrodes, each of which has either one or two exposed electrical contacts, depending on the array model. The effective electrode surface area for these MED-EL electrodes is 0.13–0.14 mm^2.

EI Data Acquisition

The main study aims were to describe the trends of EI in a large sample and highlight individuals who deviate from this. A single manufacturer and limited number of arrays were chosen to minimize the hardware variability with a view to focusing primarily on the soft or biological mechanisms for impedance evolution. Importantly, the method of voltage acquisition and impedance calculation varies significantly between manufacturers. The method used by the MED-EL telemetry system is shown in **Supplementary Figure S1**. The change in EI can be separated into two components; access resistance and polarization impedance. The latter reflects the physical properties of the electrode surface and is therefore affected by protein adsorption, surface area increase and localized ionic changes (Tykocinski et al., 2005; Newbold et al., 2010). The stimulation-induced EI reduction, which occurs rapidly following device activation, is dominated by this component (Newbold et al., 2014). Access resistance is known to reflect the bulk material around the electrode such as fluid, cells and tissue and is likely to change over longer time scales. Clinically available impedance telemetry does not allow the two components to be measured separately; however, using the MED-EL system allows both impedance components to be captured. Therefore, changes occurring over different time scales give some indication of the relative contribution of the two components. The impedance measurement is performed using monopolar, low-amplitude bi-phasic current pulses, similar to those used for stimulation via the device. Total impedance (Z_t) can calculated using total voltage which is measured at the end of the current pulse (See **Supplementary Figure S1**). Total impedance comprises the developing polarization component (Z_p) and the access resistance component (R_a). EI is calculated as: $Z_t = V_t/I$.

EI Data Management

Data were exported from MED-EL Maestro in Microsoft Access format. A custom database query was then used to return anonymized individual patients with their age at implant, implanted ear, date of birth, electrode activation status, electrode specific EI and corresponding date stamp. The difference between the date of implant and date stamp for each EI measurement was used to normalize data to a 0 date (day 0 is date of implantation) for each patient. Subsequent EI measurements were split according to the 12 individual electrodes and then averaged into 3-month time bins. All query results were exported in Microsoft spreadsheet format. MathWorks MATLAB (R2018a) was used to read data from excel spreadsheets and plot **Figures 2–8**.

Deactivated Electrode Data Filtering

It is very common for CI users to have electrodes deactivated by clinicians. As discussed, several studies show an increasing EI in the absence of electrical stimulation. Therefore, to minimize the effect of this upward bias on the analysis, only data from actively stimulating electrodes (black dots in **Figure 2**) were included in analyses from **Figure 5** onward; deactivated electrodes (red dots in **Figure 2**) were automatically removed from the analysis using a custom MATLAB script.

Electrode Numbers Were Corrected for Extra-Cochlea Position

During surgery, it is common for the electrode array not to be fully inserted in the cochlea, meaning that electrodes (referred to by position along the array) may be shifted relative to the cochlear anatomy. We corrected for this effect to allow meaningful comparison of electrode positions between patients. Surgical records were interrogated to determine presence/number of extra-cochlear electrodes. The following correction was applied: correct electrode number = [original electrode number + number of extra cochlear electrodes; maximum of 12]. **Figure 1** shows how this results in new electrode numbers being assigned to intra-cochlear electrodes. This does not allow for an estimation of insertion depth, but it does enable analysis of electrodes from "most basal" onward. This correction is applied to all data in **Figures 2**, **3**, **5–8**. The correction is not applied to **Figure 4** (analysis of reasons for deactivation) as it would mask extra-cochlear deactivations.

Statistical Analysis

The software program MathWorks MATLAB was used for data analysis. The adult and pediatric groups were analyzed separately. Least-squares linear regression lines were fitted to the average impedance data (Matlab polyfit) (**Figure 5**).

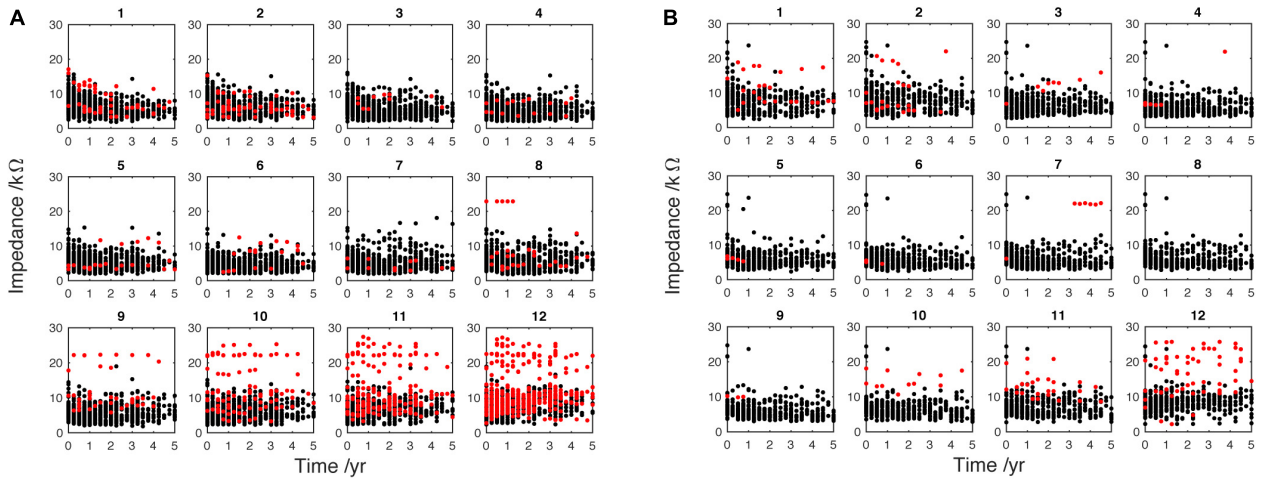

FIGURE 2 | Electrode impedance (kΩ) measured over 5 years from implantation. **(A)** (adult, n = 176) and **(B)** (pediatric, n = 66) data are split into separate electrodes, from apical (1) to basal (12). Each dot represents the 3-month-average EI for one individual patient. The timeline for each patient begins with their respective device activation (time 0). Black dots, active electrodes; Red dots, deactivated electrodes. These data have been adjusted to correct for extra-cochlea position (see **Figure 1**).

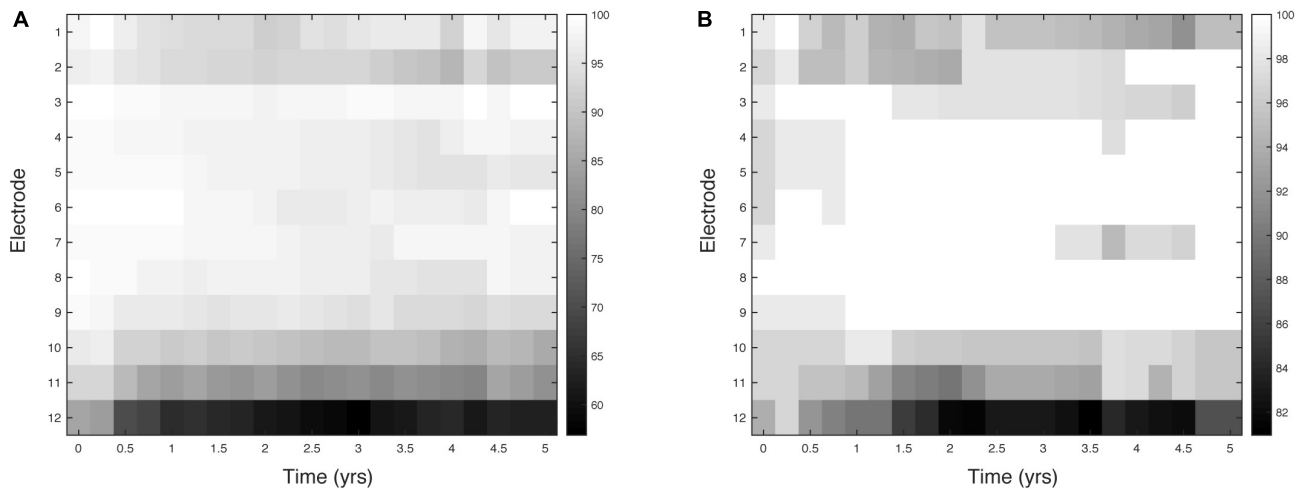

FIGURE 3 | Percentage activation for 12 electrodes over 5 years. Each square represents a 3-month epoch for a given electrode. **(A)** (adult, n = 176) and **(B)** (pediatric, n = 66).

Using MATLAB, an outlier-labeling rule was applied to identify instances of raised EI (**Figures 7**, **8** and **Supplementary Material**)

$$T = Q_u + k\,(Q_u - Q_l)$$

(Hoaglin et al., 1986):

where Q_u and Q_l are the upper and lower quartiles, respectively, and T is the threshold for an outlier. The constant k was fixed at 2.2, equivalent to a 5% probability of any given measurement being an outlier, for the adult and pediatric sample sizes tested (Hoaglin and Iglewicz, 1987). Cases were highlighted as statistically raised EI (SEI) when the EI was greater than T in $\geq$2 time bins within the first 2 years of CI use. Current methods of "high impedance" detection are based on the upper limits of the stimulus delivery hardware for individual cases. Our new approach allows investigation of raised, but not extreme, levels of EI that would otherwise be considered sub-clinical.

Highlighted cases of SEI are split into "basal" (9–12) and "non-basal" (1–8) depending on the position of the electrode showing raised EI. Basal electrodes, which are nearest to the insertion site, are expected to show significantly stronger immune-mediated tissue development: previous studies show significantly greater EI corresponding to this region. A judgment was made to categorize electrodes that are likely to be in the hook region as "basal." This is the straight region of the first cochlear turn, which extends 9 mm from the round window before it curves (Clark et al., 1990). The MED-EL Standard and Flex28 electrode arrays have contacts spaced at 2.2 and 1.9 mm,

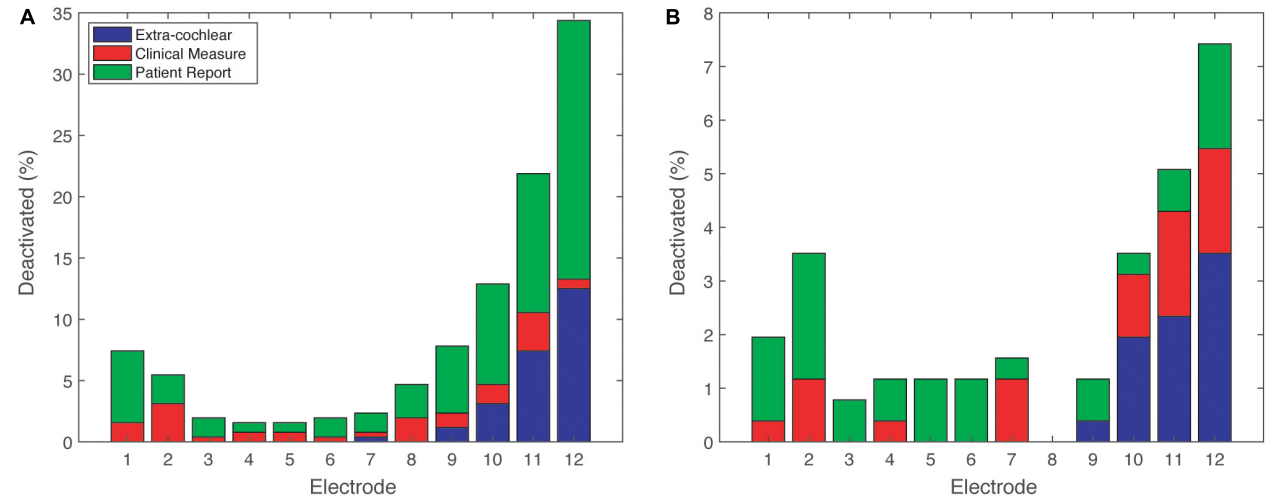

FIGURE 4 | Reasons for deactivation across 12 electrodes. Patient Report (e.g., poor sound quality), Clinical Measure (e.g., impedance telemetry). **(A)** (adult, $n = 176$) and **(B)** (pediatric, $n = 66$).

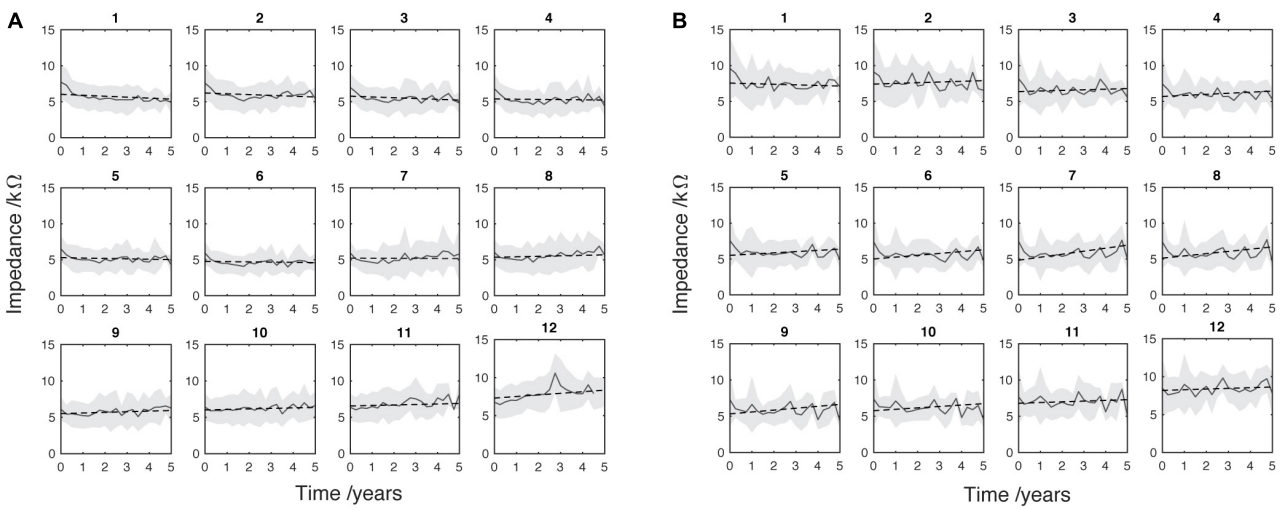

FIGURE 5 | Mean EI (solid gray line) with SD (light gray shading). Regression line of least-squares (black dotted line) was fitted. **(A)** (adult, $n = 176$) and **(B)** (pediatric, $n = 66$) data are split into separate electrodes from apical (1) to basal (12). At this stage of analysis data from deactivated electrodes were removed and electrode number was corrected to account for basal extra-cochlear electrodes. The timeline for each patient begins with their respective device activation (time 0) and subsequent points represent 3-month intervals.

respectively (Med-El, 2013). This means that the basal portion of the array (electrodes 9–12) spans 8.8 and 7.6 mm for Standard and Flex-28 electrodes, respectively.

RESULTS

Data from 242 ears (176 adult and 66 pediatric) were included in the main analysis of EI changes over time. **Figure 2** shows subplots representing 12 separate electrodes. The magnitude of EI is plotted against time from initial CI activation to 5 years later. Each single dot represents the average EI level for a single patient over 3 months. Impedance data measured from actively stimulating electrodes are indicated by black dots whereas data measured at deactivated electrodes are indicated by red dots. The subplots both show a large number of deactivated electrodes, particularly at the most apical and basal electrodes (1 and 12, respectively), the reasons for which are analyzed below. **Figure 2A** identifies a high number of deactivated basal electrodes for the adult population. Note that there are fewer dots at later time points, as not all patients had been using the device for the whole 5-year study period. The EI data were corrected to account for electrodes that were positioned outside the cochlea (see Section "Materials and Methods" and **Figure 1**). This was done to allow alignment of impedance data around an approximate physical position in the cochlea.

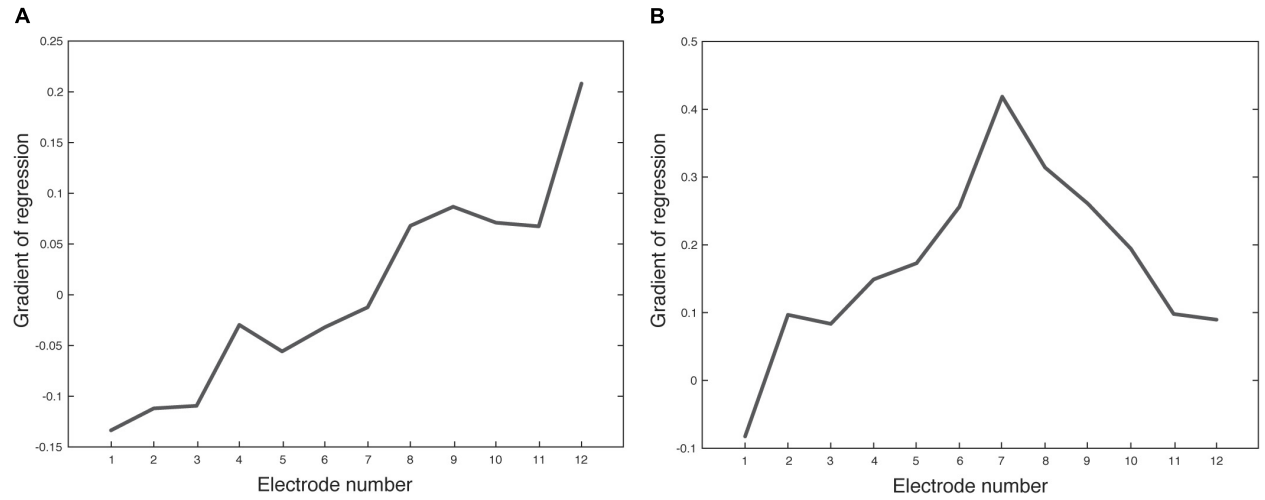

FIGURE 6 | Gradient of regression lines (**Figure 5**) for each electrode. **(A)** (adult, *n* = 176) and **(B)** (pediatric, *n* = 66). Positive gradient values represent a trend of EI increase over time and negative gradient values represent a trend of EI decrease over time.

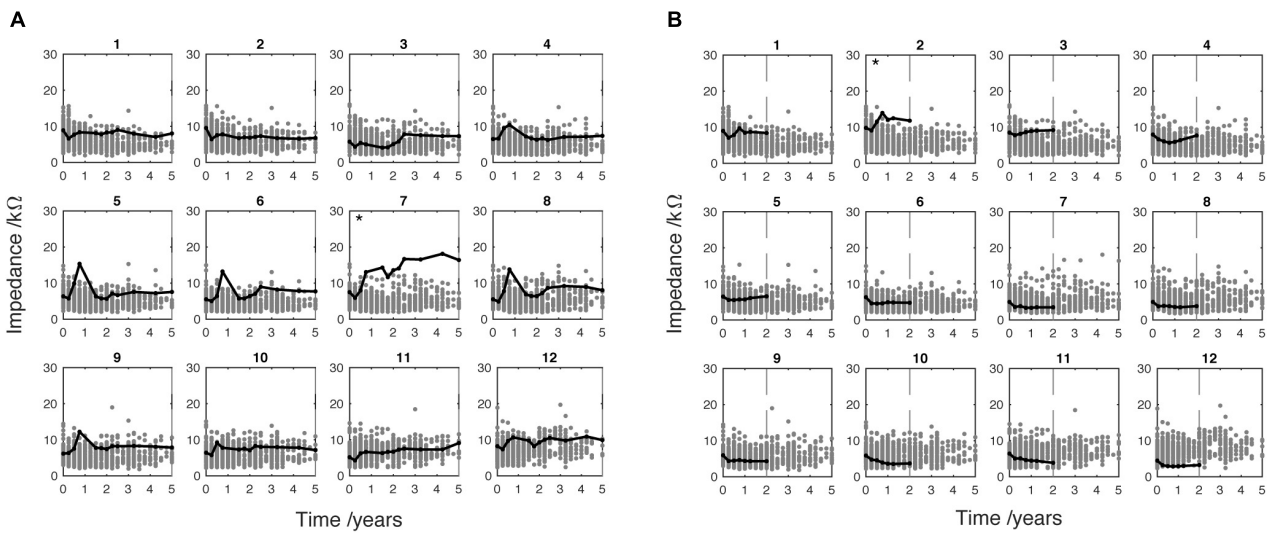

FIGURE 7 | Two individual adult cases showing EI at active electrodes only. Case **(A)** shows 5 years CI use. Case **(B)** shows 2 years CI use indicated by vertical dotted line. Electrode marked by * met the SEI criteria which indicates high EI compared to the sample distribution. These data have been adjusted to correct for extra-cochlea position (see **Figure 1**).

The proportion of deactivated electrodes in the population is shown in **Figure 3**. Deactivation is clearly most common in the most basal electrodes for both adults and children. The figure also shows an increasing number of deactivations over the first 1–2 years of CI use. The peak number of deactivations was higher in the adult group (**Figure 3A**) than the pediatric group (**Figure 3B**). Both groups had most deactivations at electrode 12, which can be seen as black at 2.25 years. At that epoch, only 60% of adult electrodes were active while 81% of pediatric electrodes were active. Electrode 11 showed the second highest number of deactivations for both groups. For example, 80% of adults had electrode 11 remaining active at 2.5, 3.25, 4 and 4.25 years. There was a slight increase in deactivations at the most apical electrodes compared to the mid-array for both adults and children. For example, adults had 88% of electrode 2 remaining active at 4 years. The children had 92% of electrode 1 remaining active at 4.5 years. A difference between the two groups was the mid-array electrodes were mostly active in the pediatric group, indicated by white area in **Figure 3B**. Although the adults were initially 100% active at electrodes 3 and 6, a few deactivations were made in the next 3-month epoch. In contrast, the children had 100% activation for the majority of the 5-year study period in electrodes 4, 5, 6 and 7.

The patterns of deactivation seen above are better understood in light of the clinical reasons for deactivation shown in **Figure 4**. Electrodes in the most basal portion of the array were deactivated

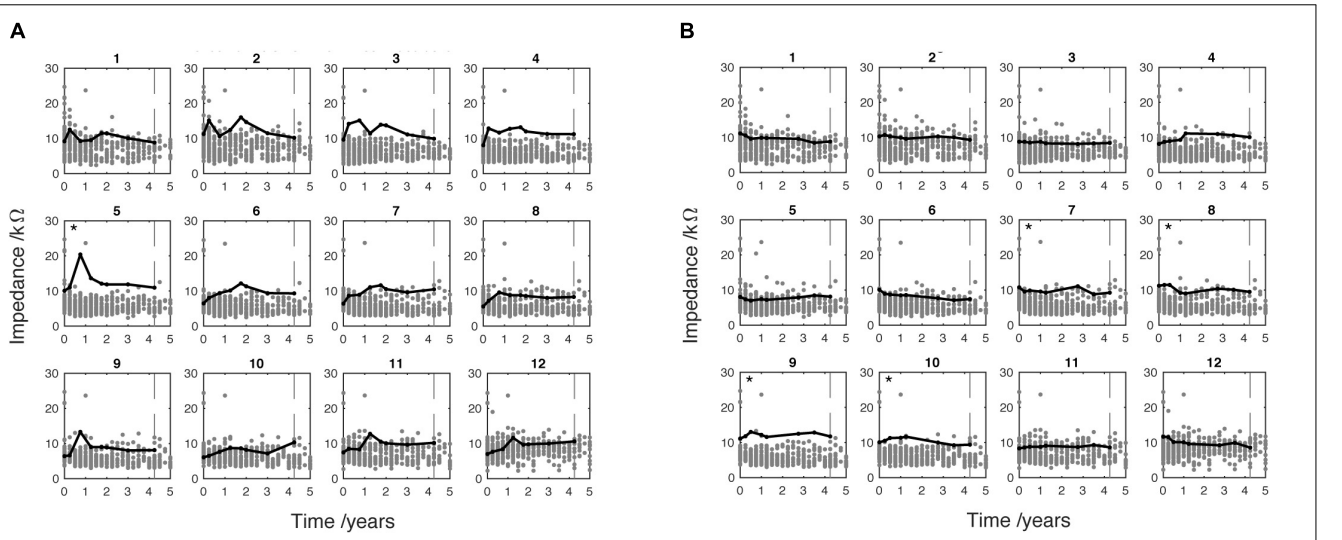

FIGURE 8 | Two individual pediatric cases showing EI at active electrodes only. Case **(A)** shows 4.25 years CI use (indicated by vertical dotted line). Case **(B)** shows 4.25 years CI use (indicated by vertical dotted line). Electrode marked by * met the SEI criteria which indicates high EI compared to the sample distribution. These data have been adjusted to correct for extra-cochlea position (see **Figure 1**).

because they were outside the cochlea (extra-cochlear). In the basal electrodes (9–12), extra-cochlear position accounted for about one third of the adult reasons (**Figure 4A**), and about half of the pediatric reasons (**Figure 4B**). The majority of deactivations, however, in the adult group were informed by the patient reports of their subjective experience, such as "poor sound quality" (See **Supplementary Figure S2** for a complete list of deactivation reasons); there were relatively few deactivations owing to "Clinical Measures" which offer objective information. The percentage of subjective "Patient Report" reasons is highly likely to be biased by the age of the CI user: many of the children are very young and could not communicate their perception of sound. As shown in **Figure 3**, the children had significantly fewer deactivations overall.

Data points acquired at deactivated electrodes were removed at this stage of the analysis (red dots in **Figure 2**). **Figure 5** shows the mean EI for the adults (**Figure 5A**) and the children (**Figure 5B**). Least-squares linear regression lines were fitted to the average impedance data (Matlab polyfit) for each electrode to show the trend of EI change over time. The adult group show a tendency for EI reduction at apical electrodes (negative slope), increase at basal electrodes (positive slope) and no change for mid electrodes. The pediatric group shows a different pattern of regression lines across the electrodes. All of the electrodes in this group, except electrode 1 show a positive slope. This suggests a difference in long-term EI evolution in children compared to adults, although the mean is more variable in this age group. This is probably caused by the lower overall sample size and fluctuation of sample size in each time window (i.e., by chance fewer individuals were seen in some 3-month epochs).

The data above indicates that EI changes over time in a way that varies with electrode position. We describe this EI change over time using a regression line for each electrode in **Figure 5**. The gradient of each line is plotted for each electrode in **Figure 6**. The adult group (**Figure 6A**) shows a positive relationship between gradient and electrode number. Each consecutive electrode shows a general increase in gradient with electrode number. The largely monotonic relationship between gradient and electrode fits the consensus in the literature and highlights the phenomena quite simply. Another observation is that the crossover point from EI reduction (negative gradient) to increase (positive gradient) is at electrode 7, which is roughly the middle of the electrode array. This shows that EI evolution varies from base to apex in a continuous fashion. The relationship between fit-line gradient and electrode number in the pediatric group (**Figure 6B**) shows that EI largely increases over the 5-year period for all electrodes except number 1. The increase is steepest at electrode 7. We note that the regression lines are an approximate linear fit and hence describe general trends. The pediatric sample shows a large degree of variability between timepoints because of the relatively low sample size and irregular frequency of clinical appointments. The peaks and troughs of mean EI cause some biasing of the fit lines so we have been conservative in our interpretation of differences between age groups.

In the adult group, 14 patients met the SEI criteria (8%): one in basal electrodes, three in both basal and non-basal and 10 in non-basal electrodes only. The case shown in **Figure 7A** was implanted with a standard electrode array and the clinical record did not include the hearing-loss etiology. The case shown in **Figure 7B** was implanted with a Flex28 electrode array and the clinical record showed head injury as the cause of hearing loss. **Figure 7A** shows an EI increase at electrode 7 over the 5 years of CI use. This electrode is highlighted by (*) to indicate that EI level met the SEI criteria. A key observation is the difference in temporal development and absolute level of EI of this electrode compared to its immediate neighbors. This difference is unusual for non-basal electrodes where the EI is often mirrored in

neighboring electrodes. The absolute EI level shown in **Figure 7B** is lower than **Figure 7A** although the SEI criteria have been met at electrode 2.

In the pediatric group, three cases met the SEI criteria (5%): two in non-basal and one in both basal and non-basal electrodes. **Figure 8** shows the EI measurements taken from two pediatric cases. Each was found to meet the SEI criteria in one of two implanted ears. The black line shows that EI is greater in these cases than the other cases in the sample (gray dots) which are mostly clustered around or below 10 kΩ. The case shown in **Figure 8A** was implanted with a Flex-28 electrode. Clinical records show they were diagnosed with congenital hearing loss associated with Pendred syndrome. This case met the SEI criteria at electrode 5 (indicated by *). After the initial activation and tuning appointment, the EI increased relatively rapidly to peak around 1 year of CI use. A similarly sharp reduction is shown in the following 3-month period before EI plateau around 12 kΩ. This case shows a general tendency for raised EI over the duration of observed CI use. This is especially marked in electrodes 2, 3 and 4, although the level did not meet the criterion for SEI. The case shown in **Figure 8B** was fitted with a Standard electrode array. The clinical record showed a diagnosis of genetic mutation of the gene GJB2 (connexin26). The case shown in **Figure 8B** met the SEI criteria at electrode 7, 8, 9 and 10. Unlike the pattern shown in **Figure 8A**, the EI tracked a stable level across the period of use.

DISCUSSION

This retrospective study of clinical data from a large sample of MED-EL CI users showed population-level trends in EI across time and between cochlear regions, and also yielded a potential new approach to define EI outliers for whom further clinical action may need to be taken. The analysis showed that most adult electrode deactivations were made because of reported experiences rather than clinical measures such as neural-response telemetry or electrode-impedance telemetry. The population-based method of outlier detection used here offers an objective insight into intra-cochlear tissue status to inform decisions to deactivate electrodes. Ongoing challenges for neuroprostheses include biocompatibility and functional longevity (Adewole et al., 2017). Performance decrement, as contrasted with frank failure, is difficult to monitor and almost impossible to predict using current approaches. The consensus in the field of CI for clinical assessment of soft failure recommends a broad-spectrum approach. This includes patient interview, medical investigations such as X-ray imaging, audiological and hardware testing (Balkany et al., 2005). This relies on the CI user having well-established linguistic abilities. In children the consensus is that the clinician should record and interpret the user's behaviors, although this has limited reliability (Moberly et al., 2013). The methods presented here allow deeper enquiry into the telemetry data that is already routinely gathered. Our results suggest that a minority of raised impedance cases can be detected in a population, which may aid triaging of patients, including those who can provide only limited verbal reports.

We describe the evolution of EI for adults and children at 12 electrodes along the MED-EL array. The measurement at the first (0 months) and second time points (3 months) identifies a drop in EI across all conditions. The drop is consistent with an increase in electrode surface area due to the electrolytic activity (Brummer and Turner, 1977), and/or clearance and reorganization of organic molecules, cells, tissues on and around the electrode (Marsella et al., 2014). The main observation in the adult group is EI growth at basal electrodes and EI reduction at apical electrodes. Growth in basal-electrode EI is likely to be caused by fibrosis and osteogenesis based on its slow evolution over time. Previous findings from a post-mortem study of cochleae from CI users have shown the levels of fibrotic and bone tissue to be greatest in the basal turn of the cochlea (Fayad et al., 2009). The magnitude of fibrosis is also correlated with the level of trauma caused by surgery (Richard et al., 2012). It is also possible that there are differences in capacity for inflammatory response in different regions of the cochlea, e.g., due to anatomical variations such as vasculature, nerve supply or cochlear-duct width.

We observed the trend that children show an increase in EI for all electrodes except electrode 1. This data shows more variability over time than the adults, possibly due to the lower number of cases analyzed. If a difference exists, the likely explanation is a difference in the chronic tissue response to surgery in children and adults (i.e., developmental stage) or differences in etiology among children vs. adults. Previous studies have shown increasing EI for basal, mid and apical electrodes in children compared to the adult group which only showed increase at the base (Hughes et al., 2001; Busby et al., 2002). Our data appear to support this although no formal age-group comparison was made. There is some published evidence of differences in hearing preservation between adults and children. One study showed a small trend toward better residual hearing in children (Zanetti et al., 2015), although another found no effect of age (Skarzynski et al., 2013). The findings of the present study suggest an increased growth of intra-cochlear tissue around the base that is particularly clear in the adult group.

The fact that gradual increases in basal impedance were observed is indicative of a slow proliferation of tissue indicative of immune-mediated fibrosis. Studies have shown that such reactions lead to structurally organized fibrotic tissue and bone (Li et al., 2007; Somdas et al., 2007), which would begin to emerge within the same timeframe as the impedance increase shown here, i.e., months to years. It should be noted that the exclusion of deactivated (mainly basal electrodes) would suggest that our findings under-estimate the extent of basal tissue growth. The data shows individual variability in EI, which may reflect surgical approach, age, etiology, noise exposure or other factors. The cases included were implanted using either cochleostomy (approximately one third) or round window insertion (approximately two thirds). No formal assessment of surgical approach and its impact on EI was carried out. Evidence shows that this variable has no significant effect on EI or listening performance for phonemes or sentences (Cheng et al., 2018).

We have limited understanding of the wide variability in performance and outcomes for CI users. A wealth of evidence suggests that the biological response to the implant

is pivotal to its long-term functionality. It is possible to measure the response using impedance telemetry, although the currently available tools are limited to detection of extreme high or low EI levels. In order to address this, we applied a statistical method of outlier-labeling to detect cases of raised impedance (SEI). This is distinct from the absolute threshold used by the MED-EL and other manufacturers, which serves to highlight high and low impedances that are extreme enough to prevent normal current delivery. These cases mostly indicate hardware faults and extra-cochlear electrode position. The cost of using high threshold methods for detecting raised impedance is the relative insensitivity to biological perturbations associated with EI changes below 20 k**Ω**. Our technique could be validated by measuring CI performance following customization of processor maps where electrodes with SEI levels are deactivated. If validated, this would provide a quicker and more clinically useful method to guide electrode deactivation as compared with more challenging and time-consuming methods based on psychophysical measurements proposed in the literature: Mathew et al. (2017) and Zhou (2017). Further work to determine any correlation between the sorts of psychophysical methods proposed by these authors and the proposed outlier-EI values would help to further validate this approach.

The long-term pattern of change of EI in those individuals identified as outliers may inform the underlying mechanism. Results show EI increase at discrete electrodes, some developing slowly over the 5-year study period. In several cases (13 of 14) the SEI criteria was met at non-basal electrodes, which is counter to the model that the tissue development driven by inflammation is most prevalent at the base near the site of array implantation (Richard et al., 2012; Bas et al., 2015). In some cases, gradual EI differences are specific to particular non-basal electrodes. For example, electrode 7 in **Figure 7A** shows a pronounced example of EI increase that develops slowly over many months. In most cases, this was limited to one, or at most, very few electrodes, which suggests the change is driven by spatially localized factors. No hardware malfunctions were detected, and the electrode remained actively stimulated for the duration of the studied time period. One possible explanation is the presence of a spatially discrete trigger of inflammation such as mechanical trauma. This might have occurred during surgery as the electrode array tip passed through this region of the cochlear duct causing an abrasion, as lateral wall damage is known to elicit fibrotic changes (Li et al., 2007). To further understand the cause of raised but not "open-circuit" EI in particular electrode regions, the ability to cross-reference with newer and more sensitive imaging methods (Aschendorff, 2011) could also lead to a greater understanding of whether localized surgical trauma, cochlear anatomy, or other factors, predispose some individuals to showing higher EI values in apical or mid-cochlear regions.

Electrical stimulation is known to electro-chemically effect the endo-cochlear environment. When charge is delivered within safe tolerances the predominant mechanisms are ionic transfer and platinum hydrogen plating (Brummer and Turner, 1977). These processes are safe and reversible when bi-phasic charge-balanced pulses are used. It has been suggested that such charge delivery mediates the process of protein adsorption onto platinum electrodes and can affect the organization and density of the fibrotic capsule (Newbold et al., 2010). It is well documented that electrode deactivation contributes to EI increase, so ideally clinicians would access objective evidence before making electrode deactivations that make future reactivation more difficult. Neuburger et al. (2009) presents further evidence of the effect of electrical stimulation on impedance. They observed cases of increasing EI in CI users with high rates of stimulation, which necessitate short pulse-width and high current to produce the desired perceived loudness. A therapeutic intervention involving increased pulse-width along with antibiotics and steroids proved effective at significantly reducing EI. The author suggests that the original EI increase could be caused by the occurrence of out-of-compliance charge delivery leading to slight asymmetries in bi-phasic pulses. Early detection of increasing impedance could therefore be clinically important: it will inform stimulus parameter adjustments, which could lower impedance levels before they cause voltage compliance problems.

Recent work has identified improved preservation of spiral ganglion neurones after dexamethasone elution in chronically stimulated animals (Scheper et al., 2017). Another study of dexamethasone eluting CI electrodes in guinea pigs showed significant reductions in fibrotic tissue and EI compared to no-steroid controls (Wilk et al., 2016). A complementary result was shown in humans where the cochlea was perfused with the steroid triamcinolone; long-term EI levels were significantly lower in the treatment group compared to controls (De Ceulaer et al., 2003). Systemic delivery of the steroid methylprednisolone in another study did not reduce EI spikes (Choi et al., 2017), which suggests the anti-inflammatory action of steroids is most effective when topically administered. It would be interesting to study the benefit of steroid based intervention that is directed by the outlier-labeling rule used here.

Our analysis of the proportion of deactivated electrodes in children and adults was quite telling. Generally, both age groups showed a pattern of electrode deactivation primarily at basal electrodes. However, the reasons for deactivations were overwhelmingly patient feedback from adults whereas the most common reason in children was extra-cochlear position. In addition, deactivation was less common in children than in adults. One possible explanation for this was that clinical decisions about deactivations are more cautious with children, or, rather, that adult feedback to clinicians does lead to choice of deactivation of electrodes with more fibrous tissue grown/higher EI (e.g., primarily basal). This begs the question of whether choice to deactivate electrodes is optimal, and in particular whether the smaller proportion of basal electrode deactivations among children in particular is clinically appropriate or whether deactivation of basal electrodes in adults is excessive. Cross-referencing with the outlier method of EI analysis and other methods noted above could help to determine the answer to these questions. Alternatively, it may be that some differences in etiology and/or anatomy pre-dispose the child's cochlea to be more susceptible to other types of problem (e.g., non-auditory stimulation).

CONCLUSION

An important outcome of this work is the insight gained from applying a custom analysis protocol to existing clinical data. Our approach was to characterize sample-wide trends and apply an outlier detection rule that could improve our early detection of sub-optimal performance. A key benefit of using this method alongside manufacturer-specific proprietary telemetry systems is the sensitivity to changes of lower magnitude that may be associated with performance. This offers clinicians and researchers working in neuroprosthetics a method for interrogating their existing population data to identify incremental changes in device behavior, without extra financial, technical or ethical burden.

Our first question addressed the trend of impedance change over time for different electrode positions. The results showed that electrodes exhibit distinct trends of impedance evolution over 5 years. In the adult group growth in the basal electrodes contrasted with reduction for apical electrodes. The results also describe the range of the adult and pediatric dataset, which provides useful insights into individual variability. One reason for characterizing the EI trends over time was to improve interpretation of any individual deviation from the normative range. We asked how many individuals show statistically raised EI. The main analysis showed 8% of adults and 5% of children exhibited raised EI levels compared to the sample distribution. These cases were detected using a statistical outlier-labeling rule, which could be used to inform electrode deactivations with improved objectivity. Indeed, our findings show that clinical decisions to deactivate electrodes for adults were most commonly informed by patient subjective reports. The fact that adults had proportionally more electrodes deactivated than children may be caused by differences in capacity and confidence for verbal communication. The method used here to detect raised impedance in individuals of a clinical population may offer an opportunity to activate or deactivate electrodes long before the current device-specific floor or ceiling levels are reached. We determine that the information extracted from populations of users can be used alongside subjective reports to inform clinical management of individual patients. More work is needed to explore the sensitivity of this method as a biomarker of CI performance decrement.

The immediate benefit of these methods and findings is to give clinicians fresh insight into their existing data. The increasing size and accessibility of clinical datasets presents an opportunity to professionals working with neuroprosthetics. Population-wide norms can be used to better interpret measurements from individual patients. The aim is to personalize clinical management to improve the function and biocompatibility of the implant interface over a user's lifetime.

AUTHOR CONTRIBUTIONS

AS conceived the research idea in conversation with TN and CV (academic supervisory team), performed the data collection, design of analysis, and literature review, and wrote the manuscript with guidance from TN and CV. ER wrote the custom MathWorks MATLAB code used for main analyses (as detailed in section "Materials and Methods") and automated generation of **Figures 2–4**, **5**, **7**, **8** with contribution from AS. AS, ER, TN, and CV performed the final manuscript editing and proofreading process with equal contribution.

ACKNOWLEDGMENTS

We thank K. Hough (Institute of Sound and Vibration Research, Faculty of Engineering and the Environment, University of Southampton) for manuscript proofreading and supporting discussions of biological responses to CI. We also thank M. Grasmeder for data extraction (MED-EL Maestro) and supporting discussions of clinical implications of findings, S. Cross for the management of clinical data (MED-EL Maestro and local patient database), and all patients of the Auditory Implant Service (Auditory Implant Service, Faculty of Engineering and the Environment, University of Southampton). We would like to acknowledge that the lead author's contributions to this work were made as part of a Ph.D. studentship funded by the Engineering and Physical Sciences Research Council (EPSRC Grant Code is 513830136) via a Doctoral Training Partnership with the University of Southampton, United Kingdom.

SUPPLEMENTARY MATERIAL

The Supplementary Material for this article can be found online at: https://www.frontiersin.org/articles/10.3389/fnins.2018.01048/full#supplementary-material

REFERENCES

Adewole, D. O., Serruya, M. D., Harris, J. P., Burrell, J. C., Chen, H. I., Wolf, J. A., et al. (2017). The evolution of neuroprosthetic interfaces. *Crit. Rev. Biomed. Eng.* 44, 123–152. doi: 10.1615/CritRevBiomedEng.2016017198

Anderson, J. M., Rodriguez, A., and Chang, D. T. (2008). Foreign body reaction to biomaterials. *Semin. Immunol.* 20, 86–100. doi: 10.1016/j.smim.2007.11.004

Aschendorff, A. (2011). Imaging in cochlear implant patients. *GMS Curr. Top. Otorhinolaryngol. – Head Neck Surg.* 90, S16–S21. doi: 10.1055/s-0030-1270448

Balkany, T. J., Hodges, A. V., Buchman, C. A., Luxford, W. M., Pillsbury, C. H., Roland, P. S., et al. (2005). Cochlear implant soft failures consensus development conference statement. *Cochlear Implants Int.* 6, 105–122. doi: 10.1179/cim.2005.6.3.105

Bas, E., Goncalves, S., Adams, M., Dinh, C. T., Bas, J. M., Van De Water, T. R., et al. (2015). Spiral ganglion cells and macrophages initiate neuro-inflammation and scarring following cochlear implantation. *Front. Cell. Neurosci.* 9:303. doi: 10.3389/fncel.2015.00303

Biedron, S., Westhofen, M., and Ilgner, J. (2009). On the number of turns in human cochleae. *Otol. Neurotol.* 30, 414–417. doi: 10.1097/MAO.0b013e3181977b8d

Brummer, S. B., and Turner, M. J. (1977). Electrochemical considerations for safe electrical stimulation of the nervous system with platinum electrodes. *IEEE Trans. Biomed. Eng.* 24, 59–63. doi: 10.1109/TBME.1977.326218

Busby, P. A., Plant, K. L., and Whitford, L. A. (2002). Electrode impedance in adults and children using the Nucleus 24 cochlear implant system. *Cochlear Implants Int.* 3, 87–103. doi: 10.1002/cii.55

Carlson, M. L., Archibald, D. J., Dabade, T. S., Gifford, R. H., Neff, B. A., Beatty, C. W., et al. (2010). Prevalence and timing of individual cochlear implant electrode failures. *Otol. Neurotol.* 31, 893–898. doi: 10.1097/MAO.0b013e3181d2d697

Causon, A., Verschuur, C. A., and Newman, T. A. (2013). Trends in cochlear implant complications: implications for improving long-term outcomes. *Otol. Neurotol.* 34, 259–265. doi: 10.1097/MAO.0b013e31827d0943

Cheng, X., Wang, B., Liu, Y., Yuan, Y., Shu, Y., and Chen, B. (2018). Comparable electrode impedance and speech perception at 12 months after cochlear implantation using round window versus cochleostomy: an analysis of 40 patients. *Orl* 200031, 1–11. doi: 10.1159/000490764

Choi, J., Payne, M. R., Campbell, L. J., Bester, C. W., Newbold, C., Eastwood, H., et al. (2017). Electrode impedance fluctuations as a biomarker for inner ear pathology after cochlear implantation. *Otol. Neurotol.* 38, 1433–1439. doi: 10.1097/MAO.0000000000001589

Christo, S. N., Diener, K. R., Bachhuka, A., Vasilev, K., and Hayball, J. D. (2015). Innate immunity and biomaterials at the nexus: friends or foes? *Biomed Res. Int.* 2015:342304. doi: 10.1155/2015/342304

Clark, G. M., Tong, C. T., and Patrick, J. F. (1990). *Cochlear Prostheses*. 1st Edn, ed. G. M. Clark, C. T. Tong, and J. F. Patrick (London: Longman Group UK Limited).

Clark, G. M., Shute, S. A., Shepherd, R. K., and Carter, T. D. (1995). Cochlear implantation: osteoneogenesis, electrode-tissue impedance, and residual hearing. *Ann. Otol. Rhinol. Laryngol.* 166, 40–42.

Clark, G. M. (2003). *Cochlear Implants: Fundamentals and Applications*, ed. Robert T. Beyer (New York: Springer-Verlag New York, Inc.). doi: 10.1007/b97263

De Ceulaer, G., Johnson, S., Yperman, M., Daemers, K., Offeciers, F. E., O'Donoghue, G. M., et al. (2003). Long-term evaluation of the effect of intracochlear steroid deposition on electrode impedance in cochlear implant patients. *Otol. Neurotol.* 24, 769–774. doi: 10.1097/00129492-200309000-00014

Dorman, M. F., Smith, L. M., Dankowski, K., McCandless, G., and Parkin, J. L. (1992). Long-term measures of electrode impedance and auditory thresholds for the Ineraid cochlear implant. *J. Speech Hear. Res.* 35, 1126–1130. doi: 10.1044/jshr.3505.1126

Ear Foundation (2016). *Cochlear Implants Information Sheet*. Available at: http://www.earfoundation.org.uk/files/download/1221

Fayad, J. N., Makarem, A. O., and Linthicum, F. H. (2009). Histopathologic assessment of fibrosis and new bone formation in implanted human temporal bones using 3D reconstruction. *Otolaryngol. – Head Neck Surg.* 141, 247–252. doi: 10.1016/j.otohns.2009.03.031

Gifford, R. H., Shallop, J. K., and Peterson, A. M. (2008). Speech recognition materials and ceiling effects: considerations for cochlear implant programs. *Audiol. Neurotol.* 13, 193–205. doi: 10.1159/000113510

Grill, W. M., and Thomas Mortimer, J. (1994). Electrical properties of implant encapsulation tissue. *Ann. Biomed. Eng.* 22, 23–33. doi: 10.1007/BF02368219

Hassler, C., Boretius, T., and Stieglitz, T. (2011). Polymers for neural implants. *J. Polym. Sci. Part B Polym. Phys.* 49, 18–33. doi: 10.1002/polb.22169

Henkin, Y., Kaplan-Neeman, R., Kronenberg, J., Migirov, L., Hildesheimer, M., and Muchnik, C. (2006). A longitudinal study of electrical stimulation levels and electrode impedance in children using the Clarion cochlear implant. *Acta Otolaryngol.* 126, 581–586. doi: 10.1080/00016480500443391

Henkin, Y., Kaplan-Neeman, R., Muchnik, C., Kronenberg, J., and Hildesheimer, M. (2003). Changes over time in electrical stimulation levels and electrode impedance values in children using the Nucleus 24M cochlear implant. *Int. J. Pediatr. Otorhinolaryngol.* 67, 873–880. doi: 10.1016/S0165-5876(03)00131-9

Hillard, C., Fowler, J. D., Barta, R., and Cunningham, B. (2017). Silicone breast implant rupture: a review. *Gland Surg.* 6, 163–168. doi: 10.21037/gs.2016.09.12

Hoaglin, D. C., and Iglewicz, B. (1987). Fine-tuning some resistant rules for outlier labeling. *J. Am. Stat. Assoc.* 82, 1147–1149. doi: 10.1080/01621459.1987.10478551

Hoaglin, D. C., Iglewicz, B., and Tukey, J. W. (1986). Performance of some resistant rules for outlier labeling. *J. Am. Stat. Assoc.* 81, 991–999. doi: 10.1080/01621459.1986.10478363

Hughes, M. L., Vander Werff, K. R., Brown, C. J., Abbas, P. J., Kelsay, D. M., Teagle, H. F., et al. (2001). A longitudinal study of electrode impedance, the electrically evoked compound action potential, and behavioral measures in nucleus 24 cochlear implant users. *Ear. Hear.* 22, 471–486. doi: 10.1097/00003446-200112000-00004

Jia, H., Venail, F., Piron, J. P., Batrel, C., Pelliccia, P., ArtierÌes, F., et al. (2011). Effect of surgical technique on electrode impedance after cochlear implantation. *Ann. Otol. Rhinol. Laryngol.* 120, 529–534. doi: 10.1177/000348941112000807

Kamakura, T., and Nadol, J. B. (2016). Correlation between word recognition score and intracochlear new bone and fibrous tissue after cochlear implantation in the human. *Hear. Res.* 339, 132–141. doi: 10.1016/j.heares.2016.06.015

Kawano, A., Seldon, H. L., Clark, G. M., Msden, R. T., and Raine, C. H. (1998). Intracochlear factors contributing to psychophysical percepts following cochlear implantation: a case study. *Acta Otolaryngol.* 104, 54–57. doi: 10.1080/00016489850183386

Leone, C. A., Mosca, F., Grassia, R., and Hospital, M. (2017). Temporal changes in impedance of implanted adults for various cochlear segments. *Acta Otorhinolaryngol. Ital.* 37, 312–319. doi: 10.14639/0392-100X-1471

Li, P. M., Somdas, M. A., Eddington, D. K., and Nadol, J. B. (2007). Analysis of intracochlear new bone and fibrous tissue formation in human subjects with cochlear implants. *Ann. Otol. Rhinol. Laryngol.* 116, 731–738. doi: 10.1177/000348940711601004

Lim, H. J., Lee, E. S., Park, H. Y., Park, K., and Choung, Y. H. (2011). Foreign body reaction after cochlear implantation. *Int. J. Pediatr. Otorhinolaryngol.* 75, 1455–1458. doi: 10.1016/j.ijporl.2011.08.004

Marsella, P., Scorpecci, A., Pacifico, C., Resca, A., Vallarino, M. V., Ingrosso, A., et al. (2014). Safety and functional results of early cochlear implant switch-on in children. *Otol. Neurotol.* 35, 277–282. doi: 10.1097/MAO.0000000000000259

Mathew, R., Undurraga, J., Li, G., Meerton, L., Boyle, P., Shaida, A., et al. (2017). Objective assessment of electrode discrimination with the auditory change complex in adult cochlear implant users. *Hear. Res.* 354, 86–101. doi: 10.1016/j.heares.2017.07.008

Med-El (2013). *Electrode Arrays: Designed for Atraumatic Implantation Providing Superior Hearing Performance*. Available at: http://www.medel.com/data/pdf/21617.pdf

Moberly, A., Welling, B., and Nittrouer, S. (2013). Detecting soft failures in pediatric cochlear implants: relating behavior to language outcomes. *Otol. Neurotol.* 34, 1648–1655. doi: 10.1016/j.pmrj.2014.02.014. Lumbar

Nadol, J. B., O'Malley, J. T., Burgess, B. J., and Galler, D. (2014). Cellular immunologic responses to cochlear implantation in the human. *Hear. Res.* 318, 11–17. doi: 10.1016/j.heares.2014.09.007

Neuburger, J., Lenarz, T., Lesinski-Schiedat, A., and Büchner, A. (2009). Spontaneous increases in impedance following cochlear implantation: suspected causes and management. *Int. J. Audiol.* 48, 233–239.

Newbold, C., Mergen, S., Richardson, R., Seligman, P., Millard, R., Cowan, R., et al. (2014). Impedance changes in chronically implanted and stimulated cochlear implant electrodes. *Cochlear Implants Int.* 15, 191–199. doi: 10.1179/1754762813Y.0000000050

Newbold, C., Richardson, R., Millard, R., Huang, C., Milojevic, D., Shepherd, R., et al. (2010). Changes in biphasic electrode impedance with protein adsorption and cell growth. *J. Neural Eng.* 7:056011. doi: 10.1088/1741-2560/7/5/056011

Nguyen, S., Cloutier, F., Philippon, D., Côté, M., Bussières, R., and Backous, D. D. (2016). Outcomes review of modern hearing preservation technique in cochlear implant. *Auris Nasus Larynx* 43, 485–488. doi: 10.1016/j.anl.2016.02.014

Rask-Andersen, H., Erixon, E., Kinnefors, A., Löwenheim, H., Schrott-Fischer, A., and Liu, W. (2011). Anatomy of the human cochlea – implications for cochlear implantation. *Cochlear Implants Int.* 12(Suppl. 1), S8–S13. doi: 10.1179/146701011X13001035752174

Rask-Andersen, H., Liu, W., Erixon, E., Kinnefors, A., Pfaller, K., Schrott-Fischer, A., et al. (2012). Human cochlea: anatomical characteristics and their relevance for cochlear implantation. *Anat. Rec.* 295, 1791–1811. doi: 10.1002/ar.22599

Richard, C., Fayad, J. N., Doherty, J., and Linthicum, F. H. (2012). Round window versus cochleostomy technique in cochlear implantation: histologic findings. *Otol. Neurotol.* 33, 1181–1187. doi: 10.1097/MAO.0b013e318263d56d

Saunders, E., Cohen, L., Aschendorff, A., Shapiro, W., Knight, M., Stecker, M., et al. (2002). Threshold, comfortable level and impedance changes as a function of electrode-modiolar distance. *Ear Hear.* 23, 28S–40S. doi: 10.1097/00003446-200202001-00004

Scheper, V., Hessler, R., Hu, M., Wilk, M., Jolly, C., Lenarz, T., et al. (2017). Local inner ear application of dexamethasone in cochlear implant models is safe for auditory neurons and increases the neuroprotective effect of chronic electrical stimulation. *PLoS ONE* 12:e0183820. doi: 10.1371/journal.pone.0183820

Seyyedi, M., and Nadol, J. B. Jr. (2014). Intracochlear inflammatory response to cochlear implant electrodes in humans. *Otol. Neurotol.* 35, 1545–1551. doi: 10.1097/MAO.0000000000000540

Shepherd, R. K., Matsushima, J., Martin, R. L., and Clark, G. M. (1994). Cochlear pathology following chronic electrical stimulation of the auditory nerve: II deafened kittens. *Hear. Res.* 81, 150–166. doi: 10.1016/0378-5955(94)90162-7

Skarzynski, H., van de Heyning, P., Agrawal, S., and Arauz, S. L. (2013). Towards a consensus on a hearing preservation classi fi cation system. *Acta Otolaryngol. Suppl.* 133, 3–13. doi: 10.3109/00016489.2013.869059

Somdas, M. A., Li, P. M., Whiten, D. M., Eddington, D. K., and Nadol, J. B. (2007). Quantitative evaluation of new bone and fibrous tissue in the cochlea following cochlear implantation in the human. *Audiol. Neurotol.* 12, 277–284. doi: 10.1159/000103208

Stöver, T., and Lenarz, T. (2009). Biomaterials in cochlear implants. *Laryngorhinootologie* 88, S12–S31. doi: 10.3205/cto000062

Tykocinski, M., Cohen, L. T., and Cowan, R. S. (2005). Measurement and analysis of access resistance and polarization impedance in cochlear implant recipients. *Otol. Neurotol.* 26, 948–956. doi: 10.1097/01.mao.0000185056.99888.f3

Tykocinski, M., Duan, Y., Tabor, B., and Cowan, R. S. (2001). Chronic electrical stimulation of the auditory nerve using high surface area (HiQ) platinum electrodes. *Hear. Res.* 159, 53–68. doi: 10.1016/S0378-5955(01)00320-3

Wilk, M., Hessler, R., Mugridge, K., Jolly, C., Fehr, M., Lenarz, T., et al. (2016). Impedance changes and fibrous tissue growth after cochlear implantation are correlated and can be reduced using a dexamethasone eluting electrode. *PLoS One* 11:e0147552. doi: 10.1371/journal.pone.0147552

Wilson, B. S., and Dorman, M. F. (2008). Cochlear implants: a remarkable past and a brilliant future. *Hear. Res.* 242, 3–21. doi: 10.1016/j.heares.2008.06.005

Wolfe, J., Baker, R., and Wood, M. (2013). Clinical case study review: steroid-responsive change in electrode impedance. *Otol. Neurotol.* 34, 227–232. doi: 10.1097/MAO.0b013e31827b4bba

Xu, J., Shepherd, R. K., Millard, R. E., and Clark, G. M. (1997). Chronic electrical stimulation of the auditory nerve at high stimulus rates: a physiological and histopathological study. *Hear. Res.* 105, 1–29. doi: 10.1016/S0378-5955(96)00193-1

Zanetti, D., Nassif, N., Redaelli De Zinis, L. O., and Civili, S. (2015). Factors affecting residual hearing preservation in cochlear implantation. *Acta Otorhinolaryngol. Ital.* 35, 433–441. doi: 10.14639/0392-100X-619

Zhou, N. (2017). Deactivating stimulation sites based on low-rate thresholds improves spectral ripple and speech reception thresholds in cochlear implant users. *J. Acoust. Soc. Am.* 141, EL243–EL248. doi: 10.1121/1.4977235

Conflict of Interest Statement: The authors declare that the research was conducted in the absence of any commercial or financial relationships that could be construed as a potential conflict of interest.

frontiers in Neuroscience

ORIGINAL RESEARCH
published: 19 March 2019
doi: 10.3389/fnins.2019.00253

Intradural Spinal Cord Stimulation: Performance Modeling of a New Modality

David J. Anderson[1,2], Daryl R. Kipke[1], Sean J. Nagel[3], Scott F. Lempka[2], Andre G. Machado[3], Marshall T. Holland[4], George T. Gillies[5], Mathew A. Howard III[4] and Saul Wilson[4]**

[1] NeuroNexus Technologies, Ann Arbor, MI, United States, [2] Department of Biomedical Engineering, University of Michigan, Ann Arbor, MI, United States, [3] Center for Neurological Restoration, Cleveland Clinic, Cleveland, OH, United States, [4] Department of Neurosurgery, University of Iowa Hospitals & Clinics, Iowa City, IA, United States, [5] Department of Mechanical and Aerospace Engineering, University of Virginia, Charlottesville, VA, United States

Introduction: Intradural spinal cord stimulation (SCS) may offer significant therapeutic benefits for those with intractable axial and extremity pain, visceral pain, spasticity, autonomic dysfunction and related disorders. A novel intradural electrical stimulation device, limited by the boundaries of the thecal sac, CSF and spinal cord was developed to test this hypothesis. In order to optimize device function, we have explored finite element modeling (FEM).

Methods: COMSOL®Multiphysics Electrical Currents was used to solve for fields and currents over a geometric model of a spinal cord segment. Cathodic and anodic currents are applied to the center and tips of the T-cross component of the electrode array to shape the stimulation field and constrain charge-balanced cathodic pulses to the target area.

Results: Currents from the electrode sites can move the effective stimulation zone horizontally across the cord by a linear step method, which can be diversified considerably to gain greater depth of penetration relative to standard epidural SCS. It is also possible to prevent spread of the target area with no off-target action potential.

Conclusion: Finite element modeling of a T-shaped intradural spinal cord stimulator predicts significant gains in field depth and current shaping that are beyond the reach of epidural stimulators. Future studies with *in vivo* models will investigate how this approach should first be tested in humans.

Keywords: spinal cord stimulation, intradural, modeling, power efficiency, fiber targeting, selectivity

OPEN ACCESS

Edited by:
Andrew Joseph Fuglevand, The University of Arizona, United States

Reviewed by:
David Borton, Brown University, United States
Burak Güçlü, Boğaziçi University, Turkey

***Correspondence:**
Sean J. Nagel
nagels@ccf.org
Saul Wilson
saul-wilson@uiowa.edu

Specialty section:
This article was submitted to Neuroprosthetics, a section of the journal Frontiers in Neuroscience

Received: *14 October 2018*
Accepted: *04 March 2019*
Published: *19 March 2019*

Citation:
Anderson DJ, Kipke DR, Nagel SJ, Lempka SF, Machado AG, Holland MT, Gillies GT, Howard MA III and Wilson S (2019) Intradural Spinal Cord Stimulation: Performance Modeling of a New Modality. Front. Neurosci. 13:253. doi: 10.3389/fnins.2019.00253

INTRODUCTION

All commercially available spinal cord stimulators in clinical use at present are intended for implantation in the epidural space. That is, the electrode lead or array is positioned dorsal to the dura matter that forms the thecal sac containing the spinal cord and the intervening layer of CSF. While some of the original stimulator arrays were inserted intradurally, the epidural space proved

Abbreviations: CSF, cerebrospinal fluid; FDA, Food and Drug Administration; FEM, finite element modeling; IP, I-patch; MRG, McIntyre–Richardson–Grill model; SCS, spinal cord stimulation; SSEP, somatosensory evoked potential.

simpler to access, and avoided CSF leakage. Taken together, these and other clinical and technical advantages (Gibson-Corley et al., 2014) have driven the field to the present paradigm.

There are currently as many as 50,000 epidural devices implanted annually worldwide (American Association of Neurological Surgeons, 2018). Decades of intense industrial activity and system refinements (Levy, 2013) sparked this change with many patients being the beneficiaries of this progress (Taylor et al., 2014; Kapural et al., 2016). Even so, there are fundamental limitations to the epidural approach that prevent selective neuromodulation of deeper fiber tracts beyond a thin superficial layer of spinal cord. This is in sharp contrast to the direct interface that exists between deep brain stimulator electrodes and neuromodulation targets within the brain. As a result, the capacity of conventional spinal cord stimulators to selectively deliver current to the spinal cord has largely reached a plateau (Zhang et al., 2014). This stimulus delivery limitation may contribute in part to the observation that many patients do not achieve relieve of their symptoms or experience loss of therapeutic effect over time (Hayek et al., 2015; Geurts et al., 2017). Because of these limitations of epidural SCS, our group has explored intradural stimulation as a means of achieving selective, high-efficacy neuromodulation of fiber tracts deep within the spinal cord in order to more effectively treat patients with neuropathic pain (Reddy et al., 2018), visceral pain (Nagel et al., 2018b), and spasticity (Nagel et al., 2017).

In its original conception, the electrode array of our intradural device, termed the I-Patch, was designed to rest directly on the pial surface of the spinal cord (Howard et al., 2011a; Song et al., 2013). The position was gently stabilized by a compliant configuration of lead loops (Oliynyk et al., 2013) that traversed the dura and were anchored to the laminectomy defect (Dalm et al., 2016). Human-scale prototypes were built and their biomechanical performance characteristics were evaluated using both *in vitro* anthropomorphic spinal cord surrogates (Howard et al., 2011b; Oya et al., 2012; Wilson et al., 2012) and *in vivo* large animal (ovine) models (Gibson-Corley et al., 2012; Oya et al., 2013; Safayi et al., 2014). The design parameters were derived from rigorous assessments of the spinal cord geometries across a large number ($n = 50$) of patients (Viljoen et al., 2013a). This was done to insure that the implanted stimulator array would remain fixed to the pial surface of the cord as it moves within the thecal sac during flexion and extension of the back (Viljoen et al., 2014). The mechanical robustness of the device was also investigated by experiment (Viljoen et al., 2013b) and FEM (Grosland et al., 2014). In parallel, SSEPs were recorded in sheep during acute SCS experiments to confirm and quantify the potential advantages of the approach. The findings included post-presentation persistence of stimulation-induced effects (Flouty et al., 2012) and significantly reduced voltage thresholds for evoking SSEPs as compared with epidural stimulation (Flouty et al., 2013). This work culminated in the development of an ovine model of moderate spinal cord injury capable of serving as a test bed for quantifying the response to intradural SCS therapy of animals with mild spasticity (Safayi et al., 2015). Taken collectively, our preliminary data suggested that it would be technically feasible to create a device that could be safely positioned on the surface of the spinal cord and directly modulate targeted spinal cord neural pathways. Explicit advantages of this approach included increased selectivity of deeper neural fibers and a significant reduction in the pulse generator's power requirements (Dalm et al., 2014).

Ultimately, in order for a new medical device to achieve a substantial impact on public health, many factors must be considered beyond the single issue of potential efficacy. These include cost, ease of use, and the perceived risk vs. benefit ratio of a new device and implantation procedure. For example, when surgeons perceive existing SCS devices as being moderately effective, they will be hesitant to adopt a new device that in theory will be substantially more effective but will require a longer, more technically demanding implantation procedure associated with increased risks. The original I-Patch (IP1) fell into this category because the electrode array was placed directly on the spinal cord surface, and the dural closure technique was technically demanding and did not achieve an immediate watertight seal. The present report describes a second-generation I-Patch (IP2) that is designed to capture the stimulus delivery benefits of an intradural device, without the limitations of increased procedure time and risk associated with the IP1. The IP2 achieves these objectives through design features that enable intradural implantation and the creation of an immediate watertight dural seal using minimally invasive surgical techniques, and with procedure times and risk that are comparable to that of a standard paddle lead stimulator. We anticipate that the implementation of this approach will result in several advantages, including (1) the elimination of risk of lead migration because the electrode array is secured to the dura, (2) no blockage of intrathecal CSF flow because of the thin profile of the intradural component, and (3) much improved penetration depth and target selectivity of the electrical stimuli delivered to the spinal cord, as discussed in detail below.

The IP2 device concept is shown in **Figure 1**. As suggested there, an intradural plate with the stimulator's electrode array on the distal side has been inserted inside the thecal sac. A hollow threaded stud on the top of the intradural plate extends through the durotomy slot and the overlying extradural plate. A fixation nut is used to secure closure of the durotomy by sandwiching the dura matter between the intradural and extradural plates. Each plate has a gasket consisting of a thin lining of either a dural substitute or some other suitable compressible material on the

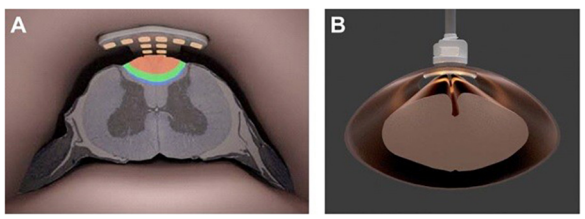

FIGURE 1 | (A) Artist's rendering of the intradural IP2 electrode array projecting current into the dorsal column of the thoracic spinal cord. **(B)** Face-on view of the IP2 array fixed to the spinal dura.

surfaces contacting the dura, in order to ensure a watertight seal with no significant risk of dural tissue necrosis (Nagel et al., 2019). The leads from the individual electrodes on the intradural array form a bundle that passes through the axial lumen of the threaded stud. The device is secured in place using standard epidural stimulator anchoring techniques, providing stress relief for the lead bundle to ensure that the electrode array remains suspended stably above the spinal cord and does not make contact with it. At its proximal end, the lead bundle is connected to the system's implantable pulse generator (not shown), used to create and control the stimulation montages.

Our goal here is to present the results of a detailed FEM effort that will optimize the design and location of the intradural electrode array of the hybrid device. This will enable maximal selectivity when targeting of neural fibers within the spinal cord. In particular, we demonstrate that selectivity and depth of stimulation of myelinated nerve fibers in the dorsal columns can be improved by bipolar or tripolar currents emanating from sites on the cross of a T-shaped configuration of electrodes (termed the "T-Array" or "T-Patch") on the intradural array. Selectivity and depth can be accentuated by lowering the array closer to the dorsal columns (i.e., deeper within the CSF) and perhaps scaling the array down in size to be more specific to the central portion. Additional benefits can be derived by incorporating epidural stimulation sites into the strategy as well. In general, we anticipate that this approach will be able to package reduced power consumption with an enlarged therapeutic window in an easily deployed device.

In what follows, we provide a brief overview of the important role played by modeling in the design, development and clinical use of spinal cord stimulators, with emphasis on intradural approaches. We then present the electro-mechanical details of the hybrid stimulator that has been the focus of our work and describe the COMSOL Multiphysics®representation of it, along with the computational approach used to generate the stimulation patterns of interest within the spinal cord and its environs. The results of the work consist of activation mappings of the targeted fiber populations, estimates of power consumption during stimulation sessions, and establishment of the charge density limits for reversible vs. irreversible tissue damage, all as functions of device configuration, location, and stimulation current levels. We then discuss our findings relative to those of others, explore the implications for implementation of novel modes of intradural stimulation, and lay out a program for future studies that will include validation of the model via experimentation and assessment of the issues to be resolved prior to eventual clinical trials.

MATERIALS AND METHODS

Ultimately, the effectiveness of any SCS device depends on its capacity to modulate targeted neural elements selectively within the spinal cord, while at the same time sparing non-targeted structures. At the most elementary level this means controlling or steering the electrical fields generated by the currents delivered from the electrode contacts; this usually involves both spatial and temporal control attributes. The spatial distribution of the field strength and gradient determines which neural elements are affected. Current flow through the axons passing into these fields may be susceptible to exogenously triggered depolarization. The temporal pattern of the fields also will influence the axonal action potentials. From this summated response to the field strength and temporal application emerges the 'selectivity' and the desired modulation of neural activity.

Our objective is to show how an intradural stimulation device enhances the effectiveness of field control by its closer proximity to the targeted neural elements and by removing the electrical resistance of the dura from the current path. This will dramatically reduce power and contain diffusion of current flow. To carry out this analysis, we have employed FEM, which has been used extensively over the past 30 years to create quantitative bioelectrical descriptions of SCS (Coburn, 1980; Coburn and Sin, 1985; Holsheimer et al., 1991; Holsheimer and Wesselink, 1997; McIntyre and Grill, 2001; Manola et al., 2007; Hernández-Labrado et al., 2011; Holsheimer and Buitenweg, 2015), including high frequency stimulation (Lempka et al., 2015; Arle et al., 2016) and, in a few cases, intradural stimulation (Howell et al., 2014; Huang et al., 2014).

Model

COMSOL®Multiphysics Electrical Currents is used to solve for electrical fields and currents over axial and transverse segments of the spinal cord deep to the dural membrane. Data and graphics are exported for illustration and use by MATLAB-based programs that reconstruct complex fields and simulate the effect of the fields on axons of various sizes within the dorsal column.

Geometry

Figures 2A,B are renderings of the present version of the implantation tool and intradural stimulator. The device design as shown there reflects the results of careful studies of several different electrode-array arrangements, with the final version optimized for performance in terms of minimizing the overall surface area of the array vs. maximizing the targeting specificity during stimulation. After the dura is opened, the surgeon uses the tool to insert the electrode array within the thecal sac. The inner shaft of the tool gently tightens a closure nut onto the surface of the extradural compression plate. This clamps the dura between the gasket materials on either side of the compression plates and secures the electrode array in place. The outer shaft of the implantation tool is then rotated to release it from the opposing tongue-and-groove joints on the extradural plate, and removed. The lead bundle is connected to one channel of the pulse generator, thus completing the procedure.

The scale and contour of the intradural electrode array is matched to that of the adult spinal cord at vertebral levels T8 to T10, which would be the typical locational range for the therapeutic applications discussed later. The features of the human spinal cord captured in geometry for computational purposes are shown in **Figure 3**. For our simulations, these included (1) a gray matter core, (2) white matter surrounding the gray matter, (3) a CSF layer bounded by the spinal cord and the dura, and (4) the dura itself, which is the outer layer of the

FIGURE 2 | Three-dimensional renderings of prototypes of **(A)** the intradural stimulator implantation tool, and **(B)** the T-shaped intradural electrode array on the distal end of the implantation tool prior to insertion.

model and includes both the dural layer and the extra-dural fat. The boundary condition simulating the dura is a conductive layer which allows current to exit the model and pass to ground. This is not a detailed geometry of the external environment, but it does account for shunting of some internal electric currents, thus reducing the current projected to the excitable tissue and affecting the neural thresholds. The intradural device provides a much higher impedance path for current to enter the extradural space than the traditional paddle positioning.

Also per **Figure 3**, an electrical conductivity was assigned to each volume. All the conductivities are scalars apart from that of the white matter, which has different longitudinal and radial conductances. Electrical continuity is assumed between each volume. While the volume outside the dura is complex, we are modeling the extradural volume with a single low conductivity material grounded at its outer surface. The cross section of the cord was held constant over the 80 mm of cord simulated. Dimensions, biophysical and electrical quantities are within the range found in the spinal modeling literature (Coburn and Sin, 1985; Holsheimer, 2002; Nagel et al., 2018a), which provides the generally accepted properties of the relevant intradural structures. The substrate holding the 12 sites is positioned just beneath the dura and projects 0.3 mm below the dura in the CSF space. The electrode substrate is not conductive but there is some current leakage beyond the edges of the substrate into the dura and the external space.

Internal Physics and Boundary Conditions

The continuity condition for zero charge creation ($\nabla\sigma\nabla V = 0$) holds everywhere in the model interior, all surfaces at the ends of the cord have zero potential ($V = 0$), the outer elliptical surface representing the extra-dural space is conductive and grounded. The sites are current sources such that: $\int_{\partial\Omega} J \bullet nds = I_0$. The actual distribution of the current over each site is determined by the surrounding electrical environment. V is the dependent variable representing the internal scalar potential voltage, σ is the conductivity scalar or tensor.

The geometry and boundary conditions are used to solve the electrical fields. This is done by discretizing the volume of the model with tetrahedral meshing and then employing the finite element method, both of which are implemented within COMSOL®.

Field Evaluation

Several post-processing methods are available within COMSOL®to produce important data products from the field solutions. Among these are visualizations of the fields and currents superimposed on the geometry, calculation of quantiles such as maximums, minimums, averages, integrals etc. over points, lines, surfaces or volumes, and export of any of the products.

Basis Function Method for Field Reconstruction

When performing many serial computations on fields under different drive conditions, it is convenient to use a basis method to reconstruct each new field dictated by new electrode current delivery. This is accomplished by solving the model for each site excited alone with a unity current (1 mA) while the other sites are set to zero current. A portion of the voltage field covering the mostly white matter and adjoining gray matter is transferred to MATLAB®using the COMSOL®suite of link functions with the voltage of each site. A complex field generated by several sites with different currents can be approximated accurately by superposition of the basis fields scaled by the current from the sites. In a like manner, the voltage on each site is determined and the power calculated. This method was used when computations such as neural simulation were performed using the MATLAB®platform outside COMSOL®.

Neural Models

There are several variations of models for the active nodes of axons, the propagation of neural spikes in myelinated axons and how electrical field potentials can initiate them. The minimum construction is a string of nodes consisting of a capacitive membrane populated by simulators of different voltage-controlled channel species for Sodium and Potassium and held at an equilibrium potential by diffusion potentials. The nodes are then capable of an action potential upon sufficient

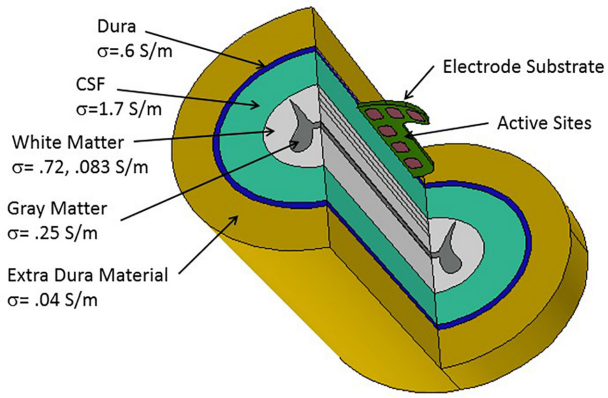

Model Dimension Table

Boundaries	width (mm)	Height (mm)	Length (mm)
Pia over White Matter	8.2	6	80
Inner Dura above CSF	14.6	11	80
Outer Dura Boundary	15.4	11.8	80
Model Exterior Boundary (ground)	11.4	17.8	80

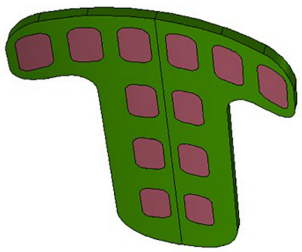

Substrate and Site Dimensions

Substrate	Thickness	.3 mm
	Main Width	4.19 mm
	Main Length	14.17 mm
	Wing Width	3 mm
	Wing Length	9 mm
Sites	Length	1.8 mm
	Width	.99 mm
	Vert. Seperation	3.04 mm
	Hor. Separation	1.5 mm

FIGURE 3 | Geometric configuration, conductance parameters, and dimensions of the spinal cord and T-shaped electrode array used in the modeling study.

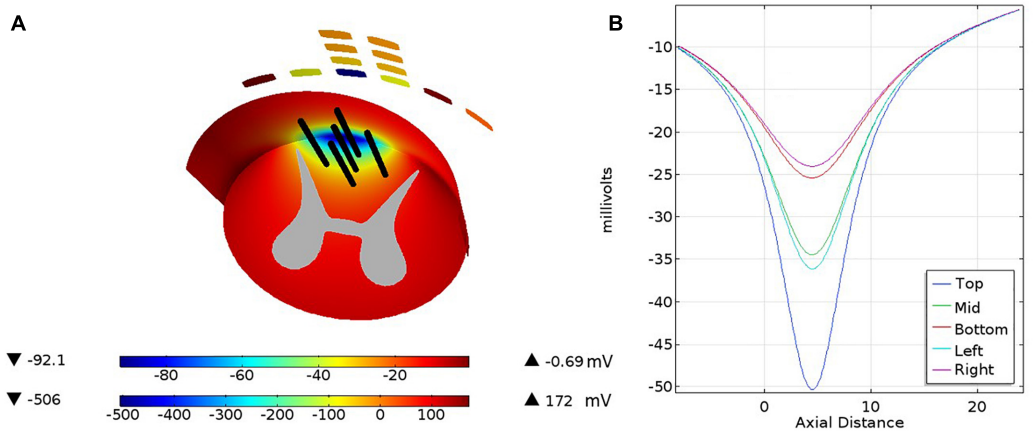

FIGURE 4 | The pia covering of the white matter is viewed from below with a cross section across the white matter and the gray matter cross section. A color coded electrical potential (lower color scale) resulting from a current drive on the cross of the T sites is projected on the pia surface and the white matter cross section (upper color scale). The black lines shown in **(A)** are test lines that are voltage-sampled and displayed in **(B)**.

depolarization of the membrane. When the nodes are connected by conductive and perfectly insulated axonal interiors, it is then possible to propagate action potentials from one node to another through depolarization of adjacent nodes by action potential-driven currents.

The triggering mechanism is the following: electrical stimulation causes initiation of the first action potential by positive second potential differences external to nodes. This will drive the currents causing depolarization of a single node or group of nodes within the influence of a sufficiently strong second difference. Thus, both field strength and field shape are important for initiating action potentials. For example, a constant field potential or a constant potential gradient cannot initiate an action potential in an axon.

Figure 4A is a view from under the pia surface. The pia and a cross section plane are colorized with a representation of the potential field. In addition, lines parallel to the axis of the cord are inserted to mark locations of waveform samples shown in **Figure 4B**. The negative peaking of these spatial waveforms clearly indicate a positive second spatial derivative or difference surrounded by a lesser negative spatial second derivative. **Figure 5** shows waveforms of the several axon nodes as several nodes near the electrode substrate are depolarized and ignited into action potentials. Nodes further from the electrode come under the influence of the first to respond and the action potential propagates in both directions from the initiation with nearly identical waveforms but delayed in time.

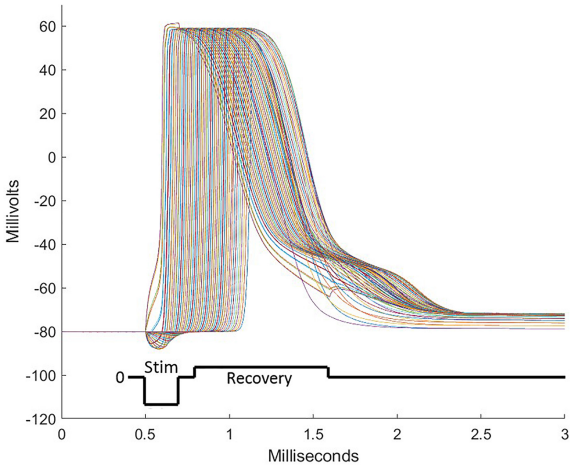

FIGURE 5 | During stimulation pulses, electrode sites over the intended target deliver currents balanced over the several sites of the electrode array. These consist of cathodic depolarizing pulses of short duration on some sites and anodic pulses on other sites, sending some nodes of neurons into action potentials followed by propagation of the action potential in both directions from the initialization. To assure that all sites are individually charge balanced, a recovery pulse is delivered which is opposite in polarity, longer in duration, and lower in amplitude than the stimulation pulse. To achieve the focusing effect to avoid stimulation of off-target tissue, anodic first pulses are delivered peripheral to the central electrode sites. A well-designed pulse complex prevents spread of stimulation from the target area and does not induce off-target action potentials.

To visualize neural activation in the model white matter, we create a grid of points in the white matter and adjacent portion of gray matter cross section-spaced 0.1 mm from each other. Each point is populated by three neurons differing in size. The particular axons chosen have node separations of 750, 1250, and 1450 μm corresponding to 7.3, 11.5, and 15 μm diameters, respectively, from Table 1 of McIntyre et al. (2002), which is the MRG model. The calculation proceeds by scanning the grid of points in the white matter by deriving the spatial waveform for that point. Each neuron is tested using the spatial waveform derived for the grid point, resampling to the node spacing and submitting sample points and axon parameters to the MATLAB®ODE solver ode45. The solver proceeds with the activation of the test axon with a 200 μs pulse. If any node in the axon passes +5 mV, the solution stops and the axon is recorded as activated. If the smallest axon is activated, the other two are not tested and the grid point is marked with a red x. Similarly, if the medial sized axon is activated, the largest one is not tested and a green x is placed at the grid point. If only the largest axon is activated, a blue x is placed at the grid point. A mark is not placed if no activation is achieved. If activation occurs in the gray matter, a white x is placed on that grid point. These activity cross sections are used in the following figures to indicate excitation within the white matter.

From this minimally complex axon model, several features can be added which increase the fidelity of the simulation. These include better models of the myelinated axon by adding piece-wise cable properties to the conductive segments and more refined populations of channels to the nodes, among others. For instance, the full MRG model separates the membrane/myelin lumped circuit into membrane leakage and capacitance in series with a myelin leakage and capacitance. In addition, a conductive space is added between the membrane and the myelin and this network is often distributed into several networks along the internode. This model adds two differential equations per internode network, which may be repeated as many as ten times. Details in the model matter particularly when investigating complex temporal aspects of stimulation signals but have been suppressed here for simplicity.

RESULTS

Tissue Targeting and Selectivity

The flow of current from any single site on the implant will spread preferentially in the CSF because it has the highest conductivity of any media in the model, e.g., ≈20 times the lateral component of the white matter conductivity tensor. The equipotential lines in the gray and white matter of the spinal cord will tend to be straight lines therefore cutting across not only the white matter but also the gray matter leading to unintended stimulation of cells in the gray matter. The solution is to excite central sites of the implant with a cathodic potential while exciting lateral sites on the tips of the T with an anodic potential. This limits the cathodic potentials from spreading laterally, thus missing the dorsal horns of the gray matter. **Figure 6** illustrates this for nine different current levels in the central two sites of the T. As the current from the central sites is diminished, the balancing currents contributed from the tip sites and the base sites are not only reduced to match but also re-proportioned to favor the base sites.

The neural activities shown in the cross sections of **Figure 6** are expressed in **Figure 7** as areas consisting of large diameter neurons only (squares), middle and large sizes (diamonds), and all sized neurons (triangles). As the anionic current stimulation progresses from all tip sites to all base sites during the nine-step sweep from the left dorsal horn to the center, the areas of all neuron classes decrease somewhat uniformly. The trace with black circles shows that the total power for each trial experiences a dramatic quadratic reduction from maximum tip site involvement to minimal tip site involvement. Note that the reduction of total neural activation does not begin to decrease until the fourth trial, indicating that a considerable power saving (about 75%) can be obtained for the deepest activity profile by involving the base sites.

As with achieving greater stimulation depth, currents from sites on the T can be manipulated to move the effective stimulation zone horizontally across the cord. **Figure 8** illustrates how sweeping of current sources across the T can position the center of stimulation with high spatial resolution. Nine steps are shown but more instances can be placed within the progression thus creating an increased resolution of position. The linear step method utilized to achieve progression of the stimulation center across the cord can be diversified considerably to gain greater depth and perhaps a more skewed pattern by departing from the symmetry of the montage as practiced in the example. The power

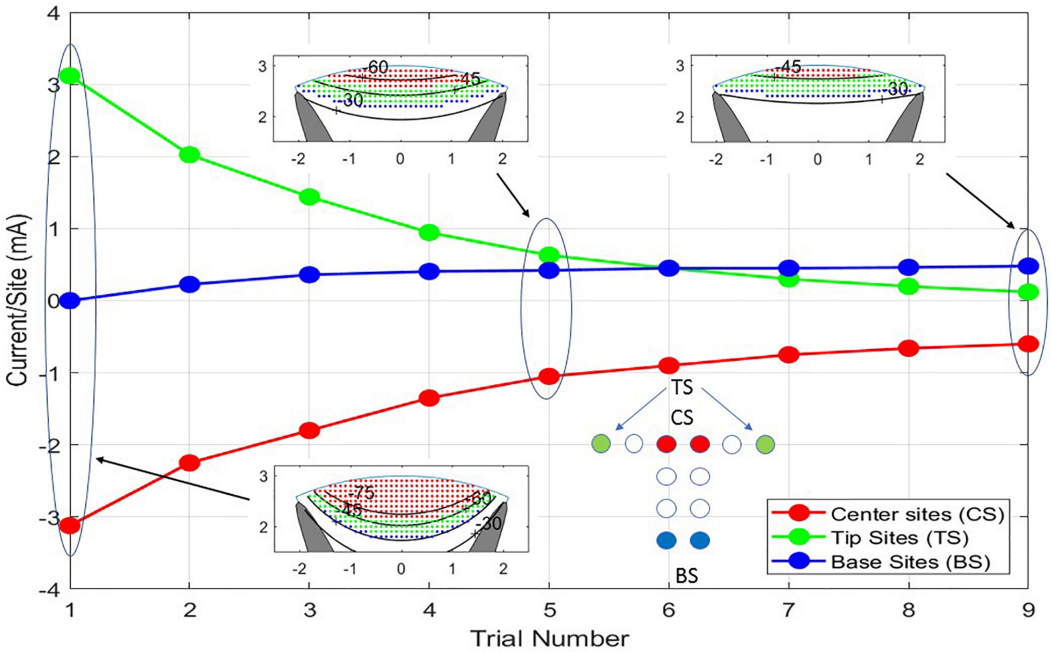

FIGURE 6 | The nine trials shown are a progression from balanced cathodic and anodic currents between the center sites (CS) and the tip sites (TS) of the T cross to balanced currents from the center sites to the base sites (BS) producing different depths of stimulation. As the transition from TS to BS is progressing, all the currents are being scaled down to prevent excitation of neurons outside the white matter. In Trial No. 1, a large current is flowing between CS and TS causing iso-potential lines of the cross section insert to bow downward at the midline of the model. In Trial No. 9, the iso-potential lines are almost horizontal across the model.

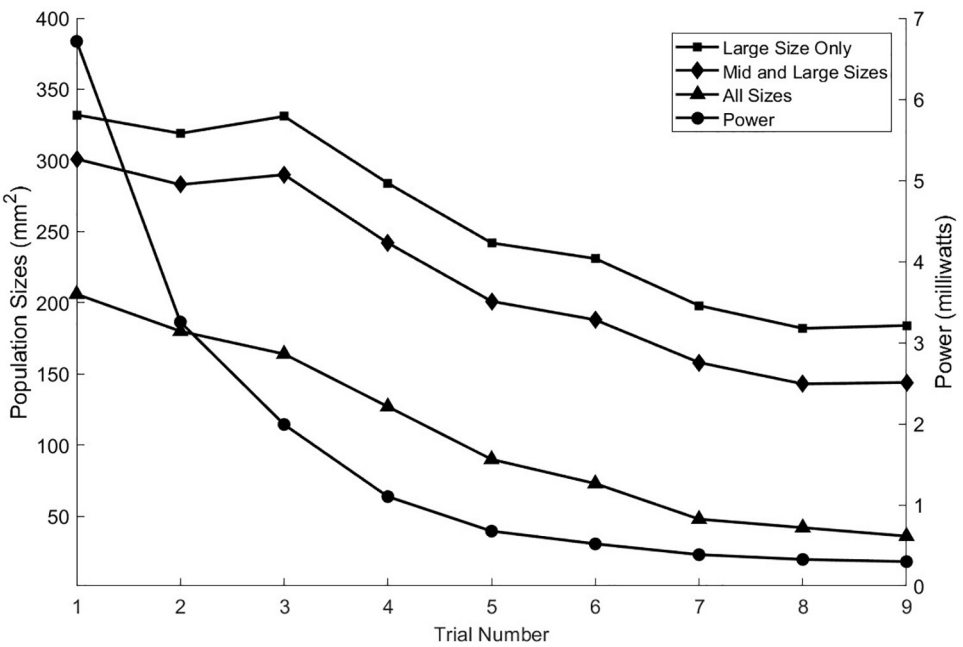

FIGURE 7 | As seen in the previous figure, the depth of stimulation in the white matter can be controlled while preventing unintended stimulation of the gray matter. This is achieved by increasing the anodic currents at the tip sites in greater proportion to the increases in cathodic currents at the central sites. That process can also be viewed in terms of the activation levels of the different sized axon populations as shown here for the nine stimulation trials. The power consumption increases approximately quadratically with the increase in the activities of the three axon classes.

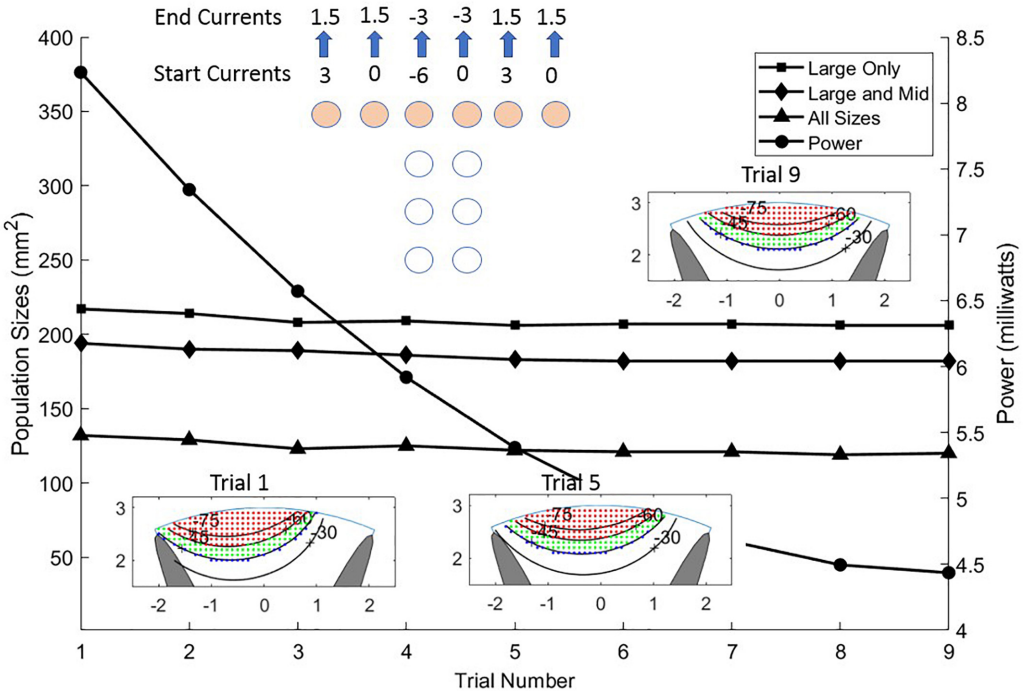

FIGURE 8 | Sliding the stimulus profile across the cross of the T allows selecting different populations of axons laterally across the upper layers of the white matter. This is accomplished by making a linear sweep of current values coming from the six sites of the T cross as shown in the top center of the Figure. Almost identical activation profiles for all three sizes of neurons are seen to progress across the cord from left to center as shown in the three colored graphics and the area curves. The power (circles) is shown for each trial diminishing from left to center to right as current is distributed more evenly over the six sites on the T cross.

consumption for the different trials in **Figure 8** is not constant but reduces as more sites take part in the stimulation. The first trial uses only three sites, while the ninth uses six sites.

When shaping the stimulation field, we can constrain the cathodic pulse to a target area but the electrochemistry of the electrode sites requires that there be a recovery phase of the stimulus waveform that charge-balances the net stimulation to zero. This means that the tissue volume not included in the target will receive a cathodic current during the recovery phase that may excite neurons in an unintended volume. The method that is usually used makes the recovery current much smaller than the stimulation phase over a longer time. The requirement for this factor in the stimulus design may limit the depth and selectivity strategy in some cases.

Power Consumption

Electrically bypassing the dura achieves a large power saving due largely to the impedance of the dura with respect to the subdural materials such as the CSF. In addition to the extra voltage drop over the dura, some of the current from the sites leaks out of the dural layer and never reaches the CSF. Depending on the exact geometry and the materials at the interface, additional work now underway indicates that this loss can be in excess of 10% of the current delivered by the sites if the seal to the upper surface of the dura is perfect, and more if there is scar tissue between the dura and the device. This leakage must be made up in extra current through the sites to achieve results comparable to the subdural device. This feature can result in longer battery life. In addition, the subdural device projects slightly (0.3 mm) into the CSF space bringing the electrode sites closer to the excitable elements of the white mater and thus less current spread within the CSF. This better proximity improves the ability to steer or focus the electrical potential within the white matter, but is not evident in this simulation due to the low profile of the device below the dura.

Independent of the reduced impedance barrier and improved proximity, curving of the iso-potentials is needed to obtain selectivity and improved depth. **Figure 6** shows improved depth by passing more current through the central sites and through the tip sites on the ends of the T cross. However, the improvement of depth obtained from no involvement of the tips sites on the ends of the T cross to maximal involvement of them requires an 18-fold increase in power. **Figure 7** shows that much of this power increase can be mitigated by passing some of the anionic current through the base sites of the electrode array. Any large current places an electrochemical stress on the electrode materials and also on the tissues just under the pia mater. To determine the limits, a safety analysis is required as discussed below.

Safety Limits

There are two important safety considerations required for long-term sustainability of neural stimulation devices. The primary consideration is the tissue's tolerance to current density and total charge per pulse-phase, but prevention of electrode failure is also paramount (McCreery et al., 1990; Cogan et al., 2016). Site

corrosion can lead to failure of a device and poisoning of the target tissue. The electrode sites used in the IP2 are small by the standards of dorsal column stimulation devices. This is justified by the proximity of the sites to the target tissue and the absence of the impedance and distance barrier presented by the dura. The area of the sites is 1.72 mm^2 and the accepted safe charge delivery per phase for platinum (Kelliher and Rose, 1987; Grill, 2005) is 50 $\mu C/cm^2$ yielding 0.86 μC as the charge limit per phase for the T-array site. (We note that this value of 50 $\mu C/cm^2$ refers to the threshold for the onset of electrochemical effects for platinum electrodes, and not to the threshold for the onset of neurological tissue damage. The latter has a different value and it is discussed separately below). Thus, for a 200 μs pulse, the largest current allowed is 4.3 mA. We further assume that the capacitance of the electrode's surface is 0.45 F/m^2. In principle, materials with higher effective capacitance might also be considered for this application, but platinum is typically chosen because its properties allow for high charge densities with relatively low risk of Faradaic reactions.

As an example, a pulse sequence consisting of a 200 μs cathodic phase of 2 mA followed by a 400 μs anodic phase at 1 mA uses about half the capacity of the site. The average interface voltage and the drive voltage will be equal as the sequence starts but diverge as the site becomes charged. As the sequence begins, the drive voltage jumps to overcome the spreading resistance then ramps downward due to (1) the increased average charge across the site and (2) to lower efficiency of charge transfer resulting from greater charge at the periphery. This rapid accumulation of charge at the site edge results from increased current flow there. If the sites and pulse protocols are not designed to control edge currents, site corrosion can occur. During the first few microseconds of a pulse, the imbalance between center and edge current can be somewhat extreme, but as time progresses, the current density across the site becomes more even. At the end of the cathodic phase, the potential difference due to extra charge at the edge is about 100 mV. The magnitude of the edge current at the beginning of the pulse can be reduced by several ways. (1) Keeping the curvature of the site perimeter to a minimum is important. Circular sites are the most efficient when used alone. (2) Shaping the pulse's leading edge to have a longer rise-time allows charge to build up more slowly, thus reducing the maximum current density at the edge (Wang et al., 2014). (3) Preventing adjacent sites from having extreme polarity differences will prevent large currents from flowing directly from site to site. Evenness of this current is promoted by parallel edges of adjacent sites. This is another cost of target selectivity. (4) Adding a resistive layer over the site forces the current flow to be more evenly distributed, but at the cost of additional power because of the resistive voltage drop and a less efficient current flow into the media. **Figure 9** shows an example of the current distributions for the sites and the pial surface of the white matter at the instant the cathodic stimulation phase is started. The pial surface current density distribution changes minimally over the charge injection pulse because of the gap between the site and target, but the current distribution on the sites changes considerably as described above.

None of the examples used in this paper exceed the threshold for the onset of electrochemical effects in platinum of 50 $\mu C/cm^2$. Similarly, there are limits of current density that can be tolerated by neural tissue. The maximum current density seen in our maximum depth-of-excitation figure is 1.33 mA/cm^2, which for the 200 μs pulse is 0.266 $\mu C/cm^2$, well below the commonly accepted boundary of 30 $\mu C/cm^2$ (McCreery et al., 1990; Cogan et al., 2016).

DISCUSSION

Comparison With Results of Others

Huang et al. (2014) carried out an early effort to model stimulation profiles of the original version of the I-Patch, in which the electrode array rested directly on the dorsal pial surface of the spinal cord and compared them against epidural stimulation. The COMSOL® implementation employed a volume conductor model with domains for the CSF, white matter, gray matter and a pair of electrodes, and the nerve fiber model of McNeal (McNeal, 1976). They found that the current threshold for axonal recruitment in the dorsal columns was over 10 times smaller for direct intradural vs. epidural stimulation, with equally improved depth of stimulation. Moreover, these findings were consistent with the outcome of an *in vivo* study of acute intradural stimulation in an ovine model (Flouty et al., 2013). While pointing the way toward potentially greater therapeutic efficacy, the invasive implantation procedure for a clinically useful device placed directly on the surface of the spinal cord would have carried greater surgical risk than a device placed in the extradural space. The present configuration of the IP2, per the device depicted in **Figure 2**, addresses this limitation by placing an intradural electrode array flush with the inner surface of the dura, and not in direct contact with the spinal cord.

For purposes of comparison with our findings, those of Howell et al. (2014) are perhaps the most relevant. Their detailed report covered the COMSOL®-based modeling and acute clinical testing of intradural SCS, as carried out both epidurally and intradurally with an AD-TECH® Spencer Probe Depth Electrode. They found that there was a $>$ 90% reduction in the power needed to activate dorsal column fibers with intradural stimulation relative to epidural stimulation, and that there was likewise a significant improvement in stimulation selectivity. The specific configurations investigated involved having the electrodes (a) 1 mm above the dura matter, (b) 1 mm above the spinal cord, and (c) 1 mm below the dura matter, with the alignments directly above the midline and also at 10 and 20° angular offsets from the midline. The configurations where the electrodes were just below the dura would bear the closest resemblance to the intradural T-array IP2 described here.

Although the vast majority of all the other efforts aimed at modeling SCS have focused on epidural methods, the goals have typically been similar to ours, i.e., to investigate the selectivity of stimulation and optimize the potential for therapeutic benefit. The University of Twente Spinal Cord Stimulation Software in particular has been used extensively to study how different configurations of electrodes and stimulation montages can enable

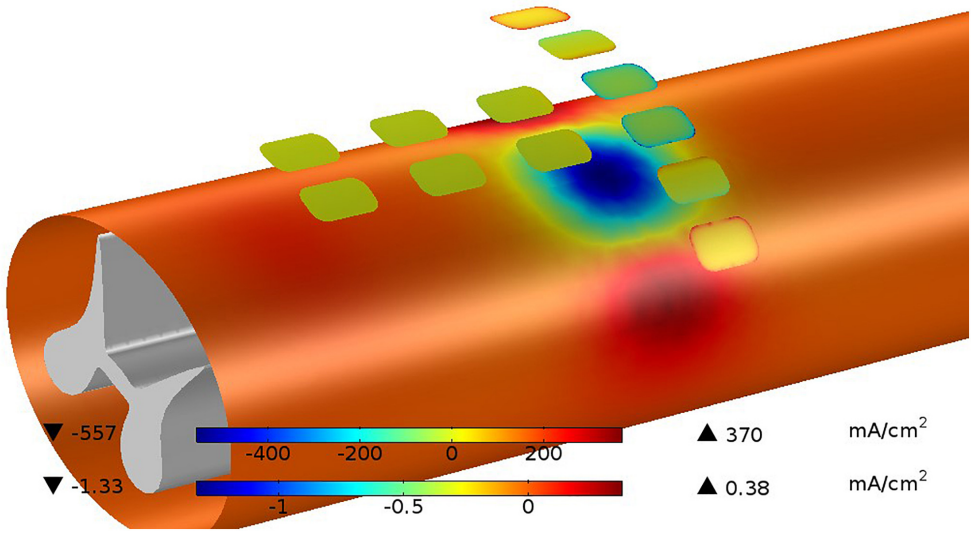

FIGURE 9 | Current distributions are shown for sites and the pia surface of the white matter at the instant the cathodic stimulation phase is started. The current on the site edges (upper color bar) are very large with respect to the average current but this quickly disappears as the charging of the site progresses. The current passing in and out of the white matter (lower color bar) is much less than the current at the sites because of the shunting effect of the CSF. While the total current at the cathodic sites is 4 mA, the current passing into the white matter is only 0.13 mA or 3.25%.

steering of the current distributions (Sankarasubramanian et al., 2011, 2013, 2014). One of the goals is to achieve improved recruitment of dorsal column fibers, which in our case is accomplished by sweeping the current sources across the sites on the T-array and, in general, by the closer proximity of the array to the dorsal surface of the spinal cord.

Limits of the Study and of the Device Design

The design of our intradural stimulation system incorporates the possibility of using one or more auxiliary epidural electrodes to enable comparisons between montages that are purely epidural, purely intradural or combined in nature. However, since the structure of the implant prohibits any such auxiliary site from being simultaneously positioned directly above the same tissues underlying the intradural array, it has played no role in our modeling effort.

Moreover, while there are several other possible geometrical arrangements for the electrodes of the intradural array, we report results for only the T-shaped version, as it will likely be the easiest to place intradurally of the various alternatives we have considered so far. The version of the T-array modeled here employs 12 electrode sites, whereas most standard paddle leads at present incorporate 16 sites. The need to minimize the array's surface area is partly responsible for this difference. However, as shown above, the closer proximity to the target fibers, the circumvention of the dura mater, and the unique geometric arrangement of the sites all combine to optimize the selectivity of stimulation targeting. Even with those advantages, a 12 site design may have limited compatibility with some implantable pulse generators requiring 16-line connectors.

Implications for Improved Therapies

Visceral Pain

The depth and control of the stimulation patterns achievable with intradural stimulation suggest that it may be possible to activate a narrow column (1–2 mm wide) of midline pathways perhaps up to 5 mm below the dorsal surface, thus achieving the reversible modulation equivalent of punctate midline myelotomy. The inception of this procedure was first described by Armour (1927) and termed the "commissural midline myelotomy" for the treatment of visceral cancer pain. The surgical goal of the commissural midline myelotomy was to transect the crossing fibers of the anterior lateral sensory system at the level of the patient's pain. This technique, despite years of refinement, continued to yield an elevated rate of unwanted side effects (Viswanathan et al., 2010). This is believed to be due to the need to access the ventral portion of the spinal cord via a dorsal approach, increasing the likelihood of undesired injury to surrounding spinal tissues. However, basic scientific studies have revealed the presence and importance of the newly described post-synaptic dorsal column visceral pain pathway, lesioning of which likely produces the efficacious benefits of the commissural midline myelotomy. First, the rodent model utilized by Hirshberg et al. (1996) demonstrated the anatomical presence of the post-synaptic dorsal column pathway. In this visceral pain system, the peripheral sensory neurons synapse with dorsal horn neurons within laminae II and IV. The dorsal horn neurons then project axons that ascend ipsilaterally within the dorsal columns and synapse with neurons within the nucleus gracilis or cuneatus. These third-order neurons then decussate in the brainstem and synapse in the thalamus to be relayed to higher order cortical structures. Further physiological studies confirmed that these neurons are activated by visceral pain

stimuli (Ness and Gebhart, 1988; Al-Chaer et al., 1996), and a small targeted transverse lesion in the midline dorsal column of the spinal cord resulted in decreased activity in the visceral pain pathway neurons within the ventral-posterolateral nucleus of the thalamus (Al-Chaer et al., 1996).

The localization and physiological characterization of this pathway has led to a modification of the original surgical technique of treating visceral pain described as the "punctate midline myelotomy." The first reported case of the punctate midline myelotomy involved creating a lesion at the T8 level that completely eliminated a patient's intractable, residual visceral pelvic pain following treatment of uterine cervical cancer (Nauta et al., 1997). In a later series of five patients performed by the same surgeon a lesion 5 mm in depth and 1 mm on each side of the midline was highly effective in relieving visceral pain symptoms (Nauta et al., 2000). Additionally, a percutaneous midline cervical spinal cord myelotomy technique (Kanpolat et al., 2002) has been used to effectively treat medically refractory visceral pain in patients with advanced malignancies. Currently the myelotomy procedure is used to treat only a small subset of patients with debilitating medically refractory visceral pain; typically patients with end stage malignancies. This restricted use is based on a combination of factors which have limited clinical adoption, the most significant being that the myelotomy is an ablative procedure. Based on the limited clinical series reported to-date, the risk of creating new neurological deficits that can be detected by standard clinical testing appears to be very low. However, lesions of this pathway may cause irreversible disruption of more difficult to quantify functions, such as sexual functions. In patients with end stage terminal illnesses, these risks are outweighed by the benefits of an ablative procedure that is highly effective in reducing or eliminating debilitating visceral pain.

For all patients with medically refractory visceral pain, but in particular for those with a prolonged life expectancy, it would be highly desirable to have the capacity to safely and reversibly modulate the neural pathway that is ablated during the punctate myelotomy procedure. The potential clinical indications for such a device would be expanded dramatically if its use could be extended to patients with non-cancer visceral pain. Chronic abdominal pain from inflammatory conditions is unfortunately common, and treatment modalities are limited. As pain management alternatives to the extensive use of opioids are sought, new technologies such as the present can become increasingly relevant. In addition, if improved modulation of midline pathways proves effective in relieving axial spine pain, as suggested by the results of recent experimental animal studies (Nauta et al., 2018), the relevance of this novel approach to public health will be even greater. The results of the present modeling study demonstrate that the IP2 will be capable of selectively projecting neuromodulatory current to a depth within the dorsal column that fully recapitulates the punctate midline myelotomy procedure (i.e., 5 mm). In contrast, earlier modeling work shows that standard extradural spinal cord stimulators are only capable of selectively modulating the most superficial ∼0.3 mm (<10%) of this pathway (Holsheimer, 2002; Holsheimer and Buitenweg, 2015). Carefully designed IP2 clinical studies will be required to determine how this greater than ten-fold improvement in neuromodulation capacity for the visceral pain pathway correlates with clinical efficacy.

Neuropathic Pain

The SCS is commonly used to treat select patients with medically refractory neuropathic pain. A wide range of device design and electrical stimulation parameter concepts have been reported. All of these strategies are designed to inhibit the transmission of neuropathic pain signals by applying an electrical stimulus that disrupts pathologic sensory neuron firing patterns associated with the perception of neuropathic pain. These include standard frequency stimulation protocols that evoke paresthesias, as well as more temporally complex higher frequency approaches designed to achieve paresthesia-free pain relief. Despite its frequent use, there are still limitations related to the implementation of SCS for the treatment of neuropathic pain syndromes; in particular, difficulties in driving stimulation to the dorsal columns without activating nearby dorsal rootlets. The IP2 is designed to accommodate delivery of the full range of electrical stimulation paradigms that are currently in use with extradural SCS devices. The results of this study show that the IP2 device will be capable of delivering these same stimuli to the targeted regions of the spinal cord with markedly improved power efficiency, site selectively, and volume of tissue activation, hence producing more effective stimulation with a lower probability of causing adverse or undesired effects. In addition, recently developed closed-loop sensing and stimulus adjustment technologies might be enhanced by using higher fidelity neural signals recorded from intradural IP2 electrode contacts (Russo et al., 2018).

Spasticity Following Spinal Cord Injury

In the past, at small number of centers, extradural spinal cord stimulators were placed to treat patients with medically refractory spasticity. Spasticity resulting from central nervous system injury causes pathologic changes in neural processing within the spinal cord. The rationale for SCS treatment in this clinical setting is that electrical stimulation of certain targeted spinal cord structures may reverse or mitigate these post-injury changes and reduce spasticity. Results from published series were mixed and spasticity is not an approved indication for SCS placement currently (Nagel et al., 2017). Extrapolating from information derived from contemporary neuroscience research regarding the pathophysiology of spasticity, and the promising clinical results observed in some patients implanted with extradural SCS devices, it is possible that the enhanced stimulus delivery capacity of an intradural stimulator may enable a device such as the IP2 to be more consistently effective in relieving the symptoms of spasticity.

Directions of Future Work

We are presently carrying out a series of pre-clinical tests in a large animal (porcine) model using the prototype device shown in **Figure 2**. The goal of these studies is to provide evidence of the technical feasibility and safety of the IP2 device and surgical implantation procedure, in support of a future FDA approved first-in-human pilot clinical study. During that pilot clinical study

the efficacy and safety of intradural stimulus delivery will be systematically examined.

CONCLUSION

The results of the current study quantify the advantages of intradural electrical stimulation using validated stimulation modeling methods. An intradural device such as the IP2 will have the capacity to modulate key therapeutic targets within the spinal cord that cannot be selectively modulated using current devices. A future clinical trial will be required in order to determine how this enhanced stimulus delivery capacity impacts clinical efficacy.

AUTHOR CONTRIBUTIONS

DA, GG, SN, MTH, and MAH prepared the manuscript draft with important edits and intellectual input from DK, AM, SL, and SW. All authors approved the final manuscript.

ACKNOWLEDGMENTS

The authors thank Mr. Charles Romans of Merge/ProtoStudios of The University of Iowa for his assistance with the preparation of prototype IP2 devices, and Mr. Daniel O'Connell of Direct Spinal Therapeutics, Inc. for several useful technical discussions.

REFERENCES

Al-Chaer, E. D., Lawand, N. B., Westlund, K. N., and Willis, W. D. (1996). Visceral nociceptive input into the ventral posterolateral nucleus of the thalamus: a new function for the dorsal column pathway. *J. Neurophysiol.* 76, 2661–2674. doi: 10.1152/jn.1996.76.4.2661

American Association of Neurological Surgeons (2018). *Spinal Cord Stimulation*. Available at: http://www.aans.org/Patients/Neurosurgical-Conditions-and-Treatments/Spinal-Cord-Stimulation [accessed April 25,2018].

Arle, J. E., Mei, L. Z., Carlson, K. W., and Shils, J. L. (2016). High-frequency stimulation of dorsal column axons: potential underlying mechanism of paresthesia-free neuropathic pain relief. *Neuromodulation* 19, 385–397. doi: 10.1111/ner.12436

Armour, D. (1927). Surgery of the spinal cord and its membranes. *Lancet* 209, 533–537. doi: 10.1016/S0140-6736(00)75098-7

Coburn, B. (1980). Electrical-stimulation of the spinal-cord – two-dimensional finite-element analysis with particular reference to epidural electrodes. *Med. Biol. Eng. Comput.* 18, 573–584. doi: 10.1007/BF02443129

Coburn, B., and Sin, W. K. (1985). A theoretical study of epidural electrical stimulation of the spinal cord – part I: finite element analysis of stimulus fields. *IEEE Trans. Biomed. Eng.* 32, 971–977. doi: 10.1109/TBME.1985.325648

Cogan, S. F., Ludwig, K. A., Welle, C. G., and Takmakov, P. (2016). Tissue damage thresholds during therapeutic electrical stimulation. *J. Neural Eng.* 13:021001. doi: 10.1088/1741-2560/13/2/021001

Dalm, B. D., Viljoen, S., Gillies, G. T., Oya, H., and Howard, M. A. III. (2016). A novel dural reconstruction method following spinal tumor resection. *Neurosurg. Q.* 26, 215–255. doi: 10.1097/WNQ.0000000000000176

Dalm, B. D., Viljoen, S. V., Dahdaleh, N. S., Reddy, C. G., Brennan, T. J., Oya, H., et al. (2014). Revisiting intradural spinal cord stimulation: an introduction to a novel intradural spinal cord stimulation device. *Inno. Neurosurg.* 2, 13–20. doi: 10.1515/ins-2014-0005

Flouty, O. E., Oya, H., Kawasaki, H., Reddy, C. G., Fredericks, D. C., Gibson-Corley, K. N., et al. (2013). Intracranial somatosensory responses with direct spinal cord stimulation in anesthetized sheep. *PLoS One* 8:e56266. doi: 10.1371/journal.pone.0056266

Flouty, O. E., Oya, H., Kawasaki, H., Wilson, S., Reddy, C. G., Jeffery, N. D., et al. (2012). A new device concept for directly modulating spinal cord pathways: initial *in vivo* experimental results. *Physiol. Meas.* 201, 2003–2015. doi: 10.1088/0967-3334/33/12/2003

Geurts, J. W., Joosten, E. A., and van Kleef, M. (2017). Current status and future perspectives of spinal cord stimulation in treatment of chronic pain. *Pain* 158, 771–774. doi: 10.1097/j.pain.0000000000000847

Gibson-Corley, K. N., Flouty, O., Oya, H., Gillies, G. T., and Howard, M. A. III. (2014). Postsurgical pathologies associated with intradural electrical stimulation in the central nervous system: design implications for a new clinical device. *Biomed. Res. Int.* 2014:989175. doi: 10.1155/2014/989175

Gibson-Corley, K. N., Oya, H., Flouty, O., Fredericks, D. C., Jeffery, N. D., Gillies, G. T., et al. (2012). Ovine tests of a novel spinal cord neuromodulator and dentate ligament fixation method. *J. Invest. Surg.* 25, 266–274. doi: 10.3109/08941939.2012.677967

Grill, W. M. (2005). Safety considerations for deep brain stimulation: review and analysis. *Expert Rev. Med. Dev.* 2, 409–420. doi: 10.1586/17434440.2.4.409

Grosland, N. M., Gillies, G. T., Shurig, R., Stoner, K., Viljoen, S., Dalm, B. D., et al. (2014). Finite-element study of the performance characteristics of an intradural spinal cord stimulator. *ASME J. Med. Devices* 8:041012. doi: 10.1115/1.4028421

Hayek, S. M., Veizi, E., and Hanes, M. (2015). Treatment-limiting cmplications of percutaneous spinal cord stimulator implants: a review of eight years of experience froman academic center database. *Neuromodulation* 18, 603–609. doi: 10.1111/ner.12312

Hernández-Labrado, G. R., Polo, J. L., López-Dolado, E., and Collazos-Castro, J. E. (2011). Spinal cord direct current stimulation: finite element analysis of the electric field and current density. *Med. Biol. Eng. Comput.* 49, 417–429. doi: 10.1007/s11517-011-0756-9

Hirshberg, R. M., Al-Chaer, E. D., Lawand, N. B., Westlund, K. N., and Willis, W. D. (1996). Is there a pathway in the posterior funiculus that signals visceral pain? *Pain* 67, 291–305.

Holsheimer, J. (2002). Which neuronal elements are activated directly by spinal cord stimulation. *Neuromodulation* 5, 25–31. doi: 10.1046/j.1525-1403.2002._2005.x

Holsheimer, J., and Buitenweg, J. R. (2015). Review: bioelectrical mechanisms in spinal cord stimulation. *Neuromodulation* 18, 161–170. doi: 10.1111/ner.12279

Holsheimer, J., Struijk, J. J., and Rijkhoff, N. J. M. (1991). Contact combinations in epidural spinal cord stimulation. *Stereotact. Funct. Neurosurg.* 56, 220–233. doi: 10.1159/000099409

Holsheimer, J., and Wesselink, W. A. (1997). Optimum electrode geometry for spinal cord stimulation: the narrow bipole and tripole. *Med. Biol. Eng. Comput.* 35, 493–497. doi: 10.1007/BF02525529

Howard, M. A., Utz, M., Brennan, T. J., Dalm, B. D., Viljoen, S., Jeffery, N. D., et al. (2011a). Intradural approach to selective stimulation in the spinal cord for treatment of intractable pain: design principles and wireless protocol. *J. Appl. Phys.* 110:044702. doi: 10.1063/1.3626469

Howard, M. A. III., Utz, M., Brennan, T. J., Dalm, B. D., Viljoen, S., Kanwal, J. K., et al. (2011b). Biophysical attributes of an in vitro spinal cord surrogate for use in developing an intradural neuromodulation system. *J. Appl. Phys.* 110:074701. doi: 10.1063/1.3642976

Howell, B., Lad, S. P., and Grill, W. M. (2014). Evaluation of intradural stimulation efficiency and selectivity in a computational model of spinal cord stimulation. *PLoS One* 9:e114938. doi: 10.1371/journal.pone.0114938

Huang, Q., Oya, H., Flouty, O. E., Reddy, C. G., Howard, M. A. III., Gillies, G. T., et al. (2014). Comparison of spinal cord stimulation profiles from intra-and extradural electrode arrangements by finite element modelling. *Med. Biol. Eng. Comput.* 52, 531–538. doi: 10.1007/s11517-014-1157-7

Kanpolat, Y., Savas, A., Ucar, T., and Torun, F. (2002). CT-guided percutaneous selective cordotomy for treatment of intractable pain in patients with malignant pleural mesothelioma. *Acta Neurochir.* 144, 595–599. doi: 10.1007/s00701-002-0945-2

Kapural, L., Yu, C., Doust, M. W., Gliner, B. E., Valleuo, R., Sitzman, B. T., et al. (2016). Comparison of 10-kH high-frquency and traditional low-frequency spinal cord stimulation for the treatment of chronic back and leg pain: 24-month results from a multicenter, randomized, controlled pivotal trial. *Neurosurgery* 79, 667–677. doi: 10.1227/NEU.0000000000001418

Kelliher, E. M., and Rose, T. L. (1987). Evaluation of charge injection properties of thin film redox materials for use as neural stimulation electrodes. *Mater. Res. Soc. Symp. Proc.* 110, 23–25. doi: 10.1557/PROC-110-23

Lempka, S. F., McIntyre, C. C., Kilgore, K. L., and Machado, A. G. (2015). Computational analysis of kilohertz frequency spinal cord stimulation for chronic pain management. *Anesthesiology* 122, 1362–1376. doi: 10.1097/ALN.0000000000000649

Levy, R. M. (2013). Progress in the technology of neuromodulation: the emperor's new cloths? *Neuromodulation* 16, 285–291. doi: 10.1111/ner.12103

Manola, L., Holsheimer, J., Veltink, P. H., Bradley, K., and Petersen, D. (2007). Theoretical investigation into longitudinal cathodal field steering in spinal cord stimulation. *Neuromodulation* 10, 120–132. doi: 10.1111/j.1525-1403.2007.00100.x

McCreery, D. B., Agnew, W. F., Yuen, T. G. H., and Bullara, L. (1990). Charge density and charge per phase as cofactors in neural injury induced by electrical stimulation. *IEEE Trans. Biomed. Eng.* 37, 996–1001. doi: 10.1109/10.102812

McIntyre, C. C., and Grill, W. M. (2001). Finite element analysis of the current-density and electric field generated by metal microelectrodes. *Ann. Biomed. Eng.* 29, 227–235. doi: 10.1114/1.1352640

McIntyre, C. C., Richardson, A. G., and Grill, W. M. (2002). Modeling the excitability of mammalian nerve fibers: influence of after potentials on the recovery cycle. *J. Neurophysiol.* 87, 995–1006. doi: 10.1152/jn.00353.2001

McNeal, D. R. (1976). Analysis of a model for excitation of myelinated nerve. *IEEE Trans. Biomed. Eng.* 23, 329–337. doi: 10.1109/TBME.1976.324593

Nagel, S. J., Helland, L., Woodroffe, R. W., Frizon, L. A., Holland, M. T., Machado, A. G., et al. (2019). Durotomy surrogate and seals for intradural spinal cord stimulators: apparatus and review of clinical methods and materials. *Neuromodulation* doi: 10.1111/ner.12913 [E-pub ahead of print],

Nagel, S. J., Reddy, C. G., Frizon, L. A., Chardon, M. K., Holland, M., Machado, A. G., et al. (2018a). Spinal dura mater: biophysical characteristics relevant to medical device development. *J. Med. Eng. Technol.* 42, 128–139. doi: 10.1080/03091902.2018.1435745

Nagel, S. J., Reddy, C. G., Frizon, L. A., Holland, M. T., Machado, A. G., Gillies, G. T., et al. (2018b). Intrathecal therapeutics: device design, access methods, and complication mitigation. *Neuromodulation* 21, 625–640. doi: 10.1111/ner.12693

Nagel, S. J., Wilson, S., Johnson, M. D., Machado, A., Frizon, L., Chardon, M. K., et al. (2017). Spinal cord stimulation for spasticity: historical approaches, current status and future directions. *Neuromodulation* 20, 307–321. doi: 10.1111/ner.12591

Nauta, H. J., Mcilwrath, S. L., and Westlund, K. N. (2018). Punctate midline myelotomy reduces pain responses in a rat model of lumbar spine pain: evidence that the postsynaptic dorsal column pathway conveys pain from the axial spine. *Cureus* 10:e2371. doi: 10.7759/cureus.2371

Nauta, H. J., Soukup, V. M., Fabian, R. H., Lin, J. T., Grady, J. J., Williams, C. G., et al. (2000). Punctate midline myelotomy for the relief of visceral cancer pain. *J. Neurosurg.* 92, 125–130. doi: 10.3171/spi.2000.92.2.0125

Nauta, H. J. W., Hewitt, E., Westlund, K. N., and Willis, W. D. (1997). Surgical interruption of a midline dorsal column visceral pain pathway - case report and review of the literature. *J. Neurosurg.* 86, 538–542. doi: 10.3171/jns.1997.86.3.0538

Ness, T. J., and Gebhart, G. F. (1988). Characterization of neurons responsive to noxious colorectal distension in the T13-L2 spinal cord of the rat. *J. Neurophysiol.* 60, 1419–1438. doi: 10.1152/jn.1988.60.4.1419

Oliynyk, M. S., Gillies, G. T., Oya, H., Wilson, S., Reddy, C. G., and Howard, M. A. (2013). Dynamic loading characteristics of an intradural spinal cord stimulator. *J. Appl. Phys.* 113:026103. doi: 10.1063/1.4775835

Oya, H., Howard, M. A. III., Shurig, R., and Gillies, G. T. (2012). Spinal canal surrogate for testing intradural implants. *J. Med. Eng. Technol.* 36, 407–410. doi: 10.3109/03091902.2012.712204

Oya, H., Safayi, S., Jeffery, N. D., Viljoen, S., Reddy, C. G., Dalm, B. D., et al. (2013). Soft-coupling suspension system for an intradural spinal cord stimulator: biophysical performance characteristics. *J. Appl. Phys.* 114:164701. doi: 10.1063/1.4827195

Reddy, C. G., Miller, J. W., Abode-Iyamah, K. O., Safayi, S., Wilson, S., Dalm, B. D., et al. (2018). Ovine model of neuropathic pain for assessing mechanisms of spinal cord stimulation therapy via dorsal horn recordings, von Frey filaments, and gain analysis. *J. Pain Res.* 11, 1147–1162. doi: 10.2147/JPR.S139843

Russo, M., Cousins, M. J., Brooker, C., Taylor, N., Boesel, T., Sullivan, R., et al. (2018). Effective relief of pain, and associated symptoms with closed-loop spinal cord stimulation system: preliminary results of the Avalon study. *Neurmodulation* 21, 38–47. doi: 10.1111/ner.12684

Safayi, S., Jeffery, N. D., Fredericks, D. C., Viljoen, S., Dalm, B. D., Reddy, C. G., et al. (2014). Biomechanical performance of an ovine model of intradural spinal cord stimulation. *J. Med. Eng. Technol.* 38, 269–283. doi: 10.3109/03091902.2014.914257

Safayi, S., Jeffery, N. D., Shivapour, S. K., Zamanighomi, M., Zylstra, T. J., Bratsch-Prince, J., et al. (2015). Kinematic analysis of the gait of adult sheep during treadmill locomotion: parameter values, allowable total error, and potential for use in evaluating spinal cord injury. *J. Neurol. Sci.* 358, 107–112. doi: 10.1016/j.jns.2015.08.031

Sankarasubramanian, V., Buitenweg, J. R., Holsheimer, J., and Veltink, P. (2011). Triple leads programmed to perform as longitudinal guarded cathodes in spinal cord stimulation: a modeling study. *Neuromodulation* 14, 401–411. doi: 10.1111/j.1525-1403.2011.00383.x

Sankarasubramanian, V., Buitenweg, J. R., Holsheimer, J., and Veltink, P. (2014). Performance of transverse tripoles vs. longitudinal tripoles with anode intensification (AI) in spinal cord stimulation: computational modeling study. *Neuromodulation* 17, 457–463. doi: 10.1111/ner.12124

Sankarasubramanian, V., Buitenweg, J. R., Holsheimer, J., and Veltink, P. H. (2013). Staggered transverse tripoles with quadripolar lateral anodes using percuaneous and surgical leads in spinal cord stimulation. *Neurosurgery* 72, 483–491. doi: 10.1227/NEU.0b013e31827d0e12

Song, S.-H., Gillies, G. T., Howard, M. A. III., Kuhnley, B., and Utz, M. (2013). Power and signal transmission protocol for a contactless subdural spinal cord stimulation device. *Biomed. Microdevices* 15, 27–36. doi: 10.1007/s10544-012-9684-1

Taylor, R. S., Desai, M. J., Rigoard, P., and Taylor, R. J. (2014). Failed back surgery syndrome: a systematic review and meta-regression analysis. *Pain Pract.* 14, 489–505. doi: 10.1111/papr.12095

Viljoen, S., Dalm, B. D., Reddy, C. G., Wilson, S., Smittkamp, C., Gillies, G. T., et al. (2013a). Optimization of intradural spinal cord stimulator designs via analysis of thoracic spine imaging data. *J. Med. Biol. Eng.* 33, 193–198. doi: 10.5405/jmbe.1317

Viljoen, S., Oya, H., Reddy, C. G., Dalm, B. D., Shurig, R., Odden, K., et al. (2013b). Apparatus for simulating dynamic interactions between the spinal cord and soft-coupled intradural implants. *Rev. of Sci. Instrum.* 84:114303. doi: 10.1063/1.4831801

Viljoen, S., Smittkamp, C. A., Dalm, B. D., Wilson, S., Reddy, C. G., Gillies, G. T., et al. (2014). MR-based measurement of spinal cord motion during flexion of the spine: implications for intradural spinal cord stimulator systems. *J. Med. Eng. Technol.* 38, 1–4. doi: 10.3109/03091902.2013.844207

Viswanathan, A., Burton, A. W., Rekita, A., and McCutcheon, I. E. (2010). Commissural myelotomy in the treatment of intractable visceral pain: technique and outcomes. *Stereotact. Funct. Neurosurg.* 88, 374–382. doi: 10.1159/000319041

Wang, B., Petrossians, A., and Weiland, J. D. (2014). Reduction of edge effect on disk electrodes by optimized current waveform. *IEEE Trans. Biomed. Eng.* 61, 2254–2263. doi: 10.1109/TBME.2014.2300860

Wilson, S., Howard, M. A. III., Rossen, J. D., Brennan, T. J., Dalm, B. D., Dahdaleh, N. S., et al. (2012). Pulsatile spinal cord surrogate for intradural neuromodulation studies. *J. Med. Eng. Technol.* 36, 22–25. doi: 10.3109/03091902.2011.632061

Zhang, T. C., Janik, J. J., and Grill, W. M. (2014). Modeling effects of spinal cord stimulation on wide-dynamic range dorsal hornneurons: influence of stimulation frequency and GABAergic inhibition. *J. Neurophysiol.* 112, 552–567. doi: 10.1152/jn.00254.2014

Conflict of Interest Statement: MAH, SW, MTH, DA, DK, and GG are co-inventors on patents covering the I-Patch intradural spinal cord stimulator described here. MAH, SW, MTH, and GG may receive patent royalties from the commercial license of the I-Patch intradural stimulator's intellectual properties negotiated by their respective institutions. GG and MAH hold equity in the licensee and serve on its Board of Directors, respectively. SL is a shareholder and scientific advisory board member of Presidio Medical, Inc. AM has distribution rights with Cardionomics and Enspire DBS, which are not related to this technology. He is a consultant with Abbott.

The remaining author declares that the research was conducted in the absence of any commercial or financial relationships that could be construed as a potential conflict of interest.

frontiers in Neuroscience

ORIGINAL RESEARCH
published: 06 June 2019
doi: 10.3389/fnins.2019.00578

When Less Is More – Discrete Tactile Feedback Dominates Continuous Audio Biofeedback in the Integrated Percept While Controlling a Myoelectric Prosthetic Hand

Leonard F. Engels[1†], Ahmed W. Shehata[2†], Erik J. Scheme[3], Jonathon W. Sensinger[3] and Christian Cipriani[1]*

[1] The BioRobotics Institute, Scuola Superiore Sant'Anna, Pisa, Italy, [2] Division of Physical Medicine and Rehabilitation, Department of Medicine, University of Alberta, Edmonton, AB, Canada, [3] Department of Electrical and Computer Engineering, Institute of Biomedical Engineering, University of New Brunswick, Fredericton, NB, Canada

OPEN ACCESS

Edited by:
Andrew Joseph Fuglevand, The University of Arizona, United States

Reviewed by:
Sabato Santaniello, University of Connecticut, United States
Burak Güçlü, Boğaziçi University, Turkey

****Correspondence:***
Ahmed W. Shehata
ahmed.shehata@ualberta.ca;
ahmedwagdyemam@gmail.com

[†] These authors have contributed equally to this work

Specialty section:
This article was submitted to Neuroprosthetics, a section of the journal Frontiers in Neuroscience

Received: *05 February 2019*
Accepted: *21 May 2019*
Published: *06 June 2019*

Citation:
Engels LF, Shehata AW, Scheme EJ, Sensinger JW and Cipriani C (2019) When Less Is More – Discrete Tactile Feedback Dominates Continuous Audio Biofeedback in the Integrated Percept While Controlling a Myoelectric Prosthetic Hand. Front. Neurosci. 13:578. doi: 10.3389/fnins.2019.00578

State of the art myoelectric hand prostheses can restore some feedforward motor function to their users, but they cannot yet restore sensory feedback. It has been shown, using psychophysical tests, that multi-modal sensory feedback is readily used in the formation of the users' representation of the control task in their central nervous system – their internal model. Hence, to fully describe the effect of providing feedback to prosthesis users, not only should functional outcomes be assessed, but so should the internal model. In this study, we compare the complex interactions between two different feedback types, as well as a combination of the two, on the internal model, and the functional performance of naïve participants without limb difference. We show that adding complementary audio biofeedback to visual feedback enables the development of a significantly stronger internal model for controlling a myoelectric hand compared to visual feedback alone, but adding discrete vibrotactile feedback to vision does not. Both types of feedback, however, improved the functional grasping abilities to a similar degree. Contrary to our expectations, when both types of feedback are combined, the discrete vibrotactile feedback seems to dominate the continuous audio feedback. This finding indicates that simply adding sensory information may not necessarily enhance the formation of the internal model in the short term. In fact, it could even degrade it. These results support our argument that assessment of the internal model is crucial to understanding the effects of any type of feedback, although we cannot be sure that the metrics used here describe the internal model exhaustively. Furthermore, all the feedback types tested herein have been proven to provide significant functional benefits to the participants using a myoelectrically controlled robotic hand. This article, therefore, proposes a crucial conceptual and methodological addition to the evaluation of sensory feedback for upper limb prostheses – the internal model – as well as new types of feedback that promise to significantly and considerably improve functional prosthesis control.

Keywords: internal model, prosthetics, sensory feedback, psychophysics, motor learning, electromyography

INTRODUCTION

The ease with which adults use their hands is owed to an intricate feedforward-feedback mechanism that has been honed since birth (Johansson and Cole, 1992). To those who have lost a hand (i.e., amputees) or were born without it, some feedforward motor functions can be restored with hand prostheses. However, while prostheses with myoelectric control represent the clinical state of the art (Schmidl, 1973), current commercial devices do not intentionally provide sensory feedback, and only few sensory feedback systems have found their way out of the research labs (Antfolk et al., 2013; Clemente et al., 2016; Ortiz-Catalan et al., 2017).

Feedforward control of myoelectric hand prostheses is chiefly influenced by two factors: (1) the robustness of the control of the movements of the prosthesis, which is affected by the method of recording and decoding the users' intent (i.e., their signals) (Geethanjali, 2016). (2) the users' ability to produce these control signals that is dependent on their understanding of the system – how it is represented in the central nervous system – which is known as the internal model (Kawato, 1999). In the unimpaired individual, internal models are continuously updated through multi-modal sensory feedback (tactile, visual, and auditory) during and after any movement (Imamizu et al., 2000). In amputees wearing a prosthesis, this differs due to the poor implicit sensory feedback available. Prosthesis users rely, chiefly, on proprioception in the remaining muscles (sense of contraction), visual feedback and, to some extent, on the incidental feedback that motor noise, and socket vibration provide (Simpson, 1973; Childress, 1980; Antfolk et al., 2013; Markovic et al., 2018b). Consequently, they cannot adequately hone their internal model, which negatively affects their ability to control the prosthesis (Lum et al., 2014; Shehata et al., 2018c). When highly reliable efferent signals are available for control, incomplete sensory inputs may suffice to retain the internal model (Hermsdörfer et al., 2008; Saunders and Vijayakumar, 2011; Ninu et al., 2014; Dosen et al., 2015b; Markovic et al., 2018b). However, it is a desirable goal to restore natural closed-loop control with supplementary (explicit) sensory feedback.

To address this goal, researchers have devised and assessed ways of providing feedback through invasive and non-invasive methods (Childress, 1980; Antfolk et al., 2013). Invasive peripheral nerve stimulation holds the promise of eventually being able to restore close-to-natural, modality- and somatotopically matched sensations (Riso, 1999; Graczyk et al., 2016). So far, however, realization of this hope has proven difficult; truly natural "touch" sensations have only been reported once (Tan et al., 2014). Non-invasive feedback does not directly interface with the nerves and is thus potentially less informative, but it is preferred by prospective users (Engdahl et al., 2015). It has also proven capable to improve functional performance in prosthetic hand users (Chatterjee et al., 2008; Ninu et al., 2014; Raspopovic et al., 2014; Clemente et al., 2016; Dosen et al., 2016; Markovic et al., 2017, 2018a). All these studies demonstrated new technological devices and methods, produced new knowledge, and revived the interesting question on the need/effectiveness of sensory feedback and how to assess it. However, no study had assessed the effects of sensory feedback on the internal model within a formalized framework.

In an attempt to reduce this gap, we recently proposed to assess the internal model strength developed while controlling myoelectric prostheses by using a psychophysical framework borrowed and modified from motor adaptation studies (Johnson et al., 2017; Shehata et al., 2018a,c). This framework uses parameters, such as sensory and control noise, to compute uncertainties in the developed internal model. Our recent work (Shehata et al., 2018c) showed that this framework can be used to investigate the effect of the feedback level on internal model strength. As a test bed for assessing this new method, we developed a versatile non-invasive human-machine interface that included a classifier for control and an audio sensory feedback system conveying continuous information about the control inputs of the classifier (EMG biofeedback) (Shehata et al., 2018a,b). The psychophysical framework proved that the strength of the internal model depends on the sensory input received (Shehata et al., 2018c). In particular, it showed that when audio biofeedback was added to vision, it outperformed the visual feedback alone in terms of internal model strength and performance in a functional task – both in a virtual environment and while using a multi-DoF hand prosthesis (Shehata et al., 2018a,b).

Based on these results, we sought to further enhance the sensory input available to the user, with complementary cues, in order to assess whether and how this could result in an even stronger internal model, and better performance in a functional task. To this aim we assessed and compared four sensory feedback conditions while controlling a myoelectric research hand prosthesis in psychophysical and functional tests. The three main conditions differed regarding the amount of complementary information: "visual-only (V)," "visual-plus-audio (VA)," and "visual-plus-audio-plus-tactile (VAT)." To disentangle the effects of the tactile component on the outcomes of the VAT feedback, the fourth condition was "visual-plus-tactile (VT)." The tactile feedback was provided by means of short-lasting vibrotactile cues (time-discrete) rather than continuous feedback, according to our previous work (Cipriani et al., 2014; Crea et al., 2015; Clemente et al., 2016; Barone et al., 2017; Aboseria et al., 2018) and the *discrete event-driven sensory feedback control* (DESC) policy (Johansson and Cole, 1992; Johansson and Edin, 1993; Johansson and Flanagan, 2009). The latter is a neuroscientific hypothesis of the mechanisms involved in human sensorimotor control, which posits that manipulation tasks are organized by means of multi-modally encoded discrete sensory events, e.g., resulting from object contact and lift-off.

Our findings show that all augmented feedback types significantly improved the performance compared to vision alone in the functional task, but only the audio biofeedback (VA) had an effect on the internal model strength, as measured by the psychophysical framework/metrics. Conversely, the tactile feedback demonstrated poor psychophysical metrics without

Abbreviations: DESC, discrete event-driven sensory control; DoF, degree of freedom; EMG, electromyography/electromyographic; iVE, instrumented virtual egg; V, visual feedback; VA, visual + audio biofeedback; VAT, visual + audio + tactile feedback; VT, visual + tactile feedback.

(VT) and in combination with the audio biofeedback (VAT). These results on how the different inputs combine (either constructively or destructively) in the integrated sensory percept contribute to the scientific debate on the internal model and suggest ways for providing effective supplementary sensory feedback to prosthetic hand users.

MATERIALS AND METHODS

Study Participants

We collected data from 28 healthy participants without any limb difference [13 females; age: 25 ± 4.5 (mean and standard deviation)]. All participants had normal or corrected-to-normal vision, were right-handed, and had no previous experience with myoelectric control. We had already collected the data for the "visual-only (V)" and "visual-plus-audio (VA)" groups (14 participants) and presented some aspects of it in our previous study (Shehata et al., 2018a). Written informed consent according to the University of New Brunswick Research and Ethics Board and the Scuola Superiore Sant'Anna Ethical Committee was obtained from all participants before conducting the experiments (UNB REB 2014-019 and SSSA 02/2017). The protocol used in this study was approved by the University of New Brunswick Research and Ethics Board and the Scuola Superiore Sant'Anna Ethical Committee.

Experimental Setup

The experimental setup was similar to that of our previous study (Shehata et al., 2018a) and is briefly described here. It comprised an array of eight custom-made myoelectric sensors in a bracelet; a right-handed sensorized research hand prosthesis (IH2 Azzurra hand, Prensilia S.r.l., IT) that was mounted on a bypass attached to the participant's forearm; a PC running the control and feedback algorithms; standard commercial headphones (MDRZX100, Sony, JP) for the audio feedback; a vibrotactor for the tactile feedback (Pico Vibe 312-101, Precision Microdrives, United Kingdom); and an instrumented test object [57 mm × 57 mm × 57 mm, ca. 180 g; (Controzzi et al., 2017; **Figure 1**)].

The myoelectric sensor bracelet was placed around the forearm of the participant and recorded the muscle activity used to control the robotic hand. We limited robotic hand movements to two degrees of freedom (DoF): (1) flexion/extension of the thumb, index and middle fingers, and (2) abduction/adduction of the thumb. Each of the four directions of movement of the robotic hand was mapped to one of four specific wrist movements: flexion and extension of the wrist corresponded to flexion/extension of the digits, while wrist abduction and adduction corresponded to abduction/adduction of the thumb. To implement the mapping, i.e., to interpret the electromyographic (EMG) signals, we used a Support Vector Regression algorithm that provided two regression-based control signals, which could simultaneously activate the two DoFs (e.g., thumb adduction and finger flexion) (Shehata et al., 2017, 2018c). These signals were then gated by a classifier; that means, the hand only moved in one direction at a time (**Figure 2**).

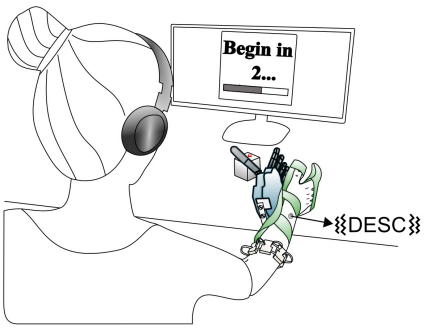

FIGURE 1 | Overview of the setup. The robotic hand was attached to the participant via bypass. The EMG signals recorded from the electrode bracelet around the forearm controlled the hand. A vibrotactor on the dorsal forearm provided discrete feedback i.e., discrete event-driven sensory feedback control (DESC), and the headphones provided continuous feedback. If the grasping force on the test object exceeded a breaking threshold in fragile mode, its red LED turned on. Modified from Shehata et al. (2018a), used under CC BY 4.0.

Biofeedback is the technique of providing biological information to participants in real-time that would otherwise be unknown (Giggins et al., 2013). Accordingly, the audio biofeedback continuously relayed the two outputs of the regression-based controller to the participant, in the form of four distinct tones. Wrist flexion and extension were mapped to tones of 400 and 500 Hz, wrist abduction and adduction to 800 and 900 Hz, respectively. The amplitude of the tones was proportional to the output of the regression algorithm (max volume = 53 ± 3 dB Sound Pressure Level). With this architecture (**Figure 2**), while the hand moved only one DoF at a time, the audio biofeedback provided richer information about the participant's myoelectric signals, which encompassed both proprioceptive and motor output information.

The tactile feedback provided information about the physical interactions of the robotic hand with the environment through the vibrotactor on the dorsal forearm. It delivered a short-lasting vibration burst (60 ms, 150 Hz, peak-to-peak force amplitude of ca. 0.3 N) upon contact, liftoff, replacement, and release of the test object. These events are known to be highly significant for the normal grasp-and-lift control, as per the DESC policy (Johansson and Cole, 1992; Johansson and Edin, 1993; Cipriani et al., 2014).

The test object – called an iVE – contained load cells measuring the grasp and load forces. The iVE could virtually break when a grasp exceeded a force of ca. 3 N, which was signaled to the participant by the activation of a red-colored LED on the iVE (Controzzi et al., 2017).

Experimental Protocol

Participants were divided into four groups (7 persons each) according to the kind of feedback they received: "visual-only (V)," "visual-plus-audio (VA)," "visual-plus-tactile (VT)," and "visual-plus-tactile-plus-audio (VAT)." They performed two tests according to a previously developed psychophysical framework (Shehata et al., 2018c): the "adaptation rate test" to measure the rate of optimization of grasping due to the feedback, and the

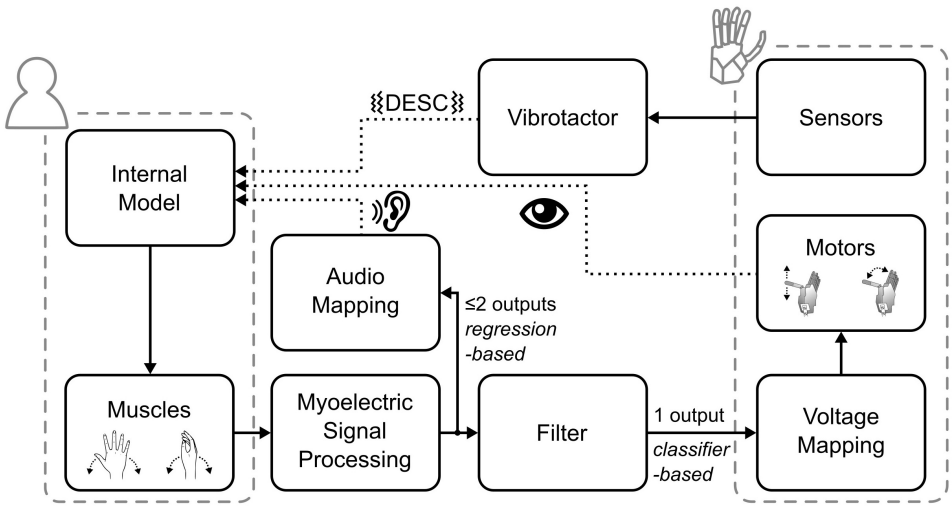

FIGURE 2 | Overview of the control and feedback loop. The dotted lines indicate the three types of feedback provided to the participants.

"just-noticeable difference (JND) test" to measure the threshold of perceiving a control perturbation. A third "functional test" was added in order to measure the ability to use the robotic hand in a manipulation task (Clemente et al., 2016).

In the adaptation rate test, the participants had 40 trials and were asked to grasp, lift, and replace the iVE as quickly as possible without breaking it. The iVE was placed in front of the participant so that the LED faced upward and the two instrumented sides could be grasped without the need to turn the object. A limit of 5 s was given to execute each trial, after which the hand automatically reopened. During trials 1–25, breaking was signaled through a red LED (fragile mode); during trials 26–40, the breaking was no longer signaled (rigid mode). This was done to keep subjects engaged with the task and prepare them for the following test.

In the JND test, the participants grasped the iVE (fragile mode) in two consecutive trials, lasting 4 s each (after which the hand automatically reopened). In one of the two, a stimulus perturbed the control of the hand. Participants were told to identify the altered trial (two-alternative forced choice) by pressing a key on a keypad placed near their unconstrained hand. The stimulus was calculated using an adaptive staircase procedure with a target probability set to 0.84 and a step size of 67 degrees and repeated until 23 reversals were achieved, as in our previous work (Shehata et al., 2018c).

In the functional test, for 20 trials of 10 s each, the participants attempted to grasp, and transfer the iVE over a barrier (H: 14.5 cm × W: 25 cm) without breaking it (fragile mode), akin to the well-known Box and Block test (Mathiowetz et al., 1985; Clemente et al., 2016). For a more detailed description of the tests please refer to (Shehata et al., 2018a).

In all groups, participants first trained freely to become familiar with the control and then trained to grasp and lift the test object. After that, they completed the three tests receiving only visual feedback. Subsequently, participants repeated the training and the three tests with either V, VA, VT, or VAT feedback. Ergo, each participant completed training and the three tests twice.

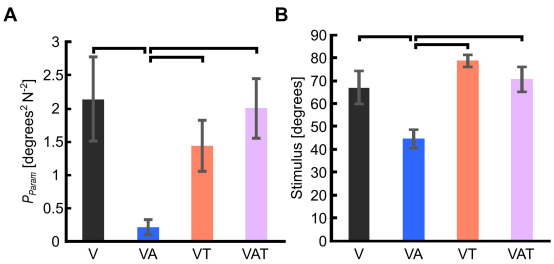

FIGURE 3 | (A) Internal model uncertainty (P_{param}). **(B)** Sensorimotor threshold (JND). Horizontal bars denote $p < 0.05$. Error bars show the standard error of the mean for each group.

The four groups were thus different and received the following feedback (in order): V-V, V-VA, V-VT, and V-VAT. In between the tests, the participants took short breaks; they took additional breaks during the (long-lasting) JND (every 12 min, or more often if desired). Each trial of the three tests was started with the hand fully opened and ended with the hand (automatically) returning to this starting pose. In the adaptation rate test and in the JND test, the thumb was fully adducted, meaning that participants had to activate only one DoF to close the hand [see also Figure 3 in Shehata et al., 2018a]. In the functional test, the fingers were extended, and the thumb fully abducted in resting position, meaning that the participants had to activate the two DoFs, mimicking the control of a multi-DoF prosthetic hand.

Outcome Measures

The internal model developed while using the robotic hand was reconstructed from the data of the second repetition of the tests, by extracting four metrics from the adaptation rate and the JND tests, following the procedure described in our previous study (Shehata et al., 2018a). These are termed *psychophysical metrics* and consist of:

- P_{param}: Internal model uncertainty. This measure describes the confidence participants have in their developed internal model, and it is computed from the outcomes of the adaptation rate test and the JND test (Shehata et al., 2018c and their Supplementary Materials).
- JND: Just-noticeable difference (or sensorimotor threshold). It describes, in degrees, the smallest external control perturbation from the trajectory (generated by the participant) that the participant perceived. The JND was defined as the final noticeable stimulus after 23 reversals of the adaptive staircase in the JND test (Shehata et al., 2018c).
- R: Sensory uncertainty. R determines the participants' trust in the sensory information they receive from the system (Shehata et al., 2018c). It is derived from the JND and the controller noise (Q) as follows:

$$R = \frac{JND^2}{2} - Q \quad (1)$$

Q was extracted from the adaptation rate test as the variance in the control signal between the start of each trial and the first activation of the muscles (ca. 100–200 ms).

- $-\beta_1$: Adaptation rate. This is a measure of the participants' modification of the feedforward control signal (from one trial to the next) based on the perceived error between the optimal and their actual movement (Bastian, 2008; Johnson et al., 2017). It was computed from each trial in the adaptation rate test by analyzing the first 150–300 ms window of the output signal from the controller (Shehata et al., 2018b). This window was selected to truly assess modifications in the control signals before integration of the visual feedback (Elliott and Allard, 1985). Since this test required only flexion of the digits, any other activations were considered self-generated errors (Shehata et al., 2017). Participants were incentivized to minimize these errors while executing the task as quick as possible without (virtually) breaking the object. We computed the $-\beta_1$ as follows:

$$error_{n+1} - error_n = \beta_1 \times error_n + \beta_0 \quad (2)$$

where *error* is the angle between the ideal and the actual hand trajectory, β_0 is the linear regression constant, β_1 is the adaptation rate, and n is the trial number. A unity value for β_1 indicates perfect adaptation, i.e., an internal model that is modified to perfectly compensate for errors. Higher or lower adaptation rates suggest over- or under-compensation.

In addition – to infer the way participants used the sensory input to control the robotic hand to grasp and lift the object – we computed the number of sub-movements from the second block of data in the adaptation test. Sub-movements are defined as the number of zero-crossing pairs of the third derivative of the grasp force profile per trial (Fishbach et al., 2007). This measure describes the real-time (or closed-loop) regulation of the grasp force and depends on the received feedback (Doeringer and Hogan, 1998; Kositsky and Barto, 2001; Dipietro et al., 2009). Specifically, a higher number of sub-movements indicates closed-loop regulation of the grasp force.

Finally, the completion rate (defined as the proportion of successful transfers) and the mean completion time (the average time needed to successfully transfer the object) were computed from the second repetition of the functional test, akin to our previous studies (Clemente et al., 2016).

Statistical Analysis

We tested all parameters for homogeneity in variances of the data by using Levene's test in SPSS (IBM Corp., United States). If data variances were homogenous, one-way ANOVAs were used to assess differences among metrics for the feedback types tested. If statistical significance was found, Bonferroni *post hoc* analysis test was performed. However, if data variances were found to be non-homogeneous, robust Welch ANOVA was used instead and followed by *post hoc* analysis using Games-Howell test. The confidence interval was calculated using the standard deviation (95% CI = mean $\pm$ 1.96 $\times$ SD).

RESULTS

The internal model uncertainty, P_{param}, proved significantly lower with the audio augmented feedback (VA) compared to all other conditions [robust Welch ANOVA ($F(3, 24) = 8.6$, $p = 0.006$) and Games-Howell *post hoc* tests $p < 0.05$] (**Figure 3A**). No other statistical differences were observed. In contrast to our expectations, with VAT, P_{param} (2.0 ± 0.45) was larger than VA (0.22 ± 0.11) and VT (1.4 ± 0.4), and not statistically different from V (2.14 ± 0.64). In other words, adding the tactile component to the audio biofeedback not only produced a lower confidence on the internal model than the two components (VA and VT) individually, but it degraded to the level of visual feedback alone.

The JND was 67 ± 7.2 degrees for V, 44.6 ± 3.9 degrees for VA, 78.6 ± 2.5 degrees for VT, and 70.6 ± 5.4 degrees for VAT. Its trend matched with that of P_{param}. Indeed, it was lowest for the VA condition (one-way ANOVA with Bonferroni *post hoc* tests, $p < 0.05$), while no other statistical differences were found among the conditions (**Figure 3B**).

Akin to P_{param} and JND, the sensory uncertainty (R) was lowest under VA and largest under VT (**Figure 4A**).

The adaptation rate was 0.82 ± 0.1 for V, 1.2 ± 0.1 for VA, 0.98 ± 0.1 for VT and 1.03 ± 0.1 for VAT. These outcomes indicated that, when using the VA feedback, participants adapted more than when using the other types, although this difference was statistically significant only in comparison to V (**Figure 4B**; Shehata et al., 2018a). No other statistical differences could be observed across conditions. It is worth noting that the controller noise Q extracted from this test was consistent across all conditions (<20%; not shown). This means that any variability in R is an effect of the sensory feedback, not of the variability of Q.

Altogether, the psychophysical metrics all indicated VA as the condition yielding the strongest internal model, as assessed by a lower JND and sensory uncertainties, higher adaptation rate, and a stronger internal model.

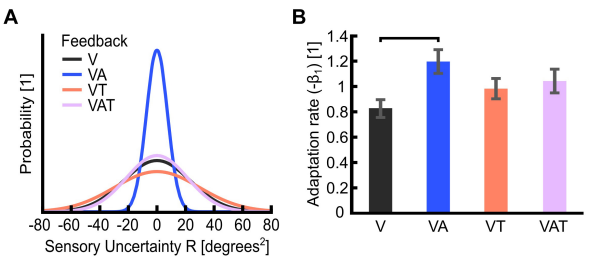

FIGURE 4 | (A) Sensory uncertainty, R. The graph is a visualization of the variance of each feedback strategy in the probability curve. It displays Gaussian curves constructed with a variance of R and an arbitrary area under the curve of 1 unit. Visual-plus-audio biofeedback (VA) shows the narrowest variance, i.e., the lowest uncertainty. Conversely, visual-plus-tactile (VT) shows the widest variance, i.e., the highest uncertainty. **(B)** Adaptation rate ($-\beta_1$). The adaptation rate describes the extent to which participants adapted to the self-generated error, i.e., how well they could optimize their control from one trial to the next. Horizontal bars denote $p < 0.05$. Error bars show the standard error of the mean for each group.

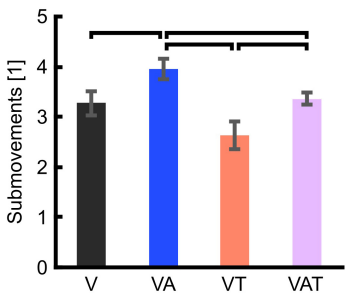

FIGURE 5 | Trial sub-movements. The graph shows significantly more sub-movements with VA than with all other feedback types. VAT lead to significantly more sub-movements than VT. VT and V are not statistically different. Horizontal bars denote $p < 0.05$. Error bars show the standard error of the mean for each group.

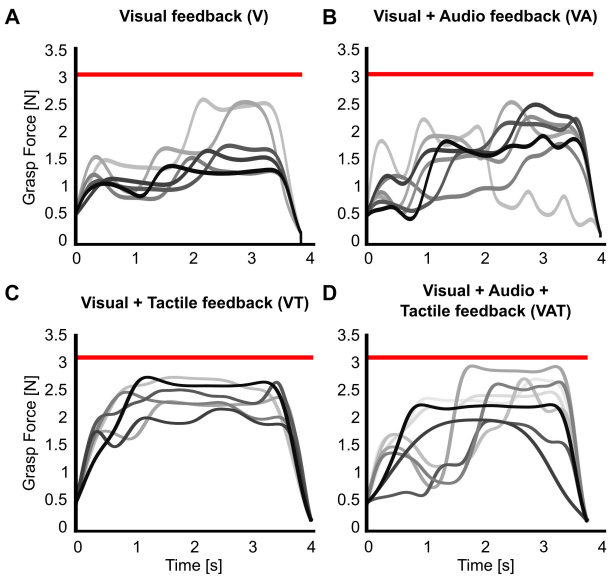

FIGURE 6 | Grasp force profiles. Representative grasp force profiles from individual trials during the adaptation rate test for all feedback types. A participant using **(A)** only visual feedback had lower variance in their grasping patterns over trials, **(B)** visual-plus-audio adjusted their grasping force throughout the trials and had higher variance in their grasping patterns, **(C)** visual-plus-tactile had automated grasping patterns with very low variance, and **(D)** visual-plus-audio-plus-tactile seemed to have highly variable grasping pattern in the initial trials but more automated grasping pattern at the final trials. Earlier trials are in lighter, later trials in darker shades of gray. The red horizontal bar indicates the breaking threshold. Incomplete trials in which the iVE was broken are not shown.

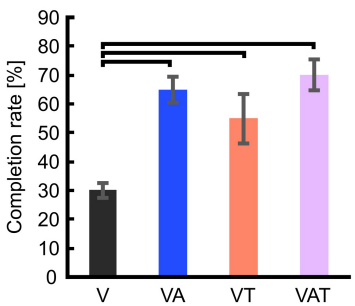

FIGURE 7 | Completion rate. The figure shows that the percentage of successful transfers (i.e., the iVE was not broken) was significantly higher when the participants received any kind of augmented feedback compared to visual alone. Horizontal bars denote $p < 0.05$. Error bars show the standard error of the mean for each group.

The analysis on the sub-movements highlighted a statistically significant difference across conditions (one-way ANOVA; $p = 0.001$) (**Figure 5**). Participants using VA adjusted their control signals significantly more than participants using the other feedback types (Bonferroni *post hoc* tests, $p < 0.05$). In other words, the participants tended to use the audio biofeedback in real-time, in order to modulate their grasp force to prevent breaking the object. Conversely, participants using the VT performed significantly less sub-movements than participants using the audio biofeedback (VAT and VA) (Bonferroni *post hoc* tests, $p < 0.05$). No other statistical differences were observed. These general behaviors were nicely captured by the time series of the grasp forces during the adaptation rate test (**Figure 6**). The evolution of the grasp force profiles, under the different conditions, suggest that, in the VAT, the participants used the audio biofeedback in the initial trials (light gray traces in **Figure 6**), and the discrete tactile feedback in the later trials (dark gray traces).

Regarding the functional test, the completion rate with visual feedback only (V) proved significanly worse than with VA, VT, and VAT (One-way ANOVA; Bonferroni *post hoc* tests, $p < 0.05$). Further, there may be a slight trend toward more successful transfers with VAT (70 ± 5.4) compared to VT (55 ± 8.5) and VA (65 ± 4.6) but it did not reach significance ($p = 0.3$ and $p = 0.6$, respectively) (**Figure 7**).

The mean completion time was not affected by the different feedback types and was 8.4 ± 0.65 s for V, 8.3 ± 0.74 s for VA, 8.6 ± 0.32 s for VT, and 8.4 ± 0.34 s for VAT.

DISCUSSION

Many researchers have explored ways of providing hand prostheses with supplementary sensory feedback, showing that it could indeed improve the performance in functional tasks. Yet, very little consideration has been given to the causes underpinning improved performance; in particular, it is still unknown how feedback contributes and combines to build strong internal models of the myoelectric control system. Here, we hypothesized that increasing the sensory information provided to a myoelectric hand user could result in a stronger internal model and better performance in a functional task. Hence, we combined continuous audio biofeedback with event-based vibratory tactile feedback in a myocontrolled prosthetic hand. Furthermore, we also explored the complex interactions between different feedback types (i.e., continuous visual and audio, and discrete tactile feedback) and their effects on the internal model strength.

Audio biofeedback provided continuous information about intensity of the control signal but not about the actual grasp, whereas time-discrete tactile feedback exclusively conveyed precise information about the interactions between the robotic hand and the environment. According to Johansson and colleagues (reviewed in Johansson and Flanagan, 2009), these interactions are processed and signaled to the nervous system through discrete sensory events and are crucial for developing efficient and natural feed-forward grasping in humans.

In this study we confirmed our previous findings (Shehata et al., 2018a): adding complementary audio biofeedback to visual feedback enables the development of a stronger internal model for controlling a myoelectric hand, as assessed by all psychophysical metrics (P_{param}, JND, R, and $-\beta_1$). The fact that the VA feedback yielded a lower sensory uncertainty (or variance) than V (cf. **Figure 3A**) suggests that the audio component dominates the integrated visual-audio percept, according to the maximum-likelihood estimate theory (Ernst and Banks, 2002). In other words, when the visual input is complemented with a coherent audio biofeedback, participants would likely rely more on the latter to execute the motor task. This is in agreement with current understanding of human sensorimotor control: the nervous system can never be completely certain about the relevance of visual information, as it provides only indirect information about the motor task, and the interactions with the environment (Johansson and Flanagan, 2009; Wei and Kording, 2009). Whether these results are due to the modality of the biofeedback (i.e., audio) or to the nature of the biofeedback itself (i.e., the sensory input which closely matches the intended motor output), remains to be assessed. Interestingly our results align with those of Dosen et al. (2015a), who conveyed EMG biofeedback using a visual interface.

The reconstructed internal model did not further improve when another piece of redundant information – this time about the touch event – was added to visual and audio biofeedback. In fact, the VAT condition yielded significantly worse psychophysical metrics compared to VA, showing results closer to the basic condition V (and also to VT). These results – if the psychophysical metrics are a truthful and complete description of the internal model – indicate that adding sensory information, albeit consistent with the already available information, may not necessarily enhance the formation of the internal model in the short term. In fact, it could even degrade it. A possible explanation for this is given by the causal inference hypothesis (Knill, 2003; Ernst, 2006; Körding et al., 2007), which posits that the nervous system interprets cues in terms of their causes. When the cues are very different from one another in space and time, the nervous system will infer that they are not related and thus should be processed separately. The visual and audio cues were indeed caused by the same process (i.e., the control input) while the tactile cues were due to the interaction of the robot hand with the environment (the control input is also causal of touch but through a transformation that involves extrinsic factors as well).

Combined in the VAT, the tactile component apparently dominated in the so-integrated percept, as indicated by the sub-movements and grasp force profiles (**Figures 5**, **6**) and also shown by the clear degradation of the psychophysical metrics. This suggests that, when combined and during grasping, (extrinsic) tactile sensory cues are more relevant to the central nervous system than (intrinsic) biofeedback cues – at least in the time frame explored. It is interesting to observe that this degradation was not immediate, as the tactile feedback only became predominant after several trials (**Figure 6**). This could mean that, when both types are present, audio biofeedback may be easier to pick-up in the initial phases – perhaps because it is very informative and closely matches the motor output – whereas it becomes less relevant in the later stages – possibly because it is more cognitively taxing compared to the tactile input. This argument would be supported by the literature on motor adaptation (Wei and Kording, 2009) and sensorimotor control of dexterous manipulation tasks (Johansson and Flanagan, 2009). Another possible reason for favoring the continuous feedback in the initial phases is related to how people expect to receive information of the grasp based on their top-down knowledge of the interactions of the body with the environment: in nature these interactions are continuous (although they may be processed differently by the nervous system). However, why and how the tactile input corrupted the psychophysical metrics (instead of enhancing them), remains unclear so far. Future tests could investigate whether the internal model is updated more efficiently with audio biofeedback than with tactile feedback after disturbances, for example by doing a pick-and-lift task with unexpectedly changing object weight (Jenmalm et al., 2006).

The degradation of the psychophysical metrics with VAT is, nevertheless, interesting, as one would expect that the tactile feedback should barely interfere in such tests, contrary to what we observed. The JND tested how well the participants could perceive discrepancies in the control input. Here, audio biofeedback provided a lot of relevant information, visual some (because the hand was not always, and completely under visual control) but tactile only notified the participants about touching the object (which was expected to be meaningless in the JND). In the adaptation rate test – where the task was to grasp and lift the object – tactile info conveyed some more information about

the final result of the control, i.e., a successful or unsuccessful grasp. In fact, in the adaptation rate test, tactile information (VT and VAT) yielded optimal results ($-\beta_1$ close to 1) whereas with only audio feedback (VA) participants overcompensated ($-\beta_1 > 1$). While the near-perfect adaptation with VT and VAT may be due to the saliency of the time-discrete sensory feedback policy (Johansson and Cole, 1992; Johansson and Edin, 1993; Johansson and Flanagan, 2009), we argue that audio feedback alone – being a reliable and continuous sensory input coherent with vision – induced the participants to adapt continuously. However, it is still unclear whether this difference between VA and VT/VAT (and V and VT/VAT) is meaningful.

The results from the functional test were complementary to those from the psychophysical tests. We found that all kinds of augmented feedback (VA, VAT, and VT) enabled users to perform significantly better than with vision alone (**Figure 7**). It was expected that VT would allow for better performance than V alone (Clemente et al., 2016). Further, this result advocates that continuous audio biofeedback can enhance motor control of a myoelectric prosthesis [in agreement with the work of Dosen et al. (2015a) and our previous study (Shehata et al., 2018a)]. However, it also reveals a significant deviation from the results of the other tests. Indeed, while participants with VT or VAT integrated the sensory input and exhibited a predictive control behavior, participants with VA used it for continuously regulating their grip force in real-time, in a closed-loop manner (as seen in the data from the adaptation test in **Figures 5**, **6B**). We believe this was due to the nature of the feedback: the time-discrete sensory cues could only be used by participants as checkpoints for the motor task (Johansson and Edin, 1993; Clemente et al., 2016), whereas the audio biofeedback – as discussed above – induced the participants to use it constantly, even when the grasp was successful. Both approaches seem to be equally adequate to improve grasping performance with a prosthetic hand.

During object manipulation, the brain uses sensory predictions and afferent signals to adapt the motor output to the physical properties of the manipulated object, as well as to monitor and update task performance (Johansson and Flanagan, 2009). In this way, humans can predict and use an adequate level of grip force required to lift an object by producing highly coordinated grasping and lifting forces and correcting their actions in the case of unexpected events (e.g., object slip or incorrectly predicted weight). Sensory feedback plays a crucial role in building and keeping the motor control repertoire updated. However, neural delays make continuous closed-loop control of dynamic motor behaviors impractical at frequencies above 1 Hz (Hogan et al., 1987; Johansson and Edin, 1993). Hence, natural grasping largely involves predictive feedforward rather than closed-loop (servo control) mechanisms. With this in mind, and considering that the VAT and VT yielded a successful predictive control behavior in the functional test (a sign of a mature internal model), we suspect that the psychophysical tests used may not grasp all the facets of the internal model. In particular, they may not be capable to properly assess the contribution of touch-related sensory information, or, alternatively, the discrete tactile feedback may have masked the measurements.

ETHICS STATEMENT

Written informed consent according to the University of New Brunswick Research and Ethics Board and the Scuola Superiore Sant'Anna Ethical Committee was obtained from all participants before conducting the experiments (UNB REB 2014-019 and SSSA 02/2017). This work is not a clinical trial. All experiments were conducted in a lab and not in a clinic.

AUTHOR CONTRIBUTIONS

All authors took part in conceiving and designing the study, discussed the results, and contributed to manuscript revision, read, and approved the submitted version. AS and LE conducted the study and wrote the manuscript. AS analyzed the data.

FUNDING

This work was supported by the Natural Sciences and Engineering Research Council of Canada (NSERC), the New Brunswick Health Research Foundation (NBHRF), and the European Commission (DeTOP – #687905). The work by CC was also funded by the European Research Council (MYKI – #679820).

ACKNOWLEDGMENTS

The authors thank Francesco Clemente and Michele Bacchereti for their maintenance of the IH2 Azzurra Hand and the iVE.

REFERENCES

Aboseria, M., Clemente, F., Engels, L. F., and Cipriani, C. (2018). Discrete vibrotactile feedback prevents object slippage in hand prostheses more intuitively than other modalities. *IEEE Trans. Neural Syst. Rehabil. Eng.* 26, 1577–1584. doi: 10.1109/TNSRE.2018.2851617

Antfolk, C., D'Alonzo, M., Rosén, B., Lundborg, G., Sebelius, F., and Cipriani, C. (2013). Sensory feedback in upper limb prosthetics. *Expert Rev. Med. Devices* 10, 45–54. doi: 10.1586/erd.12.68

Barone, D., D'Alonzo, M., Controzzi, M., Clemente, F., and Cipriani, C. (2017). A cosmetic prosthetic digit with bioinspired embedded touch feedback. *IEEE Int. Conf. Rehabil. Robot* 2017, 1136–1141. doi: 10.1109/ICORR.2017.8009402

Bastian, A. J. (2008). Understanding sensorimotor adaptation and learning for rehabilitation. *Curr. Opin. Neurol.* 21, 628–633. doi: 10.1097/WCO.0b013e328315a293.Understanding

Chatterjee, A., Chaubey, P., Martin, J., and Thakor, N. (2008). Testing a prosthetic haptic feedback simulator with an interactive force matching task. *J. Prosthetics Orthot.* 20, 27–34. doi: 10.1097/01.JPO.0000311041.61628.be

Childress, D. S. (1980). Closed-loop control in prosthetic systems: historical perspective. *Ann. Biomed. Eng.* 8, 293–303. doi: 10.1007/BF02363433

Cipriani, C., Segil, J. L., Clemente, F., Weir, R. F., and Edin, B. (2014). Humans can integrate feedback of discrete events in their sensorimotor control of a robotic hand. *Exp. brain Res.* 232, 3421–3429. doi: 10.1007/s00221-014-4024-4028

Clemente, F., D'Alonzo, M., Controzzi, M., Edin, B. B., and Cipriani, C. (2016). Non-invasive, temporally discrete feedback of object contact and release improves grasp control of closed-loop myoelectric transradial prostheses. *IEEE Trans. Neural Syst. Rehabil. Eng.* 24, 1314–1322. doi: 10.1109/tnsre.2015.2500586

Controzzi, M., Clemente, F., Pierotti, N., Bacchereti, M., Cipriani, C., Superiore, S., et al. (2017). "Evaluation of hand function trasporting fragile objects: the virtual eggs test," in *Myoelectric Control Symposium*, eds W. Hill and J. Sensinger (New Brunswick, CA: University of Salford).

Crea, S., Cipriani, C., Donati, M., Carrozza, M. C., and Vitiello, N. (2015). Providing time-discrete gait information by wearable feedback apparatus for lower-limb amputees: usability and functional validation. *IEEE Trans. Neural Syst. Rehabil. Eng.* 23, 250–257. doi: 10.1109/TNSRE.2014.2365548

Dipietro, L., Krebs, H. I., Fasoli, S. E., Volpe, B. T., and Hogan, N. (2009). Submovement changes characterize generalization of motor recovery after stroke. *CORTEX* 45, 318–324. doi: 10.1016/j.cortex.2008.02.008

Doeringer, J. A., and Hogan, N. (1998). Intermittency in preplanned elbow movements persists in the absence of visual feedback. *J. Neurophysiol.* 80, 1787–1799. doi: 10.1152/jn.1998.80.4.1787

Dosen, S., Markovic, M., Somer, K., Graimann, B., and Farina, D. (2015a). EMG Biofeedback for online predictive control of grasping force in a myoelectric prosthesis. *J. Neuroeng. Rehabil.* 12:55. doi: 10.1186/s12984-015-0047-z

Dosen, S., Markovic, M., Wille, N., Henkel, M., Koppe, M., Ninu, A., et al. (2015b). Building an internal model of a myoelectric prosthesis via closed-loop control for consistent and routine grasping. *Exp. Brain Res.* 233, 1855–1865. doi: 10.1007/s00221-015-4257-4251

Dosen, S., Markovic, M., Strbac, M., Perovic, M., Kojic, V., Bijelic, G., et al. (2016). Multichannel electrotactile feedback with spatial and mixed coding for closed-loop control of grasping force in hand prostheses. *IEEE Trans. Neural Syst. Rehabil. Eng.* 4320, 1–1. doi: 10.1109/TNSRE.2016.2550864

Elliott, D., and Allard, F. (1985). The utilization of visual feedback information during rapid pointing movements. *Q. J. Exp. Psychol.* 37A, 407–425. doi: 10.1080/14640748508400942

Engdahl, S. M., Christie, B. P., Kelly, B., Davis, A., Chestek, C. A., and Gates, D. H. (2015). Surveying the interest of individuals with upper limb loss in novel prosthetic control techniques. *J. Neuroeng. Rehabil* 12:53. doi: 10.1186/s12984-015-0044-42

Ernst, M. O. (2006). "A Bayesian view on multimodal cue integration," in *Human Body Perception from the Inside Out*, eds G. Knoblich, I. Thornton, M. Grosjean, and M. Shiffrar (New York, NY: Oxford University Press), 105–131.

Ernst, M. O., and Banks, M. S. (2002). Humans integrate visual and haptic information in a statistically optimal fashion. *Nature* 415, 429–433. doi: 10.1038/415429a

Fishbach, A., Roy, S. A., Bastianen, C., Miller, L. E., and Houk, J. C. (2007). Deciding when and how to correct a movement: discrete submovements as a decision making process. *Exp. Brain Res.* 177, 45–63. doi: 10.1007/s00221-006-0652-y

Geethanjali, P. (2016). Myoelectric control of prosthetic hands: state-of-the-art review. *Med. Devices Evid. Res.* 9, 247–255. doi: 10.2147/MDER.S91102

Giggins, O. M., Persson, U. M. C., and Caulfield, B. (2013). Biofeedback in rehabilitation. *J. Neuroeng. Rehabil.* 10, 6–19. doi: 10.1186/1743-0003-10-60

Graczyk, E. L., Schiefer, M. A., Saal, H. P., Delaye, B. P., Bensmaia, S. J., and Tyler, D. J. (2016). The neural basis of perceived intensity in natural and artificial touch. *Sci. Transl. Med.* 142, 1–11. doi: 10.1126/scitranslmed.aaf5187

Hermsdörfer, J., Elias, Z., Cole, J. D., Quaney, B. M., and Nowak, D. A. (2008). Preserved and impaired aspects of feed-forward grip force control after chronic somatosensory deafferentation. *Neurorehabil. Neural Repair* 22, 374–384. doi: 10.1177/1545968307311103

Hogan, N., Bizzi, E., Mussa-Ivaldi, F. A., and Flash, T. (1987). Controlling multijoint motor behavior. *Exerc. Sport Sci. Rev.* 15, 153–190.

Imamizu, H., Tamada, T., Yoshioka, T., and Pu, B. (2000). Human cerebellar activity reflecting an acquired internal model of a new tool. *Nature* 403, 192–195. doi: 10.1038/35003194

Jenmalm, P., Schmitz, C., Forssberg, H., and Ehrsson, H. H. (2006). Lighter or heavier than predicted: neural correlates of corrective mechanisms during erroneously programmed lifts. *J. Neurosci.* 26, 9015–9021. doi: 10.1523/jneurosci.5045-05.2006

Johansson, R. S., and Cole, K. J. (1992). Sensory-motor coordination during grasping and manipulative actions. *Curr. Opin. Neurobiol.* 2, 815–823. doi: 10.1016/0959-4388(92)90139-C

Johansson, R. S., and Edin, B. B. (1993). Predictive feed-forward sensory control during grasping and manipulation in man. *Biomed. Res.* 14, 95–106.

Johansson, R. S., and Flanagan, J. R. (2009). Coding and use of tactile signals from the fingertips in object manipulation tasks. *Nat. Rev. Neurosci.* 10, 345–359. doi: 10.1038/nrn2621

Johnson, R. E., Kording, K. P., Hargrove, L. J., and Sensinger, J. W. (2017). Adaptation to random and systematic errors: comparison of amputee and non-amputee control interfaces with varying levels of process noise. *PLoS One* 12:e0170473. doi: 10.1371/journal.pone.0170473

Kawato, M. (1999). Internal models for motor control and trajectory planning. *Curr. Opin. Neurobiol.* 9, 718–727. doi: 10.1016/s0959-4388(99)00028-8

Knill, D. C. (2003). Mixture models and the probabilistic structure of depth cues. *Vision Res.* 43, 831–854. doi: 10.1016/S0042-6989(03)00003-8

Körding, K. P., Beierholm, U., Ma, W. J., Quartz, S., Tenenbaum, J. B., and Shams, L. (2007). Causal inference in multisensory perception. *PLoS One* 2:e943. doi: 10.1371/journal.pone.0000943

Kositsky, M., and Barto, A. G. (2001). The emergence of multiple movement units in the presence of noise and feedback delay. *Adv. Neural Inf. Process. Syst.* 14, 43–50.

Lum, P. S., Black, I., Holley, R. J., Barth, J., and Dromerick, A. W. (2014). Internal models of upper limb prosthesis users when grasping and lifting a fragile object with their prosthetic limb. *Exp. Brain Res.* 232, 3785–3795. doi: 10.1007/s00221-014-4071-4071

Markovic, M., Karnal, H., Graimann, B., Farina, D., and Dosen, S. (2017). GLIMPSE: google glass interface for sensory feedback in myoelectric hand prostheses. *J. Neural Eng.* 14:036007. doi: 10.1088/1741-2552/aa620a

Markovic, M., Schweisfurth, M. A., Engels, L. F., Bentz, T., Wüstefeld, D., Farina, D., et al. (2018a). The clinical relevance of advanced artificial feedback in the control of a multi-functional myoelectric prosthesis. *J. Neuroeng. Rehabil.* 15:28. doi: 10.1186/s12984-018-0371-371

Markovic, M., Schweisfurth, M. A., Engels, L. F., Farina, D., and Dosen, S. (2018b). Myocontrol is closed-loop control: incidental feedback is sufficient for scaling the prosthesis force in routine grasping. *J. Neuroeng. Rehabil.* 15:81. doi: 10.1186/s12984-018-0422-427

Mathiowetz, V., Volland, G., Kashman, N., and Weber, K. (1985). Adult norms for the box and block test of manual dexterity. *Am. J. Occup. Ther.* 39, 386–391. doi: 10.5014/ajot.39.6.386

Ninu, A., Dosen, S., Muceli, S., Rattay, F., Dietl, H., and Farina, D. (2014). Closed-loop control of grasping with a myoelectric hand prosthesis: which are the relevant feedback variables for force control? *IEEE Trans. Neural Syst. Rehabil. Eng.* 22, 1041–1052. doi: 10.1109/TNSRE.2014.2318431

Ortiz-Catalan, M., Mastinu, E., Brånemark, R., and Håkansson, B. (2017). Direct neural sensory feedback and control via osseointegration. *XVI World Congr. Int. Soc. Prosthetics Orthot.* 11, 1–2.

Raspopovic, S., Capogrosso, M., Petrini, F. M., Bonizzato, M., Rigosa, J., Di Pino, G., et al. (2014). Restoring natural sensory feedback in real-time bidirectional hand prostheses. *Sci. Transl. Med.* 6:222ra19. doi: 10.1126/scitranslmed.3006820

Riso, R. R. (1999). Strategies for providing upper extremity amputees with tactile and hand position feedback – moving closer to the bionic arm. *Technol. Heal. Care* 7, 401–409. doi: 10.1080/09640560701402075

Saunders, I., and Vijayakumar, S. (2011). The role of feed-forward and feedback processes for closed-loop prosthesis control. *J. Neuroeng. Rehabil.* 8:60. doi: 10.1186/1743-0003-8-60

Schmidl, H. (1973). The INAIL-CECA Prostheses. *Orthot. Prosthetics* 27, 6–12.

Shehata, A. W., Engels, L. F., Controzzi, M., Cipriani, C., Scheme, E. J., and Sensinger, J. W. (2018a). Improving internal model strength and performance of prosthetic hands using augmented feedback. *J. Neuroeng. Rehabil.* 15:70. doi: 10.1186/s12984-018-0417-414

Shehata, A. W., Scheme, E. J., and Sensinger, J. W. (2018b). Audible feedback improves internal model strength and performance of myoelectric prosthesis control. *Sci. Rep.* 8:8541. doi: 10.1038/s41598-018-26810-w

Shehata, A. W., Scheme, E. J., and Sensinger, J. W. (2018c). Evaluating internal model strength and performance of myoelectric prosthesis control strategies. *IEEE Trans. Neural Syst. Rehabil. Eng.* 26, 1046–1055. doi: 10.1109/TNSRE.2018.2826981

Shehata, A. W., Scheme, E. J., and Sensinger, J. W. (2017). The effect of myoelectric prosthesis control strategies and feedback level on adaptation rate for a target acquisition task. *Int. Conf. Rehabil. Robot* 2017, 200–204. doi: 10.1109/ICORR.2017.8009246

Simpson, D. C. (1973). "The control and supply of a multimovement externally powered upper limb prosthesis," in *Proceedings of the 4th International Symposium on External Control of Human Extremities*, (Dubrovnik), 247–254.

Tan, D. W., Schiefer, M. A., Keith, M. W., Anderson, J. R., Tyler, J., and Tyler, D. J. (2014). A neural interface provides long-term stable natural touch perception. *Sci. Transl. Med.* 6:257ra138. doi: 10.1126/scitranslmed.3008669

Wei, K., and Kording, K. (2009). Relevance of error: what drives motor adaptation? *J. Neurophysiol.* 101, 655–664. doi: 10.1152/jn.90545.2008

Conflict of Interest Statement: CC is co-founder and holds shares of Prensilia S.r.l., which manufactures and sells the IH2 Azzurra hand used in this study.

The remaining authors declare that the research was conducted in the absence of any commercial or financial relationships that could be construed as a potential conflict of interest.

frontiers in Neuroscience

ORIGINAL RESEARCH
published: 24 July 2019
doi: 10.3389/fnins.2019.00773

Investigating the Feasibility of Epicranial Cortical Stimulation Using Concentric-Ring Electrodes: A Novel Minimally Invasive Neuromodulation Method

Ahmad Khatoun[1,2], *Boateng Asamoah*[1,2] *and Myles Mc Laughlin*[1,2]*

[1] Research Group Experimental Oto-Rhino-Laryngology (ExpORL), Department of Neurosciences, KU Leuven, Leuven, Belgium, [2] The Leuven Brain Institute, KU Leuven, Leuven, Belgium

Background: Invasive cortical stimulation (ICS) is a neuromodulation method in which electrodes are implanted on the cortex to deliver chronic stimulation. ICS has been used to treat neurological disorders such as neuropathic pain, epilepsy, movement disorders and tinnitus. Noninvasive neuromodulation methods such as transcranial magnetic stimulation and transcranial electrical stimulation (TES) show great promise in treating some neurological disorders and require no surgery. However, only acute stimulation can be delivered. Epicranial current stimulation (ECS) is a novel concept for delivering chronic neuromodulation through subcutaneous electrodes implanted on the skull. The use of concentric-ring ECS electrodes may allow spatially focused stimulation and offer a less invasive alternative to ICS.

Objectives: Demonstrate ECS proof-of-concept using concentric-ring electrodes in rats and then use a computational model to explore the feasibility and limitations of ECS in humans.

Methods: ECS concentric-ring electrodes were implanted in 6 rats and pulsatile stimulation delivered to the motor cortex. An MRI based electro-anatomical human head model was used to explore different ECS concentric-ring electrode designs and these were compared with ICS and TES.

Results: Concentric-ring ECS electrodes can selectively stimulate the rat motor cortex. The computational model showed that the concentric-ring ECS electrode design can be optimized to achieve focused cortical stimulation. In general, focality was less than ICS but greater than noninvasive transcranial current stimulation.

Conclusion: ECS could be a promising minimally invasive alternative to ICS. Further work in large animal models and patients is needed to demonstrate feasibility and long-term stability.

Keywords: transcranial electrical stimulation, neuromodulation, concentric-ring electrode, motor cortex stimulation, direct cortical stimulation

OPEN ACCESS

Edited by:
Kai J. Miller,
Mayo Clinic, United States

Reviewed by:
Peter Brunner,
Albany Medical College, United States
Robert A. Gaunt,
University of Pittsburgh, United States

***Correspondence:**
Myles Mc Laughlin
myles.mclaughlin@kuleuven.be

Specialty section:
This article was submitted to Neuroprosthetics, a section of the journal Frontiers in Neuroscience

Received: *04 December 2018*
Accepted: *10 July 2019*
Published: *24 July 2019*

Citation:
Khatoun A, Asamoah B and Mc Laughlin M (2019) Investigating the Feasibility of Epicranial Cortical Stimulation Using Concentric-Ring Electrodes: A Novel Minimally Invasive Neuromodulation Method. Front. Neurosci. 13:773. doi: 10.3389/fnins.2019.00773

INTRODUCTION

Electrical and magnetic brain stimulation can successfully treat a wide range of neurological and psychiatric disorders. In general, these neuromodulation methods fall into two categories: invasive or noninvasive. Invasive neuromodulation methods, such as deep brain stimulation (DBS) and invasive cortical stimulation (ICS, often simply referred to as motor cortex stimulation), require the implantation of an electrode array in a specific brain area to deliver chronic electrical stimulation. The advantage of invasive neuromodulation is that relatively strong stimulation can be chronically delivered to a very focused target. The main disadvantage is the highly invasive nature of the implantation procedure: a burr hole or craniotomy is required and the patient is often awake during parts of the surgery to ensure correct electrode placement. This surgical procedure exposes the patient to significant risk and discomfort and increases therapy cost. Noninvasive neuromodulation methods such as transcranial magnetic stimulation (TMS), transcranial direct current stimulation and transcranial alternating current stimulation (both referred to as transcranial electrical stimulation or TES) have the advantage that no surgery is required, thus significantly reducing patient risk and discomfort, in addition to reducing costs associated with hospitalization and surgery. However, noninvasive neuromodulation methods have a number of significant disadvantages: Stimulation can only be delivered in an acute clinical or laboratory setting. The neuromodulatory effects of TES are typically relatively weak and not well focused. While the effects of TMS are stronger and more focused, it requires expensive and bulky equipment to generate the strong magnetic fields required.

Recently, a novel minimally invasive approach to neuromodulation has emerged – epicranial current stimulation (ECS). In ECS an electrode array is implanted under the scalp and on, or in close proximity to, the skull. ECS has a number of potential advantages over standard invasive and noninvasive neuromodulation methods. The implantation of an ECS device is much less invasive than an ICS or DBS device and could potentially be done under local anesthesia. This would allow delivery of chronic stimulation at a significantly reduced cost, in addition to reduced patient risk and discomfort. With TES most of the delivered current is shunted by the scalp, resulting in relatively weak neuromodulatory effects. By stimulating under the skin, ECS could potentially deliver much stronger neuromodulation. ECS has been tested in animal models and shown to be an effective method for controlling epileptic seizures (Besio et al., 2007; Berényi et al., 2012; Besio et al., 2013). Beyond epilepsy, ECS could offer an alternative approach to treating the wide range of neurological and psychiatric disorders that are currently treated with standard neuromodulation methods. For example ICS is used to treat neuropathic pain (Tsubokawa et al., 1991; Tsubokawa et al., 1993; Nguyen et al., 2000) and has been investigated as a treatment for movement disorders (Pagni et al., 2005; Canavero and Bonicalzi, 2007; Priori and Lefaucheur, 2007; Moro et al., 2011) and depression (Nahas et al., 2010; Kopell et al., 2011). ECS has the potential to offer a less invasive neuromodulation therapy for these disorders. ECS has not yet been tested in humans but systems for patient use are currently in development (Lee et al., 2007).

The aim of the current study was to investigate the feasibility and limitations of using concentric-ring electrodes for ECS in humans. Concentric-ring electrodes consist of an inner disk electrode surrounded by an outer ring and have the potential to deliver more focused stimulation than standard mono or bipolar electrode configurations (Datta et al., 2008; Bortoletto et al., 2016; Gbadeyan et al., 2016; Heise et al., 2016; Martin et al., 2017). We first tested the feasibility of using ECS concentric-ring electrodes in a rat experiment. We verified that we could achieve selective stimulation of the motor cortex by measuring stimulation induced limb movements and comparing the results to that of unfocused stimulation. We then used an MRI based electro-anatomical human head computational model to simulate the electric field strength and focality that could be achieved in patients with ECS concentric-ring electrodes. We used the model to investigate the effect of different ECS concentric-ring electrode designs on electric field strength and focality. Finally, we compared the strength and focality of the cortical electric field generated by ECS with that generated by both ICS and TES.

MATERIALS AND METHODS

Concentric-Ring ECS: Proof-of-Concept in Rats

Animals

Six male Wistar rats (391 ± 91 g, Janvier labs, France) were used. They were housed in a rat colony at ∼19°C and maintained on a 14/10 h light/dark cycle (lights on at 7:00 a.m.). Rats had unrestricted access to food and water. All procedures were approved by the KU Leuven ethics committee for laboratory experimentation (project P096/2015).

Surgery and Preparation

On experiment days rats were anaesthetized with an IP injection of a combination of ketamine (45 mg/kg, Anestekin, Eurovet, Belgium) and medetomidine HCl (0.3 mg/kg, Narcostart, Kela Veterinaria, Belgium), placed in a stereotaxic frame (Narishige type SR-6, No. 7905) on a heating pad and the core temperature monitored via a metal rectal probe. Anesthesia level was routinely monitored using the toe-pinch reflex. The anesthesia level was held constant by giving an additional IP injection of around 100 μL of the ketamine-medetomidine mixture approximately every hour. The skull was exposed by making an incision and then retracting the scalp. A tripolar concentric-ring electrode (CRE medical, Kingston, United States, outer ring diameter: 5.5 mm, inner ring diameter 5 mm and center disk diameter 2 mm) was used to target the hind-limb area of the motor cortex. The general location was determined stereotactically using coordinates from the Paxinos and Watson rat brain atlas (Paxinos and Watson, 2007). The specific location was then found by slowly moving the electrode while delivering electrical stimulation. Using this approach the electrode was finally positioned on the skull over the motor cortex at a location that could elicit a limb movement.

Electrical Stimulation

Electrical stimulation was delivered using a DS5 current source (Digitimer, Hertfordshire, United Kingdom) controlled by an analog voltage waveform input. The voltage waveform was generated using an output channel on a data acquisition card (NI USB-6343, National Instruments, TX, United States) and controlled via custom written MATLAB software (MathWorks, MA, United States) at a sample rate of 20 kHz. Electrical stimulation was delivered through the central disc of the concentric-ring electrode and returned through the outer ring. Stimulation consisted of biphasic rectangular pulses (300 μs per phase) delivered in a pulse train (10 pulses per train, 300 pulses per second) and repeated every one second. These parameters were already shown to induce measurable and reproducible kick-like limb movements (Khatoun et al., 2017). We measured the limb movement when the stimulation amplitude was increased from 1 to 8 mA in 1 mA steps while keeping all other parameters the same. This stimulation amplitude range is enough to cover the variability in the limb movement threshold that occurs between the different rats. The complete sweep (i.e., all amplitudes from 1 to 8 mA) was repeated four times with a 1 min break between repetitions. To deliver unfocused (or monopolar) stimulation, the concentric-ring electrode was kept in the same location. However, now stimulation was only delivered through the central ring. No current was returned through the outer ring, instead current was returned through a large disk electrode (9 mm diameter) placed on the midline 9 mm posterior to bregma. For unfocused electrode configuration, stimulation parameters were exactly the same, except that the stimulation amplitude was increased from 1 to 4 mA. For the same current amplitude, an unfocused electrode configuration gives a stronger electric field, meaning that lower current amplitudes are needed to cause a limb movement.

Limb Movement Measurements and Quantification

To monitor the limb movement two tri-axial accelerometers (ADXL353, Analog Devices, MA, United States) were used. One accelerometer was attached to the targeted limb contralateral to the stimulation site and the other was attached to another limb of interest. Comparing data from both accelerometers showed that we selectively stimulated the motor area controlling the targeted limb, while avoiding stimulation of the motor area controlling the other limb. The six axes (three from each accelerometer) were digitized (NI USB-6216, National Instruments) at 4 kHz sample rate, displayed and recorded for off-line analysis using custom written MATLAB software (MathWorks, MA, United States).

After the experiment, the raw acceleration data were band pass filtered between 3 and 500 Hz (second-order Butterworth) and integrated twice to give the limb displacement in arbitrary units. Principal component analysis was used to combine the three displacement axes and limb displacement was defined as the first principal component. The difference between the minimum and maximum limb displacement occurring after stimulation was then calculated to give limb displacement amplitude for each stimulus presentation.

Concentric-Ring ECS: Feasibility in Humans

An electro-anatomical human head computational model was used to investigate the feasibility of applying ECS in humans and to explore possible electrode designs. The anatomical model enabled us to obtain a quantitative estimate of electric field strength in the different tissue layers during ECS and to explore the effect of different electrode designs. Additionally, we used the model to compare the results with other electrical neuromodulation techniques such as ICS and TES.

MIDA Anatomical Model

The model is based on modified data from the MIDA study: a publicly available homogenous head model, which was built by combining different tissue classes from a multimodal imaging–based detailed anatomical (MIDA) model of human head and neck (FDA, Center for Devices and Radiological Health, MD, United States, and IT'IS Foundation, Zurich, Switzerland) (Iacono et al., 2015). The MIDA model was imported into ScanIP 7 (Simpleware Ltd., Exeter, United Kingdom) as a series of 116 surface meshes – each mesh representing a different tissue type. We first simplified the model by reducing it to tissue types relevant for this study and with known conductivity values. To do this we converted the meshes to volumes (masks). Then merged tissue volumes to obtain just five tissue types and assigned them the following standard electrical conductivity values (σ): skin 0.465 S/m; skull 0.01 S/m; CSF 1.65 S/m; gray matter 0.27 S/m; and white matter 0.126 S/m (Peters et al., 2001; Akhtari et al., 2002; Datta et al., 2009; Gabriel et al., 2009).

Addition of ECS With Concentric-Ring Electrode to Anatomical Model

ECS concentric-ring was modeled as an inner disc electrode and an outer ring electrode both embedded in an insulating silicon material (polydimethylsiloxane or PDMS, typically used for invasive electrode designs) (Meacham et al., 2008; Guo et al., 2013; Ochoa et al., 2013; Salam et al., 2014). The electrode was placed in contact with the skull with the disc and ring electrodes facing the skull and the silicon layer in contact with the skin. We assumed that the electrode pushed the overlaying skin tissue resulting in a slight skin bulge. This was modeled by dilating the skin layer above the electrode with similar dimensions to the electrode. The edges of the dilation were further smoothed to mimic skin stretch. The silicon layer was modeled as a subcutaneous 1.6 mm thick layer of polydimethylsiloxane (PDMS) with 10^{-14} S/m conductivity (Mark, 1999; Danial et al., 2017), with a radius of 80 mm.

Effect of ECS Concentric-Ring Electrode Design

We used the model to explore the effect of two ECS concentric-ring electrode design parameters: (1) the spacing between the central disc electrode and the outer ring electrode (referred

TABLE 1 | List of the ECS concentric-ring electrode dimensions investigated in the study.

	Disc-ring spacing			Central disc size		
	Far	**Standard**	**Close**	**Large**	**Medium**	**Small**
Central electrode diameter (mm)	8	8	8	16	8	4
Ring electrode diameters (mm)	Inner: 52 Outer: 55.8	Inner: 26 Outer: 33	Inner: 13 Outer: 24.1	Not applicable	Not applicable	Not applicable

to as disc-ring spacing) and (2) the size of the central disc electrode (referred to as disc size). Both parameters are expected to effect the strength and focality of the electric field reaching the cortex. The central disc was always positioned in the center of the same silicon layer. Firstly, we fixed the central disc to have a diameter of 8 mm (50.25 mm^2 surface area) and investigated the effect of disc-ring spacing using three settings for the ring electrode diameters: close, standard and far. **Table 1** provides the ring diameters. Secondly, we investigated the effect of the disc size using three sizes for the central disc: small, medium and large. **Table 1** provides the disc diameters and surface areas.

For a concentric-ring electrode, the central disc is the stimulating electrode and the current returns via the outer ring electrode. This was the standard configuration used in the model and was the configuration used to test the effect of disc-ring spacing. However, since changing the size of the central disc will also change the disc-ring spacing, we opted to use a monopolar stimulation configuration (i.e., where current returns via an implantable pulse generator located in the chest) to investigate the effect of disc size (i.e., small, medium, and large) in isolation. The MIDAS model contains the head and the neck only and does not contain a body. We modeled the body as a cube connected to the neck (135 mm × 30 mm × 100 mm dimension) and we set the bottom surface of this cube as the return electrode (135 mm × 100 mm). The chosen dimension of the body cube provides a compromise solution between computational cost and reality. Importantly, we choose a body size that completely covered the base of the neck which closely matches the real life situation. This ensures that current flow patterns are only minimally affected as they passed from the neck to the body, thus current flow patterns in the brain will also be relatively unaffected. With this approach increasing the body size would only have a minimal effect the electric field in the brain.

Comparison With ICS and TES

To compare ECS with other invasive and noninvasive neuromodulation methods, the same model was used to simulate both ICS and TES. Given its invasive nature and its direct intact with the cortex, we would expect ICS to induce a stronger and more focused cortical electric field than ECS. On the other hand, we would expect TES to induce weaker and less focused cortical field than ECS given that most of the current is shunted by skin during TES.

The ICS electrode was modeled as a 3.3 mm diameter disk electrode (Lesser et al., 2010) with thickness of 1.6 mm (Kim et al., 2011). ICS used the same monopolar configuration described above.

The TES electrode was modeled as a central disc and ring electrode configuration. The central electrode diameter was set to be 16 mm and the ring electrode's inner and outer diameters were set to be 52 and 66 mm, respectively. These dimensions are similar to those reported in TES concentric-ring electrode studies (Datta et al., 2008; Gbadeyan et al., 2016; Heise et al., 2016; Martin et al., 2017). Each TES electrode (disc and ring) were modeled as a 1.6 mm thick layer of gel with 0.3 S/m conductivity in direct contact with the scalp.

One gyral crown was manually selected from the motor cortex and the central electrodes from all the methods (ECS, ICS, and TES) were positioned rectilinearly above the same gyral crown.

Electric Field Calculation

In ScanIP, volumetric tetrahedral models were calculated for all generated models. The results were imported into COMSOL multiphysics 5.3 (COMSOL, Inc., Burlington, MA, United States) where electric field (E) and current density (J) was calculated by solving Laplace's equation,

$$\begin{aligned} \nabla \cdot \sigma \nabla \varphi &= 0 \\ E &= |\nabla \varphi| \\ J &= \sigma |E| \end{aligned} \tag{1}$$

with φ representing the electrical potential. This assumes a quasi-static approximation of Maxwell's equations, valid for alternating electric fields in the brain with frequencies < 1 MHz (Nunez and Srinivasan, 2006). Boundary conditions were set to have a positive current at the anodic central electrode with peak-amplitude equal to 1 mA and the negative current was set on the ring electrode during ECS and TES and on the bottom area of the modeled body during monopolar ICS.

To avoid a measure of maximum electric field strength that is skewed by one or two voxels containing very high values, the maximum electric field strength was calculated as the average value of the electric field strength in a 10 mm^3 volume containing the highest electric field strengths in one particular tissue. This 10 mm^3 volume was found by first ranking all voxels in one tissue from high to low electric field and then selecting the number of voxels, starting with the highest ranking and progressing to lower, which were needed to make up a 10 mm^3 volume. To quantify electric field spatial spread (i.e., a measure of focality) we calculated the half-value volume (Deng et al., 2013; Khatoun et al., 2018), this is the volume of the brain with an electric field magnitude higher than half of the maximum electric field strength. For a field that is distributed over a larger volume of brain, the half-value volume

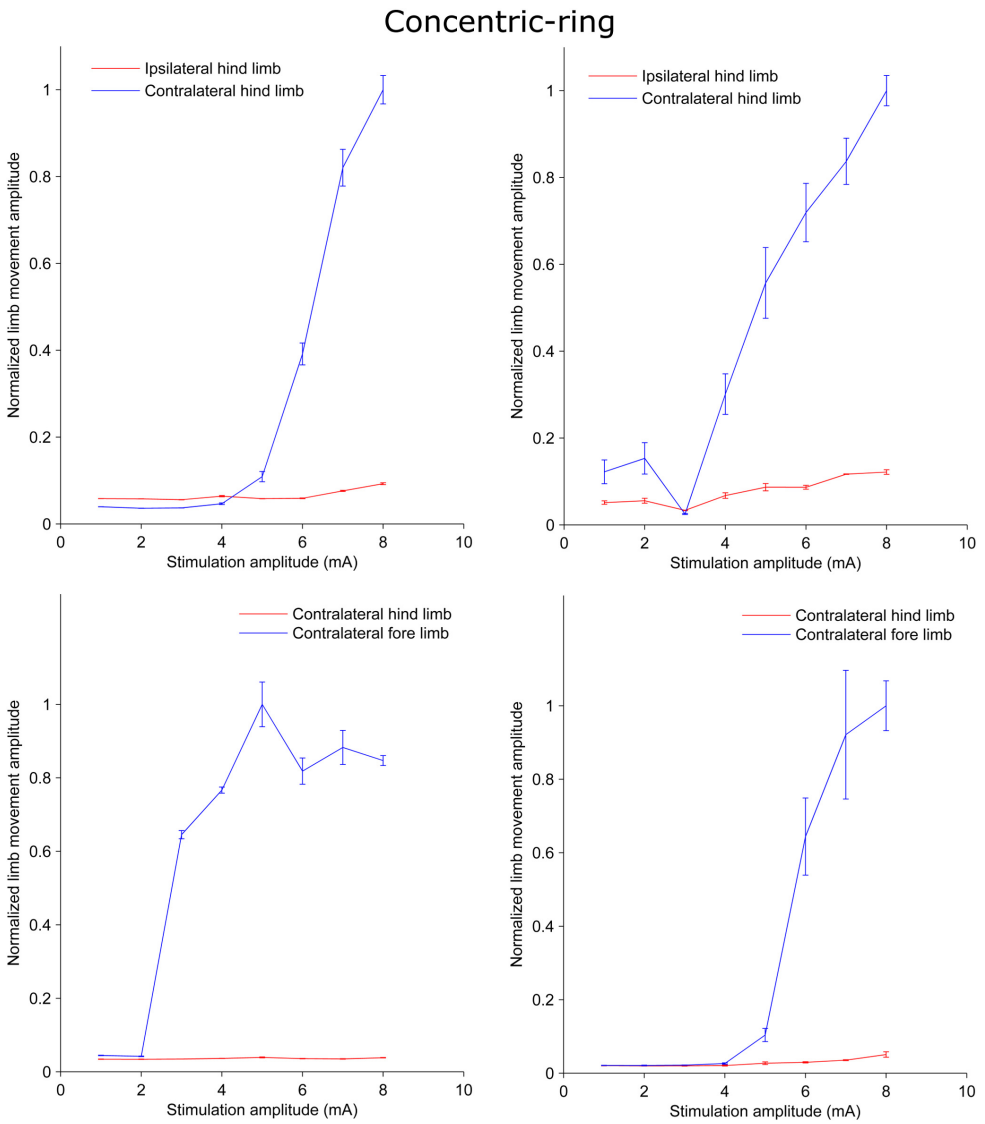

FIGURE 1 | Plots from rat experiments showing the limb movement amplitude as a function of stimulation amplitude applied to concentric-ring ECS electrode placed over the rat motor cortex. The upper panel compares the movement in the hind limbs while the lower panel compares the movement in the hind limb to that in the fore limb. Error bars represent the standard deviation. When stimulation targeted one of the hind limbs and the amplitude was below threshold (upper panel), both the hind limbs ipsilateral (red) and contralateral (blue) to the side of stimulation showed no increase in the movement amplitude. However, when stimulation amplitude was increased above threshold there was significant increase in the contralateral limb movement and no, or relatively low, ipsilateral movement. Similar results were obtained in the lower panel. However, this time stimulation targeted the fore limb cortical area. Movement was detected in the contralateral fore limb (blue) but not in the contralateral hind limb (red). This indicates that concentric-ring ECS can cause selective stimulation of the rat motor cortex.

will be higher than for a field that is distributed over a smaller volume of brain.

RESULTS

Concentric-Ring ECS: Proof-of-Concept in Rats

We used a rat experiment to demonstrate that ECS with concentric-ring electrodes can deliver focused cortical stimulation, strong enough to cause selective limb movement. The left upper panel in **Figure 1** is an example from one rat showing the amplitude of the hind limb movement as a function of the pulse-train amplitude delivered through an ECS concentric-ring electrode. When stimulation amplitude was below 4 mA, neither of the hind limbs contralateral (blue) nor the ipsilateral (red) to the stimulated hemisphere moved. When the stimulation amplitude was increased above 4 mA and up to 8 mA, the contralateral hind limb showed a corresponding increase in movement amplitude. However, the ipsilateral hind limb did not move, even at these higher amplitudes. The right upper panel in **Figure 1** shows the results from a second rat.

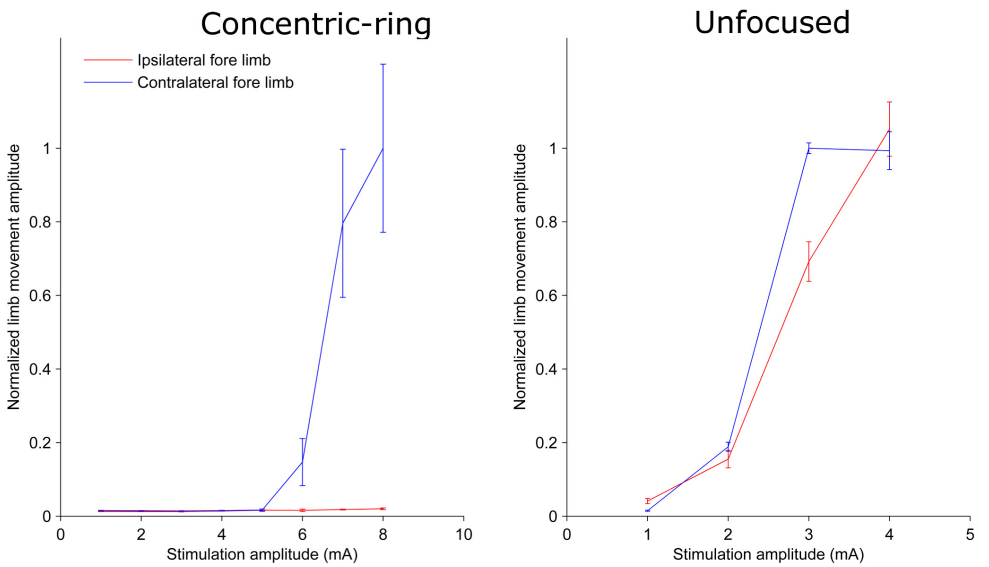

FIGURE 2 | Plots from one rat showing the limb movement amplitude as a function of stimulation amplitude using a concentric-ring ECS **(left panel)** and unfocused ECS **(right panel)**. Error bars represent the standard deviation. Note the difference in the stimulation amplitude scale between the two graphs. The concentric-ring electrode shows a selective stimulation of the contralateral fore limb (blue) with a threshold of 6 mA. On the other hand, the unfocused stimulation shows a movement in both contralateral (blue) and ipsilateral (red) fore limbs with a threshold of 2 mA. This indicates that the concentric-ring electrode provides stimulation of one specific target brain area which is not possible with an unfocused ECS electrode. However, because focused electrode produce a weaker electric field in the brain (see **Figure 4**), the concentric-ring ECS has a higher threshold than unfocused ECS.

We observed a similar effect to that of the first rat. However, the threshold for limb movement in this rat was slightly lower at around 3 mA. At higher amplitudes we also observed a small increase in the ipsilateral hind limb movement, but this was much smaller than in the contralateral hind limb. The lower panel of **Figure 1** shows similar results to the upper one but from different rats. However, this time stimulation targeted the fore limb cortical area. Movement was detected in the contralateral fore limb but not in the contralateral hind limb. The threshold for limb movement in these rats were 3 and 5 mA, respectively. Similar results to the panels in **Figure 1** were obtained from seven limbs recorded from three different rats (**Supplementary Table 1** and **Supplementary Figures 1–4**). In two of these rats we compared hind and fore limbs movements from the same side (see **Supplementary Figures 1**, **2**). The results from these measurements show a movement of the targeted contralateral limb but not the other contralateral limb. Interestingly, we compared the focality of concentric-ring to unfocused stimulations in these three rats. **Figure 2** shows an example from one rat. The left panel shows the amplitude of the hind limbs movements when the concentric-ring electrode was used and the right panel shows the movements amplitudes of the same limbs when the unfocused electrode was used. The results show that using concentric-ring electrode the stimulation was focused to the contralateral hind limb with threshold of 6 mA while no movement was recorded in the ipsilateral hind limb even at 8 mA. On the other hand, during the unfocused stimulation, the ipsilateral hind limb showed a high but slightly lower limb movement compared to the contralateral limb. In addition, the threshold for limb inducing limb movement was 2 mA which is lower than that of the concentric-ring electrode. Thus, results from the rat experiment show that ECS with concentric-ring electrodes can cause relatively strong, yet selective (i.e., focused), neuromodulation of the rat motor cortex. However, given the large differences in head size, skull thickness and morphology between rats and humans, it was unclear if ECS with concentric-ring electrode in humans would also be feasible.

Concentric-Ring ECS: Feasibility in Humans

Exploring the Feasibility of ECS

We used an electro-anatomical human head computational model to investigate the feasibility of applying ECS in humans and to explore different electrode designs. **Figure 3** shows a rendered representation from the computational model to illustrate the concept of ECS with a concentric-ring electrode. The electrode consists of a central disc and outer ring electrode (gray) embedded in a silicone layer (partially transparent). The disc and ring electrode are in contact with the skull but insulated from the skin by the silicone layer. Here, the medium disc size was used with the standard spacing (see **Table 1**). We applied a 1 mA current through the ECS electrode and calculated the electric field strength in each tissue layer. In **Figure 3** the electric field strength is color encoded on the cortical surface. It shows that ECS with a concentric-ring electrode generates a relatively focused electric field in the cortex. For 1 mA ECS using these electrode dimensions the maximum electric field strength in the cortex was 3.82 V/m.

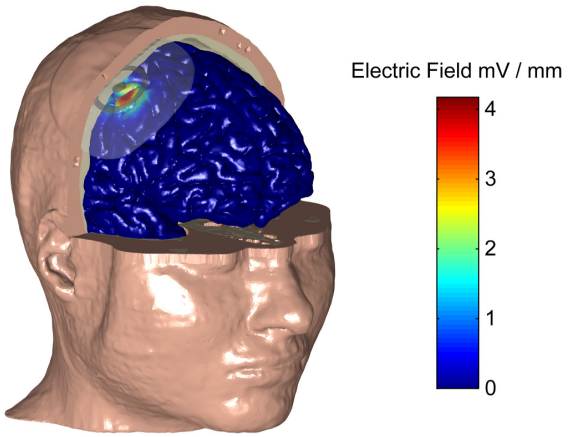

FIGURE 3 | A human head electro-anatomical computational model was used to illustrate the concept of ECS with a concentric-ring electrode. Part of the skin and skull have been made transparent to reval the ECS concentic-ring electrode, which consists of a central disc and outer ring electrode (gray) embedded in an insulating silicone layer (partially transparent). The disc and ring electrode are in contact with the skull but insulated from the skin by the silicone layer. The CSF is not shown for simplicity. The electric field strenght on the cortical surface (see color bar) caused by a 1 mA current applied through the ECS electrode is shown. Using this electrode design, 1 mA ECS creates a relatively focused electric field in the cortex with the maximum electric field strength of 3.82 V/m.

Effect of ECS Concentric-Ring Electrode Design

Next, we used the model to test the effect of disc-ring spacing on the electric field distribution. **Figure 4** shows the results for three different spacing between the central and the ring electrode: Far, standard and close (left, middle, and right column, respectively, inner ring dimensions: 52, 26, and 13 mm, respectively). The upper row in **Figure 4** shows the electric field strength generated at the cortical surface when a 1 mA current was applied through each of the electrodes. The second row shows a 2-dimensional cross-section from the same models; while the third row shows the electric field strength along a 1-dimensional line indicated by a gray arrow on the cross-section. The far spacing showed a broad electric field distribution with a half-value volume of 169.44 mm^3 and a maximum electric field strength of less than 4.13 V/m. Moving to the standard spacing (i.e., ring closer to the disc) resulted in a more focused but weaker field with values of 103.60 mm^3 and 3.82 V/m for the half-value volume and the maximum electric field strength, respectively. Reducing the spacing further to the close setting resulted in a more focused but even weaker field with values of 55.63 mm^3 and 2.70 V/m for the half-volume percentage and the maximum electric field strength, respectively. These values, along with the electric field strength in the skin and skull are summarized in **Table 2**. Thus, when keeping the current constant, changing disc-ring spacing causes a trade-off between electric field strength and focality.

Figure 5 shows the results for three different central disc sizes: large, medium and small (left, middle, and right column, respectively, disc diameters: 16, 8, and 4 mm) all with a 1 mA current amplitude. Note, that a monopolar configuration was used for all three. The large disc electrode showed a broad electric field distribution with a half-value volume of 646.81 mm^3 and a maximum electric field strength of less than 2.86 V/m. Reducing the central electrode size to medium resulted in a more focused and stronger field with values of 190.18 mm^3 and 4.16 V/m for the half-value volume and the maximum electric field strength, respectively. Reducing the central electrode size to small resulted in a more focused field with values of 118.70 mm^3 and 4.84 V/m for the half-volume percentage and maximum electric field strength, respectively. These values, along with the electric field strength in the skin and skull are summarized in **Table 2**. Thus, reducing disc size produces a stronger and more focused electric field in the brain. However, the trade-off here is with current density at the electrode-skull interface and electrode impedance. Reducing the disc size increases the current density at the electrode surface and increases the electrode impedance. For a current of 1 mA the small, medium and large disc sizes had current densities of 0.080, 0.020, and 0.005 mA/mm^2, respectively.

Comparison With ICS and TES

To put the potential neuromodulatory effects of ECS with concentric-ring electrodes into perspective we used the same model to simulate more standard neuromodulation methods, namely ICS and TES. **Figure 6** shows the model results comparing the electric field strengths generated in each tissue for the three neuromodulation methods, when the same 1 mA current was applied (from left to right: ICS, ECS with standard disc-ring spacing and medium disc size, TES). The upper row shows a 2-dimensional coronal cross-section passing through the electrode center for each neuromodulation method. The lower row shows the corresponding 1-dimensional plot of the electric field strength along the position indicated by the gray arrow in the upper panels. The figure highlights how the electric field magnitude decreases with distance from each electrode type and how the electric field is affected by the different tissues. Note, the same logarithmic scale is used to compare the electric fields across all plots. The results show that for a 1 mA current, ICS induced the strongest cortical field with the maximum electric field strength of around 42.52 V/m. For the same current amplitude, ECS showed maximum electric field strength in the cortex of 3.82 V/m with high electric fields values in the skull (greater than 100 V/m) and low field strengths in the skin with the maximum electric field strength of 0.02 V/m. As expected, TES showed the weakest cortical field and the highest fields in the skin with approximate maximum electric field strength of 0.11 and 32.8 V/m, respectively. In terms of cortical fields spatial distribution, ICS caused the most focused stimulation with the half-value volume of 5.64 mm^3 followed by ECS with a value of 103.60 mm^3 and then TES with a value of 2138.10 mm^3. Our estimated cortical electric fields are in agreement with other tES modeling studies (Datta et al., 2008; Bortoletto et al., 2016; Nikolin et al., 2019). The validity of such models has already been confirmed using invasive recordings (Lafon et al., 2017; Vöröslakos et al., 2018). In summary, the model predicts that both electric field strength and focality will be reduced by one order of magnitude when moving from the invasive ICS to

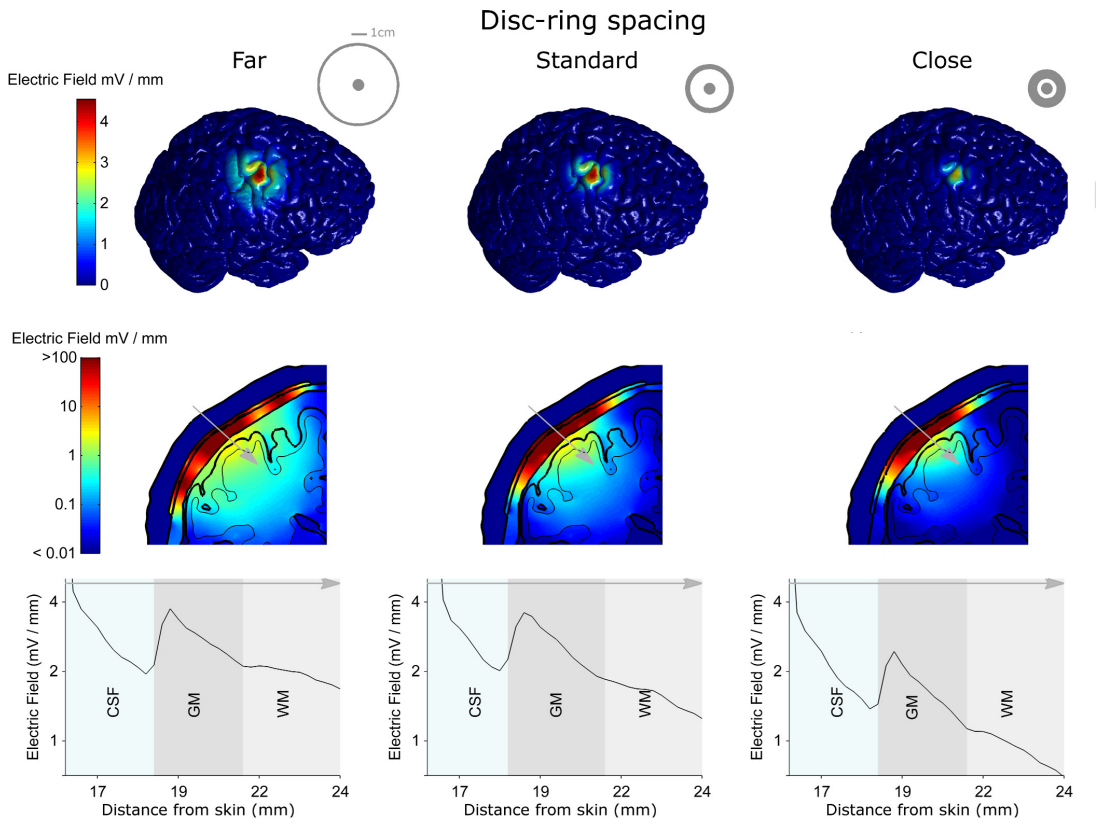

FIGURE 4 | The electro-anatomical head model was used to investigate the effect of disc-ring spacing on the focality and strength of the electric field reaching the cortex. The left, central and right columns show model data for the far, standard and close disc-ring spacing respectively (shown as insets in the top row), when the same 1 mA current is delivered through each spacing. The top row shows how reducing the disc-ring spacing causes a more focused electric field on the brain. However, as highlighted in the second and third rows this comes at the cost of reducing the electric field strength. Thus, when keeping current constant, there is always a trade-off between electric field strength and focality. A 2-dimensional coronal, partial, cross-section is shown in the middle row using a logarithmic color scale. The different model tissues are outlined in black – skin, skull, CSF, gray matter (GM) and white matter (WM). A 1-dimensional plot of the electric field strength along the position indicated by the gray arrow is shown on the bottom row. This shows how the electric field magnitude decreases with distance from the electrode, how it is affected by each tissue type (only CSF, GM, and WM shown for a clearer comparison) and by the disc-ring spacing. Note that the maximum electric field values reported in the manuscript are based on the 3-dimentional brain volume (first row) and not on the 2-dimentional (second row) or the 1-dimensional (third row) as they represent values being interpolated from the 3-dimentional data.

TABLE 2 | List of the maximum electric field strengths (E, V/m) obtained in each tissue type (skin, skull, and brain) for each of the three disc-ring spacing settings (close, standard, and far) and disc size settings (small, medium, and large) investigated.

Stim Amp		**1 mA**			**2 mA**			**10 mA**		
Max E in tissue (V/m)		E_{skin}	E_{skull}	E_{Brain}	E_{skin}	E_{skull}	E_{Brain}	E_{skin}	E_{skull}	E_{Brain}
Disc-ring spacing	Far	0.210	2.225×10^3	4.13	0.420	4.450×10^3	8.26	2.10	2.225×10^4	41.3
	Standard	0.020	2.229×10^3	3.82	0.040	4.458×10^3	7.64	0.200	2.229×10^4	38.2
	Close	0.005	2.290×10^3	2.70	0.010	4.450×10^3	5.40	0.050	2.290×10^4	27.0
Disc size	Large	0.175	839	2.86	0.350	1678	5.72	1.750	8390	28.6
	Medium	0.175	2.224×10^3	4.16	0.350	4.448×10^3	8.32	1.750	2.224×10^4	41.6
	Small	0.175	4.942×10^3	4.84	0.350	9.884×10^3	9.68	1.750	4.942×10^4	48.4
ICS		0.21	15.80	42.52						
TES		32.80	11.64	0.11						

Equivalent values for ICS and TES are shown. The effect of increasing the current delivered through the ECS concentric-ring electrodes to 2 and 10 mA are also shown.

the minimally invasive ECS. Then, the focality will be reduced again by another order of magnitude when going from ECS to the noninvasive TES. Thus, when the delivered current is held constant, there is a clear trade-off between the degree of invasiveness and the strength and focality of the electric field than can reach the brain.

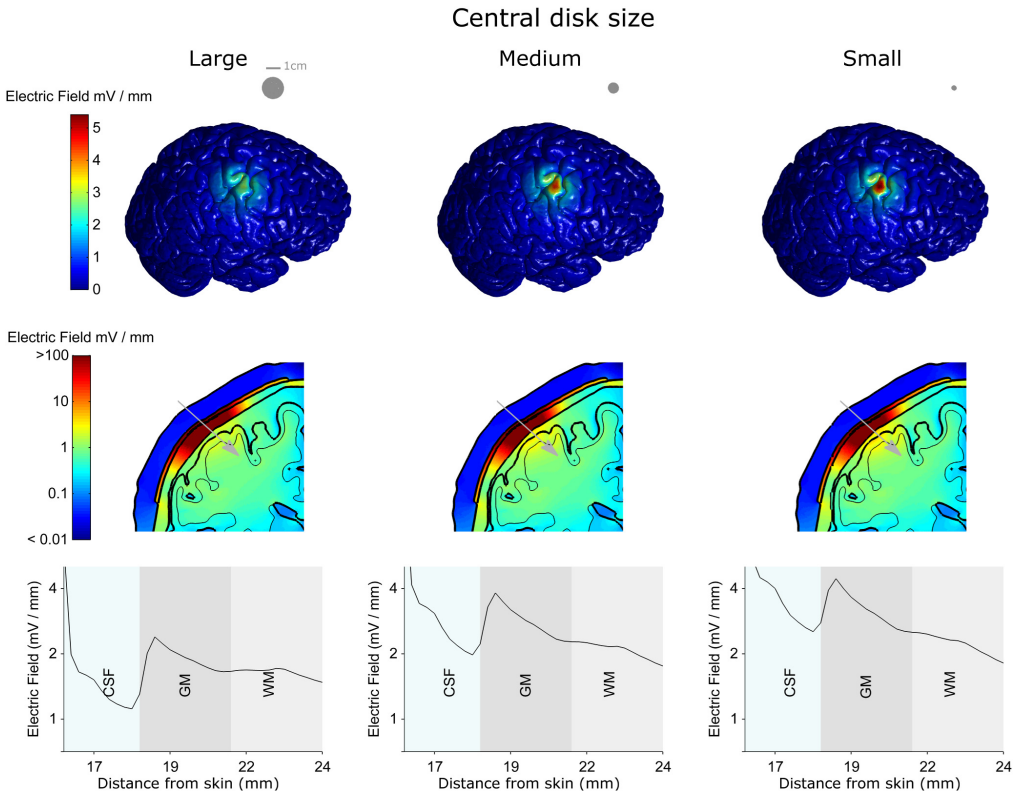

FIGURE 5 | The electro-anatomical head model was used to investigate the effect of disc size on the focality and strength of the electric field reaching the cortex. The left, central and right columns show model data for the large, medium and small disc sizes respectively, when the same 1 mA current is delivered through each spacing. Note – a monopolar configuration was used with these simulations. The top row shows how reducing the disc size (shown as insets in the top row) causes a more focused electric field on the brain. As highlighted in the second and third rows the smaller disc size also causes a stronger electric field in the brain. However, the smaller disc size increases the current density under the electrode (see text). Thus, there is always a trade-off between electric field strength and focality.
A 2-dimensional coronal, partial, cross-section is shown in the middle row using a logarithmic color scale. The different model tissues are outlined in black – skin, skull, CSF, gray matter (GM) and white matter (WM). A 1-dimensional plot of the electric field strength along the position indicated by the gray arrow is shown on the bottom row. This shows how the electric field magnitude decreases with distance from the electrode, how it is affected by each tissue type (only CSF, GM, and WM shown for a clearer comparison) and by the disc size.

Increasing ECS Stimulation Amplitude

With ECS, it may be possible to increase the strength of the electric field reaching the brain by increasing the current amplitude. To investigate the feasibility and limitations of achieving stronger electric fields in the cortex with concentric-ring ECS we simulated the effect of increasing the current amplitude delivered through the ECS electrode. This is a simple exercise, given that the model is completely linear. However, when taken in context with the ICS and TES models, the results give important insight into the potential strength of the neuromodulatory effects that could be achieved with ECS. **Table 2** shows the maximal electric field strengths in the skin, skull and cortex for a range of concentric-ring electrode designs when a 1, 2, or 10 mA current is delivered. These are compared with 1 mA TES and 1 mA ICS. Increasing the ECS current amplitude to 10 mA allows delivery of electric field strengths to the brain which are in the same range as ICS. However, even with the concentric-ring design, these fields are still less focused that those achievable with ICS.

DISCUSSION

We first evaluated ECS using concentric-ring electrodes in a rat motor cortex stimulation experiment. We demonstrated that concentric-ring ECS can produce strong and focused neuromodulation: stimulation was strong enough to cause a limb movement and focused enough to cause movement in only the target limb. This is in contrast to unfocused stimulation which always showed a movement in more than one limb. However, it is difficult to directly translate current amplitude thresholds and electric field strengths from the rat brain to the human. Therefore, we then used an electro-anatomical human head model to explore the feasibility of using concentric-ring ECS in patients. We showed that depending on the electrode design, a 1 mA current delivered through an ECS concentric-ring electrode would cause a relatively focused electric field of between 2.70 and 4.13 V/m in the cortex. To put the potential neuromodulatory effects of concentric-ring ECS into context we used the same model to simulate ICS and TES. These are both standard neuromodulation methods where the effects of the electric field strengths and effects

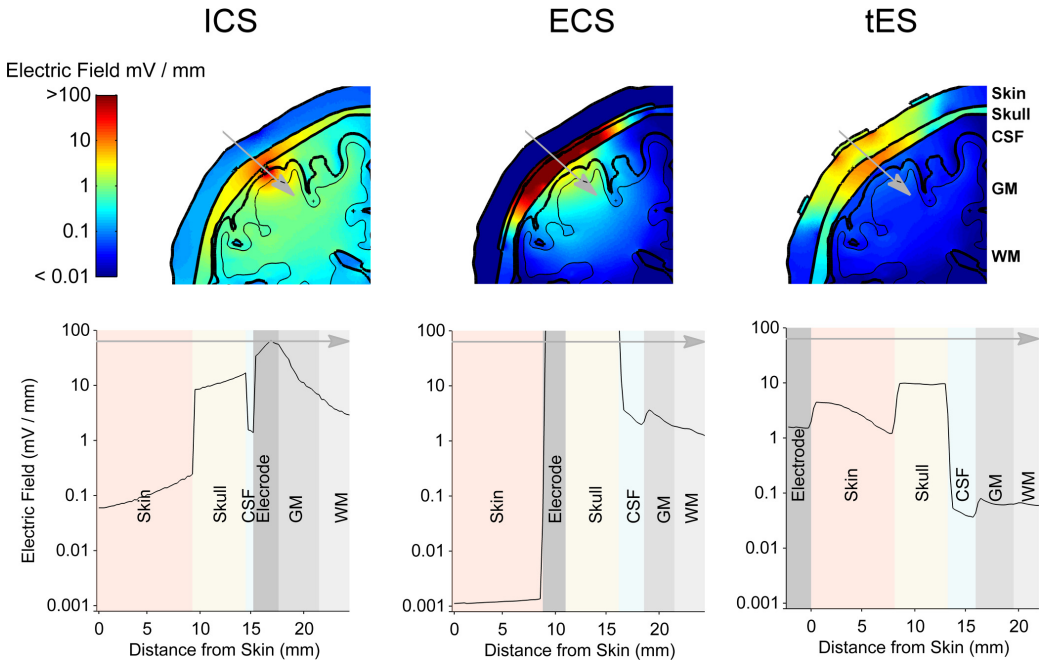

FIGURE 6 | The results from the electro-anatomical computational model comparing the electric field distribution in different tissues resulting from a 1 mA ECS to that of ICS and TES. A 2-dimensional coronal, partial, cross-section is shown in the upper row with the color scale being logarithmic. The different tissues represented in the model are indicated – skin, skull, CSF, gray matter (GM) and white matter (WM). A 1-dimensional plot of the electric field strength along the position indicated by the gray arrow is shown in the lower row. This shows how the electric field magnitude decreases with distance from the electrode and how it is affected by each tissue type. Again, note the logarithmic scale on the axis showing the electric field. ECS shows a more focused and stronger cortical field than TES, but less focused and weaker cortical field than ICS.

are reasonable well known. We showed that for the equivalent current amplitude, concentric-ring ECS could produce cortical electric fields that are an order of magnitude stronger and more focused than TES. However, for an equivalent current amplitude, ECS fields are an order of magnitude lower and less spatially focused than those achieved with ICS. Increasing ECS current amplitude to 10 mA brings the electric field strength into the same range as 1 mA ICS, but this is at the cost of stronger electric fields in the skull and skin. Within the context of these results, we now discuss potential applications for concentric-ring ECS.

Potential Applications

ECS has the potential to deliver much stronger neuromodulation than is achievable with TES, in addition to potentially delivering continuous stimulation. This could be of great value, particularly given the recent controversies in the TES field concerning: (1) the weak electric field strength in the cortex (Huang et al., 2017; Lafon et al., 2017); (2) the ongoing debate around the potential absence of neuromodulatory effects in some protocols (Lafon et al., 2017); and (3) the potential role of transcutaneous stimulation of peripheral nerves in the scalp in mediating TES effects (Asamoah et al., 2019). Our results using concentric ring electrode show that 1 mA of ECS produces an electric field in the skin that is more than three orders of magnitude weaker than that induced during 1 mA of TES. In addition, increasing the stimulation amplitude during ECS to 10 mA still induces an electric field in the skin that is much weaker than the threshold to fire an action potential in the peripheral nerves (0.2 V/m compared to 4–6 V/m) (So et al., 2004). These results indicate that it would require more than 100 mA of ECS current, using the concentric-ring electrode, before subjects perceive the stimulation in the skin. However, the potential increase in neuromodulation strength of ECS over TES comes at the cost of moving from a noninvasive to a minimally invasive method. Therefore, ECS applications are likely to be the treatment of neurological or psychiatric disorders that are severe enough to merit surgical intervention such as medically refractory epilepsy or neuropathic pain, advanced stage movement disorders, or treatment-resistant major depression. A wide range of studies have already shown that invasive neuromodulation methods such as ICS (Tsubokawa et al., 1991; Tsubokawa et al., 1993; Nguyen et al., 2000) and DBS (Benabid et al., 1991; Blond and Siegfried, 1991; Bewernick et al., 2010; Zhang et al., 2010; Volkmann et al., 2012) can be used to treat each of these conditions. Thus, for brain disorders that are already treated using invasive neurosurgical approaches, ECS may offer a less invasive alternative. The main advantage over ICS or DBS would be a much shorter and less invasive surgical approach, which could be performed under local anesthesia, thus reducing cost, risk and patient discomfort. One disadvantage of ECS over ICS, is that for the same 1 mA current, ECS will provide a much weaker and less focused neuromodulatory effect. This could potentially be compensated for by increasing the ECS current amplitude (see **Table 2**). Although, as discussed in the next section, work in large

animal models is needed to determine the safety of delivering ECS at higher current amplitudes.

Steps Toward Patient Evaluation

Our results indicate that neuromodulation with concentric-ring ECS may have a number of potentially useful patient applications. However, before these can be fully exploited a number of important steps need to be taken. Our computational model indicated that ECS will generate strong electric fields (> 100 V/m) across the skull. Thus, large animal models with skull thicknesses similar to humans should be used to investigate the safety of chronic ECS. Additionally, the redox reactions that take place at an electrode-neuron interface have been reasonably well studied (Yuen et al., 1981; Agnew et al., 1986; Agnew and McCreery, 1990; McCreery et al., 1990). For an ECS electrode similar studies should be undertake for the electrode-bone interface. As we have done here, computational models can be used to study and optimize ECS electrode design. Prototypes of these electrodes must then be manufactured and evaluated in the same large animal models. Finally, ECS needs to be evaluated in patients. Initial evaluations could be done in a noninvasive way using an approach we have recently developed (Khatoun et al., 2018): first a local anesthetic cream is used to numb the scalp; high amplitude stimulation can then be delivered through scalp electrodes to achieve a cortical electric field strength similar to ECS.

CONCLUSION

By achieving relatively strong and focused cortical stimulation, in a minimally invasive way, concentric-ring ECS has the potential to offer an alternative neuromodulation therapy for a number of severe neurological and psychiatric disorders.

ETHICS STATEMENT

All procedures were approved by the KU Leuven ethics committee for laboratory experimentation (Project P096/2015).

AUTHOR CONTRIBUTIONS

AK: computational modeling, manuscript writing, rats experiments and data analysis. BA: rats experiments, manuscript writing. MM: analysis, manuscript writing, concept. All authors reviewed the manuscript.

FUNDING

This work was supported by KU Leuven Research Funding STG/14/024 and EGM-D2929-C24/17/091 and by an EIT Health Innovation by Ideas, NEURO-WEAR Project. BA was SB Ph.D. fellow at FWO.

SUPPLEMENTARY MATERIAL

The Supplementary Material for this article can be found online at: https://www.frontiersin.org/articles/10.3389/fnins.2019.00773/full#supplementary-material

REFERENCES

Agnew, W. F., and McCreery, D. B. (1990). Considerations for safety with chronically implanted nerve electrodes. *Epilepsia* 31(Suppl. 2), S27–S32.

Agnew, W. F., Yuen, T. G., McCreery, D. B., and Bullara, L. A. (1986). Histopathologic evaluation of prolonged intracortical electrical stimulation. *Exp. Neurol.* 92, 162–185. doi: 10.1016/0014-4886(86)90132-9

Akhtari, M., Bryant, H. C., Mamelak, A. N., Flynn, E. R., Heller, L., Shih, J. J., et al. (2002). Conductivities of three-layer live human skull. *Brain Topogr.* 14, 151–167.

Asamoah, B., Khatoun, A., and Mc Laughlin, M. (2019). TACS motor system effects can be caused by transcutaneous stimulation of peripheral nerves. *Nat Commun.* 10:266. doi: 10.1038/s41467-018-08183-w

Benabid, A. L., Pollak, P., Gervason, C., Hoffmann, D., Gao, D. M., Hommel, M., et al. (1991). Long-term suppression of tremor by chronic stimulation of the ventral intermediate thalamic nucleus. *Lancet* 337, 403–406. doi: 10.1016/0140-6736(91)91175-t

Berényi, A., Belluscio, M., Mao, D., and Buzsáki, G. (2012). Closed-loop control of epilepsy by transcranial electrical stimulation. *Science* 337, 735–737. doi: 10.1126/science.1223154

Besio, W. G., Koka, K., and Cole, A. J. (2007). Effects of noninvasive transcutaneous electrical stimulation via concentric ring electrodes on pilocarpine-induced status epilepticus in rats. *Epilepsia* 48, 2273–2279. doi: 10.1111/j.1528-1167.2007.01202.x

Besio, W. G., Makeyev, O., Medvedev, A., and Gale, K. (2013). Effects of transcranial focal electrical stimulation via tripolar concentric ring electrodes on pentylenetetrazole-induced seizures in rats. *Epilepsy Res.* 105, 42–51. doi: 10.1016/j.eplepsyres.2012.12.002

Bewernick, B. H., Hurlemann, R., Matusch, A., Kayser, S., Grubert, C., Hadrysiewicz, B., et al. (2010). Nucleus accumbens deep brain stimulation decreases ratings of depression and anxiety in treatment-resistant depression. *Biol. Psychiatry* 67, 110–116. doi: 10.1016/j.biopsych.2009.09.013

Blond, S., and Siegfried, J. (1991). Thalamic stimulation for the treatment of tremor and other movement disorders. *Acta Neurochir. Suppl.* 52, 109–111. doi: 10.1007/978-3-7091-9160-6_30

Bortoletto, M., Rodella, C., Salvador, R., Miranda, P. C., and Miniussi, C. (2016). Reduced current spread by concentric electrodes in transcranial electrical stimulation (TES). *Brain Stimul.* 9, 525–528. doi: 10.1016/J.BRS.2016.03.001

Canavero, S., and Bonicalzi, V. (2007). Extradural cortical stimulation for movement disorders. *Acta Neurochir. Suppl.* 97, 223–232. doi: 10.1007/978-3-211-33081-4-25

Danial, N. S., Ramli, M. M., Halin, D. S. C., Hong, H. C., Isa, S. S. M., Abdullah, M. M. A. B., et al. (2017). Incorporation of polydimethylsiloxane with reduced graphene oxide and zinc oxide for tensile and electrical properties. *AIP Conf. Proc.* 1887:20061. doi: 10.1063/1.5003544

Datta, A., Bansal, V., Diaz, J., Patel, J., Reato, D., and Bikson, M. (2009). Gyri-precise head model of transcranial direct current stimulation: improved spatial focality using a ring electrode versus conventional rectangular pad. *Brain Stimul.* 2, 201.e1–.e207. doi: 10.1016/j.brs.2009.03.005

Datta, A., Elwassif, M., Battaglia, F., and Bikson, M. (2008). Transcranial current stimulation focality using disc and ring electrode configurations: FEM analysis. *J. Neural. Eng.* 5, 163–174. doi: 10.1088/1741-2560/5/2/007

Deng, Z.-D., Lisanby, S. H., and Peterchev, A. V. (2013). Electric field depth–focality tradeoff in transcranial magnetic stimulation: simulation comparison of 50 coil designs. *Brain Stimul.* 6, 1–13. doi: 10.1016/j.brs.2012.02.005

Gabriel, C., Peyman, A., and Grant, E. H. (2009). Electrical conductivity of tissue at frequencies below 1 MHz. *Phys. Med. Biol.* 54, 4863–4878. doi: 10.1088/0031-9155/54/16/002

Gbadeyan, O., McMahon, K., Steinhauser, M., and Meinzer, M. (2016). Stimulation of dorsolateral prefrontal cortex enhances adaptive cognitive control: a high-definition transcranial direct current stimulation study. *J. Neurosci.* 36, 12530–12536. doi: 10.1523/jneurosci.2450-16.2016

Guo, L., Guvanasen, G. S., Liu, X., Tuthill, C., Nichols, T. R., and DeWeerth, S. P. (2013). A PDMS-based integrated stretchable microelectrode array (isMEA) for neural and muscular surface interfacing. *IEEE Trans. Biomed Circuits Syst.* 7, 1–10. doi: 10.1109/TBCAS.2012.2192932

Heise, K.-F., Kortzorg, N., Saturnino, G. B., Fujiyama, H., Cuypers, K., Thielscher, A., et al. (2016). Evaluation of a Modified High-Definition Electrode Montage for Transcranial Alternating Current Stimulation (tACS) of Pre-Central Areas. *Brain Stimul.* 9, 700–704. doi: 10.1016/j.brs.2016.04.009

Huang, Y., Liu, A. A., Lafon, B., Friedman, D., Dayan, M., Wang, X., et al. (2017). Measurements and models of electric fields in the in vivo human brain during transcranial electric stimulation. *Elife* 6, 1–27. doi: 10.7554/eLife.18834

Iacono, M. I., Neufeld, E., Akinnagbe, E., Bower, K., Wolf, J., Oikonomidis, V. I., et al. (2015). MIDA: a multimodal imaging-based detailed anatomical model of the human head and neck. *PLoS One* 10:e0124126. doi: 10.13099/ViP-MIDA-V1.0

Khatoun, A., Asamoah, B., and Mc Laughlin, M. (2017). simultaneously excitatory and inhibitory effects of transcranial alternating current stimulation revealed using selective pulse-train stimulation in the rat motor cortex. *J. Neurosci.* 37, 9389–9402. doi: 10.1523/JNEUROSCI.1390-17.2017

Khatoun, A., Breukers, J., Beeck, S., Op de Nica, I. G., Aerts, J.-M., Seynaeve, L., et al. (2018). Using high-amplitude and focused transcranial alternating current stimulation to entrain physiological tremor. *Sci. Rep.* 8:4927. doi: 10.1038/s41598-018-23290-w

Kim, D., Jun, S. C., and Kim, H. (2011). Computational study of subdural and epidural cortical stimulation of the motor cortex. *Annu. Int. Conf. IEEE Eng. Med. Biol. Soc.* 2011, 7226–7229. doi: 10.1109/IEMBS.2011.6091826

Kopell, B. H., Butson, C. R., Rainey, C., Dougherty, D. D., Harsch, H., Halverson, J., et al. (2011). Epidural cortical stimulation of the left dorsolateral prefrontal cortex for refractory major depressive disorder. *Neurosurgery* 69, 1015–1029. doi: 10.1227/NEU.0b013e318229cfcd

Lafon, B., Henin, S., Huang, Y., Friedman, D., Melloni, L., Thesen, T., et al. (2017). Low frequency transcranial electrical stimulation does not entrain sleep rhythms measured by human intracranial recordings. *Nat Commun.* 8, 1–13. doi: 10.1038/s41467-017-01045-x

Lee, H., Foreman, A., Daum, W., Cohen, R., Gotman, J., and Cole, A. J. (2007). *Treatment of neurological disorders via electrical stimulation, and methods related thereto. Patent No WO2008005478 A3*. Geneva: WIPO.

Lesser, R. P., Crone, N. E., and Webber, W. R. S. (2010). Subdural Electrodes. *Clin. Neurophysiol.* 121, 1376–1392. doi: 10.1016/j.clinph.2010.04.037

Mark, J. E. (1999). *Polymer Data Handbook*. Oxford: Oxford University Press.

Martin, A. K., Dzafic, I., Ramdave, S., and Meinzer, M. (2017). Causal evidence for task-specific involvement of the dorsomedial prefrontal cortex in human social cognition. *Soc. Cogn. Affect. Neurosci.* 12, 1209–1218. doi: 10.1093/scan/nsx063

McCreery, D. B., Agnew, W. F., Yuen, T. G., and Bullara, L. (1990). Charge density and charge per phase as cofactors in neural injury induced by electrical stimulation. *IEEE Trans. Biomed. Eng.* 37, 996–1001. doi: 10.1109/10.102812

Meacham, K. W., Giuly, R. J., Guo, L., Hochman, S., and DeWeerth, S. P. (2008). A lithographically-patterned, elastic multi-electrode array for surface stimulation of the spinal cord. *Biomed Microdevices* 10, 259–269. doi: 10.1007/s10544-007-9132-9

Moro, E., Schwalb, J. M., Piboolnurak, P., Poon, Y. Y. W., Hamani, C., Hung, S. W., et al. (2011). Unilateral subdural motor cortex stimulation improves essential tremor but not Parkinson's disease. *Brain* 134, 2096–2105. doi: 10.1093/brain/awr072

Nahas, Z., Anderson, B. S., Borckardt, J., Arana, A. B., George, M. S., Reeves, S. T., et al. (2010). Bilateral epidural prefrontal cortical stimulation for treatment-resistant depression. *Biol. Psychiatry* 67, 101–109. doi: 10.1016/j.biopsych.2009.08.021

Nguyen, J. P., Lefaucher, J. P., Le Guerinel, C., Eizenbaum, J. F., Nakano, N., Carpentier, A., et al. (2000). Motor cortex stimulation in the treatment of central and neuropathic pain. *Arch. Med. Res.* 31, 263–265.

Nikolin, S., Lauf, S., Loo, C. K., and Martin, D. (2019). Effects of high-definition transcranial direct current stimulation (hd-tdcs) of the intraparietal sulcus and dorsolateral prefrontal cortex on working memory and divided attention. *Front. Integr. Neurosci.* 12:64. doi: 10.3389/fnint.2018.00064

Nunez, P. L., and Srinivasan, R. (2006). *Electric Fields of the Brain: The neurophysics of EEG*, 2nd Edn. New York, NY: Oxford University Press, doi: 10.1093/acprof:oso/9780195050387.001.0001

Ochoa, M., Wei, P., Wolley, A. J., Otto, K. J., and Ziaie, B. (2013). A Hybrid PDMS-Parylene subdural multi-electrode array. *Biomed Microdevices* 15, 437–443. doi: 10.1007/s10544-013-9743-2

Pagni, C. A., Altibrandi, M. G., Bentivoglio, A., Caruso, G., Cioni, B., Fiorella, C., et al. (2005). Extradural motor cortex stimulation (EMCS) for Parkinson's disease. History and first results by the study group of the Italian neurosurgical society. *Acta Neurochir. Suppl.* 93, 113–119. doi: 10.1007/3-211-27577-0_19

Paxinos, G., and Watson, C. (2007). *The Rat Brain in Stereotaxic Coordinates*. Amsterdam: Elsevier.

Peters, M. J., Stinstra, G., and Hendriks, M. (2001). Estimation of the electrical conductivity of human tissue. *Electromagnetics* 21, 545–557. doi: 10.1080/027263401752246199

Priori, A., and Lefaucheur, J.-P. (2007). Chronic epidural motor cortical stimulation for movement disorders. *Lancet Neurol.* 6, 279–286. doi: 10.1016/S1474-4422(07)70056-X

Salam, M. T., Gélinas, S., Desgent, S., Duss, S., Bernier Turmel, F., Carmant, L., et al. (2014). Subdural porous and notched mini-grid electrodes for wireless intracranial electroencephalographic recordings. *J. Multidiscip. Healthc.* 7, 573–586. doi: 10.2147/JMDH.S64269

So, P. P. M., Stuchly, M. A., and Nyenhuis, J. A. (2004). Peripheral nerve stimulation by gradient switching fields in magnetic resonance imaging. *IEEE Trans. Biomed. Eng.* 51, 1907–1914. doi: 10.1109/TBME.2004.834251

Tsubokawa, T., Katayama, Y., Yamamoto, T., Hirayama, T., and Koyama, S. (1991).). Chronic motor cortex stimulation for the treatment of central pain. *Acta Neurochir. Suppl.* 52, 137–139. doi: 10.1007/978-3-7091-9160-6_37

Tsubokawa, T., Katayama, Y., Yamamoto, T., Hirayama, T., and Koyama, S. (1993). Chronic motor cortex stimulation in patients with thalamic pain. *J. Neurosurg.* 78, 393–401. doi: 10.3171/jns.1993.78.3.0393

Volkmann, J., Wolters, A., Kupsch, A., Muller, J., Kuhn, A. A., Schneider, G.-H., et al. (2012). Pallidal deep brain stimulation in patients with primary generalised or segmental dystonia: 5-year follow-up of a randomised trial. *Lancet Neurol.* 11, 1029–1038. doi: 10.1016/S1474-4422(12)70257-0

Vöröslakos, M., Takeuchi, Y., Fernández-ruiz, A., Kozák, G., Buzsáki, G., Berényi, A., et al. (2018). Direct effects of transcranial electric stimulation on brain circuits in rats and humans. *Nat Commun.* 9:483. doi: 10.1038/s41467-018-02928-3

Yuen, T. G., Agnew, W. F., Bullara, L. A., Jacques, S., and McCreery, D. B. (1981). Histological evaluation of neural damage from electrical stimulation: considerations for the selection of parameters for clinical application. *Neurosurgery* 9, 292–299. doi: 10.1227/00006123-198109000-00013

Zhang, K., Bhatia, S., Oh, M. Y., Cohen, D., Angle, C., and Whiting, D. (2010). Long-term results of thalamic deep brain stimulation for essential tremor. *J. Neurosurg.* 112, 1271–1276. doi: 10.3171/2009.10.JNS09371

Conflict of Interest Statement: The authors declare that the research was conducted in the absence of any commercial or financial relationships that could be construed as a potential conflict of interest.

frontiers in Neuroscience

ORIGINAL RESEARCH
published: 10 September 2019
doi: 10.3389/fnins.2019.00891

Effect of User Practice on Prosthetic Finger Control With an Intuitive Myoelectric Decoder

Agamemnon Krasoulis[1,2]*, *Sethu Vijayakumar*[1] *and Kianoush Nazarpour*[2,3]*

[1] School of Informatics, University of Edinburgh, Edinburgh, United Kingdom, [2] School of Engineering, Newcastle University, Newcastle upon Tyne, United Kingdom, [3] Institute of Neuroscience, Newcastle University, Newcastle upon Tyne, United Kingdom

Machine learning-based myoelectric control is regarded as an intuitive paradigm, because of the mapping it creates between muscle co-activation patterns and prosthesis movements that aims to simulate the physiological pathways found in the human arm. Despite that, there has been evidence that closed-loop interaction with a classification-based interface results in user adaptation, which leads to performance improvement with experience. Recently, there has been a focus shift toward continuous prosthesis control, yet little is known about whether and how user adaptation affects myoelectric control performance in dexterous, intuitive tasks. We investigate the effect of short-term adaptation with independent finger position control by conducting real-time experiments with 10 able-bodied and two transradial amputee subjects. We demonstrate that despite using an intuitive decoder, experience leads to significant improvements in performance. We argue that this is due to the lack of an utterly natural control scheme, which is mainly caused by differences in the anatomy of human and artificial hands, movement intent decoding inaccuracies, and lack of proprioception. Finally, we extend previous work in classification-based and wrist continuous control by verifying that offline analyses cannot reliably predict real-time performance, thereby reiterating the importance of validating myoelectric control algorithms with real-time experiments.

Keywords: surface electromyography, myoelectric control, myoelectric prostheses, short-term adaptation, machine learning

OPEN ACCESS

Edited by:
Jose Luis Contreras-Vidal, University of Houston, United States

Reviewed by:
Kazutaka Takahashi, University of Chicago, United States
Sean Kevin Meehan, University of Waterloo, Canada

***Correspondence:**
Agamemnon Krasoulis
agamemnon.krasoulis@newcastle.ac.uk
Kianoush Nazarpour
kianoush.nazarpour@newcastle.ac.uk

Specialty section:
This article was submitted to Neuroprosthetics, a section of the journal Frontiers in Neuroscience

Received: *22 March 2019*
Accepted: *08 August 2019*
Published: *10 September 2019*

Citation:
Krasoulis A, Vijayakumar S and Nazarpour K (2019) Effect of User Practice on Prosthetic Finger Control With an Intuitive Myoelectric Decoder. Front. Neurosci. 13:891. doi: 10.3389/fnins.2019.00891

INTRODUCTION

State-of-the-art commercial prosthetic hands exhibit hardware capabilities that could potentially allow their users to independently control individual fingers. However, this feature is almost never utilized; instead, most current prosthetic systems still employ the conventional amplitude-based, dual-site electromyogram (EMG) mode switching paradigm for grip selection and actuation (Farina et al., 2014). Due to using a highly-non-intuitive control interface, the efficacy of this method relies on user experience gathered during daily interaction with the device. It has been previously shown, and is currently well-accepted, that humans are capable of greatly improving their control of mode switching myoelectric interfaces within only a few days of training (Bouwsema et al., 2010; Clingman and Pidcoe, 2014).

Moving toward more natural interfaces, a large body of research has investigated the potential of pattern recognition methods for providing users with the ability to directly access desired

control modes, such as hand grips and/or wrist functions. The idea of EMG signal classification for prosthetic control has been around for almost half a century (Herberts et al., 1973) and has recently found its way into commercial adoption[1]. Although classification-based control is regarded as an intuitive scheme, there has been evidence that experience can still lead to substantial performance improvement (Bunderson and Kuiken, 2012; Powell et al., 2014; He et al., 2015; Hargrove et al., 2017). This can be attributed to various causes, for example, an increase in class separability (Bunderson and Kuiken, 2012) and movement repeatability (Powell et al., 2014), even in the absence of any form of feedback (He et al., 2015). Recently, a clinical study involving transhumeral amputees having undergone targeted muscle reinnervation reported a significant increase in classification-based myoelectric control performance within 2 months of daily use (Hargrove et al., 2017).

The grip classification approach can offer a remarkable improvement of the intuitiveness and ease of use of the prosthetic device. However, it suffers from two main limitations: (1) it results in severe under-actuation of the prosthesis, which dramatically limits its functionality, as the user can only have access to a set of pre-determined modules; and (2) it is sequential in nature, that is, a single class of movement can be active at a time, as opposed to the natural continuous and asynchronous finger movement exhibited by the human hand. One way of enhancing the dexterity of powered myoelectric prostheses is via continuous and simultaneous control of multiple degrees of freedom (DOFs) (Fougner et al., 2012). Arguably, the primary focus of continuous myoelectric control has previously been on restoring wrist function (Hahne et al., 2014; Jiang et al., 2014; Muceli et al., 2014; Smith et al., 2014). Nevertheless, over the last decade several groups have also addressed the challenge of using surface EMG signals to reconstruct kinematic variables (e.g., position or velocity) of independent finger movement, both offline (Afshar and Matsuoka, 2004; Smith et al., 2008; Ngeo et al., 2014; Krasoulis et al., 2015b; Xiloyannis et al., 2017) and in real-time (Smith et al., 2009; Cipriani et al., 2011; Ngeo et al., 2013). As compared to non-invasive methods, intramuscular recordings offer the advantage of lower level of muscle cross-talk (Birdwell et al., 2013), hence making it possible to create multiple one-to-one mappings between specific muscles and prosthesis degrees of actuation (DOAs). This opportunity has been explored in the context of controlling both virtual (Birdwell et al., 2015) as well as prosthetic (Cipriani et al., 2014) hands. Besides finger position and velocity decoding, individual fingertip forces have also been reconstructed offline (Castellini et al., 2009; Nielsen et al., 2011) and in real-time (Gijsberts et al., 2014; Gailey et al., 2017; Patel et al., 2017) using surface (EMG) signals.

Continuous myoelectric control strategies, which are often referred to as *proportional* (Fougner et al., 2012), are typically intuitive, that is, they operate based on physiological associations between muscle (co)-activation patterns and prosthesis DOAs. They usually require an initial phase of data collection for subject-specific model training. A promising alternative is based on user adaptation (Dyson et al., 2018), whereby muscle signals control the prosthesis DOAs using pre-defined, subject-independent mappings. This approach heavily relies on user adaptation taking place during closed-loop control, therefore the provision of continuous feedback (e.g., visual) during user training is necessary. There has been increasing evidence that humans are able to develop novel task-specific muscle synergies, that is, muscle co-activation patterns, to achieve high-level performance in a variety of tasks, including two-dimensional cursor position control (Nazarpour et al., 2012; Pistohl et al., 2013, 2015; Antuvan et al., 2014; Dyson et al., 2017, 2018), prosthetic finger position (Pistohl et al., 2013), and high-dimensional robotic arm control (Ison and Artemiadis, 2015; Ison et al., 2016). Notably, it has been found that such synergistic patterns can be learnt even when they are not intuitive from a physiological perspective, for instance, due to requiring the co-activation of antagonist muscles (Nazarpour et al., 2012).

In comparison with non-intuitive interfaces, whereby an inverse model has to be learnt from scratch, the effect of user experience on myoelectric control performance when using an intuitive, regression-based approach is much less understood. In the context of 2-DOF continuous wrist control, a previous study showed that while three machine learning algorithms yielded statistically different offline decoding accuracies, the performance of the three algorithms was comparable during real-time myoelectric control (Jiang et al., 2014). Additionally, only weak, mainly non-significant correlations were observed between offline and real-time control performance measures. These findings support the view that user adaptation mechanisms that take place during closed-loop interaction affect ultimate real-time control performance, thereby questioning the extent to which offline myoelectric control studies can inform clinical translation of advanced upper-limb prostheses. Similar findings have been also reported in the context of myoelectric classification (Ortiz-Catalan et al., 2015; Vujaklija et al., 2017). Furthermore, a study showed that real-time, regression-based prosthetic wrist control might be less susceptible to perturbations, for example, due to noise in EMG signals, than its offline decoding counterpart (Hahne et al., 2017). This observation provides evidence that humans can user error correction mechanisms to compensate for decoding inaccuracies during closed-loop interaction with myoelectric interfaces. With regard to prosthetic finger control, several studies have attempted to push the boundaries of offline decoding accuracy (Ngeo et al., 2014; Xiloyannis et al., 2017). However, substantially less effort has been made toward understanding whether and in what manner user adaptation can affect real-time control performance.

In this work, we investigate the effect of user adaptation in continuous prosthetic finger control in able-bodied and transradial amputee subjects. We hypothesize that however intuitive a myoelectric task might be, experience gathered during interaction with the interface would still lead to performance improvement. We evaluate our hypothesis using two intuitive finger control schemes, namely, EMG-based finger position control and teleoperation with an instrumented data glove. Additionally, we investigate the effect of user experience on the power of the recorded EMG signals and the variability of the controllable DOAs. Finally, we extend previous work on

[1]https://www.coaptengineering.com/

myoelectric classification and continuous wrist control (Ortiz-Catalan et al., 2015; Vujaklija et al., 2017), by demonstrating that it is not possible to reliably predict real-time prosthetic finger control performance solely based on the outcomes of offline decoding analyses. To the best of the authors' knowledge, this is the first study to systematically demonstrate the positive impact of short-term adaptation, achieved through biofeedback user training, on intuitive, dexterous prosthetic finger control both with EMG-based decoding, as well as during robotic hand teleoperation with a data glove.

MATERIALS AND METHODS

Participant Recruitment

Ten able-bodied (nine male, one female; all right-hand dominant; median age, 26.5 years) and two male, right-hand transradial amputee subjects were recruited. Both amputees were right-hand dominant prior to amputation. Some of the able-bodied (5 out of 10) and both amputee participants had previously taken part in classification-based myoelectric control experiments (Krasoulis et al., 2017).

Hardware and Signal Acquisition

For the able-bodied group, 16 Delsys Trigno™ sensors (Delsys, Inc.) were placed on the participants' right forearm arranged in two rows of eight equally spaced sensors, without targeting specific muscles. The two rows were placed 3 and 5.5 cm, respectively, below the elbow. Photographs showing electrode placement for an able-bodied participant are shown in **Figures 1A,B**. Using a similar configuration, 13 and 12 sensors were used, respectively, for the two amputee participants, due to limited space availability on their remnant limb (right limb in both subjects). Prior to sensor placement, participants' skin was cleansed using 70% isopropyl alcohol. Elastic bandage was used to secure the sensor positions throughout the experimental sessions. Following sensor placement, the quality of all EMG channels was verified by visual inspection. The sampling frequency of EMG signals was set to 1,111 Hz.

An 18-DOF CyberGlove II data glove (CyberGlove Systems LLC) was used to record hand kinematic data from the participants' left hand (**Figures 1C,D**). For each participant, the glove was calibrated prior to data collection using dedicated software provided by the manufacturer. The sampling rate of glove data was 25 Hz.

For the real-time control experiments, we used a right model of the IH2 Azzurra hand (Prensilia s.r.l.), which is an externally-powered, underactuated (11 DOFs, 5 DOAs) anthropomorphic hand. It comprises 4 intrinsic motors controlling flexion and extension of the five digits (the ring and little fingers are mechanically coupled) and an additional motor controlling thumb rotation. The robotic hand is shown in **Figures 1E,F**.

Experimental Design

Participants sat comfortably on an office chair and rested both arms on a computer desk. Each participant completed one experimental session, which comprised two main phases: (1) *initial data collection*, and (2) *real-time robotic hand control*. Each experimental session lasted around 140 min, which included: skin preparation, electrode positioning, and signal inspection (20 min); initial data collection (60 min); short interval (20 min); and real-time control of the robotic hand (40 min).

Initial Data Collection

In the first part of the experiment, participants were asked to reproduce a series of motions instructed to them on a computer monitor. Nine exercises were selected for data collection ranging from individuated-finger to full-hand motions. The nine motions comprised: thumb flexion/extension, thumb abduction/adduction, index flexion/extension, middle flexion/extension, ring/little flexion/extension, index pointer, cylindrical grip, lateral grip, and tripod grip (**Figure S1**). All participants were asked to perform bilateral mirrored movements with both their arms resting on a computer desk.

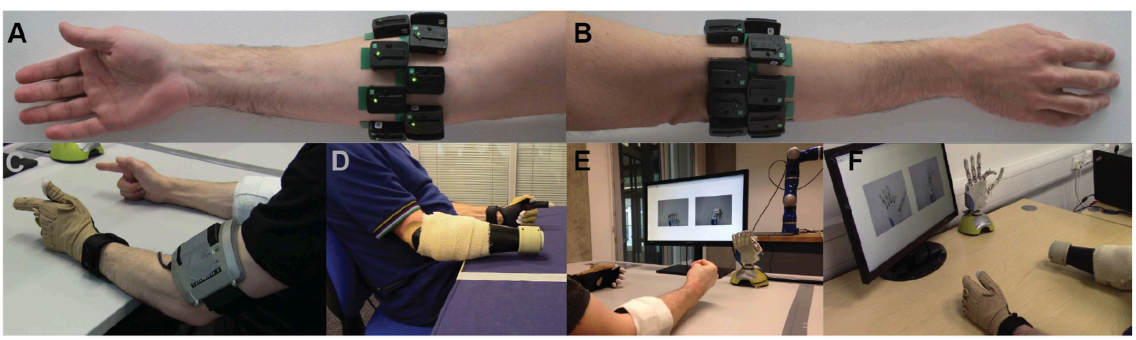

FIGURE 1 | Experimental setup. Surface EMG electrodes were placed on subjects' forearm below the elbow in two rows of equally spaced electrodes. **(A)** Palmar and **(B)** dorsal views of the forearm. Refer to main text for details on number of electrodes used for able-bodied and amputee participants. **(C,D)** Bilateral mirrored movement training. Able-bodied and amputee participants shown during initial data collection. Muscle activity was recorded from the participants' right forearm (i.e., the remnant limb for amputees), whereas hand kinematic data were recorded from the participants' left hand with an 18-DOF data glove. **(E,F)** Real-time posture matching task. Able-bodied and amputee participants shown while they modulate their muscle activity to control the finger positions of the robotic hand. The target postures for the shown trials were **(E)** full cylindrical grip and **(F)** half index flexion.

We recorded three datasets (i.e., separate blocks of trials) for each participant during this phase of the experiment: the first two (*training* and *validation* sets) comprised 10 repetitions of each motion, and the third one (*testing* set), only two. Each motion execution lasted ∼7 s and at the end of each trial subjects were instructed to return to the rest pose which corresponded to complete muscle relaxation (shown in **Figure S1A**). Succeeding trials were interleaved with intervals of 3 s and participants were also given a 10 min break after the completion of each block of trials.

Signal Pre-processing

We used a sliding window approach to process the EMG signals. The length of the window was set to 128 ms with an increment of 50 ms (60% overlap). The following time-domain features were extracted from the recorded EMG channels: Wilson amplitude, 4th-order auto-regressive coefficients, waveform length, log-variance, and slope sign change (Boostani and Moradi, 2003; Hahne et al., 2014). The columns of the design (i.e., feature) matrices were subsequently standardized via mean subtraction and inverse standard deviation scaling. Feature means and standard deviations were estimated using training data only.

For the hand kinematic data that were recorded with the data glove, we computed the mean value within the processing window for each DOF individually. The calibrated glove measurements were converted into digit positions for the prosthetic hand using a linear mapping (see **Supplementary Methods**). The columns of the target matrices containing the prosthetic hand joint positions were finally normalized in the range $[0, 1]$, where $y_j = 0$ corresponds to full extension and $y_j = 1$ to full flexion of the jth DOA, respectively.

Model Training, Prediction Post-processing, and Hyper-Parameter Optimization

Model training took place during the short resting interval between the initial data collection and real-time control evaluation. To decode finger positions from muscle activity, we deployed a regularized version of the Wiener filter, implemented using auto- and cross-correlation matrices (Perreault et al., 1999), which we have previously used to reconstruct finger position trajectories from myoelectric data offline (Krasoulis et al., 2015a,b). We have shown in previous work that the generalization of this decoder is comparable to that of non-linear regression algorithms when tested on movements outside the training set (Krasoulis et al., 2015b). The Wiener filter is a classical signal processing method for estimating a target variable using linear time-invariant filtering (e.g., spatial or temporal). In other words, at time instance n, each input x_d (i.e., EMG feature) is convolved with a finite impulse response function to produce an output y (i.e., digit position of a single DOA of the prosthetic hand):

$$y[n] = \sum_{d=1}^{D} \sum_{m=0}^{M-1} h_d[m]\, x_d[n-m], \tag{1}$$

where $h_d[m]$ accounts for the contribution of the input d at time instance m, $x_d[n-m]$ is the activation of the input d at time $n-m$, M is the filter length, and we also assume a finite number of samples $n = 1, \ldots, N$. We set the length of the linear filters to 300 ms, which corresponds to including at each time step $M = 6$ previous time lags, assuming a fixed window increment of 50 ms. The number of EMG electrodes used for decoding varied across subjects and was based on a sequential selection algorithm (described below). When the full set of sensors was used, the input dimensionality was $D = 672$ (i.e., 7 EMG features / (electrode × time bin) × 16 electrodes × 6 time bins). The output dimensionality was $K = 5$, that is, the number of DOAs of the robotic hand. For covariance matrix estimation, we used L_2 regularization to avoid inversion of potentially ill-conditioned matrices due to the high dimensionality of the input space.

We post-processed predictions using exponential smoothing to ensure smooth digit trajectories. We implemented this in the time-domain as follows:

$$\tilde{y}_j[n] = \alpha \cdot y_j[n] + (1-\alpha) \cdot \tilde{y}_j[n-1], \tag{2}$$

where $y_j[n]$ and $\tilde{y}_j[n]$ denote, respectively, the raw and smoothed predictions of the jth DOA at time step n, and α is the smoothing parameter, which is constrained by $0 \leq \alpha \leq 1$. Smaller values of α result in stronger smoothing, that is, a smaller cutoff frequency when smoothing is viewed as a low-pass filter, but also increase the prediction response latency.

We performed three types of model selection (i.e., hyper-parameter tuning) for each participant during the training phase: sensor selection, regularization, and smoothing parameter optimization. Models were initially trained using data from the training set only. Model selection was carried out by means of maximizing performance on the validation set. Following parameter optimization, the training and validation sets were merged and used to train final models. The test set was only used to evaluate and report offline performance of the final models.

Offline reconstruction accuracy was assessed using the multivariate (R^2) metric defined as:

$$R^2_{MV} = 1 - \frac{\sum_{k=1}^{K} \sum_{n=1}^{N} \left(y_{k,n} - \hat{y}_{k,n}\right)^2}{\sum_{k=1}^{K} \sum_{n=1}^{N} \left(y_{k,n} - \bar{y}_k\right)^2}, \tag{3}$$

where K denotes the dimensionality of the target variable (in our case $K = 5$), N is the number of samples in the measurement/prediction vector, $y_{k,n}$ and $\hat{y}_{k,n}$ are the nth observed and predicted values of the kth output variable, respectively, and $\bar{y}_k$ denotes the sample mean of the kth output variable.

For sensor selection, a standard sequential forward method was used (Pudil et al., 1994). That is, the selection algorithm started with an empty set and at each iteration the sensor that yielded the highest reconstruction accuracy improvement was added to the pool. The algorithm terminated execution when the inclusion of any remaining sensors caused a decrease in average performance. The number of used sensors varied from 8 to 16, with a median value of 12. To optimize the regularization parameter λ of the Wiener filter, a search was performed in the log-space $\{10^{-6}, 10^{-5}, \ldots, 10^{1}\}$ using a factor (i.e., multiplicative

step) of 10. Finally, the exponential smoothing parameter α (Equation (2)) was optimized via linear search in the range $[0, \ldots, 1]$ with a step size of 0.01. The three model selection steps were performed sequentially in the following order: sensor selection, λ optimization, and α optimization. In other words, the subset of sensors was firstly identified; using the selected subset, the regularization parameter λ was tuned; finally, using the selected sensor subset and chosen value for λ, the smoothing parameter α was optimized.

Real-Time Control and Evaluation

A real-time, biofeedback, posture matching task was designed to assess the efficacy of the regression-based control scheme and provide insight into the effect of user practice on prosthetic finger control. To that end, two scenarios were investigated: in *EMG control mode*, participants were required to modulate their muscle activity to control the prosthetic hand by making use of the regression model; in *glove control mode*, participants teleoperated the hand using the data glove worn on their contralateral hand, that is, the intact limb for the amputee participants. The glove control mode was included for two reasons: to provide an estimate of the upper-bound of prosthetic control performance for the designed experimental task (i.e., *benchmark*); and to investigate whether user practice leads to performance improvement during prosthetic finger control with a direct, natural control interface.

Participants were presented with a series of target postures on the screen and were instructed to control the hand to match the desired postures as closely as possible. Image prompts were only used at this stage, as opposed to the training data collection phase, where participants were instructed to follow video prompts. During the task, the robotic hand was connected to a base stand placed on the surface of the desk and sitting in front of the participant (**Figures 1E,F**). Nine hand postures were included, each of them with two variations, half and full activation. Therefore, the total number of postures in the real-time experiment was 18. The included hand postures were: thumb abduction, thumb flexion, index flexion, middle flexion, ring/little flexion, index pointer, cylindrical grip, lateral grip, and pinch grip (**Figure S2**).

At the start of each trial, the participants were presented with a pair of static pictures providing front and side views of the desired posture. An audio cue (waveform, sine wave; frequency, 400 Hz; duration, 500 ms) was used to signal the initiation of the trial. Participants were then given 3.5 s to drive the prosthetic hand into the desired posture. At the end of this period, a second audio cue (waveform, sine wave; frequency, 800 Hz; duration, 500 ms) was used to signal the initiation of the evaluation phase of the trial, which lasted 1.5 s. During the evaluation phase, participants were instructed to hold the hand in the performed posture. At the end of the evaluation phase, the hand was reset to its initial posture (i.e., fully open) signaling the end of the trial. Pictures illustrating the real-time posture matching task are shown in **Figures 1E,F** for two participants, one able-bodied and one amputee.

At the end of each trial, participants received a score characterizing their performance. This score was based on the average mean absolute error (MAE) between the target and performed postures during the evaluation phase (i.e., the last 1.5 s) of the trial. Let $\boldsymbol{y}$ and $\hat{\boldsymbol{y}}$ denote K-dimensional vectors in a real vector space. In our case, the two vectors represent the target and performed postures, respectively, of the prosthetic hand at a given time step and $K = 5$ is the number of DOAs of the hand. The MAE is defined as:

$$MAE = \frac{1}{K} \left|\left| \boldsymbol{y} - \hat{\boldsymbol{y}} \right|\right|_1 = \frac{1}{K} \sum_{j=1}^{K} \left| y_j - \hat{y}_j \right|, \tag{4}$$

where y_i and $\hat{y}_i$ denote, respectively, the target and true positions of the jth DOA. The evaluation phase lasted for 1.5 s, and a finger position update was made every 50 ms, that is, the increment time of the sliding window. Thus, there were $N = 300$ distance samples associated with each trial. The average distance during the evaluation phase of a trial was estimated by computing the median across the samples of the population.

To provide the participants with an intuitive performance measure for each trial, MAEs were transformed into scores in the range of 0 to 100%. This transformation was achieved as follows: firstly, a baseline average MAE score between the target posture and random predictions was established by simulating 10^6 random predictions uniformly sampled in the range $[0, 1]$; the normalized score was then computed as:

$$\text{normalized score} = \max\left\{0, \left(1 - \frac{\overline{MAE}}{\overline{MAE_r}}\right)\right\} \times 100\%, \tag{5}$$

where $\overline{MAE}$ denotes the population average (i.e., median) MAE during the evaluation phase, and $\overline{MAE_r}$ is the pre-computed, average random prediction error for the specified posture. This transformation ensured that a perfect reproduction of the desired posture would correspond to a 100% score, whereas a randomly performed posture would yield a score close to 0%. Negative scores were not allowed by the max operation. The random seed was controlled during the experiments to ensure the use of identical random predictions for all participants.

The posture matching task was split into several blocks. Within each block, all 18 postures were presented to the participants exactly once in a pseudo-randomized order. Each participant performed six blocks for each control mode (i.e., EMG and glove control, see Results section) therefore the total number of trials for each participant was 108 (i.e., 6 blocks $\times$ 18 trials/block). The execution of each block lasted $\sim$3 min. At the end of block 3, participants were given a 1 min rest. The stimulus presentation sequence was the same for all participants, but the order of the two control modes was counter-balanced across the two participant groups (i.e., able-bodied and amputee).

Dimensionality Reduction Analysis

Dimensionality reduction analysis was performed by using principal component analysis (PCA) on the envelopes of the EMG signals. EMG envelopes were computed by using a sliding

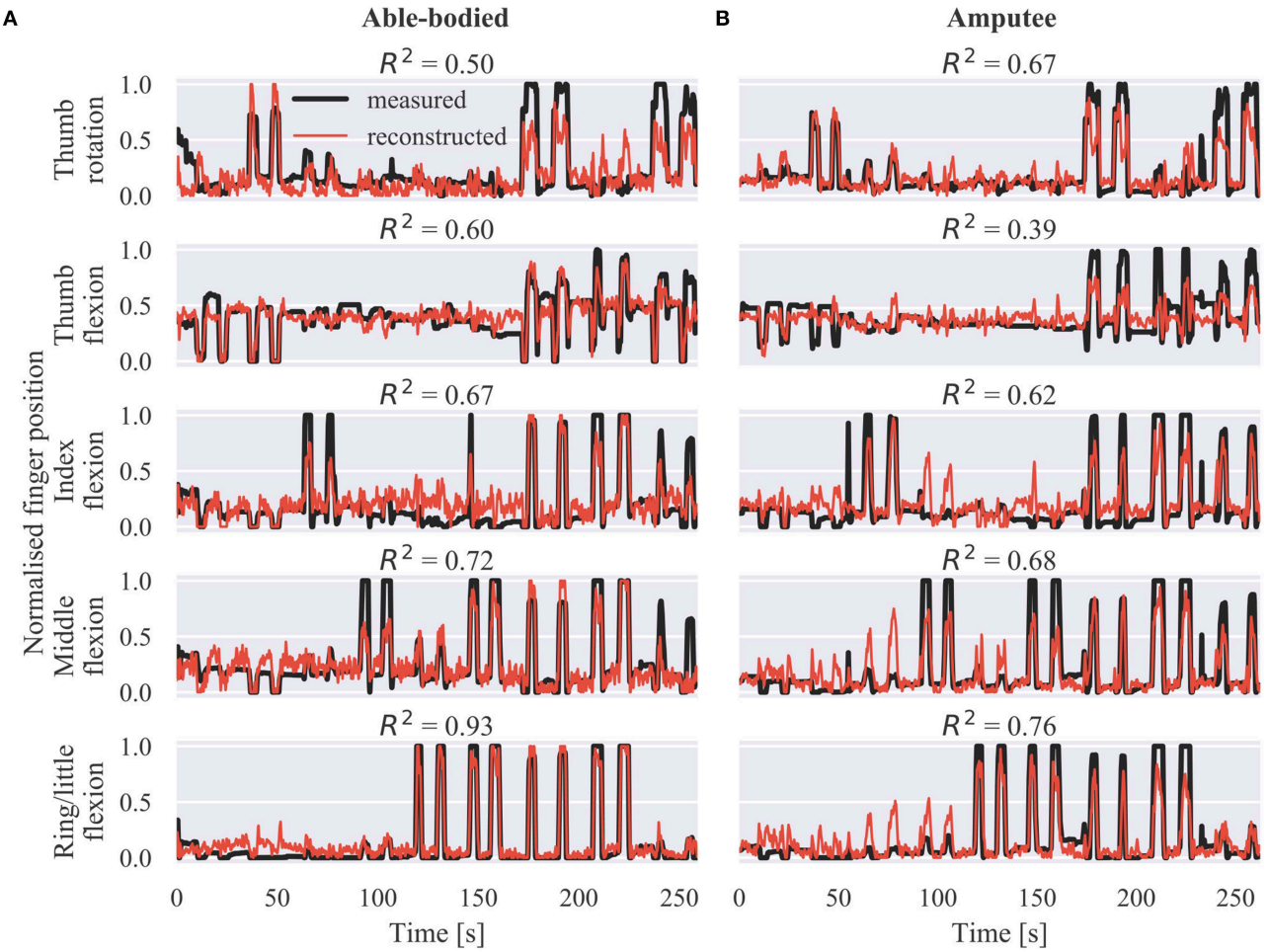

FIGURE 2 | Offline finger position reconstruction. Sample test set predictions shown for the five DOAs of the robotic hand for **(A)** an able-bodied and **(B)** an amputee subject. The shown segments of activity correspond to two repetitions of each of the movements included in the calibration phase, in the following order: thumb flexion/extension, thumb abduction/adduction, index flexion/extension, middle flexion/extension, ring/little flexion/extension, index pointer, cylindrical grip, lateral grip, and tripod grip. R^2, coefficient of determination.

window approach (length 128 ms; window increment 50 ms) and extracting the mean absolute value within the window. All EMG electrodes were used in the analysis, regardless of whether they were used for decoding, therefore the dimensionality of the problem was equal to the total number of electrodes used for each participant (i.e., 16 for able-bodied participants, 13 and 12 for the first and second amputee subjects, respectively). To compare principal components (PCs) extracted from different experimental blocks, the absolute value of the cosine similarity was used, since the sign of PC directions was of no interest; in other words, two identical PC vectors with opposite signs were considered equivalent. The cosine similarity between two vectors $\boldsymbol{a}$ and $\boldsymbol{b}$ is defined as:

$$similarity = \cos(\theta) = \frac{\boldsymbol{ab}}{\|\boldsymbol{a}\| \, \|\boldsymbol{b}\|}. \tag{6}$$

To compare PCs between two different blocks, the PCs of the blocks were first matched in terms of highest cosine similarity. The dimensionality reduction analysis was performed in Python using the scikit-learn library (v.0.19.1) (Pedregosa et al., 2011).

Statistical Analysis

For each participant, single trials were pooled together and used to compute subject-specific summaries. Depending upon the outcomes of D'Agostino-Pearson normality tests, the subject summaries used were either population means, for groups with samples following normal distributions, or medians, otherwise. The size of the summary groups equalled the total number of participants (i.e., $n = 12$). Further normality tests were used to assess the distribution of the summary group samples. For statistical comparisons between groups, paired t-tests were used in the case of normally distributed samples, and Wilcoxon signed-rank tests were used otherwise. The following effect size metrics are reported: for t-tests, the Cohen's d metric; and for Wilcoxon signed-rank tests, the common language effect size (CLES). All statistical analyses were performed in Python using the Pingouin package (Vallat, 2018).

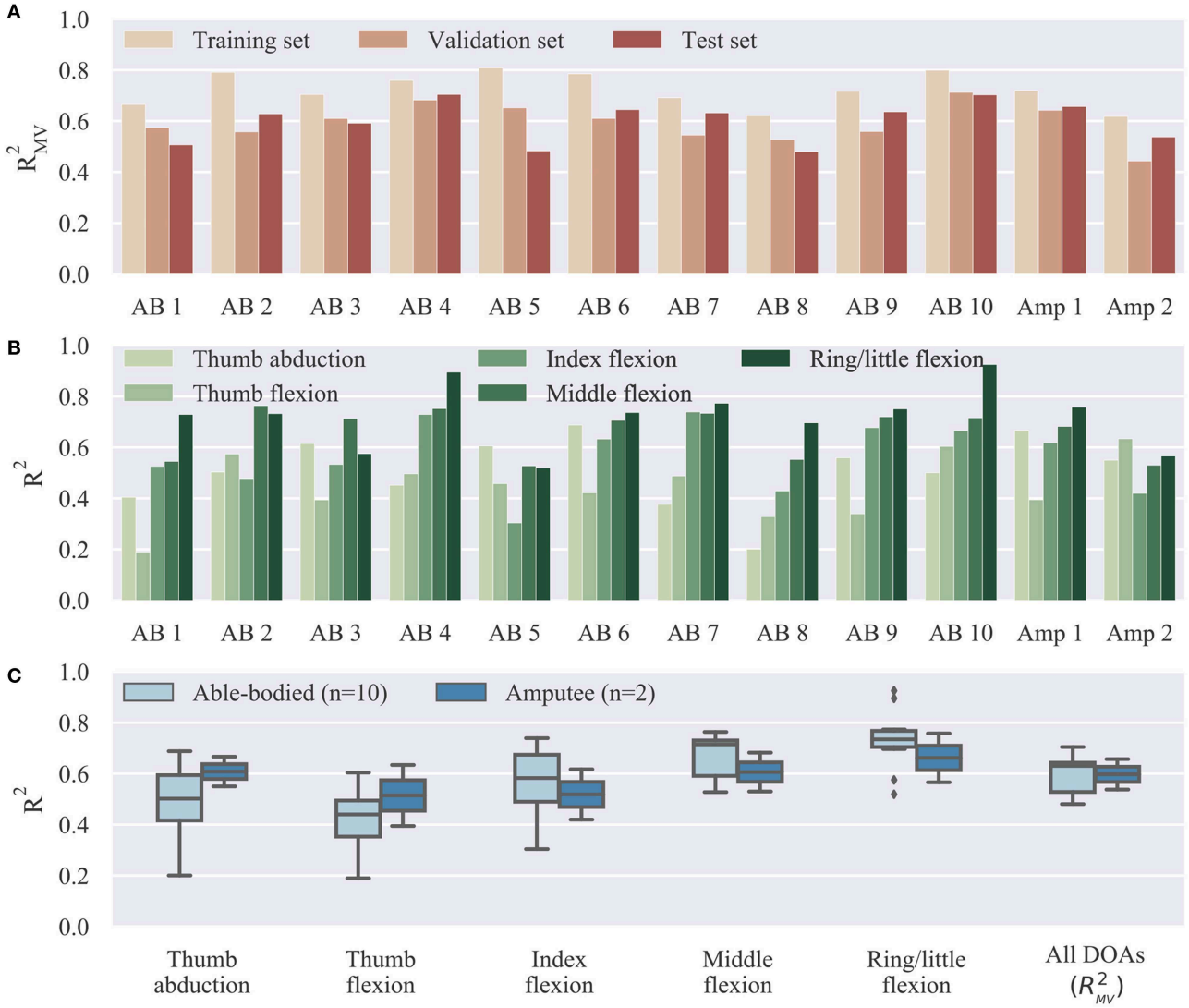

FIGURE 3 | Offline decoding results summary. **(A)** Overall reconstruction accuracy on different datasets (training, validation, and test sets) for individual subjects. The three datasets were used, respectively, for model fitting, hyper-parameter optimization, and final testing. **(B)** Offline reconstruction accuracy for individual DOAs and participants on test set. **(C)** Summary of reconstruction accuracy on test set for individual DOAs and comparison between able-bodied and amputee participants. Bars, means; straight lines, medians; solid boxes, interquartile ranges; whiskers, overall ranges of non-outlier data; diamonds, outliers; AB, able-bodied; Amp, amputee.

RESULTS

Offline Decoding Performance

Representative offline predictions of the positions of the five DOAs of the prosthetic hand are shown in **Figure 2A** for an able-bodied and **Figure 2B** for an amputee participant, respectively. Both graphs show finger trajectories (i.e., normalized positions) in the held-out testing dataset, which comprised two repetitions of each of the nine training exercises (**Figure S1**).

Offline reconstruction accuracy results are summarized in **Figure 3**. The multivariate R^2 is shown in **Figure 3A** for all participants on the three collected datasets, that is, the training, validation, and test sets. As was to be expected, performance on the validation and test sets was slightly inferior to that on the training set. The average offline decoding accuracies in the three datasets were: training set, median 0.72, range 0.19; validation set, median 0.59, range 0.27; test set, median 0.63, range 0.22. **Figure 3B** shows the test set offline accuracy for individual DOAs and participants. The highest average decoding accuracy was achieved for the ring/little fingers DOA (median 0.73, range 0.41) followed by the middle finger DOA (median 0.71, range 0.24). The worst performance was observed for the thumb flexion DOA (median 0.44, range 0.45). This pattern was observed in four out of 12 participants. Finally, an overall summary is provided in **Figure 3C**, separately for the able-bodied and amputee groups. The average accuracy scores for the two

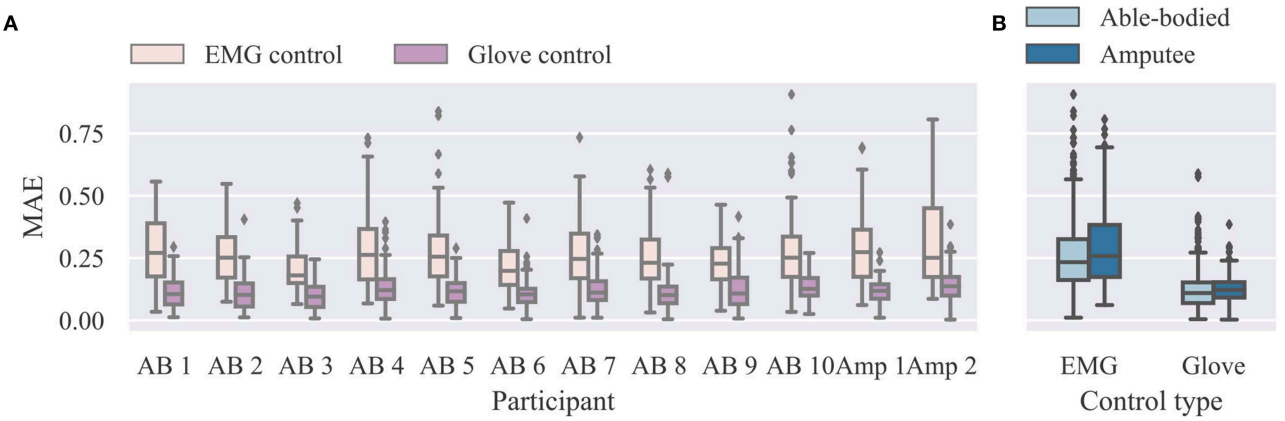

FIGURE 4 | Summary results for real-time experiment. **(A)** Individual MAE scores for EMG and glove control modes. Lower scores indicate better performance. **(B)** Summary results for able-bodied and amputee groups for the two control modes. Data from all trials and postures are shown ($n = 108$ for each participant and control mode). MAE, mean absolute error; EMG, electromyography.

groups were: able-bodied, median 0.63, range 0.22, $n = 10$; amputee, median 0.60, range 0.12, $n = 2$; n refers to number of participants in each group.

Real-Time Experiment Results

We start our analysis of the real-time control experiment by summarizing the overall performance in **Figure 4**. We report here MAE scores between target and performed postures. A similar analysis of the closely related performance scores presented to participants at the end of the trials is provided in the **Supplementary Material** (Supplementary Results section). Not surprisingly, glove control performance was significantly higher than EMG control ($p = 10^{-9}$, $d = 6.5$, $n = 12$; paired t-test; n refers to total number of participants). The median MAE scores across all participants, blocks, and trials were 0.24 (range 0.90) and 0.11 (range 0.59) for EMG and glove control, respectively. The average MAE scores across all blocks for the two groups were: EMG control, able-bodied, median 0.23, range 0.90, $n = 1080$; EMG control, amputee, median 0.26, range 0.74, $n = 216$; glove control, able-bodied, median 0.11, range 0.58, $n = 1080$; glove control, amputee, median 0.12, range 0.38, $n = 216$; n refers to number of single trials within each participant group and control mode.

We now turn our attention to the effect of user practice on performance during real-time finger control. Learning curves for the real-time task are presented in **Figure 5**, where average performance scores are plotted against the experimental block number (ranging from one to six). In all cases, an improvement in performance can be observed as the block number increases (**Figures 5A,B**). A statistical comparison of early (i.e., 1–2) vs. late (i.e., 5–6) blocks is provided in **Figure 5C**, separately for each control mode. For this analysis, able-bodied and amputee participants have been grouped together. For both control modes, average MAEs were significantly lower in late than in early blocks (EMG control, $p = 0.02$, $d = 0.612$; glove control, $p = 10^{-5}$, $d = 2.49$, paired t-tests, $n = 12$; n hereafter refers to total number of participants). A one-to-one comparison of performance in early vs. late blocks is shown in **Figure 5D**, where each point in the scatter plot corresponds to a single participant and control mode. For EMG control, the performance was higher in late blocks for nine out of 12 participants (one out of two amputees). For glove control, the performance in late blocks was consistently improved for all 12 participants (some points in the plot are overlaid and therefore not visible). Two videos showing one amputee participant performing the first and last blocks of the real-time posture matching task are provided as **Supplementary Material** (**Supplementary Movies 1**, **2**).

Next, we seek to investigate whether user practice can have an effect on the user's muscular activity. As a first step, we perform dimensionality reduction on the recorded EMG envelopes using PCA. The top row of **Figure 6** shows the cosine similarities of the first (**Figure 6A**) and second (**Figure 6B**) PCs between the first and subsequent blocks. The variance explained by the first (**Figure 6C**) and first two (**Figure 6D**) PCs extracted in block 1 is plotted against the block number in the second row of **Figure 6**. In the bottom row of the (**Figures 6E,F**), the percentage of variance explained in each block is shown again against the block number, but this time the PCs used were estimated in the same blocks. For both participant groups, a decrease in similarity between the PCs in the first and subsequent blocks is observed as the block number increases. Similarly, a consistent decreasing trend is observed for the percentage of explained variance by the first two PCs estimated in the first block of trials. When using PCs extracted from the same block, the percentage of variance explained is comparable across blocks.

Additionally, we compare the power of the recorded surface EMG channels across experimental blocks. This analysis is performed separately for the set of electrodes used for real-time decoding and the non-used set. The results of this analysis are presented in **Figure 7A**. For both groups of electrodes we observe a small, but not significant, decrease in median EMG signal power between early and late trials (used electrodes, $p = 0.11$,

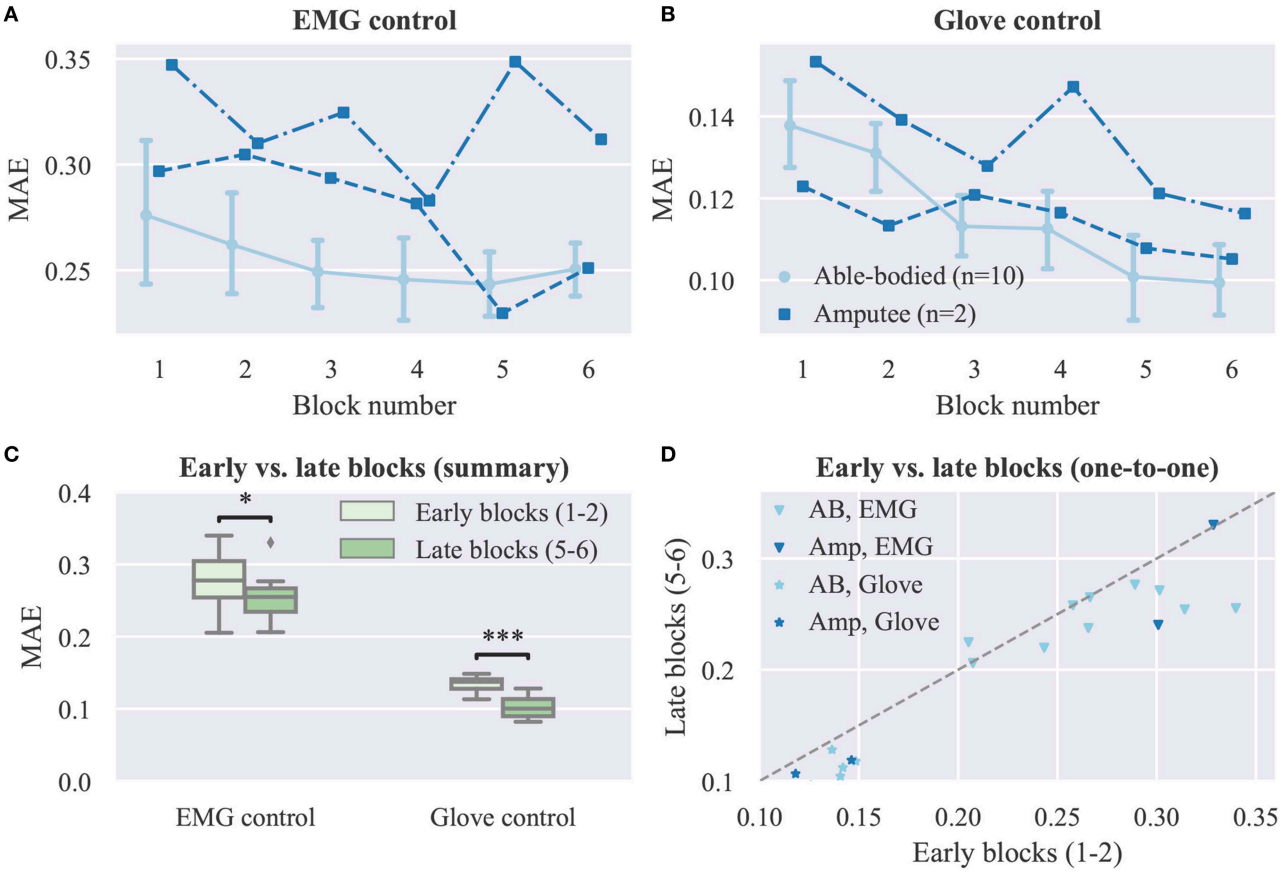

FIGURE 5 | Effect of user practice on task performance (real-time experiment). **(A,B)** MAE scores are plotted against the experimental block number for **(A)** EMG and **(B)** glove control (note different y axis scales). Data for able-bodied participants are presented as means with confidence intervals. Amputee data are shown separately for each of the two individuals. **(C)** Comparison of early vs. late blocks for grouped participants (able-bodied and amputee). Each block lasted 3 min and participants were given a 1 min rest after block 3, therefore blocks 1 and 5 were ~13 min apart. Data shown correspond to subject averages across blocks for all participants (i.e., 10 able-bodied and two amputees). Within each block, participants replicated 18 hand postures presented to them exactly once in a pseudo-randomized order. **(D)** One-to-one comparisons of early vs. late block averages for all participants. Each point in the scatter plot corresponds to a single participant and control mode. Points, means; error bars, 95% confidence intervals estimated via bootstrapping (1,000 iterations); $^{*}p < 0.05$; $^{***}p < 0.001$.

$CLES = 0.632$; non-used electrodes, $p = 0.12$, $CLES = 0.636$; $n = 12$ in both cases, Wilcoxon signed-rank tests). Similarly, we assess the effect of user practice on the variability of the controllable DOAs, that is, the robotic hand finger positions. Variability is assessed in terms of standard deviation during the evaluation phase of the posture matching task. The results of this analysis are presented in **Figure 7C** separately for EMG and glove control. For EMG control, a significant decrease in finger position variability between early and late blocks is observed ($p = 0.01$, $CLES = 0.778$). Conversely, for glove control, there is no difference between early and late blocks ($p = 0.84$, $CLES = 0.556$, $n = 12$, Wilcoxon signed-rank tests). One-to-one comparisons of average EMG power and finger position variability between early and late blocks are shown in **Figures 7C,D**, respectively, where each point in the scatter plots corresponds to a single participant and decoding condition.

Finally, we investigate whether offline decoding accuracy can provide a reliable predictor of real-time control performance. For this reason, we compute the average MAE for each subject across all trials and blocks and compare this metric to the respective offline reconstruction accuracy score for the same subject on the test set. The results of this analysis are presented in **Figure 8**, where each point in the plot corresponds to a single participant. A very weak, non-significant ($p = 0.69$, $n = 12$) negative correlation is observed between offline reconstruction accuracy (i.e., multivariate R^2) and average real-time error (i.e., MAE). Based on this observation, we conclude that it is not possible to predict the performance of real-time finger position control solely based on offline accuracy scores.

DISCUSSION

The goal of this study was to investigate the effect of user practice on performance during intuitive, individual finger prosthesis control. A large body of previous work has shown that controlling a prosthesis using a non-intuitive interface, such as two-site EMG

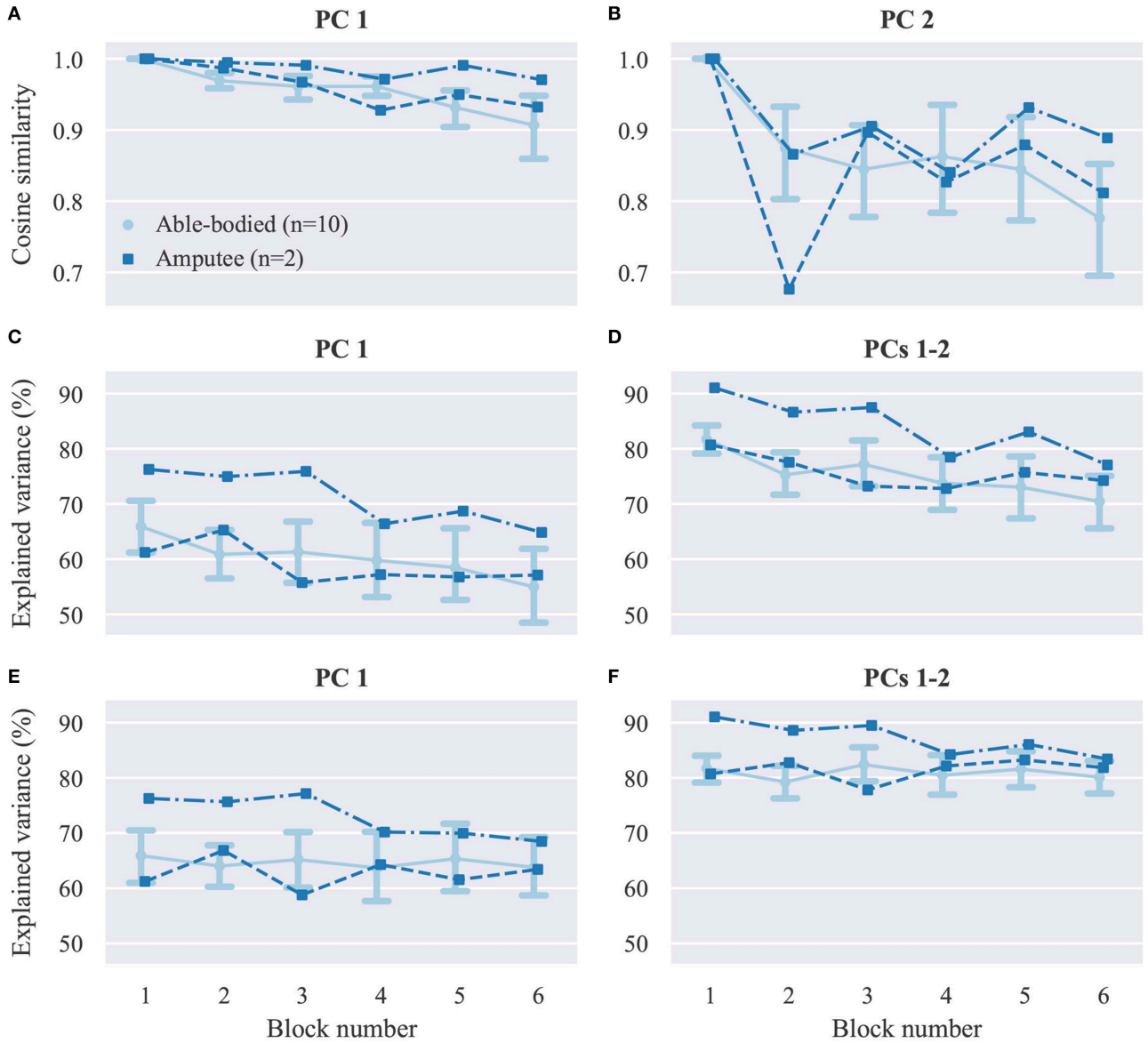

FIGURE 6 | Dimensionality reduction analysis. **(A,B)** Average cosine similarities between **(A)** first **(B)** and second PCs in each block with the respective PCs computed in block 1. **(C,D)** Percentage of explained variance in each block by the **(C)** first and **(D)** first two PCs computed in block 1. **(E,F)** Percentage of explained variance in each block by **(E)** first and **(F)** first two PCs computed in the same block. PC, principal component. Data for able-bodied participants are presented as means with confidence intervals. Amputee data are shown separately for each of the two individuals.

mode switching, requires motor skills that can be developed via frequent interaction with the device (Bouwsema et al., 2010; Clingman and Pidcoe, 2014). With regard to proportional, that is, continuous myoelectric control, there has been evidence that experience can lead to formation of novel, task-specific muscle synergies when the association between muscle co-activations and the DOFs of the output device is non-intuitive from a physiological perspective (Radhakrishnan et al., 2008; Nazarpour et al., 2012; Pistohl et al., 2013; Ison and Artemiadis, 2015). Therefore, non-intuitive paradigms may require training before a user is able to control a prosthesis at its full capacity. On the other hand, the use of more intuitive interfaces, such as those based on multi-site EMG signal classification, can alleviate some of this burden due to relying on a natural association between muscle contractions and prosthesis activations. Previous work has shown that even in the case of intuitive interfaces, user practice results in substantial control performance improvement (Bunderson and Kuiken, 2012; Powell et al., 2014; He et al., 2015; Hargrove et al., 2017). However, these studies were concerned with classification-based control, which still lacks complete intuitiveness due to the discrete and sequential nature of the hand actuation mechanism. Here, we investigated the effect of user adaptation on myoelectric

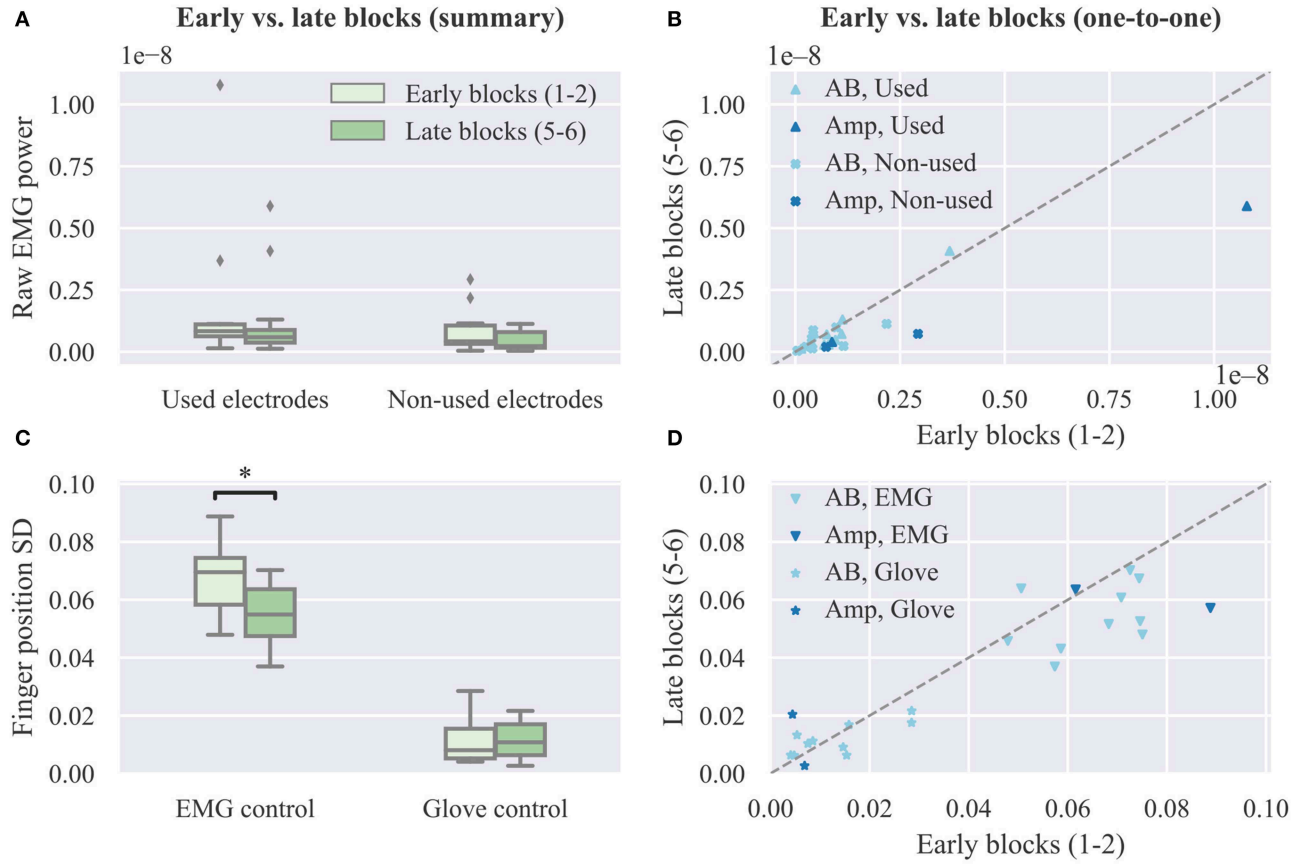

FIGURE 7 | Effect of user practice on muscle force and output variability. **(A)** Average raw EMG power of used and non-used electrodes for real-time decoding in early vs. late blocks. **(B)** One-to-one comparison of raw EMG power between early and late blocks. **(C)** Average finger position variability during the evaluation phase of the real-time posture matching task in early vs. late blocks for EMG and glove control. **(D)** One-to-one comparison of finger position variability between early and late blocks. SD, standard deviation.

control when using a decoder mapping EMG features onto prosthetic digit positions.

We found evidence that the performance of intuitive, independent prosthesis finger control can benefit from user experience gathered during real-time, closed-loop interaction with the control interface. In our experiment, two types of feedback were provided, namely, visual, since the prosthetic hand was within the visual field of the participant and responded to their control input, and a performance score, which was presented to the participants at the end of each trial. We hypothesized that despite the intuitiveness of the controller, experience should allow users to improve their performance. Indeed, we observed a significant decrease in target posture mismatch within ∼20 min of interaction with the prosthesis (**Figure 5**).

Of particular interest is the question of whether the observed improvement in performance can be retained during long-term use. Previous work has demonstrated an increase in classification-based myoelectric performance after a 6–8 weeks home trial (Hargrove et al., 2017). Whether a similar pattern can be observed with individual finger control remains to be investigated. Furthermore, it shall be compelling to investigate whether long-term performance improvement is accompanied by permanent changes in forward neuromotor control (i.e., motor learning). Our study has demonstrated that users can adapt rather quickly to improve performance on a specific task based on feedback. However, to assess long-term adaptation, a more extended study spanning across multiple sessions and testing generalization on novel tasks might be needed (Kantak and Winstein, 2012).

The dimensionality reduction analysis (**Figures 6A,B**) revealed that over the course of our experiments, substantial changes occurred in the covariance structure of the recorded EMG signal envelopes, and therefore the direction and variance explained by the first two PCs (**Figures 6C,D**). Although such temporal changes in muscle co-activation patterns might in part reflect the non-stationary nature of surface EMG recordings, when combined with the observed increase in task performance, these changes may be primarily mediated by user adaptation in muscle recruitment. It is worth mentioning that although the extracted PCs reflect muscle co-activation patterns, they do not directly correspond to muscle synergies, as we did not target specific muscles during electrode positioning. However, by taking

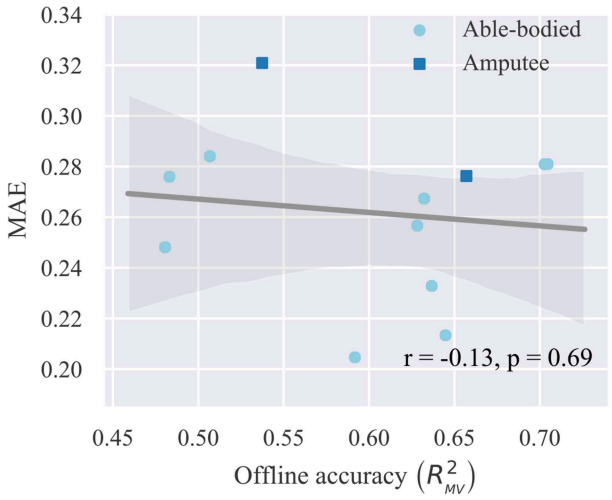

FIGURE 8 | Relationship between offline reconstruction accuracy (multivariate R^2) and real-time performance (MAE). Circles/squares, individual observations (i.e., one for each participant); line, linear regression fit; translucent band, 95% confidence intervals estimated via bootstrapping (1,000 iterations); *r*, correlation coefficient; *p*, significance value.

into consideration that the EMG electrodes record in this setting a superposition of the activity of different muscles, and also given that PCA produces a linear transformation of the input space, it is reasonable to expect that similar results would have been obtained had we targeted specific muscles. It is also worth noting that the dimensionality reduction analysis was performed on the EMG envelopes, that is, the mean absolute value of the recorded signals, whereas various non-linear feature transformations were used for decoding finger positions from EMG signals. Therefore, there is no direct correspondence between the estimated PCs and the principal directions of the regression problem (Krasoulis et al., 2015a), which has a substantially higher dimensionality. It can be observed in **Figures 6C,D** that the first two PCs explained a higher percentage of the overall variance in the two amputee than in the able-bodied participants. We attribute this to the smaller number of electrodes used in the former case (i.e., 12 and 13 electrodes for amputees as opposed to 16 electrodes for able-bodied participants). The percentage of explained variance in each block by the PCs computed in the same block remained constant during the experiment (**Figures 6E,F**). This observation rules out the possibility that the decrease in explained variance by the PCs extracted in the first block (**Figures 6C,D**) is due to exogenous parameters, hence further suggesting that this reduction is caused by changes in muscle co-activation patterns emerging from short-term user adaptation.

Force field adaptation studies have previously shown that humans learn to optimize limb impedance to minimize metabolic costs and movement error simultaneously (Burdet et al., 2001). In addition to a decrease in movement error, we also observed a small, however non-significant, reduction in overall EMG power exerted by the participants' muscles and a significant decrease in the variability of the controllable DOAs (**Figure 7**). Both of these observations are compatible with the notion of limb impedance optimization. Notably, we did not observe a decrease in finger position variability with glove control, hence implying that the respective reduction with EMG control should be indeed attributed to changes in the recorded muscle signals. A key difference between our study and previous work (Burdet et al., 2001) is that the user and the device were not mechanically linked, but in both cases the effector was unstable and with practice subjects learned to enhance its stability. The decrease in median EMG power was non-significant ($p = 0.10$) and therefore no definitive conclusions can be drawn regarding whether and how user training can lead to a reduction in muscle metabolic cost during myoelectric control. Future experiments with amputee participants wearing a prosthetic hand can reveal the extent to which energy-efficient control can be achieved. It is unlikely that the observed trend is due to muscle fatigue, since it is known that the latter is associated with an increase in EMG power with a simultaneous reduction of median frequency of the EMG spectrum (Luttmann et al., 2000; Bartuzi and Roman-Liu, 2014).

A previous study that made use of a performance score that was similar to the one presented to the participants at the end of the trials reported an increase from 0 to 40% after ∼200 trials (Pistohl et al., 2013). In the current study, the average performance with EMG control increased from 33.48 to 36.50% corresponding to a decrease in average MAE from 0.28 to 0.26 (**Figure 5A**) after 108 trials. Although this improvement is smaller than the one reported previously, this finding should not be surprising; the previous study used a pre-determined, fixed, and non-intuitive mapping from muscle activity to the DOAs of the prosthetic hand, and thus, participants had to learn the underlying control principle, that is, an inverse model of the interface (Dyson et al., 2018) from scratch. Conversely, in our study, the mappings were based on regression models trained with user-specific data; hence, the mappings were intuitive for all participants and the baseline performance at the start of the experiment was well above zero.

Our results agree with previous work suggesting that experience can help humans improve their performance at myoelectric control tasks, even in the case of intuitive interfaces (Radhakrishnan et al., 2008). A question that may naturally arise is why one should expect such improvement when using biomimetic, intuitive myoelectric decoders. Before addressing this sensible question, one should first note that in our experiments an increase in performance was also observed in the case of robotic hand teleoperation using the data glove, despite the very high level of intuitiveness of this particular task. With this important information in mind, we seek to provide the following justification: despite being intuitive from a physiological perspective, the myoelectric controller is still far from natural; this is due to many differences between the human and robotic hands, including, but not limited to, the number of DOFs, the finger anatomical structure, and the range of finger movement. Furthermore, our control algorithm mapped recorded muscle activity onto finger joint positions without taking into account joint velocities or digit forces which, in the human body, are also controlled by muscle contractions. In the case of EMG control, although decoding accuracy was relatively

high, it was still far from perfect (**Figure 3**). Therefore, it is likely that participants performed compensatory contractions to correct for prediction errors (Jiang et al., 2014; Hahne et al., 2017). Finally, it is worth noting that the lack of proprioception in amputees can only exacerbate the challenges outlined above. Taking everything into consideration, it is clear that despite our best efforts, it is still impossible to develop biomimetic myoelectric control schemes that feel entirely natural to the user, unless all the following conditions are simultaneously met: the end device is a perfect replication of the human hand, sensing technologies and decoding algorithms allow for near-perfect reconstruction of movement intent and, finally, artificial proprioceptive information is fed back to the user. In any other case, a certain amount of adaptation is still very likely to take place during interaction with the device, which has the potential to substantially improve control performance.

In addition to an increase in control accuracy, user training may have additionally resulted in a reduction in reaction time. However, given the long preparation window, in combination with the fact that performance was only assessed with respect to the final posture and not the followed trajectories, it seems unlikely that this factor could explain the observed increase in control performance. One such example is given in **Figure S5**, where two trials are compared for the same participant and posture, one at the start and one at the end of the experimental session. For the shown example, after training, the participant was able to reach the desired posture in less time and with better accuracy. However, in both cases, the final posture was achieved before the start of the evaluation phase. Hence, the difference in performance scores is only due to the higher accuracy of the end posture in the late trial. The length of the preparation window was set during pilot trials to the chosen value (i.e., 3.5 s), as this was found to offer a good compromise between the desired task difficulty and the ability to assess performance without being influenced by a potential decrease in user reaction time.

In the context of myoelectric classification, it has been previously shown that a discrepancy exists between offline accuracy and real-time control performance (Ortiz-Catalan et al., 2015). With regard to continuous wrist control, it has been shown that only a weak correlation exists between offline R^2 and metrics characterizing real-time performance during a target achievement control test, such as completion rate, completion time, overshoots, throughput, speed, and efficiency coefficient (Jiang et al., 2014). To assess whether a similar statement could be made about continuous finger position control, we compared offline reconstruction accuracy to performance scores during the real-time posture matching task. In agreement with previous work (Jiang et al., 2014; Ortiz-Catalan et al., 2015), a very weak, non-significant correlation was found between offline accuracy and real-time performance. Such differences between offline decoding and real-time control, which may be primarily attributed to user adaptation taking place during closed-loop interaction, further reiterate the need for testing prosthetic control methodologies with real-time experiments (Jiang et al., 2012, 2014; Ortiz-Catalan et al., 2015; Vujaklija et al., 2017).

In this study, we focused on non-invasive, continuous position control of individual digits. In line with previous work (Cipriani et al., 2011), we have shown that it is feasible, in principle, to use surface EMG measurements from the forearm of able-bodied and transradial amputee subjects to decode finger positions and subsequently use these estimates to control the individual digits of a prosthesis in real-time. The set of controllable DOAs included flexion of all fingers and thumb opposition. The ring and little fingers were controlled together because of mechanical coupling in the robotic device used in our experiments. Offline analysis revealed that thumb movement (flexion and rotation) was the most challenging to decode (**Figure 3**). This is not surprising, given that thumb muscles are either intrinsic or located in the distal part of the forearm. In this work, however, we focused on transradial amputation and, therefore, recorded EMG activity from the proximal part of the forearm only.

The continuous finger position controller has two main advantages: intuitiveness and dexterity. As has already been pointed out, training regression models using muscle signals and glove data recorded from the end-user creates an intuitive association between muscle activity and finger movement and, thus, the user does not need to learn a new mapping from scratch. Dexterity naturally arises from the fact that the user can control individual digits in a continuous space. One particular advantage of this scheme over discrete control schemes, for example, classification-based grip selection, is the ability to move from one type of grip to another without the need for executing an intermediate hand opening action. The high level of dexterity, however, comes at a price; decoding independent finger movement is a much more challenging task than classifying EMG activity into hand postures. In its current form, the proposed scheme is unlikely to be suitable for clinical adoption by amputees, as significant improvements are required to ensure its long-term viability. For example, one simplification made in this study was that the posture of the participants' forearm was kept fixed throughout the experimental sessions. This simplification would not occur in a realistic scenario and, thus, it is expected that performance would deteriorate due to the limb position effect (Fougner et al., 2011). Nevertheless, given the potential of this method to achieve intuitive and truly dexterous prosthetic control, we consider it is worthwhile pursuing further research in this direction.

It is worth mentioning that an invasive approach might indeed be required to achieve robust finger position control. Intramuscular EMG recordings have been previously used for continuous finger control of both virtual (Birdwell et al., 2015) and robotic (Cipriani et al., 2014) hands. Both of these studies, however, had the following two limitations: firstly, they used a one-to-one mapping from individual pairs of muscles to DOAs of the hand; secondly, they were limited to able-bodied participants. An alternative avenue would be to investigate the use of multivariate regression models in mapping the activity of multiple muscles onto prosthesis DOAs, as opposed to the previously used one-to-one mapping schemes. Another compelling possibility would be to test the performance of continuous finger control in patients having undergone targeted

muscle reinnervation. It has been previously demonstrated that hand/wrist movements can be classified with high accuracy in targeted muscle reinnervation patients (Kuiken et al., 2009). Whether robust individual finger control can be achieved using a similar invasive approach remains to be investigated.

As a final note, we seek to re-emphasize the important role that user adaptation could play in myoelectric control of prosthetic fingers, regardless of the origin of control signals. We have shown here that even with an intuitive decoder, humans can improve their performance in a biofeedback myoelectric task within a short period of time. In line with previous reports from the myoelectric classification and wrist control literature (Jiang et al., 2014; Ortiz-Catalan et al., 2015), we conclude that future efforts should focus on putting the human in the loop and evaluating control methodologies with real-time, closed-loop experiments. We firmly believe that further advancements can be achieved by explicitly taking into account the remarkable plasticity of the human brain when designing myoelectric control interfaces.

DATA AVAILABILITY

The datasets collected for model training and offline evaluation are available as part of the NINAPRO database (http://ninapro.hevs.ch/DB8); and Newcastle University Data Repository (https://data.ncl.ac.uk/articles/EMG_and_data_glove_dataset_for_dexterous_myoelectric_control/9577598/1, doi: 10.25405/data.ncl.9577598.v1).

ETHICS STATEMENT

All experiments were performed in accordance with the Declaration of Helsinki and were approved by the local Ethics Committees of the School of Informatics, University of Edinburgh and School of Engineering, Newcastle University. Prior to the experiments, subjects read a participant information sheet, and gave written informed consent.

AUTHOR CONTRIBUTIONS

AK, SV, and KN conceptualized the study. AK designed and implemented the experimental protocol, analyzed the data, and prepared the figures. AK and KN conducted the experiments. All authors contributed to manuscript preparation, read, and approved the final manuscript.

FUNDING

AK was supported in part by grants EP/F500386/1 and BB/F529254/1 for the University of Edinburgh School of Informatics Doctoral Training Centre in Neuroinformatics and Computational Neuroscience from the UK Engineering and Physical Sciences Research Council (EPSRC), UK Biotechnology and Biological Sciences Research Council (BBSRC), and the UK Medical Research Council (MRC). AK was currently supported by EPSRC grant EP/R004242/1. SV was supported by the Microsoft Research RAEng. Fellowship and EPSRC grant EP/L016834/1. KN was supported by EPSRC grants EP/M025977/1, EP/N023080/1, and EP/R004242/1.

ACKNOWLEDGMENTS

The authors are grateful to the two amputee volunteers for taking part in the study. The authors would like to thank Matthew Dyson for useful discussion.

SUPPLEMENTARY MATERIAL

The Supplementary Material for this article can be found online at: https://www.frontiersin.org/articles/10.3389/fnins.2019.00891/full#supplementary-material

Supplementary Movie 1 | Real-time prosthetic finger control: amputee subject 1, block 1.

Supplementary Movie 2 | Real-time prosthetic finger control: amputee subject 1, block 6.

REFERENCES

Afshar, P., and Matsuoka, Y. (2004). "Neural-based control of a robotic hand: evidence for distinct muscle strategies," in *IEEE International Conference on Robotics and Automation, 2004. Proceedings. ICRA '04. 2004* (New Orleans, LA: IEEE), 4633–4638. doi: 10.1109/ROBOT.2004.1302448

Antuvan, C. W., Ison, M., and Artemiadis, P. (2014). Embedded human control of robots using myoelectric interfaces. *IEEE Trans. Neural Syst. Rehabil. Eng.* 22, 820–827. doi: 10.1109/TNSRE.2014.2302212

Bartuzi, P., and Roman-Liu, D. (2014). Assessment of muscle load and fatigue with the usage of frequency and time-frequency analysis of the emg signal. *Acta Bioeng. Biomech.* 16, 31–39.

Birdwell, J. A., Hargrove, L. J., Kuiken, T. A., and Weir, R. F. (2013). Activation of individual extrinsic thumb muscles and compartments of extrinsic finger muscles. *J. Neurophysiol.* 110, 1385–1392. doi: 10.1152/jn.00748.2012

Birdwell, J. A., Hargrove, L. J., Weir, R. F., and Kuiken, T. A. (2015). Extrinsic finger and thumb muscles command a virtual hand to allow individual finger and grasp control. *IEEE Trans. Biomed. Eng.* 62, 218–226. doi: 10.1109/TBME.2014.2344854

Boostani, R., and Moradi, M. H. (2003). Evaluation of the forearm EMG signal features for the control of a prosthetic hand. *Physiol. Measure.* 24, 309–319. doi: 10.1088/0967-3334/24/2/307

Bouwsema, H., van der Sluis, C. K., and Bongers, R. M. (2010). Learning to control opening and closing a myoelectric hand. *Arch. Phys. Med. Rehabil.* 91, 1442–1446. doi: 10.1016/j.apmr.2010.06.025

Bunderson, N. E., and Kuiken, T. A. (2012). Quantification of feature space changes with experience during electromyogram pattern recognition control. *IEEE Trans. Neural Syst. Rehabil. Eng.* 20, 239–246. doi: 10.1109/TNSRE.2011.2182525

Burdet, E., Osu, R., Franklin, D. W., Milner, T. E., and Kawato, M. (2001). The central nervous system stabilizes unstable dynamics by learning optimal impedance. *Nature* 414:446–449. doi: 10.1038/35106566

Castellini, C., Gruppioni, E., Davalli, A., and Sandini, G. (2009). Fine detection of grasp force and posture by amputees via surface electromyography. *J. Physiol. Paris* 103, 255–262. doi: 10.1016/j.jphysparis.2009.08.008

Cipriani, C., Antfolk, C., Controzzi, M., Lundborg, G., Rosen, B., Carrozza, M. C., et al. (2011). Online myoelectric control of a dexterous hand prosthesis by

transradial amputees. *IEEE Trans. Neural Syst. Rehabil. Eng.* 19, 260–270. doi: 10.1109/TNSRE.2011.2108667

Cipriani, C., Segil, J. L., Birdwell, J. A., and Weir, R. F. (2014). Dexterous control of a prosthetic hand using fine-wire intramuscular electrodes in targeted extrinsic muscles. *IEEE Trans. Neural Syst. Rehabil. Eng.* 22, 828–836. doi: 10.1109/TNSRE.2014.2301234

Clingman, R., and Pidcoe, P. (2014). A novel myoelectric training device for upper limb prostheses. *IEEE Trans. Neural Syst. Rehabil. Eng.* 22, 879–885. doi: 10.1109/TNSRE.2014.2315046

Dyson, M., Barnes, J., and Nazarpour, K. (2017). "Abstract myoelectric control with EMG drive estimated using linear, kurtosis and Bayesian filtering." in *2017 8th International IEEE/EMBS Conference on Neural Engineering (NER)* (Shanghai:IEEE), 54–57. doi: 10.1109/NER.2017.8008290

Dyson, M., Barnes, J., and Nazarpour, K. (2018). Myoelectric control with abstract decoders. *J. Neural Eng.* 15:056003. doi: 10.1088/1741-2552/aacbfe

Farina, D., Jiang, N., Rehbaum, H., Holobar, A., Graimann, B., Dietl, H., and Aszmann, O. C. (2014). The extraction of neural information from the surface EMG for the control of upper-limb prostheses: emerging avenues and challenges. *IEEE Trans. Neural Syst. Rehabil. Eng.* 22, 797–809. doi: 10.1109/TNSRE.2014.2305111

Fougner, A., Scheme, E. J., Chan, A. D., Englehart, K. B., and Stavdahl, Ø. (2011). Resolving the limb position effect in myoelectric pattern recognition. *IEEE Trans. Neural Syst. Rehabil. Eng.* 19, 644–651. doi: 10.1109/TNSRE.2011.2163529

Fougner, A., Stavdahl, Ø., Kyberd, P. J., Losier, Y. G., and Parker, P. A. (2012). Control of upper limb prostheses: terminology and proportional myoelectric control–A review. *IEEE Trans. Neural Syst. Rehabil. Eng.* 20, 663–677. doi: 10.1109/TNSRE.2012.2196711

Gailey, A., Artemiadis, P., and Santello, M. (2017). Proof of concept of an online EMG-based decoding of hand postures and individual digit forces for prosthetic hand control. *Front. Neurol.* 8:7. doi: 10.3389/fneur.2017.00007

Gijsberts, A., Bohra, R., Sierra González, D. S., Werner, A., Nowak, M., Caputo, B., et al. (2014). Stable myoelectric control of a hand prosthesis using non-linear incremental learning. *Front. Neurorobot.* 8:8. doi: 10.3389/fnbot.2014.00008

Hahne, J. M., Biebmann, F., Jiang, N., Rehbaum, H., Farina, D., Meinecke, F. C., et al. (2014). Linear and nonlinear regression techniques for simultaneous and proportional myoelectric control. *IEEE Trans. Neural Syst. Rehabil. Eng.* 22, 269–279. doi: 10.1109/TNSRE.2014.2305520

Hahne, J. M., Markovic, M., and Farina, D. (2017). User adaptation in myoelectric man-machine interfaces. *Sci. Rep.* 7:4437. doi: 10.1038/s41598-017-04255-x

Hargrove, L. J., Miller, L. A., Turner, K., and Kuiken, T. A. (2017). Myoelectric pattern recognition outperforms direct control for transhumeral amputees with targeted muscle reinnervation: a randomized clinical trial. *Sci. Rep.* 7:13840. doi: 10.1038/s41598-017-14386-w

He, J., Zhang, D., Jiang, N., Sheng, X., Farina, D., and Zhu, X. (2015). User adaptation in long-term, open-loop myoelectric training: implications for EMG pattern recognition in prosthesis control. *J. Neural Eng.* 12:046005. doi: 10.1088/1741-2560/12/4/046005

Herberts, P., Almström, C., Kadefors, R., and Lawrence, P. D. (1973). Hand prosthesis control via myoelectric patterns. *Acta Orthop. Scand.* 44, 389–409. doi: 10.3109/17453677308989075

Ison, M., and Artemiadis, P. (2015). Proportional myoelectric control of robots: muscle synergy development drives performance enhancement, retainment, and generalization. *IEEE Trans. Robot.* 31, 259–268. doi: 10.1109/TRO.2015.2395731

Ison, M., Vujaklija, I., Whitsell, B., Farina, D., and Artemiadis, P. (2016). High-density electromyography and motor skill learning for robust long-term control of a 7-DoF robot arm. *IEEE Trans. Neural Syst. Rehabil. Eng.* 24, 424–433. doi: 10.1109/TNSRE.2015.2417775

Jiang, N., Dosen, S., Müller, K.-R., and Farina, D. (2012). Myoelectric control of artificial limbs –is there a need to change focus? [In the spotlight]. *IEEE Signal Proc. Mag.* 29, 152–150. doi: 10.1109/MSP.2012.2203480

Jiang, N., Vujaklija, I., Rehbaum, H., Graimann, B., and Farina, D. (2014). Is accurate mapping of EMG signals on kinematics needed for precise online myoelectric control? *IEEE Trans. Neural Syst. Rehabil. Eng.* 22, 549–558. doi: 10.1109/TNSRE.2013.2287383

Kantak, S. S., and Winstein, C. J. (2012). Learning–performance distinction and memory processes for motor skills: a focused review and perspective. *Behav. Brain Res.* 228, 219–231. doi: 10.1016/j.bbr.2011.11.028

Krasoulis, A., Kyranou, I., Erden, M. S., Nazarpour, K., and Vijayakumar, S. (2017). Improved prosthetic hand control with concurrent use of myoelectric and inertial measurements. *J. NeuroEng. Rehabil.* 14:71. doi: 10.1186/s12984-017-0284-4

Krasoulis, A., Nazarpour, K., and Vijayakumar, S. (2015a). Towards low-dimensional proportional myoelectric control. In *Conf. Proc. Eng. Med. Biol. Soc.* 2015, 7155–7158. doi: 10.1109/EMBC.2015.7320042

Krasoulis, A., Vijayakumar, S., and Nazarpour, K. (2015b). "Evaluation of regression methods for the continuous decoding of finger movement from surface EMG and accelerometry," in *2015 7th International IEEE/EMBS Conference on Neural Engineering (NER)* (Montpellier: IEEE), 631–634. doi: 10.1109/NER.2015.7146702

Kuiken, T. A., Li, G., Lock, B. A., Lipschutz, R. D., Miller, L. A., Stubblefield, K. A., et al. (2009). Targeted muscle reinnervation for real-time myoelectric control of multifunction artificial arms. *JAMA* 301, 619–628. doi: 10.1001/jama.2009.116

Luttmann, A., Jäger, M., and Laurig, W. (2000). Electromyographical indication of muscular fatigue in occupational field studies. *Int. J. Indust. Ergon.* 25, 645–660. doi: 10.1016/S0169-8141(99)00053-0

Muceli, S., Jiang, N., and Farina, D. (2014). Extracting signals robust to electrode number and shift for online simultaneous and proportional myoelectric control by factorization algorithms. *IEEE Trans. Neural Syst. Rehabil. Eng.* 22, 623–633. doi: 10.1109/TNSRE.2013.2282898

Nazarpour, K., Barnard, A., and Jackson, A. (2012). Flexible cortical control of task-specific muscle synergies. *J. Neurosci.* 32, 12349–12360. doi: 10.1523/JNEUROSCI.5481-11.2012

Ngeo, J. G., Tamei, T., and Shibata, T. (2014). Continuous and simultaneous estimation of finger kinematics using inputs from an EMG-to-muscle activation model. *J. NeuroEng. Rehabil.* 11:122. doi: 10.1186/1743-0003-11-122

Ngeo, J. G., Tamei, T., Shibata, T., Orlando, M. F. F., Behera, L., Saxena, A., et al. (2013). Control of an optimal finger exoskeleton based on continuous joint angle estimation from EMG signals. *Conf. Eng. Med. Biol. Soc.* 2013, 338–341. doi: 10.1109/EMBC.2013.6609506

Nielsen, J. L., Holmgaard, S., Jiang, N., Englehart, K. B., Farina, D., and Parker, P. A. (2011). Simultaneous and proportional force estimation for multifunction myoelectric prostheses using mirrored bilateral training. *IEEE Trans. Biomed. Eng.* 58, 681–688. doi: 10.1109/TBME.2010.2068298

Ortiz-Catalan, M., Rouhani, F., Brånemark, R., and Håkansson, B. (2015). "Offline accuracy: a potentially misleading metric in myoelectric pattern recognition for prosthetic control," in *2015 37th Annual International Conference of the IEEE Engineering in Medicine and Biology Society (EMBC)* (Milan: IEEE) 1140–1143. doi: 10.1109/EMBC.2015.7318567

Patel, G. K., Nowak, M., and Castellini, C. (2017). Exploiting knowledge composition to improve real-life hand prosthetic control. *IEEE Trans. Neural Syst. Rehabil. Eng.* 25, 967–975. doi: 10.1109/TNSRE.2017.2676467

Pedregosa, F., Varoquaux, G., Gramfort, A., Michel, V., Thirion, B., Grisel, O., et al. (2011). Scikit-learn: machine learning in Python. *J. Mach. Learn. Res.* 12, 2825–2830.

Perreault, E. J., Kirsch, R. F., and Acosta, A. M. (1999). Multiple-input, multiple-output system identification for characterization of limb stiffness dynamics. *Biol. Cybern.* 80, 327–337. doi: 10.1007/s004220050529

Pistohl, T., Cipriani, C., Jackson, A., and Nazarpour, K. (2013). Abstract and proportional myoelectric control for multi-fingered hand prostheses. *Ann. of Biomedical Eng.* 41, 2687–2698. doi: 10.1007/s10439-013-0876-5

Pistohl, T., Joshi, D., Ganesh, G., Jackson, A., and Nazarpour, K. (2015). Artificial proprioceptive feedback for myoelectric control. *IEEE Trans. Neural Syst. Rehabil. Eng.* 23, 498–507. doi: 10.1109/TNSRE.2014.2355856

Powell, M. A., Kaliki, R. R., and Thakor, N. V. (2014). User training for pattern recognition-based myoelectric prostheses: improving phantom limb movement consistency and distinguishability. *IEEE Trans. Neural Syst. Rehabil. Eng.* 22, 522–532. doi: 10.1109/TNSRE.2013.2279737

Pudil, P., Novovičová, J., and Kittler, J. (1994). Floating search methods in feature selection. *Patt. Recogn. Lett.* 15, 1119–1125.

Radhakrishnan, S. M., Baker, S. N., and Jackson, A. (2008). Learning a novel myoelectric-controlled interface task. *J. Neurophysiol.* 100, 2397–2408. doi: 10.1152/jn.90614.2008

Smith, L. H., Kuiken, T. A., and Hargrove, L. J. (2014). Real-time simultaneous and proportional myoelectric control using intramuscular EMG. *J. Neural Eng.* 11:066013. doi: 10.1088/1741-2560/11/6/066013

Smith, R. J., Huberdeau, D., Tenore, F., and Thakor, N. V. (2009). "Real-time myoelectric decoding of individual finger movements for a virtual target task," in *2009 Annual International Conference of the IEEE Engineering in Medicine and Biology Society* (Minneapolis, MN: IEEE), 2376–2379. doi: 10.1109/IEMBS.2009.5334981

Smith, R. J., Tenore, F., Huberdeau, D., Etienne-Cummings, R., and Thakor, N. V. (2008). "Continuous decoding of finger position from surface EMG signals for the control of powered prostheses," in *2008 30th Annual International Conference of the IEEE Engineering in Medicine and Biology Society* (Vancouver, BC: IEEE), 197–200.

Vallat, R. (2018). Pingouin: statistics in python. *J. Open Source Software* 3:331. doi: 10.21105/joss.01026

Vujaklija, I., Roche, A. D., Hasenoehrl, T., Sturma, A., Amsüss, S., Farina, D., et al. (2017). Translating research on myoelectric control into clinics' Are the performance assessment methods adequate? *Front. Neurorobot.* 11:7. doi: 10.3389/fnbot.2017.00007

Xiloyannis, M., Gavriel, C., Thomik, A. A. C., and Faisal, A. A. (2017). Gaussian Process autoregression for simultaneous proportional multi-modal prosthetic control with natural hand kinematics. *IEEE Trans. Neural Syst. Rehabil. Eng.* 25, 1785–1801. doi: 10.1109/TNSRE.2017.2699598

Conflict of Interest Statement: The authors declare that the research was conducted in the absence of any commercial or financial relationships that could be construed as a potential conflict of interest.

frontiers in Neuroscience

ORIGINAL RESEARCH
published: 14 October 2019
doi: 10.3389/fnins.2019.01073

Electrical Stimulation Degenerated Cochlear Synapses Through Oxidative Stress in Neonatal Cochlear Explants

Qiong Liang[1,2†], Na Shen[1,2,3†], Bin Lai[4], Changjian Xu[5], Zengjun Sun[5], Zhengmin Wang[1,2] and Shufeng Li[1,2]*

[1] Department of Otolaryngology, Eye and ENT Hospital of Fudan University, Shanghai, China, [2] National Health Commission Key Laboratory of Hearing Medicine, Shanghai, China, [3] Department of Otolaryngology, Zhongshan Hospital of Fudan University, Shanghai, China, [4] State Key Laboratory of Medical Neurobiology, Shanghai, China, [5] Shanghai Cochlear Engineering Technology Research Center, Shanghai, China

OPEN ACCESS

Edited by:
Wolfgang Freysinger, Medical University of Innsbruck, Austria

Reviewed by:
Anneliese Schrott-Fischer, Medical University of Innsbruck, Austria
Esperanza Bas Infante, University of Miami, United States
Athanasia Warnecke, Hannover Medical School, Germany

***Correspondence:**
Shufeng Li
lisf@fudan.edu.cn

[†] These authors have contributed equally to this work

Specialty section:
This article was submitted to Neuroprosthetics, a section of the journal Frontiers in Neuroscience

Received: *25 April 2019*
Accepted: *24 September 2019*
Published: *14 October 2019*

Citation:
Liang Q, Shen N, Lai B, Xu C, Sun Z, Wang Z and Li S (2019) Electrical Stimulation Degenerated Cochlear Synapses Through Oxidative Stress in Neonatal Cochlear Explants. Front. Neurosci. 13:1073. doi: 10.3389/fnins.2019.01073

Neurostimulation devices use electrical stimulation (ES) to substitute, supplement or modulate neural function. However, the impact of ES on their modulating structures is largely unknown. For example, recipients of cochlear implants using electroacoustic stimulation experienced delayed loss of residual hearing over time after ES, even though ES had no impact on the morphology of hair cells. In this study, using a novel model of cochlear explant culture with charge-balanced biphasic ES, we found that ES did not change the quantity and morphology of hair cells but decreased the number of inner hair cell (IHC) synapses and the density of spiral ganglion neuron (SGN) peripheral fibers. Inhibiting calcium influx with voltage-dependent calcium channel (VDCC) blockers attenuated the loss of SGN peripheral fibers and IHC synapses induced by ES. ES increased ROS/RNS in cochlear explants, but the inhibition of calcium influx abolished this effect. Glutathione peroxidase 1 (GPx1) and GPx2 in cochlear explants decreased under ES and ebselen abolished this effect and attenuated the loss of SGN peripheral fibers. This finding demonstrated that ES induced the degeneration of SGN peripheral fibers and IHC synapses in a current intensity- and duration-dependent manner *in vitro*. Calcium influx resulting in oxidative stress played an important role in this process. Additionally, ebselen might be a potential protector of ES-induced cochlear synaptic degeneration.

Keywords: cochlear explants, electrical stimulation, oxidative stress, calcium influx, ebselen, synapses, spiral ganglion neuron

INTRODUCTION

Neurostimulation devices, for example visual prosthetics, auditory prosthetics, deep brain stimulation device, prosthetics for pain relief, motor prosthetics and brain-computer interfaces, are promising therapeutics for neurological disorders by supplanting or supplementing the input and/or output of the nervous system. These devices were initially designed to bypass neural deficits that occurred as a result of injuries or diseases. Currently, neurostimulation devices are

even developed to modulate existing neural function to improve performance, especially in the application of future brain-computer interfaces. Cochlear implants (CIs) are the most widely used neural prosthetic. Traditional CIs restore hearing perception by delivering electrical signals converted from sound information to spiral ganglion neurons (SGNs), bypassing the defective or missing mechanosensory structures of the organ of Corti, i.e., hair cells. In the last decade, electric-acoustic stimulation (EAS) technology was newly developed for patients with severe or profound high-frequency hearing loss and residual low-frequency hearing (Von Ilberg et al., 1999; Gantz and Turner, 2003; Kiefer et al., 2005). This technology uses a short electrode array in the basal to middle part of the cochlear duct, leaving the apical part intact to preserve the residual low-frequency hearing. Patients are then able to receive acoustic signals at the apical part of the cochlea and electrical stimulation (ES) at the basal and middle part of the cochlea, simultaneously. Compared to full-insertion CI, EAS technology significantly improves music appreciation and speech recognition in background noise (Turner et al., 2004, 2008; Gfeller et al., 2006). Accordingly, the preservation of residual low-frequency hearing is critical to EAS recipients. Unfortunately, clinical trials showed that 30–75% of EAS recipients experienced delayed progressive loss of residual low-frequency hearing over time after the activation of EAS (Gantz et al., 2009; Gstoettner et al., 2009; Santa Maria et al., 2013). Understanding how existing hearing function deteriorates under EAS might benefit not only the preservation of the residual hearing of EAS recipients but also the protection of existing neural functions on which, other neurostimulation devices depend. However, the mechanism of this delayed hearing impairment is largely unknown. Animal studies suggested that reduced endocochlear potential due to lateral wall or stria vascularis damage (Wright and Roland, 2013) and disturbed traveling wave due to fibrosis or new bone growth (Choi and Oghalai, 2005) were associated with the hearing loss of EAS recipients. Nevertheless, there is still a lack of strong evidence to support these theories. Previous animal studies demonstrated that ES did not cause any morphological changes in hair cells or SGNs (Ni et al., 1992; Shepherd et al., 1994; Coco et al., 2007; O'Leary et al., 2013). Notably, to the best of our knowledge, the status of synapses between SGNs and inner hair cells (IHCs) in EAS-induced hearing loss has not yet been investigated. However, the loss of IHC synapses has been shown to play an important role in noise-induced hearing loss (Kujawa and Liberman, 2009; Lin et al., 2011) and in age-related hearing loss (Makary et al., 2011; Sergeyenko et al., 2013).

Cochlear implants use charge-balanced biphasic pulses to stimulate SGNs. The depolarization of the SGN membrane caused by ES results in calcium influx through various types of voltage-dependent calcium channels (VDCCs). Excessive calcium influx could lead to the injuries of SGN (Hegarty et al., 1997; Roehm et al., 2008) and hair cells (Fridberger et al., 1998). Oxidative stress also plays important roles in hearing loss induced by noise, aminoglycoside antibiotics, cisplatin and aging (Choi and Choi, 2015; Sheth et al., 2017; Tavanai and Mohammadkhani, 2017). We postulated that excessive calcium influx through VDCCs and the resulting increase in oxidative stress might be involved in the loss of residual hearing due to chronic ES.

In this study, we used cochlear explants culture with ES of charge-balanced biphasic pulses to investigate the impact of ES on SGN peripheral fibers, hair cells and their synapses. We demonstrated that CI with ES could induce the degeneration of IHC synapses and SGN peripheral fibers through calcium influx and resulting oxidative stress.

MATERIALS AND METHODS

Cochlear Explant Culture

All procedures were approved by the Ethics Review Board of Eye and ENT Hospital of Fudan University (No. 2013024). Sprague Dawley rat pups of 4–6 postnatal days old of both sexes were provided by Shanghai SIPPR-Bk Lab Animal Co., Ltd. The cochlear explant culture was previously used to investigate the excitotoxic damage of IHC-SGN synapses (Wang and Green, 2011). Briefly, the cochlea were dissected out in ice-cold PBS. The osseous labyrinth, stria vascularis and spiral ligament were carefully removed. With the organ of Corti and modiolus preserved intact, Reissner's membrane and tectorial membrane were carefully removed with fine forceps. After the upper and basal turns were cut off, the middle turns were cut into small pieces and plated on poly-L-lysine-treated chamber slides. We usually dissected 5 pups and collected 10 cochleae at one time. Then the middle parts of cochlear tissues were pooled together and each of them was cut into 3–4 small pieces. Six pieces of cochlear tissues were then randomly put into each chamber. Unless otherwise indicated, the explants during the whole experiments, were maintained in a 37°C humidified incubator with 5% CO_2 and in high glucose Dulbecco's modified eagle's medium (DMEM, Life Technologies, 11965) with N2 supplement (Life Technologies, 17502-048), 10% fetal bovine serum (Gibco, 10099-141), 10 μg/ml insulin (Sigma-Aldrich, I6634), 50 ng/ml neurotrophin-3 (NT-3, Sigma-Aldrich, N1905) and 50 ng/ml brain-derived neurotrophic factor (BDNF, Sigma-Aldrich, B3795). The explants were first allowed to settle down on the chamber floor for 24 h before the following treatments. The floating explants were discarded and the adherent ones were used for the following experiments.

Chamber Slide With ES

To investigate the impact of ES on cochlear structures, we established a culture system of cochlear explants under ES (**Figure 1**). Briefly, two parallel platinum-iridium wires were introduced into a four-well chamber slide system (154526, Thermo Scientific) through four holes at four corners against the chamber floor. The holes were sealed with silicon glue to secure the wires which were connected to a multichannel charge-balanced biphasic pulse generator (Listent Medical Tech Co., Ltd.). The charge-balanced biphasic pulses used for ES held adjustable amplitudes with a 65-μs pulse width, 8-μs open-circuit interphase gap, and 4862-μs short-circuit phase at a frequency of 200 Hz. The distance between the two paralleling wires was

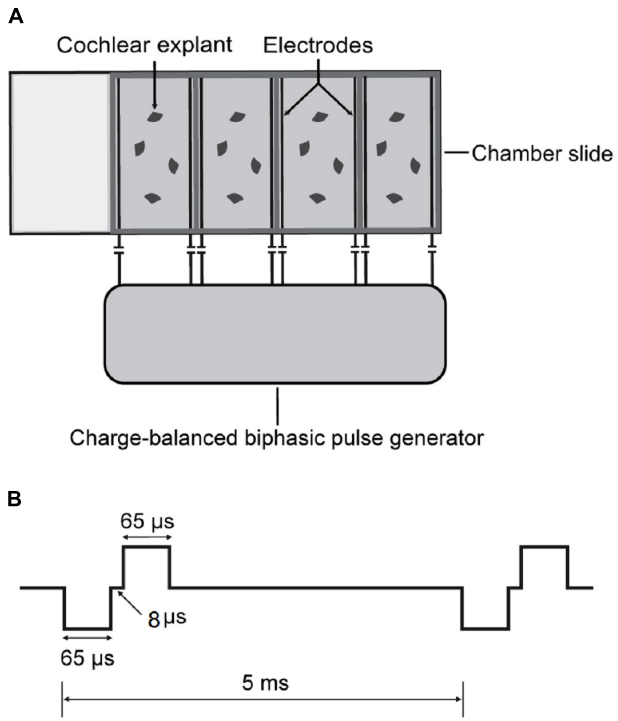

FIGURE 1 | Schematics of cochlear explant culture under charge-balanced biphasic ES. **(A)** Four-well chamber slides were used in cochlear explant culture. Two parallel platinum-iridium wires were introduced into each chamber against the floor through four holes at four corners. The wires were then connected with a charge-balanced biphasic pulse generator. **(B)** The charge-balanced biphasic pluses for ES had adjustable amplitudes, a 65-μs pulse width, an 8-μs open-circuit interphase gap, a 4862-μs short-circuit phase, and a 200 Hz frequency.

1 cm and the volume of culture medium in each chamber was 0.6 ml. The maximum charge density used in this study was 0.043 μC/cm^2/phase when a maximum current intensity of 400 μA was used. This charge intensity was far less than 15 to 65 μC/cm^2/phase which was suggested as the maximum level of charge intensity in commercial CIs (Zeng et al., 2008).

Application of VDCC Blocker, Ebselen and H_2O_2

Various VDCC blockers, ebselen (40 μM; Sigma, E3520) and H_2O_2 (0.25 mM; Aladdin, H112517) were added to the culture medium. The VDCC blockers included the L-type channel blocker verapamil (VPL, 10 μM; Sigma, V4629), the N-type channel blocker ω–conotoxin GVIA (GVIA, 1 μM; Sigma, C9915), the P/Q-type channel blocker ω-agatoxin IVA (IVA, 1 μM; Sigma, A6719), the mixture of the three above blockers (CCBM, 10 μM VPL/1 μM GVIA/1 μM IVA), and the non-selective calcium channel blocker cadmium chloride (Cd, 10 μM; Sigma-Aldrich, 439800). For the calcium-free environment, the culture medium was completely replaced by calcium-free DMEM (Gibco, 21068028) with 1 mM EDTA, N2, BDNF, NT3, and insulin.

Immunocytochemistry

Cochlear explant cultures were fixed with 4% paraformaldehyde for 15 min and permeabilized with 0.2% Triton X-100 and 10% donkey serum in PBS for 1 h. For immunostaining, the tissues were sequentially incubated with primary at 4°C overnight and with secondary antibodies for 1 h at room temperature diluted in PBS with 10% donkey serum. Primary antibodies were used as follows: anti-NF200 (1:400; Sigma, N0142) to label the SGNs and their peripheral fibers, anti-PSD95 (1:1000; Millipore, MABN68) to label postsynaptic densities (PSDs) in SGNs, and anti-Myo7A (1:800; Proteus BioSciences, 25-6790) or Alexa Fluor 647 phalloidin (1:200; Thermo Fisher Scientific, A22287) to label hair cells. Secondary antibodies were conjugated with Alexa Fluor 488, Alexa Fluor 546 and Alexa Fluor 647 (1: 800; Thermo Fisher Scientific).

Measuring Reactive Oxygen Species (ROS)/Reactive Nitrogen Species (RNS) Activity

The total ROS/RNS activity was measured by a ROS/RNS Assay Kit (Cell Biolabs, STA-347-5) according to the provided procedure. Briefly, cochlear explant cultures under different conditions were removed and rapidly homogenized under ice-cold conditions. The homogenates were then centrifuged, and the supernatants were reacted with dichlorofluorescein in a DiOxyQ probe for spectrofluorimetric measurement.

Real-Time PCR

For real-time PCR, PCR was conducted using an Applied Biosystems 7500 Real-time PCR System. Cochlear explants were harvested from cover slips and total RNA was purified with an RNeasy Plus Micro Extraction Kit (Qiagen, 74034). Then the RNA was reverse transcribed with a High Capacity RNA-to-cDNA kit (TaKaRa, RR036A) (Applied Biosystems, Foster City, CA, United States). The following primer pairs were designed using Primer3 software: β-actin, (F) CCTCTATGCCAACACAGT and (R) AGCCACCAATCCACACAG, with amplicon lengths of 155 bp; and glutathione peroxidase 2 (Gpx2), (F) AGACACTGGGAA ACCGAAGC and (R) AAGGAA ATGGGTGGCAGGAA, with amplicon lengths of 65 bp.

Quantitative Analysis of SGN Peripheral Fibers, IHC Synapses and Hair Cells

Digital images of immunostained cochlear explants were acquired by a Leica SP8 confocal microscope. Serial images of each explant at a 0.3 μm interval (*z*-axis) were recorded to generate a z-stack of images that could be projected onto a single plane (z-projection). Images of hair cells, IHC synapses and SGN peripheral fibers were simultaneously obtained with a 60×, 1.5 numerical aperture objective, while hair cells and SGN peripheral fibers were scanned at 40×, in different experiments. Then, the images were analyzed with ImageJ software. The number of SGN-IHC synapses was determined by counting the numbers of PSD-95 puncta on IHCs and in contact with NF200-positive neurites slice by slice. Each puncta was counted in the

first slice in which it appeared in focus to avoid being counted again. In the NF200 images, SGN peripheral nerve fibers in the area near the inner hair cell were crossing and overlapping. As a result, the fibers were hard to distinguish and count. We used the gray value of immunofluorescence in NF200 images to quantify the relative density of SGN peripheral nerve fibers. Images of each SGN peripheral fibers were captured using the same exposure time and light intensity and at the same sitting. At first, MYO7A and NF200 images from same location were converted to 8-bit grayscale images and constituted to a stack in ImageJ. A rectangle area with the dimension of 40 × 200 pixels was selected closely against to the base of inner hair cells in MYO7A images. That area coincided with the region that PSD-95 puncta distributed. Images of each SGN peripheral fibers were captured using the same exposure time and light intensity and at the same sitting. Then the mean gray value of the same area subtracted by that of background area in NF200 images was measured and determined as the relative density of SGN peripheral nerve fibers (**Figure 2**).

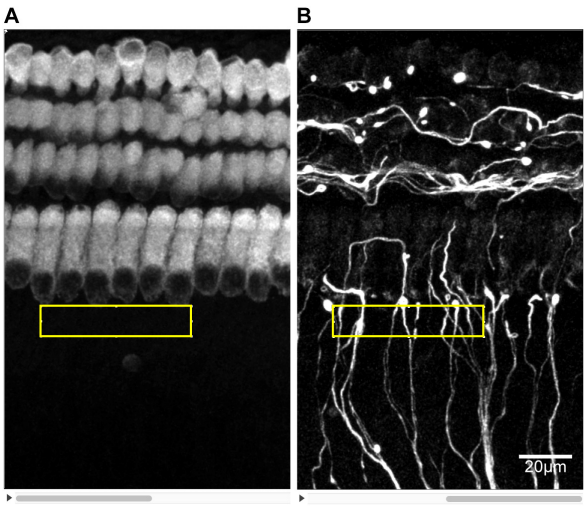

FIGURE 2 | Measuring the density of SGN peripheral fibers. The z-stacks of PSD95 and NF200 8-bit grayscale images of the same area were prepared in ImageJ. **(A)** A certain rectangular area of 40 × 200 pixels was selected just against the base of IHCs in PSD95 images. **(B)** The mean grayscale of the same selected area in NF200 images minus that of a background area of the same size was determined as the density of SGN peripheral fibers.

Statistical Analysis

Statistical analysis was performed by GraphPad Prism 7 (GraphPad Software, Inc., CA, United States). Unless otherwise indicated, significances of differences among various conditions were compared by one-way ANOVA followed by Dunnett's multiple comparisons test.

RESULTS

ES Decreased the Quantity of SGN Peripheral Fibers and IHC Synapses but Not the Quantity of Hair Cells

To investigate the impact of ES on cochlear structure, we cultured cochlear explants in a chamber slide system with multichannel charge-balanced biphasic pulse generators (**Figure 1**), which has been demonstrated in our previous work (Shen et al., 2016). The cochlear explants were electrically stimulated by charge-balanced biphasic electrical pulses with an amplitude of 50 or 100 μA amplitude for 8, 24, or 48 h. Cochlear explants cultured for the same duration and without ES were used as the control groups, respectively (non-ES group). The quantity of outer hair cells (OHCs), IHCs and anti-PSD95-labeled puncta and the density of SGN peripheral fibers (fiber density) near IHCs were measured after respective immunofluorescence-labeling. The ratio of the number of OHCs to IHCs number (OHC/IHC ratio) and the ratio of the number of PSD95 puncta number to IHCs (PSD95/IHC ratio) was used to evaluate the quantity of hair cells and IHC synapses, respectively. After 8 h or 24 h, there was no statistical difference in the OHC/IHC ratio, fiber density and PSD95/IHC ratio among the non-ES, 50 and 100 μA groups (*P* values in **Table 1** and **Figures 3A–C**). After 48 h, PSD95/IHC ratio of 48 h/50 μA group were also comparable to that of non-ES group ($P = 0.9170$, **Figures 3C,F,J**), but the fiber density was less than that in non-ES group ($P = 0.0097$, **Figures 3B,E,G,I,K**). Compared to with non-ES explants, cochlear explants electrically stimulated with a 100 μA pulse for 48 h showed significantly decreased fiber density and PSD95/IHC ratio ($P < 0.0001$, **Figures 3B,C,M–O**). However, after 24 h or 48 h, the OHC/IHC ratio in explants treated with 50 μA or 100 μA ES was still comparable to that in non-ES explants (24 h/50 μA group $P > 0.9999$, 24 h/100 μA group $P = 0.5872$, 48 h/50 μA group $P = 0.6174$, 48 h/100 μA group $P = 0.3631$, respectively when compared with non-ES group, **Figure 3A**). Additionally, there was no obvious difference between the hair cell morphology of ES explants and non-ES explants (**Figures 3D,H,L**).

TABLE 1 | *P* value of OHC/IHC ratio, fiber density and PSD95/IHC ratio of the 50 and 100 μA group compared with Non-ES group.

	8 h		24 h		48 h	
	50 μA	100 μA	50 μA	100 μA	50 μA	100 μA
OHC/IHC	0.8955	0.4851	>0.9999	0.5872	0.6174	0.3631
PSD95/IHC	0.4526	0.7005	0.5011	0.3921	0.9170	<0.0001
Fiber Density	0.9096	0.8528	0.4702	0.4854	0.0097	<0.0001

OHC/IHC, the ratio of OHC number to IHC number; PSD95/IHC, the ratio of PSD95 puncta number to IHC number.

The Quantity of IHC Synapses and SGN Peripheral Fibers Decreased Synchronously Under ES

We further used higher intensities of biphasic charge-balanced pulses to stimulate the cochlear explants for 48 h. Compared to the non-ES group with PSD95/IHC ratio counting to 25.38, PSD95/IHC ratios of 100, 200, and 400 μA groups significantly decreased to 20.06, 14.21, and 6.64, respectively (**Figure 4S**).

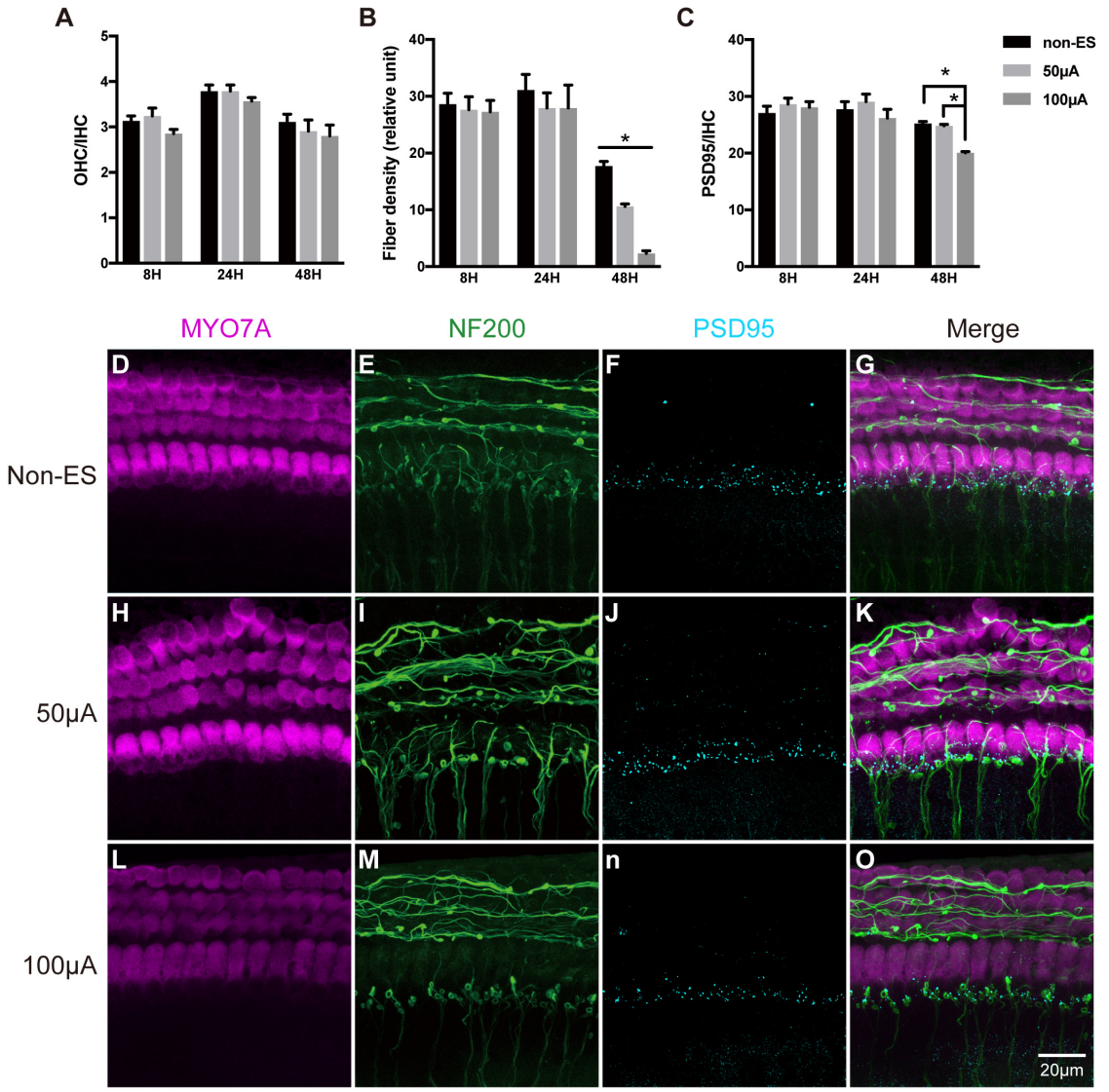

FIGURE 3 | ES did not change the quantity and morphology of hair cells in cochlear explants but induced the loss of IHC synapses and SGN peripheral fibers. **(A)** After 8, 24 or 48 h of ES, the OHC/IHC ratio was comparable in cochlear explants without ES (non-ES group), under 50 μA ES and 100 μA ES (8 h/50 μA, $P = 0.8955$; 8 h/100 μA, $P = 0.4851$; 24 h/50 μA, $P > 0.9999$; 24h/100 μA, $P = 0.5872$; 48 h/50 μA, $P = 0.6174$ and 48 h/100 μA, $P = 0.3631$), $n = 9$–20 in each group. **(B)** The density of SGN peripheral fibers significantly decreased after 48 h/50 μA and 48 h/100 μA ES compared to the non-ES group ($P = 0.0097$, $P < 0.0001$, respectively), while the fiber density in explants after 8 h or 24 h ES was comparable to that in non-ES explants (8 h/50 μA, $P = 0.9096$; 8 h/100 μA, $P = 0.8528$; 24 h/50 μA, $P = 0.4702$; 24 h/100 μA, $P = 0.4854$), $n = 9$–20 in each group. **(C)** The PSD95/IHC ratio in explants with 48 h/100 μA ES was significantly different from that in non-ES explants ($P < 0.0001$), while PSD95/IHC ratio in explants with other treatments was comparable to that in non-ES explants (8 h/50 μA, $P = 0.4526$; 8 h/100 μA, $P = 0.7005$; 24 h/50 μA, $P = 0.5011$; 24 h/100 μA, $P = 0.3921$; 48 h/50 μA, $P = 0.9170$), $n = 9$–20 in each group. **(D–O)** Typical images of cochlear explants treated with 48 h/non-ES **(D–G)**, 48 h/50 μA ES **(H–K)**, and 48 h/100 μA ES **(L–O)**. The quantity and morphology of IHCs and OHCs (in magenta, labeled with anti-Myo7A) were comparable in explants treated with non-ES **(D)**, 50 μA ES **(H)** and 100 μA ES **(L)**. The density of SGN peripheral fibers (in green, labeled with anti-neurofilament-200, NF200) in explants treated with 50 μA (l) or 100 μA ES **(M)** was less than that in explants treated with non-ES **(E)**. The number of IHC synapses (in cyan, labeled with anti-PSD95) in explants treated with 100 μA ES **(N)** was much less than that in explants treated with 50 μA ES **(J)** or non-ES **(F)**. $^*P < 0.05$. Data represent the mean + SEM. Two-way ANOVA followed by Dunnett's multiple comparisons test was used in all the experiments mentioned above.

Additionally, the fiber densities of 100, 200, and 400 μA groups also significantly decreased to 4.17, 2.34, and 1.10, respectively, compared to 7.58 in the non-ES group (**Figure 4R**). The density of SGN peripheral fibers and the quantity of IHC synapses were synchronously decreased with increasing ES intensity (**Figures 4E–P**). However, there was still no significant difference in the morphology of hair cells and the OHC/IHC ratios among these groups (**Figures 4A–D,Q**). There was a significant correlation between fiber density and PSD95/IHC ratio (Pearson test, $r = 0.954$, $P = 0.046$, **Figure 4T**). These results demonstrated that ES synchronously decreased the quantity of IHC synapses and SGN peripheral fibers in a current intensity-dependent

manner, but did not change the morphology or quantity of hair cells. Thus, we only used fiber density to evaluate the change of cochlear structure in the following experiments.

Inhibition of Calcium Influx Attenuated the ES-Induced Loss of SGN Peripheral Fibers and IHC Synapses

To investigate the role of calcium influx through VDCCs in the ES-induced degeneration of SGN peripheral fibers and IHC synapses, we inhibited calcium influx in 48 h/100 μA cochlear explants by bath application of various VDCC blockers, i.e., 10 μM L-type Ca^{2+} channel blocker VPL, 1 μM N-type Ca^{2+} channel blocker GVIA, 1 μM P/Q-type Ca^{2+} channel blocker IVA and their mixture (CCBM). The fiber density and PSD/IHC ratio of 48 h/100 μA group was significantly lower than those of the non-ES group as described above ($P < 0.0001$). However, fiber density and PSD/IHC ratio of the groups treated with any VDCC blocker were comparable to those of the non-ES group (P in **Table 2** and **Figures 5A,C**). We also inhibited calcium influx in 48 h/100 μA cochlear explants by maintaining them in Ca^{2+}-free medium or in medium with 10 μM Cd, a non-selective calcium channel blocker. As a result, the fiber density and PSD/IHC ratio were also comparable to those of the non-ES group (P in **Table 3** and **Figures 5B,D**). These results suggested that calcium influx through VDCCs is vital to the ES-induced degeneration of SGN peripheral fibers and IHC synapses.

ES Increased the Activity of ROS and RNS in Cochlear Explants

To investigate whether ES caused oxidative stress in cochlear explants by increasing calcium influx, we measured ROS/RNS activity in explants under various intensities of ES for 48 h. ROS/RNS activity in explants under ES with amplitudes of 25, 50, 100, 200, and 400 μA were increased to 2.9, 2.1, 1.7, 4.4, and 6.5-fold to that of non-ES group, respectively ($P = 0.0020$, 0.0442, 0.1606, <0.0001, and <0.001, respectively when compared with the non-ES group, **Figure 6A**). In addition, ROS/RNS activity increased in an intensity-dependent manner when cochlear explants had amplitudes greater than 50 μA (**Figure 6B**). To investigate the role of calcium influx through VDCCs in the change in ROS/RNS activity, we added a mixture of VPL, GVIA and IVA to culture medium of 48 h/100 μA cochlear explants. As a result, ROS/RNS activity decreased to a level comparable to that of the non-ES group ($P = 0.1072$, **Figure 6C**). These results suggested that ES could increase ROS/RNS activity and cause oxidative stress by increasing calcium influx through VDCCs.

TABLE 2 | *P* value of fiber density and PSD95/IHC ratio of the Non-ES/CCB and 100 μA/CCB group compared with Non-ES group.

	PSD95/IHC	Fiber Density
Non-ES/Ca^{-}	0.6568	0.8194
Non-ES/Cd	0.9983	0.8073
100 μA/Ca^{-}	0.9455	0.9527
100 μA/Cd	0.8361	0.4058

VPL, verapamil; IVA, ω-agatoxin IVA; GVIA, ω-conotoxin GVIA; CCBM, the mixture of VPL; IVA and GVIA, CCB, calcium channel blockers.

ES Inhibited GPx Expression in Cochlear Explants

We hypothesized that the ES-induced increase in ROS/RNS activity in cochlear explants might be due to the altered expression of oxidative stress-related genes. We evaluated the mRNA expression levels of GPx1 and GPx2 in cochlear explants under various intensities of ES and without ES. Significant decreases in the GPx1 and GPx2 expression levels were both observed in 200 μA/48 h- and 400 μA/48 h-treated explants compared with non-ES explants, respectively (GPx1: 200 μA $P = 0.0231$ and 400 μA $P = 0.0233$, GPx2: 200 μA $P = 0.0484$ and 400 μA $P = 0.0228$, **Figures 7A,B**). The GPx1 expression level in 100 μA/48 h-treated explants also decreased compared to that in non-ES explants ($P = 0.0647$, **Figure 7A**). These results demonstrated that ES could result in downregulation of GPx1 and GPx2 mRNA expression levels.

Ebselen Prevented the Decrease of GPx Expression as Well as the Loss of SGN Peripheral Fibers in Cochlear Explants Exposed to ES

Ebselen is an organoselenium compound that acts as a GPx mimetic and is thereby able to prevent the cellular damage induced by the ROS and RNS generated and accumulated during various cellular processes. To investigate whether the ES-mediated downregulation of GPx and the increase in ROS/RNS activity caused the degeneration of SGN peripheral fibers and IHC synapses, we maintained cochlear explants in medium with 40 μM ebselen for 48 h. As a result, the GPx1 and GPx2 expression levels in 100 μA/48 h-, 200 μA/48 h- and 400 μA/48 h-treated cochlear explants were comparable level to those in non-ES explants (**Figures 7A,B**). Moreover, the density of SGN peripheral fibers in all ES-treated groups was also comparable to that in non-ES group (**Figures 7C–P**). These results indicated that ES-induced downregulation of GPx1 and GPx2 expression levels caused the degeneration of SGN peripheral fibers in cochlear explants.

Increased Oxidative Stress in Cochlear Explants Induced by H_2O_2 Treatment Resulted in the Loss of SGN Peripheral Fibers

To further investigate the role of oxidative stress in ES-induced degeneration of SGN peripheral fibers, we added H_2O_2 to cochlear explant cultures to induce oxidative stress and evaluated the density of SGN peripheral fibers. Similar to ES, maintaining cochlear explants in medium with 250 μM H_2O_2 for 8 h did not change the hair cells morphology and OHC/IHC ratio ($P = 0.9990$, **Figures 8A,E**) but did significantly decrease the density of SGN peripheral fibers ($P < 0.0001$, **Figures 8B,I,M**), compared to maintaining cochlear explants

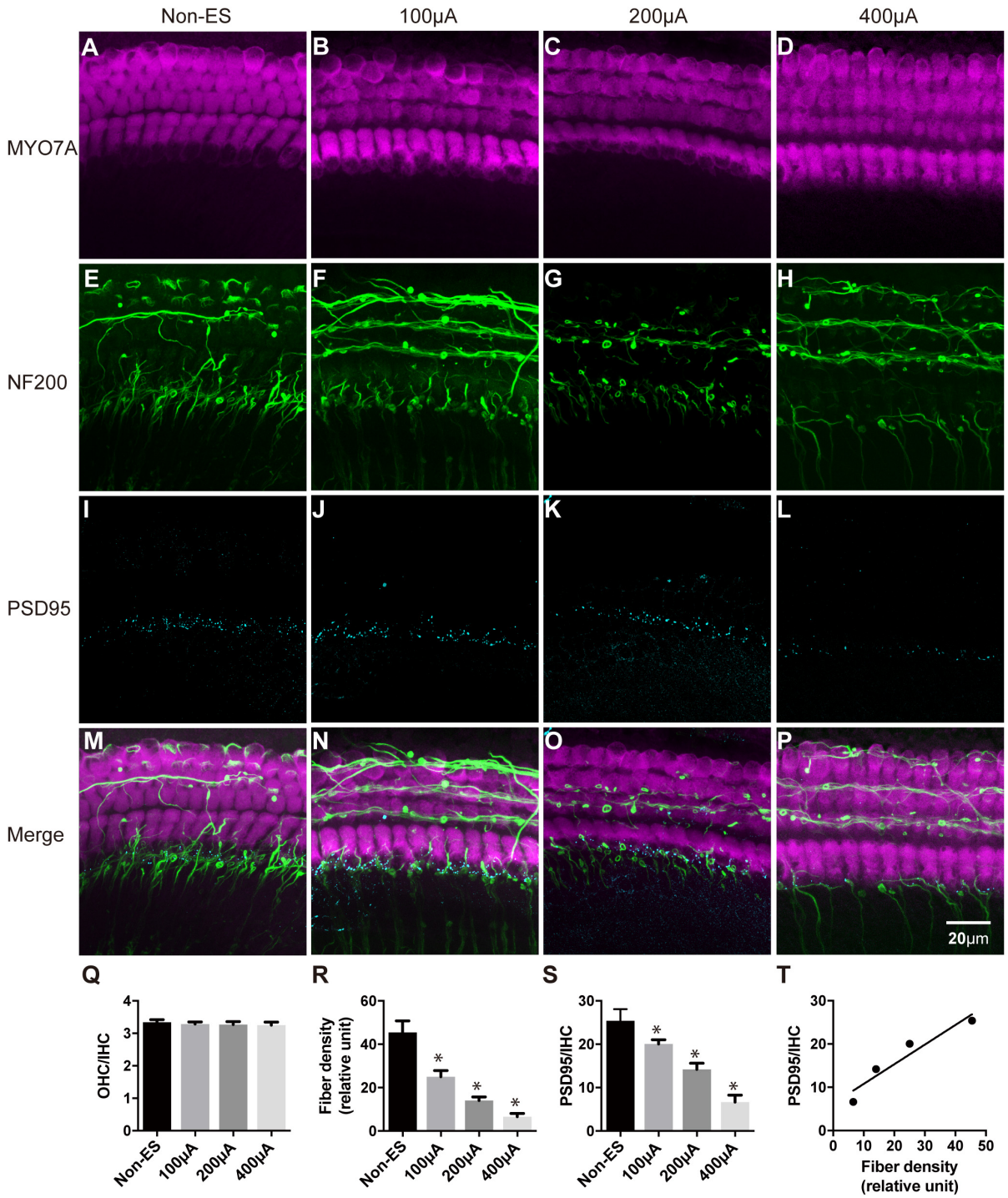

FIGURE 4 | The density of SGN peripheral fibers and the quantity of IHC synapses were synchronously decreased with increasing ES intensity. The quantity and morphology of hair cells (in magenta) were comparable in explants treated with non-ES, 100 μA ES, 200 μA ES or 400 μA ES for 48 h (**A–D**; $P = 0.6957$, $P = 0.5289$, $P = 0.3364$, compared with non-ES in panel **Q**, one-way ANOVA followed by Dunnett's multiple comparisons test, the following comparisons in this paper used the same method unless otherwise noted, $n = 5$ in each group). The density of SGN peripheral fibers (in green) in explants treated with 100, 200, and 400 μA ES for 48 h was significantly less than that in non-ES explants (**E–H**; * in panel **R**, $P = 0.0001$ when compared to non-ES, $n = 20$ in each group). The PSD95/IHC ratio in explants treated with 100, 200, and 400 μA ES for 48 h was also significantly less than that in non-ES explants (**I–L**; * in panel **S**, $P = 0.0001$ when compared to non-ES, $n = 20$ in each group). **(M–P)** The merged images of the upper three images under the same conditions, respectively. **(T)** There was a significant correlation between the change of SGN peripheral fiber density and the PSD95-punch/IHC ratio with the increase of ES intensity (Pearson test, $r = 0.9538$, $P = 0.0462$). Data represent the mean + SEM.

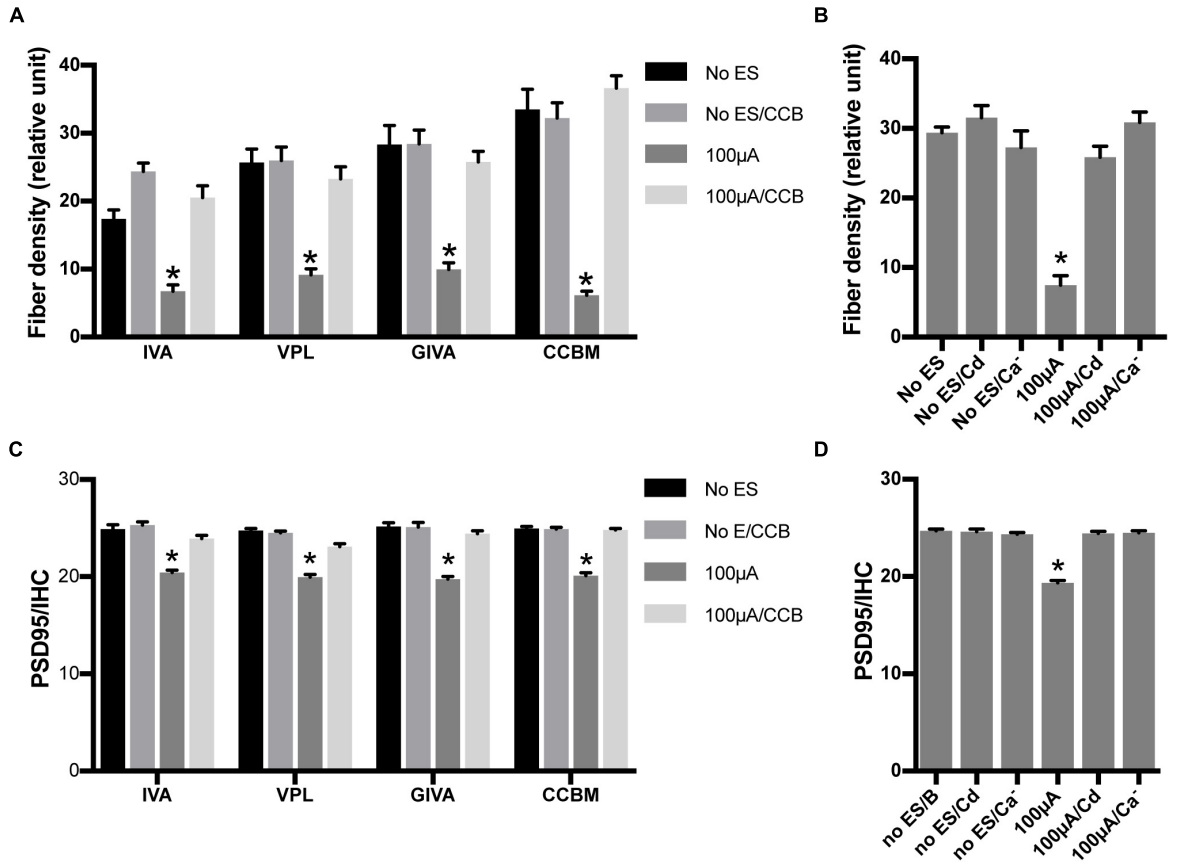

FIGURE 5 | Inhibiting calcium influx attenuated the loss of SGN peripheral fibers and IHC synapses induced by ES. **(A)** PSD95/IHC ratio was significantly decreased in explants treated with 100 μA/48 h ES compared with non-ES explants, while explants simultaneously treated with 100 μA/48 h ES and various types of voltage-dependent calcium channel blockers (CCB), including 10 μM VPL, 1 μM GVIA, 1 μM IVA and their mixture (CCBM), were not significantly different from the non-ES group $n = 7$–12 in each group. **(B)** When ES-treated explants were also treated with 10 μM Cd or maintained in calcium-free medium (Ca^-), the PSD95/IHC ratio was also comparable to that of non-ES explants $n = 9$ in each group. **(C)** The density of SGN peripheral fibers was comparable in ES-treated explants also treated with VPL, GVIA, IVA or CCB and in non-ES explants, $n = 12$ in each group. **(D)** The density of SGN peripheral fibers was also comparable in ES-treated cochlear explants also treated with Cd or maintained in calcium-free medium and in non-ES explants, $n = 12$ in each group. *$p < 0.001$ compared with any other group in the same experiment, one-way ANOVA followed by Dunnett's multiple comparisons. Data represent the mean + SEM.

without H_2O_2 treatment (**Figures 8C,G,K**). However, the quantity and morphology of HCs and the fiber density of explants simultaneously treated with 250 μM H_2O_2 and 40 μM ebselen for 8 h was not different ($P = 0.3828$, **Figures 8B,D,F,H,J,L,N**), from that of explants without treatment. These results further indicated that oxidative stress could induce the degeneration of SGN peripheral fibers.

TABLE 3 | *P* value of fiber density and PSD95/IHC ratio of the Non-ES/Ca^-, Non-ES/Cd, 100 μA/Ca^- and 100 μA/Cd group compared with Non-ES group.

	PSD95/IHC		Fiber Density	
	Non-ES	**100 μA**	**Non-ES**	**100 μA**
VPL	0.9208	0.0002	0.9995	0.7532
IVA	0.7979	0.2014	0.0041	0.3629
GVIA	0.9995	0.5060	>0.9999	0.8033
CCBM	0.9969	0.9618	0.9768	0.7404

Non-ES/Ca^-, cochlear explants without electrical stimulation in calcium-free medium; Non-ES/Cd, cochlear explants without electrical stimulation in medium with cadmium chloride; 100 μA/Ca^-, cochlear explants with 100 μA electrical stimulation in calcium-free medium; 100 μA/Cd, cochlear explants with 100 μA electrical stimulation in medium with cadmium chloride.

DISCUSSION

Electrical stimulation is used by CI and other neurostimulation devices to activate targeting neurons. The impact of ES on targeted and related neural structures when neurostimulation devices are used as modulators of existing neural function instead of as substitutes of non-functioning neural tissues, warrants additional attention. As shown in cochlea implant recipients using EAS technology, there was a delayed loss of residual low-frequency hearing function (Von Ilberg et al., 1999; Gantz and Turner, 2003; Kiefer et al., 2005). Here we show, that ES could degenerated the connection between the targeted neuron and modulated neural structures *in vitro*. In addition, calcium influx

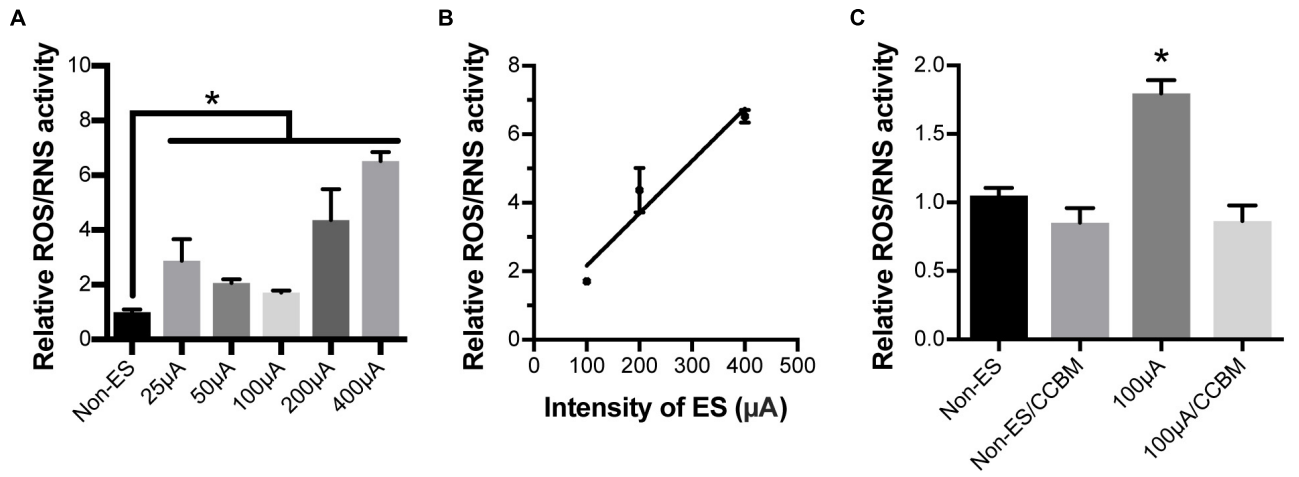

FIGURE 6 | Electrical stimulation increased ROS/RNS activity in cochlear explants but inhibiting calcium influx completely abolished this effect. **(A)** ROS/RNS activity of explants under 25, 50, 100, 200, and 400 μA ES for 48 h was significantly higher than that of non-ES explants. $^*P < 0.05$ when compared with non-ES group, $n = 3$ in each group, measurements were repeated three times. **(B)** ROS/RNS activities increased in an ES intensity-dependent manner. Pearson's test, $r = 0.9691$, $P = 0.1587$ (two-tailed). **(C)** When 100 μA/48 h ES-treated cochlear explants were also treated with CCB mixture (CCBM), the level of ROS/RNS activity was comparable to that in non-ES explants. $^*p < 0.001$ when compared with any other group, $n = 3$ in each group, measurements were repeated three times. Data represented the mean + SEM.

through VDCCs and resulting oxidative stress played important roles in this effect.

Our study suggested that continuous charge-balanced biphasic ES with an intensity up to 48 h/400 μA did not change the numbers of hair cells in cochlear explants. In accordance with our study, a recent *in vitro* study also reported that ES could induce synaptic change in cochlear tissues (Peter et al., 2019). In addition, several previous animal studies also found no morphological changes in hair cells and SGNs associated with ES (Ni et al., 1992; Shepherd et al., 1994; Coco et al., 2007; Irving et al., 2013; O'Leary et al., 2013), even though low-frequency hearing deteriorate after ES (O'Leary et al., 2013; Tanaka et al., 2014). A postmortem histopathological study also suggested that there was no significant loss of SGNs and hair cells in EAS recipients with delayed hearing loss (Quesnel et al., 2015). Our study demonstrated that SGN peripheral fibers and IHC synapses in cochlear explants decreased under the ES with charge-balanced biphasic pulses used by CIs. The charge intensities used in this study were far less than the maximum charge intensities allowed in commercial CIs. However, animal studies are warranted to further investigate whether a similar change is the cause of residual low-frequency hearing loss in EAS recipients.

Electrical stimulation can induce the activation of VDCCs and result in Ca^{2+} influx. Calcium influx through VDCCs was involved in the inhibition of SGN neurite extension induced by continuous ES or membrane depolarization accomplished by raising extracellular K^+ (Roehm et al., 2008; Shen et al., 2016). Calcium overload has been shown to cause damage to SGNs (Hegarty et al., 1997; Roehm et al., 2008). Our study suggested that blocking various types of VDCCs by bath application of VDCC blockers, by the non-selective VDCC blocker cadmium or by the removal of extracellular Ca^{2+} attenuated the ES-induced loss of SGN peripheral fibers and IHC synapses. The mixture of VPL, GVIA, and IVA also abolished the ES-induced increase in ROS/RNS activity in cochlear explants. These results suggest that calcium influx through VDCCs plays a key role in ES-induced cochlear synaptic degeneration.

The ES-induced loss of SGN peripheral terminals and IHC synapses with the preservation of hair cells and SGNs is similar to the changes that appeared in the early stage of noise-induced hearing loss (Kujawa and Liberman, 2009; Lin et al., 2011). Previous studies have suggested that the excitotoxicity and calcium overload play critical roles in noise-induced hearing loss (Le Prell et al., 2007; Kujawa and Liberman, 2009). Mimicking excitotoxicity in cochlear explant culture by brief treatment with NMDA and kainite also resulted in the loss of IHC synapses and SGN peripheral axons with the organ of Corti and SGNs intact (Wang and Green, 2011). Taken together, these findings suggest that the manifestations of cochlear explants under ES were similar to the findings in animal studies of CI chronic ES, and noise-induced hearing loss and in the *in vitro* study of excitotoxicity in cochlear explants. This suggested that excitotoxicity and calcium overload might play important roles in delayed EAS hearing loss. This theory was supported by our results that the inhibition of calcium influx prevented the loss of IHC synapses and SGN peripheral terminals. Interestingly, a close correlation between EAS hearing loss and a history of noise-induced hearing loss shown in a recent clinical study provides further support for this postulation (Kopelovich et al., 2014).

Our study showed that ES induced an increase in ROS/RNS activity in cochlear explants. The increase in ROS/RNS activity was closely correlated with the intensity of ES. After the increase in ROS/RNS activity was prevented by ebselen, the loss of SGN peripheral fibers in ES-treated cochlear explants was significantly attenuated to a level comparable to that of non-ES

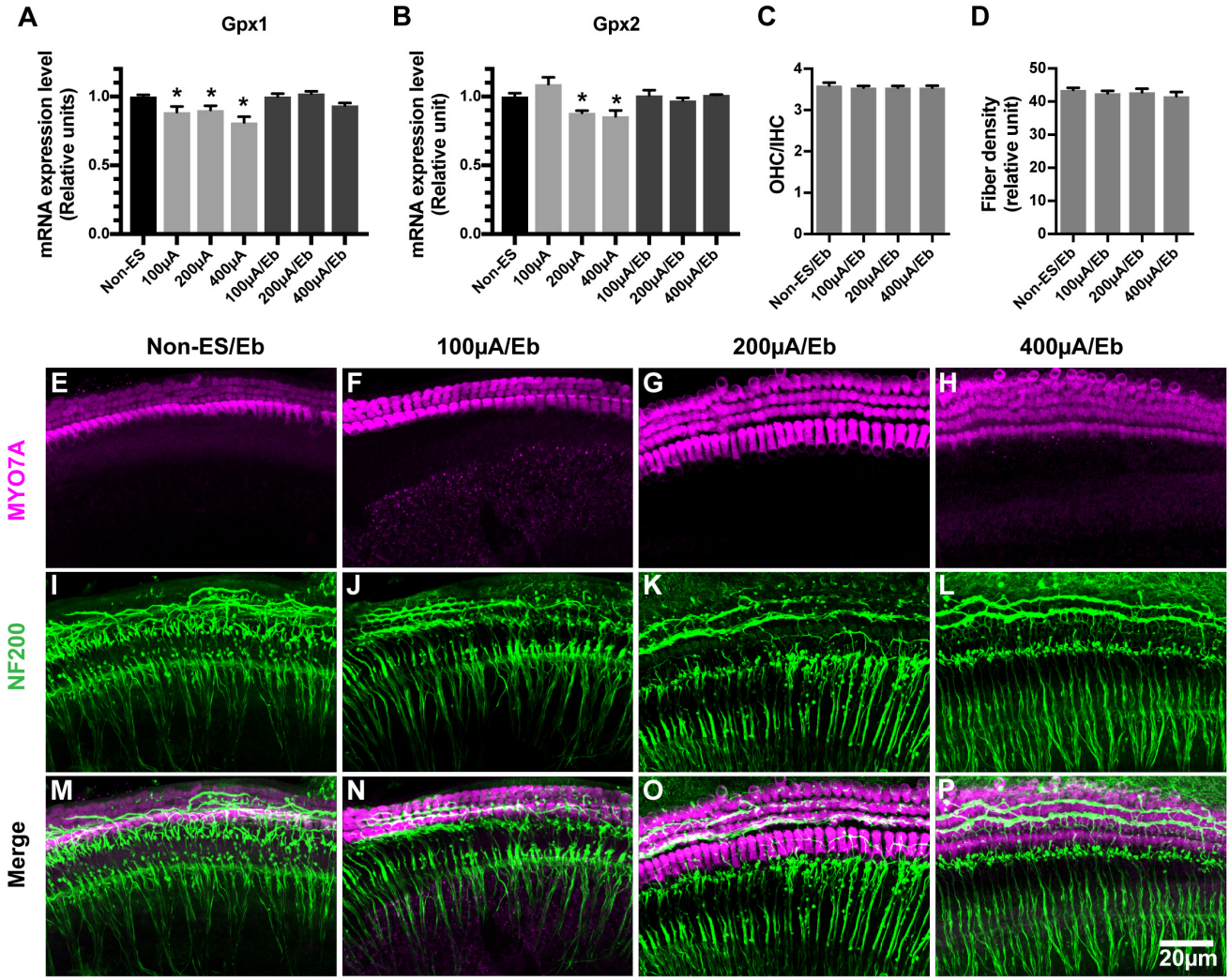

FIGURE 7 | The mRNA expression level of GPx1 and GPx2 in cochlear explants decreased under ES and ebselen abolished this effect and the loss of SGN peripheral fibers. **(A,B)** ES treatment of 200 and 400 μA/48 h both significantly decreased the mRNA expression level of both GPx1 and GPx2 in explants while 100 μA/48 h-ES treatment only decreased the mRNA expression level of GPx1 (*, GPx1: 200 μA, $P = 0.0231$; 400 μA, $P = 0.0233$; GPx2: 200 μA, $P = 0.0484$; 400 μA, $P = 0.0228$, when compared to non-ES group, $n = 3$ in each group, measurements were repeated three times). When the cochlear explants were treated with ES and 40 μM Ebselen at the same time, mRNA expression level of GPx1 and GPx2 was comparable to that in non-ES group (GPx1: 100 μA/Eb, $P > 0.9999$; 200 μA/Eb, $P = 0.9738$; 400 μA/Eb, $P = 0.4027$; GPx2: 100 μA/Eb, $P > 0.9999$; 200 μA/Eb, $P > 0.9999$; 400 μA/Eb, $P > 0.9999$ compared to non-ES group). When the cochlear explants were treated with 40 μM Ebselen, OHC/IHC ratio (**C**, $P = 0.7997$, $P = 0.7629$, $P = 0.7639$, in each group.) and the density of SGN peripheral fibers (**D**, $P = 0.7860$, $P = 0.9025$, $P = 0.3482$, $n = 20$ in each group.) in 100, 200, and 400 μA/48 h-ES groups had no significantly statistical difference from those in the non-ES group. **(E–P)** Representative images showed that there was no significant loss of hair cells (in magenta) and SGN peripheral fibers (in green) in ES-treated explants when they were maintained in medium with 40 μM Ebselen. Data represented the mean + SEM.

cochlear explants. These results suggested that oxidative stress played an important role in the ES-induced loss of SGN-IHC connections. Oxidative stress has also been reported to play important roles in hearing loss induced by noise, aminoglycoside antibiotics, cisplatin and aging (Choi and Choi, 2015; Sheth et al., 2017; Tavanai and Mohammadkhani, 2017). Excessively high ROS and RNS activity can cause damage to DNA, lipids and proteins, trigger hair cell death and result in hearing loss (Fetoni et al., 2015). We added H_2O_2 to the culture medium to induce oxidative stress and consequently caused a change similar to the ES-induced loss of IHCs-SGNs connection. These results further supported our hypothesis that ES induces cochlear synaptic degeneration through calcium influx-induced oxidative stress.

This study demonstrated that GPx1 and GPx2 expression levels significantly decreased after 200 μA/48 h and 400 μA/48 h ES. Interestingly, GPx1 expression level significantly decreased even after a relatively weak ES, i.e., 100 μA/48 h of ES, while GPx2 expression level insignificantly decreased. In accordance with our study, a decrease in GPx1 activity was shown to play an important role in noise-induced hearing loss (Kil et al., 2007). The targeted mutation of the GPx1 gene in mice

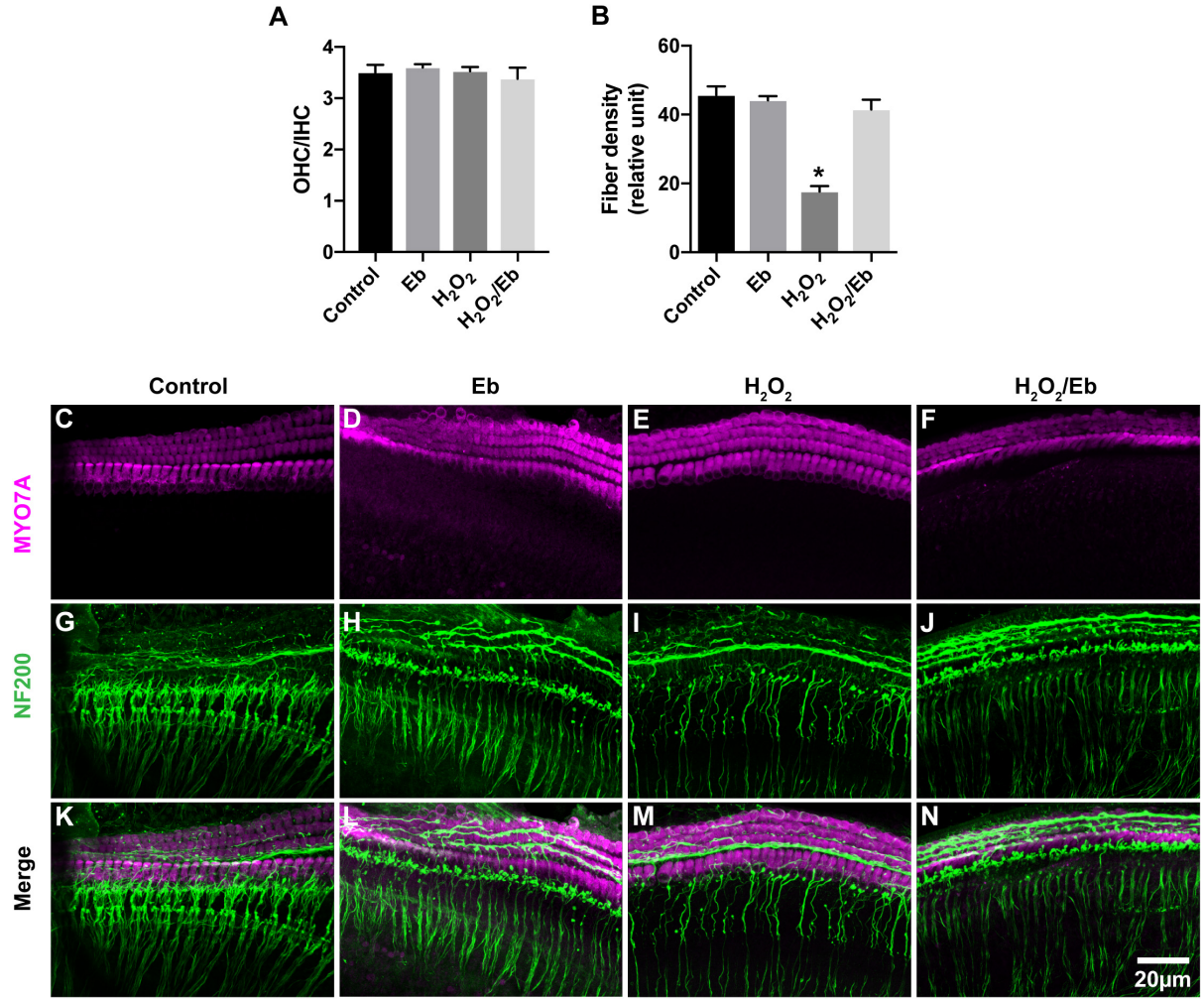

FIGURE 8 | Increased oxidative stress in cochlear explants induced by H_2O_2 treatment resulted in the loss of SGN peripheral fibers. **(A)** Treatment of explants with 250 μM H_2O_2, 40 μM ebselen or both did not cause any significant difference in the OHC/IHC (in magenta) ratio from that of explants without these treatments. $P = 0.9990$, $P = 0.9294$, $P = 0.8813$, respectively, $n = 3$–5 in each group. **(B)** Treatment of cochlear explants with 250 μM H_2O_2 significantly decreased the density of SGN peripheral fibers (in green, $^*P < 0.0001$), while treatment of cochlear explants with both 250 μM H_2O_2 and 40 μM ebselen did not decrease the density ($P = 0.3828$, $n = 8$ in each group), compared to the density in explants without H_2O_2 or ebselen treatment. **(C–N)** Typical images of cochlear explants treated with 8 h/control **(C,G,K)**, 8 h/Eb **(D,H,L)**, 8 h/H_2O_2 **(E,I,M)** and 8 h/H_2O_2 Eb **(F,J,N)**. The quantity and morphology of IHCs and OHCs (in magenta, labeled with anti-Myo7A) were comparable in explants treated with control **(C)**, Eb **(D)**, H_2O_2 **(E)**, and H_2O_2 Eb **(F)**. The density of SGN peripheral fibers (in green, labeled with anti-neurofilament-200, NF200) were similar explants treated with control **(G)**, Eb **(H)**, and H_2O_2 Eb **(J)**, while the density was less than that in explants treated with H_2O_2 **(I)**. Data represented the mean + SEM.

also increased their vulnerability to noise-induced hearing loss (Ohlemiller et al., 2000). Ebselen could inhibit iNOS (Zembowicz et al., 1993) and mimic the anti-oxidative enzyme GPx (Ohlemiller et al., 2000). Ebselen treatment reducse the severity and duration of noise-induced hearing loss of in animals as well as human beings (Pourbakht and Yamasoba, 2003; Kil et al., 2017). In our study, ebselen treatment significantly increased GPx1 and GPx2 expression levels which were decreased by ES. Additionally, the ES-induced loss of SGN peripheral fibers was completely abolished. These results strongly supported that the decrease in GPx1 and GPx2 expression levels played a vital role in ES-induced loss of IHC-SGN connections. Our study also indicated that ebselen might be a promising agent to protect the residual hearing of EAS recipients although further *in vivo* studies are needed.

In conclusion, our study demonstrated that ES with charge-balanced biphasic pulses could result in the synchronous degeneration of SGN peripheral fibers and IHC synapses in a current intensity- and duration-dependent manner *in vitro*. Calcium influx through VDCC and resulting oxidative stress played key roles in this effect. Ebselen was shown to be a potential protector of ES-induced cochlear synaptic degeneration. Our study provides novel insights into delayed hearing loss in EAS recipients as well as the impact of other neurostimulation devices on targeting neural structures. However, only middle turn of immature cochlea was used in our study. Whether

there is different impact of electrical stimulation on different part of cochlea or mature cochlear tissues should be investigated further. Notably, animal studies are also necessary to investigate the status of IHC synapses and SGN peripheral fibers under chronic ES.

DATA AVAILABILITY STATEMENT

All datasets generated for this study are included in the manuscript/supplementary files.

ETHICS STATEMENT

This study was carried out in accordance with the recommendations of the Ethics Review Board of Eye and ENT Hospital of Fudan University. The protocol was approved by the Ethics Review Board of Eye and ENT Hospital of Fudan University.

AUTHOR CONTRIBUTIONS

NS contributed the experiments of duration and intensity effect, calcium influx manipulation as well as related statistical analysis. QL performed all other experiments and related analysis. BL contributed a part of imaging work under confocal microscope. ZW contributed the design of experiments. SL contributed the design of all experiments, the writing of manuscript and preparation of figures. CX and ZS contributed the adjust of multichannel charge-balanced biphasic pulse generator.

FUNDING

This work was supported by the National Natural Science Foundation of China (NSFC, 81171482 and 81670927), the Research Special Fund for Public Welfare Industry of Health (201202001), Fund of the Science and Technology Commission of Shanghai Municipality (12DZ2251700), and Shanghai Pujiang Program (18PJD004).

REFERENCES

Choi, C. H., and Oghalai, J. S. (2005). Predicting the effect of post-implant cochlear fibrosis on residual hearing. *Hear. Res.* 205, 193–200. doi: 10.1016/j.heares.2005.03.018

Choi, S. H., and Choi, C. H. (2015). Noise-induced neural degeneration and therapeutic effect of antioxidant drugs. *J. Audiol. Otol.* 19, 111–119. doi: 10.7874/jao.2015.19.3.111

Coco, A., Epp, S. B., Fallon, J. B., Xu, J., Millard, R. E., and Shepherd, R. K. (2007). Does cochlear implantation and electrical stimulation affect residual hair cells and spiral ganglion neurons? *Hear. Res.* 225, 60–70. doi: 10.1016/j.heares.2006.12.004

Fetoni, A. R., Troiani, D., Petrosini, L., and Paludetti, G. (2015). Cochlear injury and adaptive plasticity of the auditory cortex. *Front. Aging Neurosci.* 7:8. doi: 10.3389/fnagi.2015.00008

Fridberger, A., Flock, A., Ulfendahl, M., and Flock, B. (1998). Acoustic overstimulation increases outer hair cell Ca2+ concentrations and causes dynamic contractions of the hearing organ. *Proc. Natl. Acad. Sci. U.S.A.* 95, 7127–7132. doi: 10.1073/pnas.95.12.7127

Gantz, B. J., Hansen, M. R., Turner, C. W., Oleson, J. J., Reiss, L. A., and Parkinson, A. J. (2009). Hybrid 10 clinical trial: preliminary results. *Audiol. Neurootol.* 14(Suppl. 1), 32–38. doi: 10.1159/000206493

Gantz, B. J., and Turner, C. W. (2003). Combining acoustic and electricalal hearing. *Laryngoscope* 113, 1726–1730. doi: 10.1097/00005537-200310000-00012

Gfeller, K. E., Olszewski, C., Turner, C., Gantz, B., and Oleson, J. (2006). Music perception with cochlear implants and residual hearing. *Audiol. Neurootol.* 11(Suppl. 1), 12–15. doi: 10.1159/000095608

Gstoettner, W., Helbig, S., Settevendemie, C., Baumann, U., Wagenblast, J., and Arnoldner, C. (2009). A new electrode for residual hearing preservation in cochlear implantation: first clinical results. *Acta Otolaryngol.* 129, 372–379. doi: 10.1080/00016480802552568

Hegarty, J. L., Kay, A. R., and Green, S. H. (1997). Trophic support of cultured spiral ganglion neurons by depolarization exceeds and is additive with that by neurotrophins or cyclic AMP, and requires elevation of [Ca2+]i within a set range. *J. Neurosci.* 17, 1959–1970. doi: 10.1523/jneurosci.17-06-01959.1997

Irving, S., Trotter, M. I., Fallon, J. B., Millard, R. E., Shepherd, R. K., and Wise, A. K. (2013). Cochlear implantation for chronic electrical stimulation in the mouse. *Hear. Res.* 306, 37–45. doi: 10.1016/j.heares.2013.09.005

Kiefer, J., Pok, M., Adunka, O., Sturzebecher, E., Baumgartner, W., Schmidt, M., et al. (2005). Combined electric and acoustic stimulation of the auditory system: results of a clinical study. *Audiol. Neurootol.* 10, 134–144. doi: 10.1159/000084023

Kil, J., Lobarinas, E., Spankovich, C., Griffiths, S. K., Antonelli, P. J., Lynch, E. D., et al. (2017). Safety and efficacy of ebselen for the prevention of noise-induced hearing loss: a randomised, double-blind, placebo-controlled, phase 2 trial. *Lancet* 390, 969–979. doi: 10.1016/S0140-6736(17)31791-9

Kil, J., Pierce, C., Tran, H., Gu, R., and Lynch, E. D. (2007). Ebselen treatment reduces noise induced hearing loss via the mimicry and induction of glutathione peroxidase. *Hear. Res.* 226, 44–51. doi: 10.1016/j.heares.2006.08.006

Kopelovich, J. C., Reiss, L. A., Oleson, J. J., Lundt, E. S., Gantz, B. J., and Hansen, M. R. (2014). Risk factors for loss of ipsilateral residual hearing after hybrid cochlear implantation. *Otol. Neurotol.* 35, 1403–1408. doi: 10.1097/MAO.0000000000000389

Kujawa, S. G., and Liberman, M. C. (2009). Adding insult to injury: cochlear nerve degeneration after "temporary" noise-induced hearing loss. *J. Neurosci.* 29, 14077–14085. doi: 10.1523/JNEUROSCI.2845-09.2009

Le Prell, C. G., Yamashita, D., Minami, S. B., Yamasoba, T., and Miller, J. M. (2007). Mechanisms of noise-induced hearing loss indicate multiple methods of prevention. *Hear. Res.* 226, 22–43. doi: 10.1016/j.heares.2006.10.006

Lin, H. W., Furman, A. C., Kujawa, S. G., and Liberman, M. C. (2011). Primary neural degeneration in the Guinea pig cochlea after reversible noise-induced threshold shift. *J. Assoc. Res. Otolaryngol.* 12, 605–616. doi: 10.1007/s10162-011-0277-0

Makary, C. A., Shin, J., Kujawa, S. G., Liberman, M. C., and Merchant, S. N. (2011). Age-related primary cochlear neuronal degeneration in human temporal bones. *J. Assoc. Res. Otolaryngol.* 12, 711–717. doi: 10.1007/s10162-011-0283-2

Ni, D., Shepherd, R. K., Seldon, H. L., Xu, S. A., Clark, G. M., and Millard, R. E. (1992). Cochlear pathology following chronic electrical stimulation of the auditory nerve. I: normal hearing kittens. *Hear. Res.* 62, 63–81. doi: 10.1016/0378-5955(92)90203-y

Ohlemiller, K. K., McFadden, S. L., Ding, D. L., Lear, P. M., and Ho, Y. S. (2000). Targeted mutation of the gene for cellular glutathione peroxidase (Gpx1) increases noise-induced hearing loss in mice. *J. Assoc. Res. Otolaryngol.* 1, 243–254. doi: 10.1007/s101620010043

O'Leary, S. J., Monksfield, P., Kel, G., Connolly, T., Souter, M. A., Chang, A., et al. (2013). Relations between cochlear histopathology and hearing loss in experimental cochlear implantation. *Hear. Res.* 298, 27–35. doi: 10.1016/j.heares.2013.01.012

Peter, M. N., Warnecke, A., Reich, U., Olze, H., Szczepek, A. J., Lenarz, T., et al. (2019). Influence of in vitro electrical stimulation on survival of spiral ganglion neurons. *Neurotox. Res.* 36, 204–216. doi: 10.1007/s12640-019-00017-x

Pourbakht, A., and Yamasoba, T. (2003). Ebselen attenuates cochlear damage caused by acoustic trauma. *Hear. Res.* 181, 100–108. doi: 10.1016/s0378-5955(03)00178-3

Quesnel, A. M., Nakajima, H. H., Rosowski, J. J., Hansen, M. R., Gantz, B. J., Nadol, J. B. Jr., et al. (2015). Delayed loss of hearing after hearing preservation cochlear implantation: human temporal bone pathology and implications for etiology. *Hear. Res.* 333, 225–234. doi: 10.1016/j.heares.2015.08.018

Roehm, P. C., Xu, N., Woodson, E. A., Green, S. H., and Hansen, M. R. (2008). Membrane depolarization inhibits spiral ganglion neurite growth via activation of multiple types of voltage sensitive calcium channels and calpain. *Mol. Cell. Neurosci.* 37, 376–387. doi: 10.1016/j.mcn.2007.10.014

Santa Maria, P. L., Domville-Lewis, C., Sucher, C. M., Chester-Browne, R., and Atlas, M. D. (2013). Hearing preservation surgery for cochlear implantation–hearing and quality of life after 2 years. *Otol. Neurotol.* 34, 526–531. doi: 10.1097/MAO.0b013e318281e0c9

Sergeyenko, Y., Lall, K., Liberman, M. C., and Kujawa, S. G. (2013). Age-related cochlear synaptopathy: an early-onset contributor to auditory functional decline. *J. Neurosci.* 33, 13686–13694. doi: 10.1523/JNEUROSCI.1783-13.2013

Shen, N., Liang, Q., Liu, Y., Lai, B., Li, W., Wang, Z., et al. (2016). Charge-balanced biphasic electrical stimulation inhibits neurite extension of spiral ganglion neurons. *Neurosci. Lett.* 624, 92–99. doi: 10.1016/j.neulet.2016.04.069

Shepherd, R. K., Matsushima, J., Martin, R. L., and Clark, G. M. (1994). Cochlear pathology following chronic electrical stimulation of the auditory nerve: II. Deafened kittens. *Hear. Res.* 81, 150–166. doi: 10.1016/0378-5955(94)90162-7

Sheth, S., Mukherjea, D., Rybak, L. P., and Ramkumar, V. (2017). Mechanisms of cisplatin-induced ototoxicity and otoprotection. *Front. Cell. Neurosci.* 11:338. doi: 10.3389/fncel.2017.00338

Tanaka, C., Nguyen-Huynh, A., Loera, K., Stark, G., and Reiss, L. (2014). Factors associated with hearing loss in a normal-hearing guinea pig model of Hybrid cochlear implants. *Hear. Res.* 316, 82–93. doi: 10.1016/j.heares.2014.07.011S0378-5955(14)00129-4

Tavanai, E., and Mohammadkhani, G. (2017). Role of antioxidants in prevention of age-related hearing loss: a review of literature. *Eur. Arch. Otorhinolaryngol.* 274, 1821–1834. doi: 10.1007/s00405-016-4378-6

Turner, C., Gantz, B. J., and Reiss, L. (2008). Integration of acoustic and electrical hearing. *J. Rehabil. Res. Dev.* 45, 769–778. doi: 10.1682/jrrd.2007.05.0065

Turner, C. W., Gantz, B. J., Vidal, C., Behrens, A., and Henry, B. A. (2004). Speech recognition in noise for cochlear implant listeners: benefits of residual acoustic hearing. *J. Acoust. Soc. Am.* 115, 1729–1735. doi: 10.1121/1.1687425

Von Ilberg, C., Kiefere, J., Tillein, J., Pfenningdorff, T., Hartmann, R., Stürzebecher, E., et al. (1999). Electrical-acoustic stimulation of the auditory system: new technology for severe hearing loss. *ORL J. Otorhinolaryngol. Relat. Spec.* 61, 334–340.

Wang, Q., and Green, S. H. (2011). Functional role of neurotrophin-3 in synapse regeneration by spiral ganglion neurons on inner hair cells after excitotoxic trauma in vitro. *J. Neurosci.* 31, 7938–7949. doi: 10.1523/JNEUROSCI.1434-10.2011

Wright, C. G., and Roland, P. S. (2013). Vascular trauma during cochlear implantation: a contributor to residual hearing loss? *Otol. Neurotol.* 34, 402–407. doi: 10.1097/MAO.0b013e318278509a

Zembowicz, A., Hatchett, R. J., Radziszewski, W., and Gryglewski, R. J. (1993). Inhibition of endothelial nitric oxide synthase by ebselen. Prevention by thiols suggests the inactivation by ebselen of a critical thiol essential for the catalytic activity of nitric oxide synthase. *J. Pharmacol. Exp. Ther.* 267, 1112–1118.

Zeng, F. G., Rebscher, S., Harrison, W., Sun, X., and Feng, H. (2008). Cochlear implants: system design, integration, and evaluation. *IEEE Rev. Biomed. Eng.* 1, 115–142. doi: 10.1109/RBME.2008.2008250

Conflict of Interest: The authors declare that the research was conducted in the absence of any commercial or financial relationships that could be construed as a potential conflict of interest.

frontiers in Neuroscience

ORIGINAL RESEARCH
published: 29 January 2020
doi: 10.3389/fnins.2020.00034

Motor Imagery Training With Neurofeedback From the Frontal Pole Facilitated Sensorimotor Cortical Activity and Improved Hand Dexterity

*Yuya Ota[1], Kouichi Takamoto[1,2], Susumu Urakawa[3], Hiroshi Nishimaru[1], Jumpei Matsumoto[1], Yusaku Takamura[1], Masahito Mihara[4], Taketoshi Ono[1] and Hisao Nishijo[1]**

[1] System Emotional Science, Faculty of Medicine, University of Toyama, Toyama, Japan, [2] Department of Sports and Health Sciences, Faculty of Human Sciences, University of East Asia, Shimonoseki, Japan, [3] Department of Musculoskeletal Functional Research and Regeneration, Graduate School of Biomedical and Health Sciences, Hiroshima University, Hiroshima, Japan, [4] Department of Neurology, Kawasaki Medical School, Okayama, Japan

OPEN ACCESS

Edited by:
Cuntai Guan,
Nanyang Technological University,
Singapore

Reviewed by:
Atsuhiro Tsubaki,
Niigata University of Health
and Welfare, Japan
Beatrix Barth,
University of Tübingen, Germany

***Correspondence:**
Hisao Nishijo
nishijo@med.u-toyama.ac.jp

Specialty section:
This article was submitted to
Neuroprosthetics,
a section of the journal
Frontiers in Neuroscience

Received: 14 November 2019
Accepted: 13 January 2020
Published: 29 January 2020

Citation:
Ota Y, Takamoto K, Urakawa S,
Nishimaru H, Matsumoto J,
Takamura Y, Mihara M, Ono T and
Nishijo H (2020) Motor Imagery
Training With Neurofeedback From
the Frontal Pole Facilitated
Sensorimotor Cortical Activity
and Improved Hand Dexterity.
Front. Neurosci. 14:34.
doi: 10.3389/fnins.2020.00034

To develop a real-time neurofeedback system from the anterior prefrontal cortex (aPFC) using functional near-infrared spectroscopy (fNIRS) for motor rehabilitation, we investigated the effects of motor imagery training with neurofeedback from the aPFC on hand dexterity and cerebral hemodynamic activity during a motor rehabilitation task. Thirty-one right-handed healthy subjects participated in this study. They received motor imagery training six times for 2 weeks under fNIRS neurofeedback from the aPFC, in which they were instructed to increase aPFC activity. The real group subjects (n = 16) were shown real fNIRS neurofeedback signals from the aPFC, whereas the sham group subjects (n = 15) were shown irrelevant randomized signals during neurofeedback training. Before and after the training, hand dexterity was assessed by a motor rehabilitation task, during which cerebral hemodynamic activity was also measured. The results indicated that aPFC activity was increased during the training, and performance improvement rates in the rehabilitation task after the training was increased in the real group when compared with the sham group. Improvement rates of mean aPFC activity across the training were positively correlated with performance improvement rates in the motor rehabilitation task. During the motor rehabilitation task after the training, the hemodynamic activity in the left somatosensory motor-related areas [premotor area (PM), primary motor area (M1), and primary somatosensory area (S1)] was increased in the real group, whereas the hemodynamic activity was increased in the supplementary motor area in the sham group. This hemodynamic activity increases in the somatosensory motor-related areas after the training correlated with aPFC activity during the last 2 days of motor imagery training. Furthermore, improvement rates of M1 hemodynamic activity after the training was positively correlated with

performance improvement rates in the motor rehabilitation task. The results suggest that the aPFC might shape activity in the somatosensory motor-related areas to improve hand dexterity. These findings further suggest that the motor imagery training using neurofeedback signals from the aPFC might be useful to patients with motor disability.

Keywords: fNIRS, neurofeedback, frontal pole, motor rehabilitation, primary motor cortex

INTRODUCTION

Motor rehabilitation is fundamental to management of patients with stroke as well as chronic neurological disorders such as Parkinson's disease, Alzheimer's disease, vestibular disease, etc. (Johansson, 2011; Cheng et al., 2012; Hatem et al., 2016). These neurological disorders increased in the last 25 years, and the number of patients in need of neurological cares will increase in the next decades (GBD 2015 Neurological Disorders Collaborator Group, 2015). Hemiparesis of the upper limb is the most common motor disturbance after a stroke. It affects more than 80% of patients in an acute phase, and more than 40% in a chronic phase (Cramer et al., 1997). In Parkinson's disease, the reduction of fine hand skills seriously affects daily activities (Raggi et al., 2011). In mild cognitive impairment and Alzheimer's disease, fine motor function such as hand dexterity is disturbed, impairing activities of daily living (ADL) (Scherder et al., 2008; de Paula et al., 2016). These findings suggest that to increase the patients' quality of life (QOL), and also to reduce medical costs, appropriate rehabilitation methods for upper limbs should be developed.

Motor rehabilitation ability is associated with motor skill learning (Hanlon, 1996). Motor skill learning and the resultant formation of motor memories can be defined as an improvement of motor skills through practice (Brem et al., 2013). Repetitive performance of a rehabilitation task effectively improves motor skills of the upper extremity, which is attributed to motor skill learning based on changes in brain neural circuits, especially on those in the primary motor cortex (M1) (Hatakenaka et al., 2007; Papale and Hooks, 2018). Neurofeedback is biofeedback in which sensory (usually visual or auditory) signals reflecting real-time neural activity are displayed to subjects so that they can learn to modulate activity in targeted neural substrates involved in specific behaviors or brain functions (Sitaram et al., 2016; Wang et al., 2018). Neurofeedback could induce specific neural activation patterns in target brain areas (Shibata et al., 2011; Sitaram et al., 2016), suggesting that neurofeedback training could induce changes in neural circuits for motor skill learning and, consequently, could be used for motor rehabilitation training. It is also noted that neurofeedback training could be beneficial to patients with motor disability such as stroke since patients do not need to make overt behaviors during training. Also, neurofeedback has been recently applied to motor rehabilitation in stroke patients as well as healthy adults (Mihara et al., 2012, 2013; Fujimoto et al., 2017; Wang et al., 2018). These previous studies targeted the sensorimotor related areas as neurofeedback sources: M1, primary somatosensory cortex (S1), premotor cortex (PM), and supplementary motor area (SMA).

We previously reported that hemodynamic activity in the anterior part of the prefrontal cortex (aPFC), which corresponds to the frontal pole (Brodmann area 10), was increased during motor learning in a motor rehabilitation task of hand dexterity, and correlated with the performance improvement rate in healthy subjects (Ishikuro et al., 2014). Furthermore, anodal stimulation of the aPFC improved hand dexterity in the same motor rehabilitation task in both healthy adults and patients with Parkinson's disease (Ishikuro et al., 2014, 2018). These previous results suggest that the aPFC facilitates motor skill learning, and further suggest that training with neurofeedback from the aPFC might be useful for motor rehabilitation of the hand. To develop a neurofeedback system, we applied functional near-infrared spectroscopy (fNIRS) to measure aPFC activity as neurofeedback signals. fNIRS is a neuroimaging technique that can detect changes in oxygenated-hemoglobin (Oxy-Hb), deoxygenated-hemoglobin (Deoxy-Hb), and total hemoglobin (Total-Hb) in the cerebral cortex associated with local cortical activity based on neurovascular coupling (Ferrari and Quaresima, 2012; Quaresima and Ferrari, 2019). fNIRS can be used with less body and head restraint in relatively larger spaces. Thus, fNIRS allows us to measure brain activity under conditions similar to actual clinical environments when compared with the other imaging methods such as functional magnetic resonance imaging (fMRI) and positron emission tomography (PET).

In this study, we hypothesized that neurofeedback training targeting the aPFC would improve hand dexterity through its effects on the sensorimotor cortex. To investigate the effects of training with neurofeedback from the aPFC on hand motor dexterity and cortical hemodynamic activity, we analyzed changes in hand dexterity and cortical hemodynamic activity during a motor rehabilitation task for hand dexterity before and after neurofeedback training. Here we report that cerebral hemodynamic activity in the somatosensory motor-related areas was increased during the motor rehabilitation task after neurofeedback training, which correlated to the aPFC activity during training. Furthermore, improvement rates of M1 hemodynamic activity after the training was associated with performance improvement rates in the motor rehabilitation task.

MATERIALS AND METHODS

Subjects

The inclusion criterion was right-handed healthy adults who had no history of neurological and psychological disorders, and no experience of neurofeedback training (Dieterich et al., 2003). Histories of neurological and psychological disorders were assessed based on the subjects' self-reports. Handedness was determined by the Edinburgh Handedness Inventory

(Oldfield, 1971), and all subjects included were right-handed. A total of 31 subjects participated in the current study [25.4 ± 0.7, mean age ± standard error (SE), ranging from 20 to 33 years old; 17 males and 14 females]. The subjects were randomly grouped into two groups: real group subjects (n = 16; nine males and seven females) were shown real fNIRS neurofeedback signals from the aPFC, while sham group subjects (n = 15; eight males and seven females) were shown irrelevant randomized signals during neurofeedback training. The subjects were blinded to subject grouping. All subjects were treated in strict compliance with the Declaration of Helsinki and the United States Code of Federal Regulations for the protection of human participants. We obtained written informed consents from all subjects prior to experiments. The present experimental protocol was approved by the Ethical Committee of Human Experiments at the University of Toyama.

Sample Size

The sample size for the comparison of two independent samples (two-tailed t-test) was estimated using G*Power, a tool to compute statistical power analyses[1] (Faul et al., 2007). Data in the previous study (Ishikuro et al., 2014), in which cortical hemodynamics and peg task performance were analyzed, were used for this sample size estimation. The analysis indicated an n = 11 for each group based on the following conditions; level of significance = 0.05, statistical power = 0.95, mean and standard deviation (SD) in group 1 = 11.4 and 1.31, respectively, and mean and SD in group 2 = 9.0 and 1.55, respectively.

Experimental Procedures

Subjects were randomly grouped into two groups; (1) A real group (n = 16) that was shown real fNIRS neurofeedback signals, and (2) A sham group (n = 15) that was shown irrelevant randomized signals during neurofeedback training. The experimental protocol was composed of three sessions; pre (before training)-assessment session, motor imagery training session, and post (after training)-assessment session (**Figure 1A**). In the pre-assessment session, after an fNIRS head cap and probes have been set on the head (see below in detail), hand dexterity was assessed by using the Purdue Pegboard test (see below in detail) as the baseline status. In the motor imagery training session, the subjects received motor imagery training three times a week for 2 weeks. After the last session of the training, hand dexterity was reassessed using the same Purdue Pegboard test in the post-assessment session. In the Purdue Pegboard test in the pre- and post-assessment sessions, whole-brain hemodynamic activity was also recorded (see below in detail). In the motor imagery training sessions, cortical activation in the anterior prefrontal cortex (aPFC: Brodmann area 10) (Ramnani and Owen, 2004) was assessed by real-time analysis of fNIRS signals from the aPFC (see below in detail).

The Purdue Pegboard Test

The Purdue Pegboard test (Mathiowetz et al., 1986; Vasylenko et al., 2018) was used to evaluate hand dexterity before and after the training session. Subjects sat in a chair in front of a table 755 mm in height. The Purdue Pegboard (Model 32020A, Lafayette Instrument, Co. Ltd., IN, United States) was placed on the table (**Figure 1Ba**). The Purdue Pegboard had four cups in the upper side and two rows of 25 holes each arranged vertically in the center of the board. The 25 pins (pegs) were initially placed in the extreme right cup. In the pre-assessment, the subjects received brief instructions from the experimenter. After the instructions, the subjects were allowed to briefly perform the task for practice.

In the Purdue Pegboard test, the subjects picked up one of the pegs from the right-handed cup and put into a hole using their right hands, starting at the top of the right row to the bottom. The subjects were asked to put as many pegs as possible into the holes within a 30-s period in each block of the task. The test consisted of three blocks of three phases: rest, task, and rest (each phase for 30 s) (**Figure 1Bb**). Thus, the actual inter-task rest period was 60 s [a last resting period (30 s) in the previous block plus an initial resting period (30 s) in the next block]. Performance in the Purdue Pegboard test was assessed by counting the number of pegs put into holes.

After the pre-assessment of the Purdue Pegboard test, motor imagery ability of the subjects was assessed using Movement Imagery Questionnaire-Revised Japanese Version (JMIQ-R) (Hasagawa and Hoshino, 2002). The subjects were required to score their motor imageries of four actions using own extremities.

Motor Imagery Training

After an fNIRS head cap and optodes were set on the head, the subjects sat in a chair in front of a screen and were asked to open their eyes to look at the screen (**Figure 2Aa**). The motor imagery training composed of (**Figure 2Ab**): (1) video-guided motor imagery without neurofeedback for 10 min, and (2) motor imagery with neurofeedback for 10 min (Mihara et al., 2013). In the video-guided motor imagery, the subjects in both groups were asked to perform motor imagery in the Purdue Pegboard test: picking up one of the pegs from a cup and putting it into a hole with the right hand following video instructions. After a short break of 1–2 min, motor imagery training with neurofeedback was started. In this second training, a bar to go up and down as real or randomized fNIRS feedback signals from the aPFC was shown to the subjects. The subjects in both groups were asked to look at the feedback bar as neurofeedback from the aPFC on the screen and to perform motor imagery of the Purdue Pegboard test (to keep the height and color of the feedback bar at the elevated levels; see below for details). The sham group was shown the feedback bar, height and color of which did not reflect real fNIRS signals.

Each training of motor imagery with neurofeedback consisted of 16 trials consisting of a 5-s period of the motor imagery task followed by inter-task rest periods ranging from 8 to 15 s (**Figure 2Ac**). To prevent prediction of task start by the subjects, the inter-task rest period was pseudorandomly set (mean resting time, 11.19 ± 0.53 s). In response to beep sounds indicating the start of each trial, the subjects were asked to perform the motor imagery as if they actually moved their right fingers and hand in the Purdue Pegboard test. Throughout the motor

[1] http://www.gpower.hhu.de/

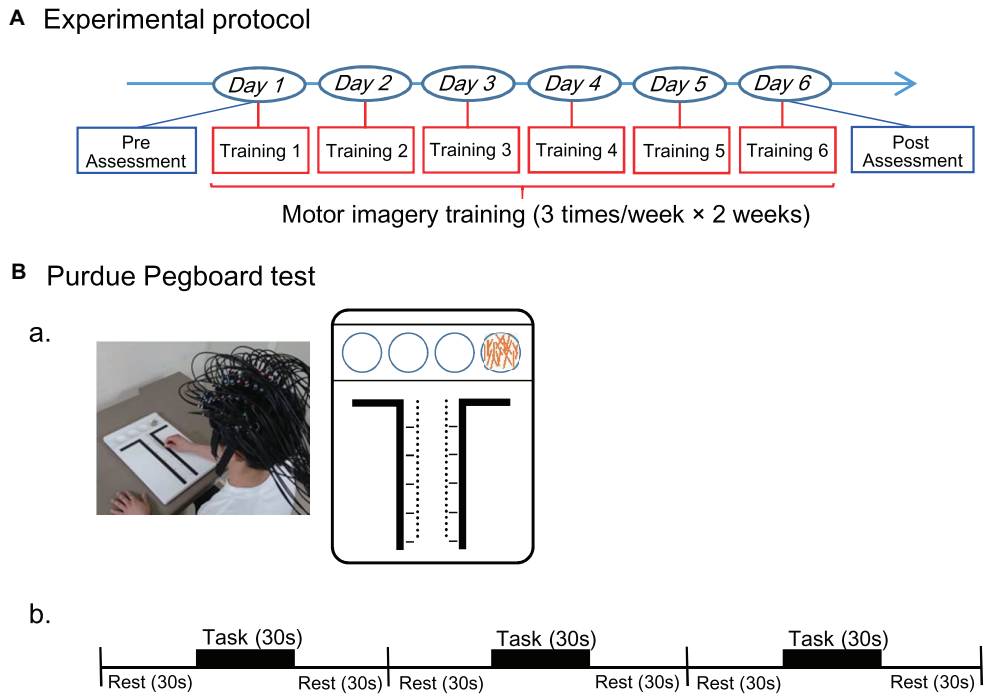

FIGURE 1 | Experimental protocol throughout this study **(A)** and that for the Purdue Pegboard test **(B)**. **(A)** The entire experimental protocol. The experimental protocol composed of three sessions; pre (before training)-assessment session, motor imagery training session, and post (after training)-assessment session. In the motor imagery training session, the subjects received motor imagery training three times a week for 2 weeks. Hand dexterity was assessed using the Purdue Pegboard test in the pre- and post-assessment sessions. **(B)** The Purdue Pegboard test protocol. **(a)** A photo of a subject with an fNIRS head cap during Purdue Pegboard testing and schematic illustration of the Purdue Pegboard are shown. The Purdue Pegboard has four cups in the upper side and two rows of 25 holes each arranged vertically in the center of the board. **(b)** The Purdue Pegboard test consisted of three blocks, and each block had three phases: each phase for 30 s (rest, task, and rest).

imagery training, behaviors of each subject were recorded in a video camera (HC-V480M, Panasonic, Co. Ltd., Osaka, Japan) to observe their posture, eyes, hand, and finger movements. All subjects opened their eyes and looked at the screen without overt changes of their posture, and overt hand and finger movements were not observed (data not shown).

Measurements of Hemodynamic Activity Using fNIRS

Two fNIRS systems (OMM 3000, Shimadzu, Co. Ltd., Kyoto, Japan) were used to measure changes in brain hemodynamic activity from the bilateral hemispheres. To measure data as the integrated system, the two fNIRS systems were connected with Ethernet and SYNC cables. One fNIRS system was used as the master, the clock signal was synchronized using the SYNC cable, and the measurement control commands were synchronized by the TCP/IP protocol using Ethernet cable. The systems were automatically calibrated using target measurement condition in advance before the experiment so that all NIRS signals were comparable.

An fNIRS head cap was placed on the subject's head. The optodes for the fNIRS instruments were fixed on the head cap and the bottom horizontal line of the frontal optodes was placed according to the international 10–20 EEG system (2 cm posterior to the subject's Fpz in the current study) (Takeuchi et al., 2009; Takamoto et al., 2010; Takakura et al., 2015). The fNIRS systems used three different wavelengths (780, 805, and 830 nm) to detect hemodynamics (oxygenated Hb [Oxy-Hb], deoxygenated Hb [Deoxy-Hb] and Total-Hb [Oxy-Hb + Deoxy-Hb]), which were estimated using a modified Lambert–Beer law (Seiyama et al., 1988; Wray et al., 1988).

The light detector optode detected hemodynamic signals around the midpoints (called "channels") between the light source and detector optodes. The hemodynamic signals include different information depending on the optode distance between light sources and detectors (Fukui et al., 2003; Niederer et al., 2008; Ishikuro et al., 2014). The fNIRS signals from optodes with 3 cm include both cerebral (brain) and extra-cerebral (scalp, skull, and cerebrospinal fluid) components, and the signals from optodes with 1.5 cm reflect extra-cerebral components. In this study, multi-distance optode arrangement was applied to remove artifacts and extract cerebral hemodynamics from all hemodynamic responses that included both extra-cerebral and cerebral components (Schytz et al., 2009; Nakamichi et al., 2018). Furthermore, to record from the somatosensory motor-related areas more densely than a conventional optode arrangement in a channel lattice of 30 × 30 mm, extra sources and probes were placed in the bilateral somatosensory motor-related areas so that fNIRS signals could be recorded in a channel lattice

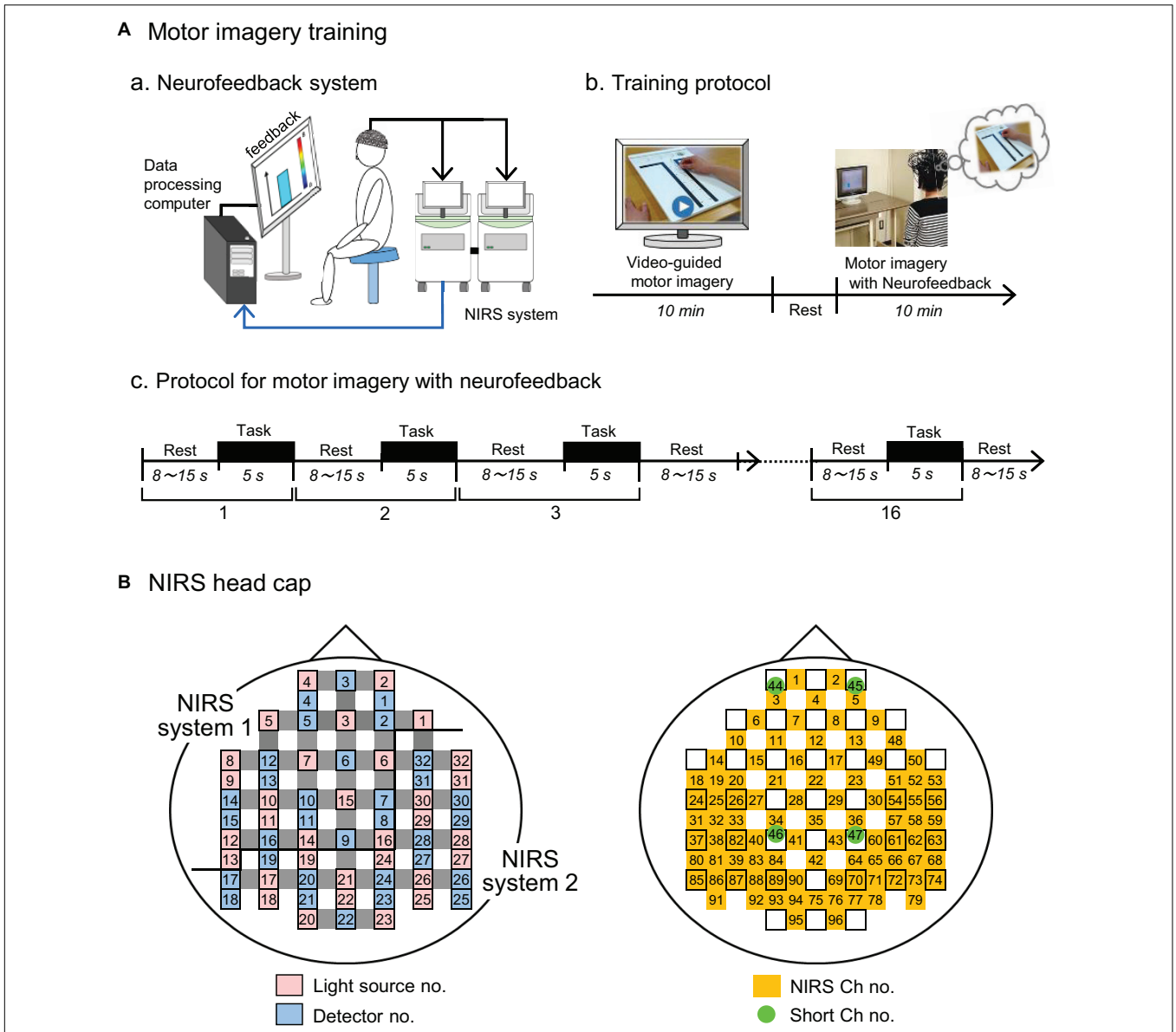

FIGURE 2 | Motor imagery training using fNIRS neurofeedback system. **(A)** Motor imagery training. **(a)** A schematic figure of the fNIRS-mediated neurofeedback system. **(b)** Protocol for motor imagery training. Motor imagery training consisted of video-guided motor imagery and motor imagery with neurofeedback. **(c)** Protocol for motor imagery with neurofeedback. The training protocol consisted of 16 trials. Each trial consists of 5-s motor imagery and 8 -15-s rest periods. **(B)** Arrangement of probes and channels in an fNIRS head cap. As the source of feedback signals, 5 fNIRS channels in the aPFC (Ch 1-5) were used. NIRS ch no., NIRS channel no. with probe distance of 3.0 cm; Short ch no., with probe distance of 1.5 cm.

of 15 × 15 mm (e.g., extra-source No. 9, 11, 13, 19, 18, 22; extra-detector No. 13, 15, 19, 18, 21 in the left hemisphere; **Figure 2B**). This high density optode arrangement is reported to improve spatial resolution (Yamamoto et al., 2002; White and Culver, 2010). Thus, hemodynamic signals were measured from 92 channels at 4 Hz using 32 light-source probes and 28 light-detector probes (**Figure 2B**), and the optodes were placed across from each other at 3 cm by an adjustment mechanism based on the Guss-Bonnet theorem (Banados et al., 1994; Cummings, 2001). Another 4 detectors (No. 1, 4, 8, 11) were positioned 1.5 cm from source optodes, resulting in 4 channels (Ch 44-47) with short distances (1.5 cm). The short channels were placed in the bilateral aPFC and somatosensory motor-related areas. The positions of the short channels were determined, so that distance between the long (3.0 cm) and short (1.5 cm) channels was relatively similar across the head.

After recording, 3-dimensional locations of the optodes were measured using a Digitizer (FASTRAK, Polhemus Inc., United States) with reference to the vertex (Cz), nasion and bilateral external auditory meatus. The anatomical locations of the fNIRS optodes and channels in each subject were normalized to standard coordinates in the Montreal

Neurological Institute (MNI) coordinate system (Singh et al., 2005). Furthermore, we identified the cortical regions covered by each channel using the MRIcro software[2], as well as the Brodmann's area image and automated anatomic labeling image (Tzourio-Mazoyer et al., 2002).

fNIRS-Mediated Neurofeedback System

In this study, we analyzed Oxy-Hb signals as cortical activity. Previous studies reported that Oxy-Hb was correlated with fMRI BOLD signals and it might be the most consistent parameter for cortical activity (Hoshi et al., 2001; Strangman et al., 2002; Yamamoto and Kato, 2002). fNIRS signals were sampled at 4 Hz, and the data were transferred to the neurofeedback system online (**Figure 2Aa**). As the source of feedbacks from a region of interest (ROI), 5 fNIRS channels (Ch 1-5 in **Figure 2B**) in the aPFC were used. Transferred fNIRS signals were initially filtered with a lowcut filter (0.0125 Hz). A sliding-windows general linear model (GLM) analysis with a least-square estimation was used for real-time analysis of signal changes by in-house programs in MATLAB (R2014b; Math Works, Natick, MA, United States). The detailed methods for real-time analysis of fNIRS signals have been reported previously (Mihara et al., 2012). The window included 80 data points, which covered at least one cycle of the task (5 s) and rest (8–15 s) periods. Each window was measured for 20 s at 4 Hz. To eliminate contamination of the extra-cerebral components, such as the influence of scalp blood flow, respiration, heart rate, and motion artifacts, a principal component analysis was simultaneously performed using data from the short distance channels (Ch 44 and 45 in **Figure 2B**). The primary principal component was included in the model as a regressor. The *t*-values were used to estimate changes in cortical activation.

The maximal *t*-values from the feedback ROI were used as the cortical feedback signals. The height and color of the feedback bar varied from 0 (blue) to 8 (red), according to the *t*-value. The *t*-values > 2.0 indicated significant activation (approximately $P < 0.05$). If *t*-values from all the 5 fNIRS channels were lower than zero, suggesting no significant cortical activation, the feedback bar was set to zero. In the sham group, random signals regardless of their own aPFC activation were generated as neurofeedback signals from prerecorded data of aPFC activity from other individuals. The prerecorded data were randomly selected from pooled data that were recorded during the same task in the real feedback condition. Thus, the height and color of the feedback bar on the screen reflected the real-time fNIRS signals in the real group, but the randomly selected prerecorded data in the sham group. The subjects in both groups were asked to keep the height and color of the feedback bar at higher levels (Mihara et al., 2013; Fujimoto et al., 2017).

Data Analysis

Behavioral Measures

To evaluate the hand dexterity, peg scores, defined as the number of the pegs put into the holes, were estimated on each assessment before and after the motor imagery training, and the scores from three blocks were averaged. "Performance gain" was defined as the peg score in the post-assessment divided by that in the pre-assessment in individual subjects. Then, the mean performance gain of the two groups was compared using unpaired *t*-test.

fNIRS Data in the Feedback ROI During Motor Imagery Training

To compare progress in motor imagery training between the two groups, feedback signals (Oxy-Hb) were analyzed. Early training data (trials 1–4 in **Figure 2Ac**) from each training day were removed from the analysis due to data instability (Fujimoto et al., 2017). Then, the mean *t*-values of the 5 channels (Ch 1-5 in **Figure 2B**) in trials 5–16 were averaged for each subject in each training day, and the mean *t*-values for each day in each group were estimated. Finally, the averaged mean *t*-values across the 6 training days were compared between the two groups using paired *t*-test. To evaluate the effects of neurofeedback training on performance gain, the relationships between performance gain and improvement rate of hemodynamic activity (Oxy-Hb gain) in the feedback ROI during training were analyzed by simple regression analysis. The Oxy-Hb gain in the feedback ROI was defined as averaged *t*-values across Ch 1-5 on training day 6 divided by those on training day 1 in individual subjects.

We also analyzed temporal changes of cerebral hemodynamic responses (Oxy-Hb, Deoxy-Hb, and Total-Hb) during motor imagery training in the aPFC. First, cerebral hemodynamic responses were estimated by simple-subtraction methods (Schytz et al., 2009; Nakamichi et al., 2018): [the whole signals with probe distance of 3.0 cm in the aPFC] minus [the extra-cerebral signals with probe distance of 1.5 cm, located nearest to corresponding whole signals]. The subtracted cerebral signals were filtered with a bandpass filter (0.01–0.1 Hz) to reduce long-term baseline drift and autonomic responses such as cardiac or respiratory activity (Tong et al., 2011; Yasumura et al., 2014). The fNIRS signals were then summed and averaged across the 12 trials (from 5th to 16th trials except the early 4 trials) in each training day. The summed data were corrected for baseline activity from −3 to 0 s before the start of motor imagery (start beep tone).

fNIRS Data During Assessment of Hand Dexterity (Purdue Pegboard Test)

The cerebral hemodynamic activity (Oxy-Hb, Deoxy-Hb, and Total-Hb) was similarly computed using simple-subtraction methods (see above). In this study, we analyzed Oxy-Hb signals as cortical activity (see above). Oxy-Hb signals were analyzed using a mass univariate GLM by statistical parametric mapping on NIRS-SPM software[3] (version 4.1) (Ye et al., 2009). In the group analysis, SPM *t*-statistic maps on the standardized brain in the MNI coordinate system were generated. Statistical significant level was set at an uncorrected threshold of $P < 0.001$ (Thornton et al., 2011; Kim et al., 2017) and the threshold setting of cluster-extent was 50 sequence (Woo et al., 2014; Theisen et al., 2017; Bansal and Peterson, 2018).

[2]http://www.MRIcro.com

[3]https://www.nitrc.org/projects/nirs_spm/

The above group analysis indicated activation in the several cortical areas including the left, but not right, somatosensory motor-related areas in the real group and SMA in the sham groups (see section "Results"). We investigated the relationship between hand dexterity during Purdue Pegboard testing and hemodynamic cortical activity in these activated areas using simple regression analysis. First, five cortical regions that showed significant activation in the SPM t-statistic maps in the post-assessment were selected as ROIs; the left premotor area (L-PM), left primary motor area (L-M1) for the hand (lateral L-M1), L-M1 except lateral L-M1 (medial L-M1), left primary somatosensory area (L-S1), and SMA. The L-M1 was divided into two parts based on the X coordinate of the MNI coordinates: the hand motor area (lateral L-M1: area with $X \leq -30$) and the remaining area (medial L-M1: area with $X \geq -29$) (Stoeckel et al., 2009; Hadoush et al., 2011; Lapborisuth et al., 2017; Schellekens et al., 2018). Second, in each ROI, the averaged *t*-values were calculated in the pre- and post-assessment sessions. Then, Oxy-Hb gain was calculated in each ROI as mean *t*-value in the post-assessment divided by that in the pre-assessment. Finally, in each ROI, a simple regression analysis was performed to analyze relationships between Oxy-Hb gain and performance gain. In these regression analyses, outliers were detected by residual analysis and were removed before the analyses. Data with standardized residuals larger than 3.29 were defined as outliers (Cook and Weisberg, 1982).

To investigate the effects of neurofeedback training on cortical activation during the Purdue Pegboard test, the relationships between the mean *t*-values in the feedback ROI on each training day and the mean *t*-values in the activated areas during the Purdue Pegboard test in the post-assessment were analyzed using simple regression analysis.

Statistical Analysis

Data normality was assessed by the Shapiro–Wilk test. Homogeneity of variance was assessed by Levene's test. Data between the real and sham groups were compared using Student's *t*-test (or Mann–Whitney *U*-test) and analysis of variance (ANOVA). The simple regression analysis was used to investigate data correlation using the data in the all subjects as well as those in the real group. These statistical analyses were performed using SPSS statistical package version 19.0 (IBM, Co. Ltd., New York, NY, United States). The statistical significant level was set at $P < 0.05$.

RESULTS

Baseline Characteristics

The baseline characteristics of the two groups are shown in **Table 1**. The mean (±SE) age in the real group was 25.4 ± 0.9 years, and that in the sham group was 25.3 ± 1.1 years. There were no significant differences between the two groups in terms of handedness [Student's *t*-test; $T(29) = 0.746$, $P > 0.05$], age [Student's *t*-test; $T(29) = 0.029$, $P > 0.05$], and sex [chi-squared test; $\chi^2(1) = 0.027$, $P > 0.05$].

TABLE 1 | Baseline subject characteristics.

	Real group (*N* = 16)	Sham group (*N* = 15)
Male (*N*)	9	8
Female (*N*)	7	7
Age (years)	25.4 ± 0.9	25.3 ± 1.1
Handedness (%)	89.2 ± 2.8	85.2 ± 4.7

Age (years) and Handedness (%) are presented as mean ± SE. There were no significant differences between the two groups in terms of sex (Chi-squared test, $P > 0.05$), age and handedness (unpaired t-test, $P > 0.05$).

Performance in the Purdue Pegboard Test

Hand dexterity was assessed by using the Purdue Pegboard test. Peg scores in the pre-assessment session were used as a control before training, and there was no significant difference in scores between the two groups (14.67 ± 0.367 in the real group, 15.76 ± 0.475 in the sham group) [Mann–Whitney *U*-test; $U(16, 15) = 71.00$, $P > 0.05$]. These mean scores are comparable to those of the normative data (around 15–16) of the healthy adults in their twenties and thirties (Yeudall et al., 1986). However, performance gain was significantly higher in the real group than the sham group (1.085 ± 0.017 in the real group, 1.034 ± 0.011 in the sham group) [Student's *t*-test; $T(29) = 2.427$, $P < 0.05$] (**Figure 3**).

After the pre-assessment of the Purdue Pegboard test, motor imagery ability of the subjects was assessed using the JMIQ-R. The mean total score in the real group was 42.94 ± 2.21, and that in the sham group was 43.93 ± 2.35. There was no significant difference in total sores between the real and sham groups [Student's *t*-test; $T(29) = 0.299$, $P > 0.05$].

Effects of Motor Imagery Training on aPFC Activity and Performance Gain

Figure 4A shows examples of cerebral hemodynamic responses in the 5 fNIRS channels in the aPFC during motor imagery training on day 6 in one subject of the real group. In Ch 1, 3, and 4, Oxy-Hb and Total-Hb concentration increased after onset, whereas Deoxy-Hb concentration gradually decreased during the task period. In Ch 2 and 5, Oxy-Hb concentration slightly increased during the task period, whereas Deoxy-Hb and Total-Hb concentrations gradually decreased after the onset. **Figure 4B** shows examples of the comparable data in one subject of the sham group. There were no apparent increases in Oxy-Hb concentration after the task onset.

Figure 5A shows a comparison of the mean *t*-values in the 5 channels of the aPFC across the 6 training days between the real and sham groups. The results showed that the mean *t*-values were significantly higher in the real group when compared with the sham group (1.520 ± 0.032 in the real group, 1.400 ± 0.039 in the sham group) [paired *t*-test; $T(5) = 4.383$, $P < 0.01$]. Trends of changes in mean *t*-values in the aPFC during motor imagery training over the trials in each training day are shown in **Supplementary Figure 1**. The difference between the two groups in **Figure 5A** could be ascribed to the difference in the appearance

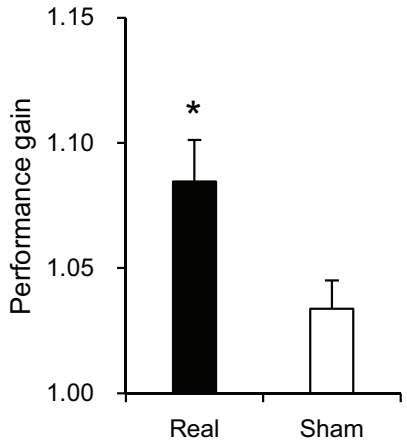

FIGURE 3 | Comparison of performance gain between the real and sham groups. *$P < 0.05$.

of the presented bar between the two groups. However, there was no significant difference in the height of the feedback bar on the screen between the real and sham feedback groups (2.274 ± 0.165 in the real group, 2.270 ± 0.274 in the sham group) [Mann–Whitney U-test; $U(16, 15) = 84.00$, $P > 0.05$]. This indicated that the observed significant difference in the mean t-values of the aPFC signals between the two groups was not due to the difference in the screen bar.

To analyze the effects of neurofeedback training on hand dexterity, the relationships between performance gain in the Purdue Pegboard test and Oxy-Hb gain in the feedback ROI (aPFC) during motor imagery training were analyzed (**Figure 5B**). When the data of all subjects were analyzed (**Figure 5Ba**), the Oxy-Hb gain in the feedback ROI was significantly and positively correlated with performance gain [$r = 0.37$, $F(1,29) = 4.726$, $P < 0.05$]. When the data were confined to the real group (**Figure 5Bb**), there was also a significant positive correlation between the Oxy-Hb gain in the aPFC and the performance gain [$r = 0.54$, $F(1,14) = 5.841$, $P < 0.05$].

Hemodynamic Responses During Purdue Pegboard Testing

Figure 6 shows the contrast image maps during Purdue Pegboard testing in the post-assessment resulting from the group analysis based on the GLM with NIRS-SPM. In the real group, task-related cortical activation was observed in the somatosensory motor-related areas: L-PM, L-M1, and L-S1 (**Figure 6Aa**). The L-M1 was further divided into the hand area (lateral L-M1) and the remaining L-M1 (medial L-M1) (see section Materials and Methods). A schematic illustration of the activated areas is shown in **Figure 6B**. The averaged MNI coordinates [(X, Y, Z) mm] of each ROI were as follows; L-PM, [Averaged MNI coordinate; (−36, −18, 68) mm]; hand area in L-M1 (lateral L-M1), [(−34, −25, 72) mm]; the remaining L-M1 (medial L-M1), [(−27, −25, 75) mm]; and L-S1, [(−29, −30, 75) mm].

In the sham group, task-related activity was observed in the SMA (**Figure 6Ab**). The averaged coordinates of the SMA were −4, 10, and 74 (X, Y, Z) mm.

Relationships Among Motor Imagery Training, Somatosensory-Motor Cortical Activity, and Performance Gain

The above data in **Figure 5B** indicated that Oxy-Hb gain in the aPFC during motor imagery training was significantly and positively correlated with performance gain. We hypothesized that motor imagery training gradually increased activity in the somatosensory motor-related areas through the aPFC, which in turn increased performance gain in the Purdue Pegboard test. First, we analyzed the relationships between aPFC activity during motor imagery training and activity in the somatosensory motor-related areas during Purdue Pegboard testing in the post-assessment (**Figure 7A**). Statistical analyses by a simple regression analysis indicated that task-related activation in the somatosensory motor-related areas (L-PM, L-M1, and L-S1) during Purdue Pegboard testing in the post-assessment significantly and positively correlated with aPFC activity on day 5 [day 5; $r = 0.41$, $F(1,29) = 5.765$, $P < 0.05$], and day 6 [day 6; $r = 0.45$, $F(1,29) = 7.284$, $P < 0.05$] in the motor imagery training. However, there were no such correlations on day 1, 2, 3, and 4 (data not shown).

Second, we then analyzed the relationships between Oxy-Hb gain in the somatosensory motor-related areas in the Purdue Pegboard test (i.e., improvement of task-related activation) and performance gain in the Purdue Pegboard test (i.e., improvement of hand dexterity). There were no significant relationships between Oxy-Hb gain in the entire activated somatosensory motor-related areas and performance gain [$r = 0.35$, $F(1,29) = 4.068$, $P > 0.05$]. However, there was a significant positive correlation between Oxy-Hb gain in the lateral L-M1 (hand motor area) and performance gain (**Figure 7B**). In the whole subject analysis (**Figure 7Ba**), data from one sample were removed as outliers by the residual analysis (standardized residual = −5.001), and there was a significant positive correlation between Oxy-Hb gain in the lateral L-M1 and performance gain [$r = 0.55$, $F(1,28) = 12.201$, $P < 0.01$]. When the data were confined to the real group (**Figure 7Bb**), data from one sample were also removed as outliers (standardized residual = −3.481), and there was also a significant positive correlation between Oxy-Hb gain in the lateral L-M1 and performance gain [$r = 0.61$, $F(1,13) = 7.786$, $P < 0.05$].

In contrast, no significant correlation was observed between Oxy-Hb gain in the SMA and performance gain in the sham group [$r = 0.39$, $F(1,12) = 2.183$, $P > 0.05$], where data from one sample were removed as outliers (standardized residual = −3.468), nor significant correlation in the whole subject analysis [$r = 0.12$, $F(1,28) = 0.429$, $P > 0.05$], where one sample data were also removed as an outlier (standardized residual = −5.200).

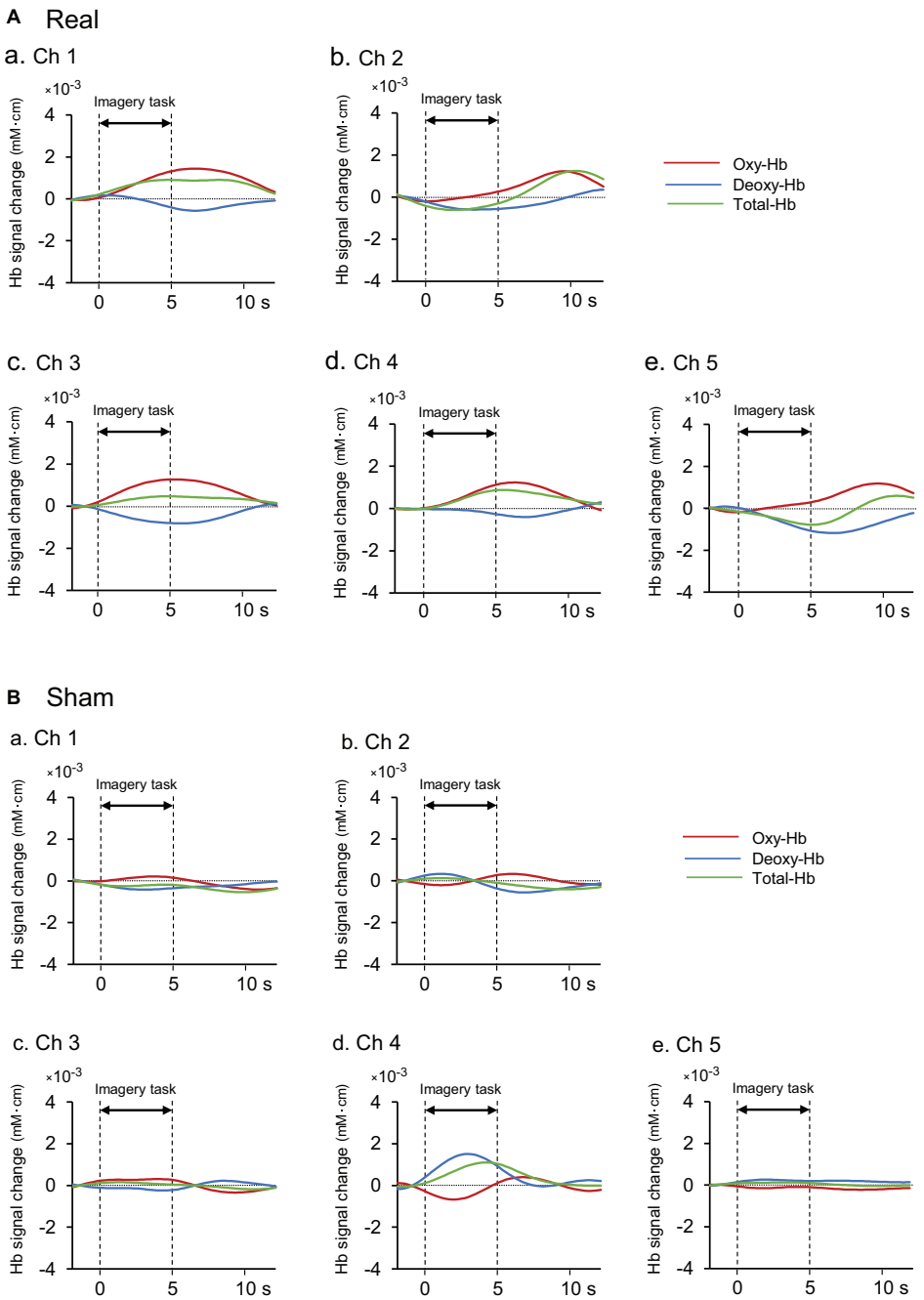

FIGURE 4 | Examples of hemodynamic responses in the feedback ROI (Ch 1-5) during motor imagery training in the real **(Aa–Ae)** and sham **(Ba-Be)** groups. **(A)** Hemodynamic responses in one subject of the real group. In Ch 1, 3, and 4, Oxy-Hb and Total-Hb concentrations increased after task onset, whereas Deoxy-Hb concentration gradually decreased during neurofeedback training. **(B)** Hemodynamic responses in one subject of the sham group. There were no apparent increases in Oxy-Hb concentration after the task onset.

DISCUSSION

Effects of Neurofeedback Training Targeting the aPFC

The neurofeedback training in healthy adult subjects significantly increased cerebral hemodynamic activity in the aPFC in the real group when compared with the sham group. These findings indicated that the subjects could volitionally control (self-regulate) aPFC hemodynamic activity. Previous studies also reported that subjects could self-regulate activity in specific brain areas including the PM, SMA, and aPFC through neurofeedback-guided motor imagery training (Mihara et al., 2012, 2013;

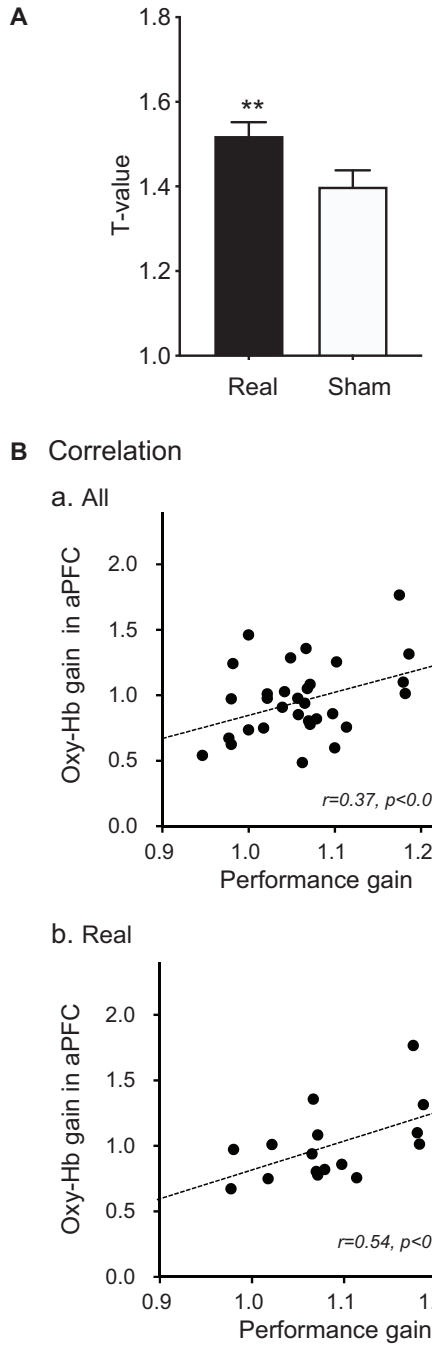

FIGURE 5 | Effects of motor imagery training on aPFC activity **(A)** and performance gain **(B)**. **(A)** Comparison of cortical activation (mean *t*-values) in the aPFC during the motor imagery task between the real and sham groups. $^{**}P < 0.01$. **(B)** Correlation between Oxy-Hb gain in the aPFC in motor imagery training and hand performance gain in the Purdue Pegboard test in all subjects **(a)** and in the real group **(b)**.

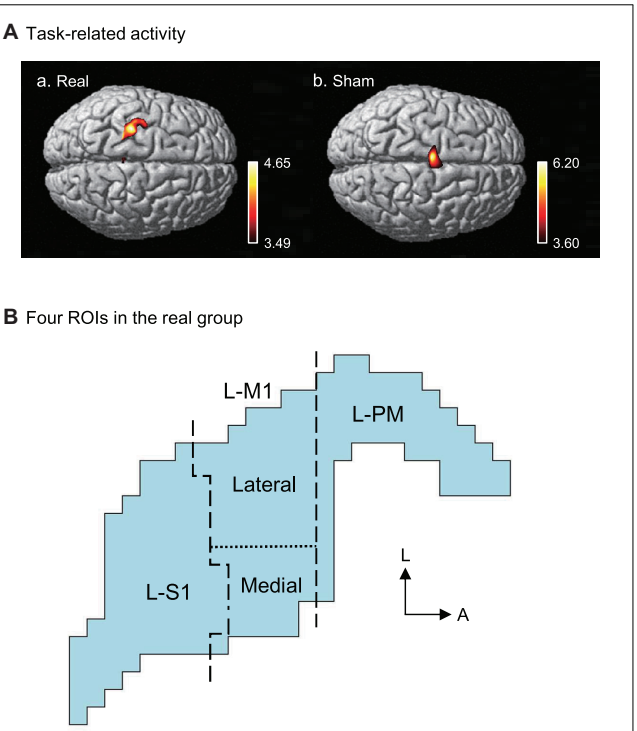

FIGURE 6 | Task-related cortical activation during the Purdue Pegboard test in the post-assessment. **(A)** NIRS-SPM T-statistic maps in the real **(a)** and sham **(b)** groups. Task-related cortical activation was observed in the somatosensory motor-related areas in the real group **(a)**, and the supplementary motor area (SMA) in the sham group. **(B)** Schematic illustration of the task-related cortical activation in the real group. The task-related activated areas were divided into 4 ROIs: left premotor area (L-PM), lateral left primary motor area (L-M1) (lateral L-M1, hand motor area), medial L-M1, and the left primary somatosensory area (L-S1). L, lateral; A, anterior.

Kinoshita et al., 2016; Subramanian et al., 2016). The present study further indicated that performance gain was significantly increased in the real group than the sham group after motor imagery training, and that motor imagery training progress (i.e., Oxy-Hb gain in the aPFC) correlated with performance improvement (i.e., performance gain) in the Purdue Pegboard test. These findings suggest that the activation of the aPFC is associated with improvement in hand motor functions. Consistent with this idea, our previous studies reported that Oxy-Hb gain in the aPFC positively correlated with performance gain during repeated training in a task similar to the Purdue Pegboard test, and that anodal stimulation of the aPFC by transcranial direct current stimulation (tDCS) increased performance in a motor rehabilitation task similar to the Purdue Pegboard test in healthy adults as well as in patients with Parkinson's disease (Ishikuro et al., 2014, 2018). Furthermore, activity in the aPFC was reported to correlate with shoulder function after surgery due to shoulder dislocation (Zanchi et al., 2017). These findings suggest that the aPFC is an important target for neurofeedback training in motor rehabilitation.

Effects of Neurofeedback Training on the Somatosensory Motor-Related Areas

In the present study, the SPM map in the group analysis indicated that hemodynamic activity in the somatosensory motor-related areas (L-PM, lateral L-M1, medial L-M1, and L-S1) increased

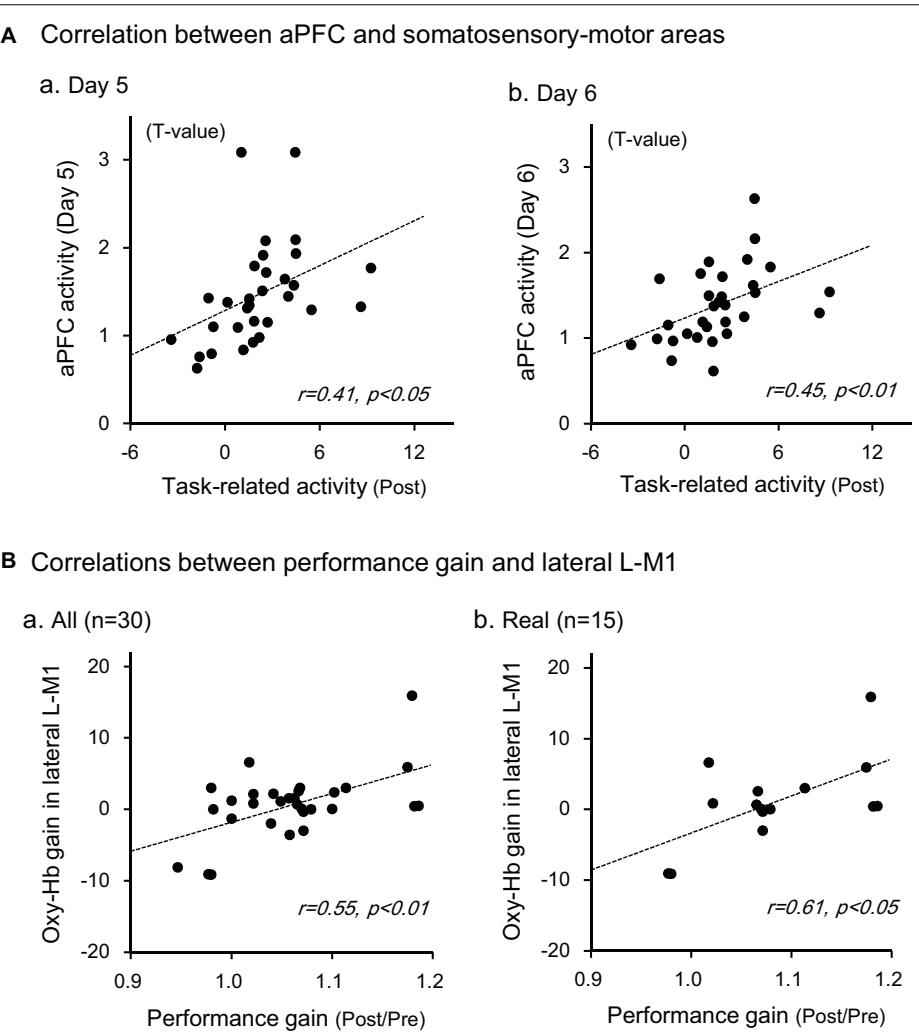

FIGURE 7 | Relationships between aPFC activity during motor imagery training and activity in the somatosensory motor-related areas during the Purdue Pegboard test **(A)**, and those between Oxy-Hb gain in the lateral L-M1 and performance gain in the Purdue Pegboard test **(B)**. **(A)** There were significant positive correlations between the activity in the somatosensory motor-related areas and that in the aPFC on day 5 **(a)** and day 6 **(b)**. **(B)** There were significant positive correlations between Oxy-Hb gain in the lateral L-M1 and hand performance gain in the Purdue Pegboard test when data in the whole subjects **(a)** and subjects in the real group **(b)** were analyzed. The data in each circle indicate data from each subject.

during Purdue Pegboard testing after neurofeedback training in the real group with hand performance improvement. The results suggest that the left somatosensory motor-related areas are essential for motor skill learning using the right hand. Consistent with the present results, recent studies suggest that the motor cortex (L-M1), which plays a prominent role in movement control, is also important in motor skill learning (Papale and Hooks, 2018), and that the somatosensory cortex (L-S1) is also involved in motor control through its direct projections to the motor cortex (Matyas et al., 2010). The premotor cortex (L-PM) is also implicated in motor learning in healthy subjects as well as patients (Mihara et al., 2012, 2013; Hardwick et al., 2013). Transcranial direct current stimulation of the premotor cortex increased hand dexterity (Pavlova et al., 2014), and increased excitability of the ipsilateral M1 area (Boros et al., 2008), suggesting that L-PM effects on performance gain might be mediated through its effects on the L-M1. Furthermore, hemodynamic activity in the aPFC was positively correlated with that in the L-PM during motor learning in a similar motor task (Ishikuro et al., 2014). These finding suggest that the aPFC might affect motor learning through the L-PM and L-M1.

Interestingly, hemodynamic activity in the SMA increased in the sham group during Purdue Pegboard testing in the post-assessment. The SMA has been implicated in learning a new association between stimuli and motor responses, and in cognitive control to inhibit a response plan (Nachev et al., 2008). Furthermore, a recent intracranial recording study suggests that the SMA functions as an action-monitoring system to emit alarm signals for incorrect responses or errors (Bonini et al., 2014). In the sham group, the subjects received random feedback signals regardless of their own aPFC activation during motor imagery of the Purdue Pegboard test. This indicates that the correct

aPFC activation that led to execution of the Purdue Pegboard test was not facilitated in the sham group, further suggesting that irrelevant aPFC activation might develop irrelevant synaptic activation in the somatosensory motor-related area in a way different from that used in the Purdue Pegboard test. Therefore, in the post-assessment of the Purdue Pegboard test, the subjects in the sham group might have to correct wrong synaptic activity formed by sham motor imagery training. Thus, the SMA activity in the sham group might increase to detect wrong synaptic activity in the somatosensory motor-related areas, to inhibit wrong responses, and to learn correct (new) association between incoming visual inputs and motor responses.

Neural Mechanisms of Performance Improvement

Hemodynamic activity in the somatosensory motor-related areas increased in the Purdue Pegboard test after neurofeedback training in the real group. This activity increase correlated with aPFC activity on days 5 and 6 during motor imagery training. Furthermore, Oxy-Hb gain in the lateral L-M1 (hand motor area) positively correlated with hand performance gain in the Purdue Pegboard test. It has been proposed that there are two stages of motor skill learning; initial fast learning (e.g., within a single session of training) and late slow learning (e.g., repeated training over a month to increase accuracy and speed) (Dayan and Cohen, 2011). In an initial fast learning, BOLD signals in the M1 decrease along with progression of learning, while BOLD signals in the M1 gradually increase along with learning in a late slow learning (see a review by Dayan and Cohen, 2011). The present results indicating significant increases in Oxy-Hb in the lateral L-M1 after repeated motor imagery training for 6 days, which were positively associated with task performance, suggest that neural mechanisms for late slow learning may be involved in the present neurofeedback training.

Our previous results indicated that response latencies in the aPFC were faster than in the somatosensory motor-related areas, and that hemodynamic activity in the aPFC correlated with that in the somatosensory motor-related areas during motor learning in a similar motor rehabilitation task (Ishikuro et al., 2014). Non-invasive studies reported indirect projections from the aPFC to the somatosensory motor-related areas (Hasan et al., 2013; Liu et al., 2013). Human neuropsychological studies suggest that the activity of the anterior part of the PFC, including the aPFC, was increased when subjects learned new motor task(s) (Jenkins et al., 1994; Floyer-Lea and Matthews, 2004), and lesions to these PFC areas delayed motor learning (de Guise et al., 1999; Richer et al., 1999). These findings suggest that the aPFC might shape synaptic activity in the somatosensory motor-related areas to improve hand dexterity during neurofeedback motor imagery training. Induction of such synaptic plasticity during feedback training might be mediated through long-term potentiation (LTP)-like and long-term depression (LTD)-like mechanisms as well as through dopaminergic activity (Sitaram et al., 2016).

Consistent with this idea, previous human studies suggest that the motor learning process during the repetition of a motor task involves synaptic plasticity in the M1 area, including LTP- and LTD-like mechanisms (Rioult-Pedotti et al., 1998; Muellbacher et al., 2002; Jung and Ziemann, 2009). The dorsolateral PFC, which receives projections from the aPFC (Liu et al., 2013), could facilitate excitability of the ipsilateral M1 area (Hasan et al., 2013), consistent with LTP induction. Second, dopaminergic neurons receive direct and/or indirect glutamatergic projections from the PFC (Kalivas, 1993; Carr and Sesack, 2000; Omelchenko and Sesack, 2007; Han et al., 2017), and dopaminergic neuronal activity correlates with that of PFC neurons (Gao et al., 2007; Zhang et al., 2012), suggesting that aPFC activity might induce dopamine release in the somatosensory motor-related areas. Furthermore, dopamine facilitates LTP induction as well as motor skill learning (Li et al., 2003; Molina-Luna et al., 2009; Hosp et al., 2011). Taken together, the aPFC might improve performance gain partly through these two mechanisms.

Limitations

There are several limitations in the present study. First, although performance in the Purdue Pegboard test was improved by motor imagery training to increase aPFC activity, motor imagery training itself could improve performance in the Purdue Pegboard test regardless of aPFC activity. Therefore, the sham group was introduced to control motor imagery training to exclude such possibility. Furthermore, the subjects were randomly assigned to the two groups, and there was no significant difference in motor imagery ability at least after the pre-assessment of the Purdue Pegboard test. However, sense of agency ("feeling of being in control": Jeunet et al., 2016) could affect motor imagery performance. Although the subjects were blinded to subject grouping, they could identify subject grouping through their sense of agency during the motor imagery training. Identification of own group could affect degree of engagement in the motor imagery training. Thus, sense of agency could affect performance gain in the Purdue Pegboard test regardless of aPFC activity. However, the present results indicated that activity in the aPFC was significantly associated with activity in the somatosensory motor-related areas and performance in the Purdue Pegboard test. These results indicated that aPFC activity during the motor imagery training is one of the important factors to improve performance in the Purdue Pegboard test.

Second, we used young healthy subjects in the present study. However, patients with stroke as well as chronic neurological disorders such as Parkinson's disease and Alzheimer's disease are expected to undergo the neurofeedback training, and would be older than the present subjects. A previous study reported that aPFC stimulation by tDCS ameliorated hand dexterity in elder patients with Parkinson's disease (Ishikuro et al., 2018), suggesting that the neurofeedback training to increase aPFC activity might be effective in elder patients. Third, we analyzed relationships between dexterity and hemodynamic activity in the left somatosensory motor-related area, since only this area was activated during the Purdue Pegboard test in the post-assessment session. However, activity in the ventral parts of the brain such the cerebellum and basal ganglia, which are also implicated in motor learning (Atallah et al., 2007; Spampinato and Celnik, 2017), were not investigated due to methodological limitation

of NIRS. Fourth, although hemodynamic activity changes based on neurovascular coupling (see section Introduction), it cannot detect whether these changes are associated with neurophysiological facilitation nor inhibition. Fifth, we observed the motor behaviors during the motor imagery training by videos instead of EMG recording since it is difficult to record EMGs from all of the many muscles involved in stretching the arm and picking up a peg. However, video inspection could miss muscle activity without overt movements during the motor imagery training. Finally, sense of agency, which is an important factor for effectiveness of intervention with neurofeedback training (Braun et al., 2018), was not evaluated in the present study. However, sense of agency is reported to be positively associated with performance in neurofeedback training (Jeunet et al., 2016), and hemodynamic activity in the aPFC during the motor imagery training was larger in the real than sham groups, suggesting that sense of agency during the training might be higher in the real than sham groups. Further studies were required to evaluate usefulness of this neurofeedback training in patients with motor disabilities.

CONCLUSION

In the present study, the healthy adult subjects were trained to increase aPFC activity by using motor imagery of the Purdue Pegboard test under real-time neurofeedback from the aPFC: the real group subjects received real feedback signals from the aPFC, whereas the sham group subjects received random signals. The motor imagery training significantly increased hemodynamic activity in the aPFC in subjects in the real group when compared with subjects in the sham group. After the training, group analysis of hemodynamic activity during Purdue Pegboard testing indicated that the somatosensory motor-related areas (L-PM, lateral L-M1, medial L-M1, and L-S1) were activated in the real group with hand performance improvement, while hemodynamic activity in the SMA was increased in the sham group. Furthermore, the hemodynamic activity in the somatosensory motor-related areas during the Purdue Pegboard test after the training correlated with the activity in the aPFC on the last two days during motor imagery training. In addition, Oxy-Hb gain in the lateral L-M1 positively correlated with hand performance gain in the Purdue Pegboard test. Motor skill learning requiring fine motor functions has been attributed to changes in neural circuits in the sensorimotor cortex (Hatakenaka et al., 2007; Papale and Hooks, 2018). The present results suggest that neurofeedback training from the aPFC might induce synaptic plasticity in the sensorimotor cortex. These findings further suggest that motor imagery training using neurofeedback from the aPFC can be applied to patients with stroke or chronic neurological disorders.

DATA AVAILABILITY STATEMENT

The data that support the findings in this study are available from the corresponding author HSN, upon reasonable request.

ETHICS STATEMENT

The studies involving human participants were reviewed and approved by the Ethical Committee of Human Experiments at the University of Toyama. The participants provided their written informed consent to participate in this study.

AUTHOR CONTRIBUTIONS

HSN, SU, and MM designed the experiment. YO performed the experiment. YO and HisN analyzed the data and wrote the manuscript. YO, HSN, KT, HRN, SU, JM, YT, MM, and TO revised the manuscript. All authors discussed the results, and approved the final manuscript.

FUNDING

This study was supported partly by the JSPS KAKENHI (Grant No. 17K01503), and research funds from University of Toyama. The funders had no role in this study.

SUPPLEMENTARY MATERIAL

The Supplementary Material for this article can be found online at: https://www.frontiersin.org/articles/10.3389/fnins.2020.00034/full#supplementary-material

REFERENCES

Atallah, H. E., Lopez-Paniagua, D., Rudy, J. W., and O'Reilly, R. C. (2007). Separate neural substrates for skill learning and performance in the ventral and dorsal striatum. *Nat. Neurosci.* 10, 126–131. doi: 10.1038/nn1817

Banados, M., Teitelboim, C., and Zanelli, J. (1994). Black hole entropy and the dimensional continuation of the Gauss-Bonnet theorem. *Phys. Rev. Lett.* 72, 957–960. doi: 10.1103/PhysRevLett.72.957

Bansal, R., and Peterson, B. S. (2018). Cluster-level statistical inference in fMRI datasets: the unexpected behavior of random fields in high dimensions. *Magn. Reson. Imaging* 49, 101–115. doi: 10.1016/j.mri.2018.01.004

Bonini, F., Burle, B., Liégeois-Chauvel, C., Régis, J., Chauvel, P., and Vidal, F. (2014). Action monitoring and medial frontal cortex: leading role of supplementary motor area. *Science* 343, 888–891. doi: 10.1126/science.1247412

Boros, K., Poreisz, C., Münchau, A., Paulus, W., and Nitsche, M. A. (2008). Premotor transcranial direct current stimulation (tDCS) affects primary motor excitability in humans. *Eur. J. Neurosci.* 27, 1292–1300. doi: 10.1111/j.1460-9568.2008.06090.x

Braun, N., Debener, S., Spychala, N., Bongartz, E., Sörös, P., Müller, H. H. O., et al. (2018). The senses of agency and ownership: a review. *Front. Psychol.* 9:535. doi: 10.3389/fpsyg.2018.00535

Brem, A. K., Ran, K., and Pascual-Leone, A. (2013). Learning and memory. *Handb. Clin. Neurol.* 116, 693–737.

Carr, D. B., and Sesack, S. R. (2000). Projections from the rat prefrontal cortex to the ventral tegmental area: target specificity in the synaptic associations

with mesoaccumbens and mesocortical neurons. *J. Neurosci.* 20, 3864–3873. doi: 10.1523/JNEUROSCI.20-10-03864.2000

Cheng, Y. Y., Hsieh, W. L., Kao, C. L., and Chan, R. C. (2012). Principles of rehabilitation for common chronic neurologic diseases in the elderly. *J. Clin. Gerontol. Geriatr.* 3, 5–13. doi: 10.1016/j.jcgg.2011.11.003

Cook, R. D., and Weisberg, S. (1982). *Residuals and Influence in Regression: Monographs on Statistics and Applied Probability*. London: Chapman and Hall.

Cramer, S. C., Nelles, G., Benson, R. R., Kaplan, J. D., Parker, R. A., Kwong, K. K., et al. (1997). A functional MRI study of subjects recovered from hemiparetic stroke. *Stroke* 28, 2518–2527. doi: 10.1161/01.STR.28.12.2518

Cummings, F. W. (2001). The interaction of surface geometry with morphogens. *J. Theor. Biol.* 212, 303–313. doi: 10.1006/jtbi.2001.2377

Dayan, E., and Cohen, L. G. (2011). Neuroplasticity subserving motor skill learning. *Neuron* 72, 443–454. doi: 10.1016/j.neuron.2011.10.008

de Guise, E., del Pesce, M., Foschi, N., Quattrini, A., Papo, I., and Lassonde, M. (1999). Callosal and cortical contribution to procedural learning. *Brain* 122, 1049–1062. doi: 10.1093/brain/122.6.1049

de Paula, J. J., Albuquerque, M. R., Lage, G. M., Bicalho, M. A., Romano-Silva, M. A., and Malloy-Diniz, L. F. (2016). Impairment of fine motor dexterity in mild cognitive impairment and Alzheimer's disease dementia: association with activities of daily living. *Braz. J. Psychiatry* 38, 235–238. doi: 10.1590/1516-4446-2015-1874

Dieterich, M., Bense, S., Lutz, S., Drzezga, A., Stephan, T., Bartenstein, P., et al. (2003). Dominance for vestibular cortical function in the non-dominant hemisphere. *Cereb. Cortex* 13, 994–1007. doi: 10.1093/cercor/13.9.994

Faul, F., Erdfelder, E., Lang, A. G., and Buchner, A. (2007). G*Power 3: a flexible statistical power analysis program for the social, behavioral, and biomedical sciences. *Behav. Res. Methods* 39, 175–191. doi: 10.3758/BF03193146

Ferrari, M., and Quaresima, V. (2012). A brief review on the history of human functional near-infrared spectroscopy (fNIRS) development and fields of application. *Neuroimage* 63, 921–935. doi: 10.1016/j.neuroimage.2012.03.049

Floyer-Lea, A., and Matthews, P. M. (2004). Changing brain networks for visuomotor control with increased movement automaticity. *J. Neurophysiol.* 92, 2405–2412. doi: 10.1152/jn.01092.2003

Fujimoto, H., Mihara, M., Hattori, N., Hatakenaka, M., Yagura, H., Kawano, T., et al. (2017). Neurofeedback-induced facilitation of the supplementary motor area affects postural stability. *Neurophotonics* 4:045003. doi: 10.1117/1.NPh.4.4.045003

Fukui, Y., Ajichi, Y., and Okada, E. (2003). Monte Carlo prediction of near-infrared light propagation in realistic adult and neonatal head models. *Appl. Opt.* 42, 2881–2887. doi: 10.1364/AO.42.002881

Gao, M., Liu, C. L., Yang, S., Jin, G. Z., Bunney, B. S., and Shi, W. X. (2007). Functional coupling between the prefrontal cortex and dopamine neurons in the ventral tegmental area. *J. Neurosci.* 27, 5414–5421. doi: 10.1523/JNEUROSCI.5347-06.2007

GBD 2015 Neurological Disorders Collaborator Group (2017). Global, regional, and national burden of neurological disorders during 1990-2015: a systematic analysis for the global burden of disease study 2015. *Lancet Neurol.* 16, 877–897. doi: 10.1016/S1474-4422(17)30299-5

Hadoush, H., Sunagawa, T., Nakanishi, K., Endo, K., and Ochi, M. (2011). Motor somatotopy of extensor indicis proprius and extensor pollicis longus. *Neuroreport* 22, 559–564. doi: 10.1097/WNR.0b013e328348e750

Han, X., Jing, M. Y., Zhao, T. Y., Wu, N., Song, R., and Li, J. (2017). Role of dopamine projections from ventral tegmental area to nucleus accumbens and medial prefrontal cortex in reinforcement behaviors assessed using optogenetic manipulation. *Metab. Brain Dis.* 32, 1491–1502. doi: 10.1007/s11011-017-0023-3

Hanlon, R. E. (1996). Motor learning following unilateral stroke. *Arch. Phys. Med. Rehabil.* 77, 811–815. doi: 10.1016/S0003-9993(96)90262-2

Hardwick, R. M., Rottschy, C., Miall, R. C., and Eickhoff, S. B. (2013). A quantitative meta-analysis and review of motor learning in the human brain. *Neuroimage* 67, 283–297. doi: 10.1016/j.neuroimage.2012.11.020

Hasagawa, N., and Hoshino, K. (2002). On relationship between skill and movement imagery with athletes. *J. Health Sports Sci. Juntendo* 6, 166–173.

Hasan, A., Galea, J. M., Casula, E. P., Falkai, P., Bestmann, S., and Rothwell, J. C. (2013). Muscle and timing-specific functional connectivity between the dorsolateral prefrontal cortex and the primary motor cortex. *J. Cogn. Neurosci.* 25, 558–570. doi: 10.1162/jocn_a_00338

Hatakenaka, M., Miyai, I., Mihara, M., Sakoda, S., and Kubota, K. (2007). Frontal regions involved in learning of motor skill—A functional NIRS study. *Neuroimage* 34, 109–116. doi: 10.1016/j.neuroimage.2006.08.014

Hatem, S. M., Saussez, G., della Faille, M., Prist, V., Zhang, X., Dispa, D., et al. (2016). Rehabilitation of motor function after stroke: a multiple systematic review focused on techniques to stimulate upper extremity recovery. *Front. Hum. Neurosci.* 10:442. doi: 10.3389/fnhum.2016.00442

Hoshi, Y., Kobayashi, N., and Tamura, M. (2001). Interpretation of near-infrared spectroscopy signals: a study with a newly developed perfused rat brain model. *J. Appl. Physiol.* 90, 1657–1662. doi: 10.1152/jappl.2001.90.5.1657

Hosp, J. A., Pekanovic, A., Rioult-Pedotti, M. S., and Luft, A. R. (2011). Dopaminergic projections from midbrain to primary motor cortex mediate motor skill learning. *J. Neurosci.* 31, 2481–2487. doi: 10.1523/JNEUROSCI.5411-10.2011

Ishikuro, K., Dougu, N., Nukui, T., Yamamoto, M., Nakatsuji, Y., Kuroda, S., et al. (2018). Effects of transcranial direct current stimulation (tDCS) over the frontal polar area on motor and executive functions in Parkinson's disease; a pilot study. *Front. Aging Neurosci.* 10:231. doi: 10.3389/fnagi.2018.00231

Ishikuro, K., Urakawa, S., Takamoto, K., Ishikawa, A., Ono, T., and Nishijo, H. (2014). Cerebral functional imaging using near-infrared spectroscopy during repeated performances of motor rehabilitation tasks tested on healthy subjects. *Front. Hum. Neurosci.* 8:292. doi: 10.3389/fnhum.2014.00292

Jenkins, I. H., Brooks, D. J., Nixon, P. D., Frackowiak, R. S., and Passingham, R. E. (1994). Motor sequence learning: a study with positron emission tomography. *J. Neurosci.* 14, 3775–3790. doi: 10.1523/JNEUROSCI.14-06-03775

Jeunet, C., N'Kaoua, B., and Lotte, F. (2016). "Advances in user-training for mental-imagery-based BCI control: psychological and cognitive factors and their neural correlates," in *Progress in Brain Research*, Vol. 228, ed. D. Coyle, (Amsterdam: Elsevier), 3–35. doi: 10.1016/bs.pbr.2016.04.002

Johansson, B. B. (2011). Current trends in stroke rehabilitation. A review with focus on brain plasticity. *Acta Neurol. Scand.* 123, 147–159. doi: 10.1111/j.1600-0404.2010.01417.x

Jung, P., and Ziemann, U. (2009). Homeostatic and nonhomeostatic modulation of learning in human motor cortex. *J. Neurosci.* 29, 5597–5604. doi: 10.1523/JNEUROSCI.0222-09.2009

Kalivas, P. W. (1993). Neurotransmitter regulation of dopamine neurons in the ventral tegmental area. *Brain Res. Brain Res. Rev.* 18, 75–113. doi: 10.1016/0165-0173(93)90008-n

Kim, H. Y., Kim, E. J., and You, J. S. H. (2017). Adaptive locomotor network activation during randomized walking speeds using functional near-infrared spectroscopy. *Technol. Health Care* 25, 93–98. doi: 10.3233/THC-171310

Kinoshita, A., Takizawa, R., Yahata, N., Homae, F., Hashimoto, R., Sakakibara, E., et al. (2016). Development of a neurofeedback protocol targeting the frontal pole using near-infrared spectroscopy. *Psychiatry Clin. Neurosci.* 70, 507–516. doi: 10.1111/pcn.12427

Lapborisuth, P., Zhang, X., Noah, A., and Hirsch, J. (2017). Neurofeedback-based functional near-infrared spectroscopy upregulates motor cortex activity in imagined motor tasks. *Neurophotonics* 4:021107. doi: 10.1117/1.NPh.4.2.021107

Li, S., Cullen, W. K., Anwyl, R., and Rowan, M. J. (2003). Dopamine-dependent facilitation of LTP induction in hippocampal CA1 by exposure to spatial novelty. *Nat. Neurosci.* 6, 526–531. doi: 10.1038/nn1049

Liu, H., Qin, W., Li, W., Fan, L., Wang, J., Jiang, T., et al. (2013). Connectivity-based parcellation of the human frontal pole with diffusion tensor imaging. *J. Neurosci.* 33, 6782–6790. doi: 10.1523/JNEUROSCI.4882-12.2013

Mathiowetz, V., Rogers, S. L., Dowe-Keval, M., Donahoe, L., and Rennells, C. (1986). The purdue pegboard: norms for 14- to 19-year-olds. *Am. J. Occup. Ther.* 40, 174–179. doi: 10.5014/ajot.40.3.174

Matyas, F., Sreenivasan, V., Marbach, F., Wacongne, C., Barsy, B., Mateo, C., et al. (2010). Motor control by sensory cortex. *Science* 330, 1240–1243. doi: 10.1126/science.1195797

Mihara, M., Hattori, N., Hatakenaka, M., Yagura, H., Kawano, T., Hino, T., et al. (2013). Near-infrared spectroscopy-mediated neurofeedback enhances efficacy of motor imagery-based training in poststroke victims: a pilot study. *Stroke* 44, 1091–1098. doi: 10.1161/STROKEAHA.111.674507

Mihara, M., Miyai, I., Hattori, N., Hatakenaka, M., Yagura, H., Kawano, T., et al. (2012). Neurofeedback using real-time near-infrared spectroscopy enhances

motor imagery related cortical activation. *PLoS One* 7:e32234. doi: 10.1371/journal.pone.0032234

Molina-Luna, K., Pekanovic, A., Röhrich, S., Hertler, B., Schubring-Giese, M., Rioult-Pedotti, M. S., et al. (2009). Dopamine in motor cortex is necessary for skill learning and synaptic plasticity. *PLoS One* 4:e7082. doi: 10.1371/journal.pone.0007082

Muellbacher, W., Richards, C., Ziemann, U., Wittenberg, G., Weltz, D., Boroojerdi, B., et al. (2002). Improving hand function in chronic stroke. *Arch. Neurol.* 59, 1278–1282. doi: 10.1001/archneur.59.8.1278

Nachev, P., Kennard, C., and Husain, M. (2008). Functional role of the supplementary and pre-supplementary motor areas. *Nat. Rev. Neurosci.* 9, 856–869. doi: 10.1038/nrn2478

Nakamichi, N., Takamoto, K., Nishimaru, H., Fujiwara, K., Takamura, Y., Matsumoto, J., et al. (2018). Cerebral hemodynamics in speech-related cortical areas: articulation learning involves the inferior frontal gyrus, ventral sensory-motor cortex, and parietal-temporal sylvian area. *Front. Neurol.* 9:939. doi: 10.3389/fneur.2018.00939

Niederer, P., Mudra, R., and Keller, E. (2008). Monte Carlo simulation of light propagation in adult brain: influence of tissue blood content and indocyanine green. *Opto Electron. Rev.* 16, 124–130. doi: 10.2478/s11772-008-0012-5

Oldfield, R. C. (1971). The assessment and analysis of handedness: the Edinburgh inventory. *Neuropsychologia* 9, 97–113. doi: 10.1016/0028-3932(71)90067-4

Omelchenko, N., and Sesack, S. R. (2007). Glutamate synaptic inputs to ventral tegmental area neurons in the rat derive primarily from subcortical sources. *Neuroscience* 146, 1259–1274. doi: 10.1016/j.neuroscience.2007.02.016

Papale, A. E., and Hooks, B. M. (2018). Circuit changes in motor cortex during motor skill learning. *Neuroscience* 368, 283–297. doi: 10.1016/j.neuroscience.2017.09.010

Pavlova, E., Kuo, M. F., Nitsche, M. A., and Borg, J. (2014). Transcranial direct current stimulation of the premotor cortex: effects on hand dexterity. *Brain Res.* 1576, 52–62. doi: 10.1016/j.brainres.2014.06.023

Quaresima, V., and Ferrari, M. (2019). A mini-review on functional near-infrared spectroscopy (fNIRS): where do we stand, and where should we go? *Photonics* 6:87. doi: 10.3390/photonics6030087

Raggi, A., Leonardi, M., Ajovalasit, D., Carella, F., Soliveri, P., Albanese, A., et al. (2011). Disability and profiles of functioning of patients with Parkinson's disease described with ICF classification. *Int. J. Rehabil. Res.* 34, 141–150. doi: 10.1097/MRR.0b013e328344ae09

Ramnani, N., and Owen, A. M. (2004). Anterior prefrontal cortex: insights into function from anatomy and neuroimaging. *Nat. Rev. Neurosci.* 5, 184–194. doi: 10.1038/nrn1343

Richer, F., Chouinard, M. J., and Rouleau, I. (1999). Frontal lesions impair the attentional control of movements during motor learning. *Neuropsychologia* 37, 1427–1435. doi: 10.1016/S0028-3932(99)00029-9

Rioult-Pedotti, M. S., Friedman, D., Hess, G., and Donoghue, J. P. (1998). Strengthening of horizontal cortical connections following skill learning. *Nat. Neurosci.* 1, 230–234. doi: 10.1038/678

Schellekens, W., Petridou, N., and Ramsey, N. F. (2018). Detailed somatotopy in primary motor and somatosensory cortex revealed by Gaussian population receptive fields. *Neuroimage* 179, 337–347. doi: 10.1016/j.neuroimage.2018.06.062

Scherder, E., Dekker, W., and Eggermont, L. (2008). Higher-level hand motor function in aging and (preclinical) dementia: its relationship with (instrumental) activities of daily life – a mini-review. *Gerontology* 54, 333–341. doi: 10.1159/000168203

Schytz, H. W., Wienecke, T., Jensen, L. T., Selb, J., Boas, D. A., and Ashina, M. (2009). Changes in cerebral blood flow after acetazolamide: an experimental study comparing near-infrared spectroscopy and SPECT. *Eur. J. Neurol.* 16, 461–467. doi: 10.1111/j.1468-1331.2008.02398.x

Seiyama, A., Hazeki, O., and Tamura, M. (1988). Noninvasive quantitative analysis of blood oxygenation in rat skeletal muscle. *J. Biochem.* 103, 419–424. doi: 10.1093/oxfordjournals.jbchem.a122285

Shibata, K., Watanabe, T., Sasaki, Y., and Kawato, M. (2011). Perceptual learning incepted by decoded fMRI neurofeedback without stimulus presentation. *Science* 334, 1413–1415. doi: 10.1126/science.1212003

Singh, A. K., Okamoto, M., Dan, H., Jurcak, V., and Dan, I. (2005). Spatial registration of multichannel multi-subject fNIRS data to MNI space without MRI. *Neuroimage* 27, 842–851. doi: 10.1016/j.neuroimage.2005.05.019

Sitaram, R., Ros, T., Stoeckel, L., Haller, S., Scharnowski, F., Lewis-Peacock, J., et al. (2016). Closed-loop brain training: the science of neurofeedback. *Nat. Rev. Neurosci.* 18, 86–100. doi: 10.1038/nrn.2016.164

Spampinato, D., and Celnik, P. (2017). Temporal dynamics of cerebellar and motor cortex physiological processes during motor skill learning. *Sci. Rep.* 7:40715. doi: 10.1038/srep40715

Stoeckel, M. C., Seitz, R. J., and Buetefisch, C. M. (2009). Congenitally altered motor experience alters somatotopic organization of human primary motor cortex. *Proc. Natl. Acad. Sci. U.S.A.* 106, 2395–2400. doi: 10.1073/pnas.0803733106

Strangman, G., Culver, J. P., Thompson, J. H., and Boas, D. A. (2002). A quantitative comparison of simultaneous BOLD fMRI and NIRS recordings during functional brain activation. *Neuroimage* 17, 719–731. doi: 10.1006/nimg.2002.1227

Subramanian, L., Morris, M. B., Brosnan, M., Turner, D. L., Morris, H. R., and Linden, D. E. (2016). Functional magnetic resonance imaging neurofeedback-guided motor imagery training and motor training for Parkinson's disease: randomized trial. *Front. Behav. Neurosci.* 10:111. doi: 10.3389/fnbeh.2016.00111

Takakura, H., Nishijo, H., Ishikawa, A., and Shojaku, H. (2015). Cerebral hemodynamic responses during dynamic posturography: analysis with a multichannel near-infrared spectroscopy system. *Front. Hum. Neurosci.* 9:620. doi: 10.3389/fnhum.2015.00620

Takamoto, K., Hori, E., Urakawa, S., Sakai, S., Ishikawa, A., Kohno, S., et al. (2010). Cerebral hemodynamic responses induced by specific acupuncture sensations during needling at trigger points: a near-infrared spectroscopic study. *Brain Topogr.* 23, 279–291. doi: 10.1007/s10548-010-0148-8

Takeuchi, M., Hori, E., Takamoto, K., Tran, A. H., Satoru, K., Ishikawa, A., et al. (2009). Brain cortical mapping by simultaneous recording of functional near infrared spectroscopy and electroencephalograms from the whole brain during right median nerve stimulation. *Brain Topogr.* 22, 197–214. doi: 10.1007/s10548-009-0109-2

Theisen, F., Leda, R., Pozorski, V., Oh, J. M., Adluru, N., Wong, R., et al. (2017). Evaluation of striatonigral connectivity using probabilistic tractography in Parkinson's disease. *Neuroimage Clin.* 16, 557–563. doi: 10.1016/j.nicl.2017.09.009

Thornton, R., Vulliemoz, S., Rodionov, R., Carmichael, D. W., Chaudhary, U. J., Diehl, B., et al. (2011). Epileptic networks in focal cortical dysplasia revealed using electroencephalography–functional magnetic resonance imaging. *Ann. Neurol.* 70, 822–837. doi: 10.1002/ana.22535

Tong, Y., Lindsey, K. P., and deB Frederick, B. (2011). Partitioning of physiological noise signals in the brain with concurrent near-infrared spectroscopy and fMRI. *J. Cereb. Blood Flow Metab.* 31, 2352–2362. doi: 10.1038/jcbfm.2011.100

Tzourio-Mazoyer, N., Landeau, B., Papathanassiou, D., Crivello, F., Etard, O., Delcroix, N., et al. (2002). Automated anatomical labeling of activations in SPM using a macroscopic anatomical parcellation of the MNI MRI single-subject brain. *Neuroimage* 15, 273–289. doi: 10.1006/nimg.2001.0978

Vasylenko, O., Gorecka, M. M., and Rodriguez-Aranda, C. (2018). Manual dexterity in young and healthy older adults. 1. Age- and gender-related differences in unimanual and bimanual performance. *Dev. Psychobiol.* 60, 407–427. doi: 10.1002/dev.21619

Wang, T., Mantini, D., and Gillebert, C. R. (2018). The potential of real-time fMRI neurofeedback for stroke rehabilitation: a systematic review. *Cortex* 107, 148–165. doi: 10.1016/j.cortex.2017.09.006

White, B. R., and Culver, J. P. (2010). Quantitative evaluation of high-density diffuse optical tomography: in vivo resolution and mapping performance. *J. Biomed. Opt.* 15:026006. doi: 10.1117/1.3368999

Woo, C. W., Krishnan, A., and Wager, T. D. (2014). Cluster-extent based thresholding in fMRI analyses: pitfalls and recommendations. *Neuroimage* 91, 412–419. doi: 10.1016/j.neuroimage.2013.12.058

Wray, S., Cope, M., Delpy, D. T., Wyatt, J. S., and Reynolds, E. O. (1988). Characterization of the near infrared absorption spectra of cytochrome aa3 and haemoglobin for the non-invasive monitoring of cerebral oxygenation. *Biochim. Biophys. Acta* 933, 184–192. doi: 10.1016/0005-2728(88)90069-2

Yamamoto, T., and Kato, T. (2002). Paradoxical correlation between signal in functional magnetic resonance imaging and deoxygenated hemoglobin content in capillaries: a new theoretical explanation. *Phys. Med. Biol.* 47, 1121–1141. doi: 10.1088/0031-9155/47/7/309

Yamamoto, T., Maki, A., Kadoya, T., Tanikawa, Y., Yamad, Y., Okada, E., et al. (2002). Arranging optical fibres for the spatial resolution improvement of topographical images. *Phys. Med. Biol.* 47, 3429–3440. doi: 10.1088/0031-9155/47/18/311

Yasumura, A., Kokubo, N., Yamamoto, H., Yasumura, Y., Nakagawa, E., Kaga, M., et al. (2014). Neurobehavioral and hemodynamic evaluation of Stroop and reverse Stroop interference in children with attention-deficit/hyperactivity disorder. *Brain Dev.* 36, 97–106. doi: 10.1016/j.braindev.2013.01.005

Ye, J. C., Tak, S., Jang, K. E., Jung, J., and Jang, J. (2009). NIRS-SPM: statistical parametric mapping for near-infrared spectroscopy. *Neuroimage* 44, 428–447. doi: 10.1016/j.neuroimage.2008.08.036

Yeudall, L. T., Fromm, D., Reddon, R., and Stefanyk, W. O. (1986). Normative data stratified by age and sex for 12 neuropsychological tests. *J. Clin. Psychol.* 42, 918–946. doi: 10.1002/1097-4679(198611)42:6<918::aid-jclp2270420617>3.0.co;2-y

Zanchi, D., Cunningham, G., Lädermann, A., Ozturk, M., Hoffmeyer, P., and Haller, S. (2017). Brain activity in the right-frontal pole and lateral occipital cortex predicts successful post-operatory outcome after surgery for anterior glenoumeral instability. *Sci. Rep.* 7:498. doi: 10.1038/s41598-017-00518-9

Zhang, D., Gao, M., Xu, D., Shi, W. X., Gutkin, B. S., Steffensen, S. C., et al. (2012). Impact of prefrontal cortex in nicotine-induced excitation of ventral tegmental area dopamine neurons in anesthetized rats. *J. Neurosci.* 32, 12366–12375. doi: 10.1523/JNEUROSCI.5411-11.2012

Conflict of Interest: The authors declare that the research was conducted in the absence of any commercial or financial relationships that could be construed as a potential conflict of interest.

frontiers in Neuroscience

BRIEF RESEARCH REPORT
published: 17 June 2020
doi: 10.3389/fnins.2020.00600

Longitudinal Case Study of Regression-Based Hand Prosthesis Control in Daily Life

Janne M. Hahne[1], Meike A. Wilke[1,2], Mario Koppe[1,3], Dario Farina[1,4] and Arndt F. Schilling[1]*

[1] Applied Rehabilitation Technology Lab, Department of Trauma Surgery, Orthopedic Surgery and Hand Surgery, University Medical Center Göttingen, Göttingen, Germany, [2] Faculty of Life Sciences, University of Applied Sciences (HAW) Hamburg, Hamburg, Germany, [3] Global Research and Innovation Hub, Ottobock SE & Co. KGaA, Duderstadt, Germany, [4] Department of Bioengineering, Imperial College London, London, United Kingdom

Hand prostheses are usually controlled by electromyographic (EMG) signals from the remnant muscles of the residual limb. Most prostheses used today are controlled with very simple techniques using only two EMG electrodes that allow to control a single prosthetic function at a time only. Recently, modern prosthesis controllers based on EMG classification, have become clinically available, which allow to directly access more functions, but still in a sequential manner only. We have recently shown in laboratory tests that a regression-based mapping from EMG signals into prosthetic control commands allows for a simultaneous activation of two functions and an independent control of their velocities with high reliability. Here we aimed to study how such regression-based control performs in daily life in a two-month case study. The performance is evaluated in functional tests and with a questionnaire at the beginning and the end of this phase and compared with the participant's own prosthesis, controlled with a classical approach. Already 1 day after training of the regression model, the participant with transradial amputation outperformed the performance achieved with his own Michelangelo hand in two out of three functional metrics. No retraining of the model was required during the entire study duration. During the use of the system at home, the performance improved further and outperformed the conventional control in all three metrics. This study demonstrates that the high fidelity of linear regression-based prosthesis control is not restricted to a laboratory environment, but can be transferred to daily use.

Keywords: Myolectric control, prosthesis, regression, simultaneous control, clinical evaluation

OPEN ACCESS

Edited by:
Jose Luis Contreras-Vidal, University of Houston, United States

Reviewed by:
Kazutaka Takahashi, The University of Chicago, United States
Melanie Gay Urbanchek, University of Michigan, United States

****Correspondence:***
Janne M. Hahne
janne.hahne@med.uni-goettingen.de

Specialty section:
This article was submitted to Neuroprosthetics, a section of the journal Frontiers in Neuroscience

Received: *03 July 2019*
Accepted: *15 May 2020*
Published: *17 June 2020*

Citation:
Hahne JM, Wilke MA, Koppe M, Farina D and Schilling AF (2020) Longitudinal Case Study of Regression-Based Hand Prosthesis Control in Daily Life. Front. Neurosci. 14:600. doi: 10.3389/fnins.2020.00600

INTRODUCTION

Losing a hand has a dramatic impact to a person's life. Myoelectric hand prostheses can reduce the repercussions and help the person to conduct activities of daily living with less restrictions. Conventionally, two electrodes placed on antagonistic muscles are used to control a single degree of freedom (DOF) of the hand (Muzumdar, 2004), i.e., opening and closing the hand. Mode-switching techniques, such as co-contraction are used control a second DOF such as a wrist rotation or other

functions, such as different grip types sequentially, which is cumbersome and limits the benefit of additional functions (Amsuess et al., 2014).

To overcome the limitations, classification techniques (Englehart and Hudgins, 2003; Oskoei and Hu, 2007; Peerdeman et al., 2011; Scheme and Englehart, 2011; Hahne et al., 2012) have been applied that compare the current electromyographic (EMG) with training-patterns with known motion. The classifier decides for the most similar class, allowing for directly accessing all functions, although typically only in a sequential manner. Recently, classification based control approaches have become clinically available (Coapt-LLC, 2019; Ottobock, 2019).

In the past years also regression algorithms have been applied in prosthetic research (Jiang et al., 2009; Ameri et al., 2014; Gijsberts et al., 2014; Hahne et al., 2014). The fundamental difference to classification is, that a regressor does not decide for a particular motion class. Instead, a regressor estimates activity levels for all DOFs simultaneously. This allows not only performing two different functions at the same time but even to control their velocity independently. Since the output reacts to any changes of the EMG input, the user can more easily compensate for disturbances, which increases the reliability (Hahne et al., 2017).

The relatively high classification/regression performance shown in laboratory conditions may not necessarily translate into good functional recovery in real prosthetic use (Jiang et al., 2012). Factors such as changes in arm position (Fougner et al., 2011; Khushaba et al., 2016; Beaulieu et al., 2017), small electrode displacements (Young et al., 2011; Hwang et al., 2017), sweat, mechanical load to the socket (Cipriani et al., 2011), or time between training and application of the algorithm (Amsuss et al., 2013; Vidovic et al., 2016) can degrade the performance and lead to an unreliable control in daily life.

Recently, we have shown a relatively high robustness of the regression approach in five prosthetic users during advanced clinical tests in the laboratory that involved challenging arm positions and the application on a second day without retraining (Hahne et al., 2018). The purpose of this eight-week case study was to test a research prosthesis controlled by linear regression (LR) under fully uncontrolled conditions in the daily life and compare it with the participant's own prosthesis with a conventional control (CC).

METHODS

Participant

The participant of this case study was a 58-year old man, who got his left hand amputated on trasradial level, 35 years before this study. Since that time he has been actively using conventional myoelectric prostheses controlled with two EMG channels. Until approximately 12 months before the beginning of this study he was wearing only single-DOF prostheses without rotation. Then he was provided with an Otto Bock Michelangelo hand and used conventional slope-control to access grasp and rotation and co-contraction to alter between the two grip functions. He had moderate experience with both classification- and regression-based control approaches from earlier experiments and was familiar with the functional tests conducted in this study. Due to his participation in our previous laboratory study (Hahne et al., 2018) with a similar system, he was already familiar with the control concept and was able to generate suitable training data. A chronologic overview on the participant's prosthetic history and this study is provided in **Figure 1E**.

Prosthesis

The research prosthesis used in this study was an Otto Bock VariPlus Speed hand with electric wrist rotator. A customized socket was built for the participant (inner socket high temperature vulcanization silicone incl. eight Otto Bock 13E200 electrodes, outer socket laminated carbon fiber). It included a customized controller, a battery pack and an easily accessible power-switch and allowed for simultaneous and proportional control of the two DOFs with LR.

The system and the training procedure were similar to those described in Hahne et al. (2018). First, four suitable phantom-limb motions were selected based on visual inspection of the EMG (phantom flexion/extension for closing/opening, pronation/little-finger flexion for rotation). The latter gave a relatively strong and clear pattern and was chosen instead supination to increase the robustness.

For the algorithmic training, data with known movement association was recorded. Therefore, the participant was asked to follow trapezoidal contraction profiles for all four motions (2 s rest, 3 s ramp-up, 3 s static contraction, and 2 s ramp-down). The entire training dataset consisted of only one repetition of each motion in neutral arm position, corresponding to a total of 40 s of data for training the algorithm (data in **Supplementary Material**).

A linear mapping model W from the eight-dimensional EMG envelopes x to the two-dimensional control signal $\hat{y}$ (Eq. 1) was established by ordinary LR (Eq. 2), where X and Y are matrices with the collected training data and labels based on the visual cues:

$$\hat{y} = W^T x \tag{1}$$

$$W = \left(XX^T\right)^{-1} XY^T \tag{2}$$

Algorithmic training of the regression model was conducted with a customized MATLAB framework on a standard PC (I7, 2 × 2.5 GHz, 16 GB RAM, and Windows 7). As previously shown (Hahne et al., 2014), a linear regressor on EMG can estimate simultaneous activations of two DOFs with a clinically feasible number of electrodes, even when trained on non-combined motions only. Following the training of the algorithm, a real-time control of a cursor in a two-dimensional coordinate system was established in position-control mode to verify proper control.

As in CC, the prosthesis was operated in velocity-control mode. The stronger the participant contracted, the faster the prosthesis moved and at relaxation, the prosthesis did not move back. The envelope output of the active EMG electrodes could be directly utilized without windowing or feature extraction.

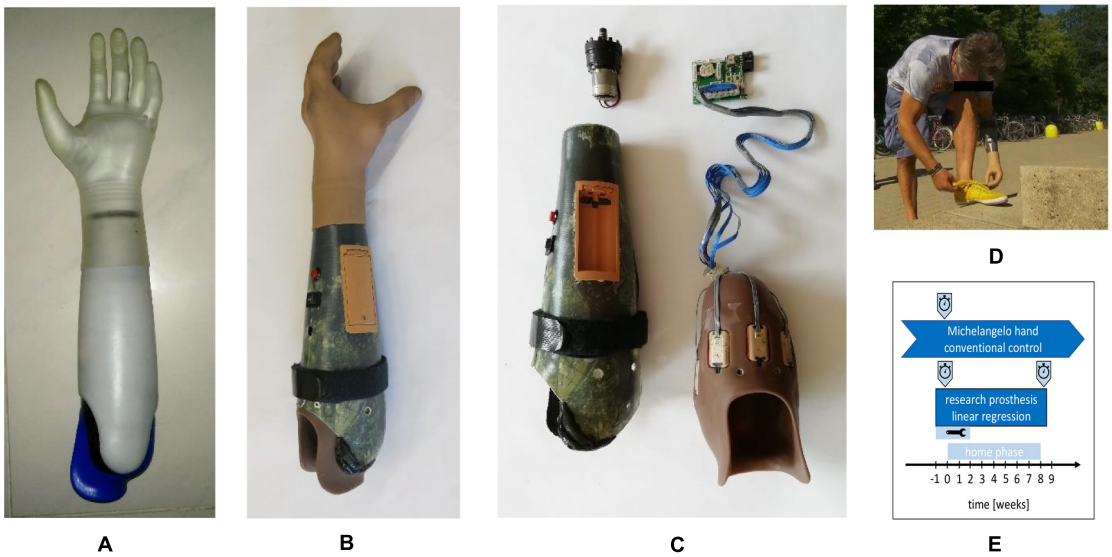

FIGURE 1 | Prostheses hardware used in this study. **(A)** Michelangelo hand owned by the participant and used as a baseline with conventional two-channel control in this study. **(B)** Research prosthesis controlled by eight channels and linear regression. **(C)** Components of the research prosthesis: rotation unit (upper left), outer socket with battery holder, power-switch and strap with hook and loop fastener to adjust the fit (lower left), inner socket made from silicone with eight integrated electrode modules (lower right), customized controller. **(D)** Use of the regression based prosthesis in uncontrolled conditions, in daily life. **(E)** Chronology of this case report indicating prosthetic use, functional assessments (stopwatch), and adjustments period (tool icon). Michelangelo hand was used already since 12 month at the study period and before the participant used single-DOF prostheses for around 35 years.

To suppress unintended motions and fine-tune the velocity of the prosthesis, two thresholds were individually adjusted for each of the four prosthetic functions that determined the level of activation and the level for that the maximal speed is reached. Additionally, the customized controller contained a real-time clock and a micro-SD card that was used for continuous recording of the EMG envelopes to allow for quantitative usage evaluation. For the analysis, we considered only reconstructed motions with speed larger than five percent of the maximal speed and a duration larger than 200 ms. A motion that included a phase with both DOFs active was counted as one multi-DOF motion. The results of this analysis were averaged over periods of 1 week of the home phase.

As a baseline, we compared our research prosthesis (controlled with LR) with the Michelangelo hand owned by the participant and used daily before this study for approximately 12 months. It was controlled by two EMG channels on the residual flexor and extensor muscles and a CC technique based on the initial EMG slope (Muzumdar, 2004). Slowly increasing EMG amplitudes would open/close the prosthesis while quickly raising contractions would rotate the hand with a velocity proportional to the EMG amplitude and a co-contraction was used to change between lateral and palmar grip.

Functional and Subjective Assessment

The functional performance of the LR-controlled research-prototype prosthesis was assessed with three standardized tests during laboratory sessions performed at the beginning of the study, 1 day after the training with the new system, and at the end of the 2-month home phase. The CC-controlled Michelangelo hand was evaluated with the same functional tests at the beginning of the study only. Since the participant had already used this fitting for 12 months in daily life, we assumed that the training with this prosthesis was finished and the performance already saturated. The functional tests performed were the Box-And-Blocks Test (Mathiowetz et al., 1985), the Clothespin-Relocation Test (Hussaini and Kyberd, 2017), and the Southampton Hand Assessment Procedure (SHAP; Kyberd et al., 2009).

The Box-And-Blocks Test requires to transfer as many wooden blocks as possible from one box into another within 60 s. The Clothespin-Relocation Test assesses the time needed to relocate three pins (10 N grip force) of the Rolyan Graded Pinch Exerciser from a horizontal to a vertical bar. For the SHAP test times for a broad spectrum of activities of daily living are measured and compared with a normative database of young healthy people (Light et al., 2002). A SHAP-score of 100 corresponds to normal and 0 to minimal functionality.

The Box-And-Blocks Test and the Clothespin-Relocation Test were performed ten times in each laboratory session, in order to reduce the scatter and test for statistically significant differences within the participant. Statistical comparisons were performed with a Wilcoxon rank-sum test with Bonferroni correction and a threshold of $p = 0.05$.

Beside the functional tests in the laboratory, we aimed to gather information regarding the reliability in other daily life situations, where disturbing factors that were not present in the laboratory tests appear. Also, we were interested in the personal opinion of the participant regarding the new control approach. Therefore, he was asked to fill in customized questionnaires

for the first and the last week of the home phase (one pencil paper form covering both prostheses, not-validated). He had to grade different aspects of the research prosthesis and his own Michelangelo hand on a scale from 0 to 10 (questions in **Supplementary Material**).

The study was conducted in accordance with the declaration of Helsinki and was approved by the local ethic commission (approval number 23/4/16) and written, informed consent was obtained.

RESULTS

Summary of Home Phase

During the home phase of this study the participant was motivated to use the LR-controlled research prosthesis as much as possible, but he was allowed to use his own Michelangelo hand. His previous single-DOF prosthesis was not used and he reported to wear a prosthesis most of the time.

In the first two weeks of the home phase, problems with the socket fitting including electrode lift offs required several iterations of corrections (**Figure 1E**). Therefore, he visited our laboratory several times and was visited by a technician once in that time. Adding a strap adjuster system to the outer socket finally allowed the subject to control the tightness of the socket to ensure proper fixation and comfortable fit and to compensate for stump volume variations.

No retraining of the regression model that transforms the eight EMG-envelopes into control signals was required during the entire study. Only the thresholds that were used as a post-processing after the regression step to fine-tune the speed and to reduce the risk of unintended activations were adjusted as the participant experienced the sensitivity of the control as too high in the first week at home. On day 13 all thresholds were therefore increased by 75%, followed by corrections for the upper thresholds for hand open and supination. These were the only adjustments made on the controller during the home phase. After these mechanical and parametrical adjustments, the participant reported to be very satisfied with the control for the rest of the study. No further laboratory visits were required during the home phase but we called him occasionally to verify that everything was ok. He used the LR prosthesis in any activity of daily life, such as cooking, eating, cleaning, dressing, or fastening his shoes (**Figure 1**). He further reported that the LR control was very intuitive and that he could easily change from CC to LR. In contrast, when changing back to CC, he always needed some time of familiarization to the slope-control. He reported unintended rotations with his Michelangelo hand, especially in situations when he was in a rush and therefore generated quickly rising EMG amplitudes; a problem that was already present before this study. Being unsatisfied with his CC, he requested that the rotation function to be removed from his Michelangelo prosthesis by his prosthetist during the time of this study. We did not modify the control of the participant's Michelangelo hand and no other changes beside removing the rotation were made externally during this study.

Despite satisfaction with the control, he, however, did not constantly wear the research prosthesis. He explained this choice with a preferred esthetic appearance of his Michelangelo hand over the VariPlus Speed hand and a more comfortable socket. He did not report any injuries, blisters, muscle aches, headaches, or similar issues related to the prostheses during the study. Overall, he indicated that he would prefer the LR control algorithm to be embedded in his own Michelangelo prosthesis and socket.

Data Log

The average amount of time the participant was wearing the research prosthesis increased within the first weeks and remained on a relatively high level between five and seven hours per day until week four (**Figure 2A**). In the second half of the study the average wear time decreased to 1–4 h per day. The wear-time of his own Michelangelo hand was not tracked as this was not possible with the commercial hardware, however, one can assume that it behalves complementary to the research prothesis, as the participant stated to wear a prothesis all day long. The number of motions he conducted per hour while wearing the research prosthesis was relatively high at the beginning of the study, with approximately 100 single-DOF motions and 80 multi-DOF motions, and decreased after the final adjustments in the end of week 2 to approximately 70 single-DOF and less than 20 multi-DOF motions per hour (**Figure 2B**). The amount of single DOF motions increased in the second half of the study to reach 120 motions per hour toward the end of the study. The multi-DOF motions on the other hand remained low in number until the end of the study. When considering the frequency of single DOF motions for each DOF separately, both DOFs were almost equally often active in the first two weeks. After week 2, however, the use of rotation decreased to approximately 10 motions per hour and remained at this level until the end of the study. The number of motions in the open/close DOF did not change in the first weeks and increased in the second half of the study from less than 60 to 80–100 motions per hour. The duration of single-DOF motions was shorter than multi-DOF motions and rotations were shorter than motions of the DOF hand open/close (**Figure 2C**). There is a small trend towards decreasing duration for all motions over the time of the study.

Functional Tests

All three functional tests were performed with the participant's own Michelangelo hand (in beginning only) and the research prosthesis (before and after home phase; **Figure 3**).

In the Box-And-Blocks Test the participant performed significantly better with LR prototype than with CC ($p < 0.05$) already before the home phase. The performance in this test did not further improve after the home phase but remained significantly better than CC in the second evaluation. Performance of the Clothespin-Relocation Test with the LR control was not significantly different with respect to CC before the home phase. However, after the home phase, the control with the regression-based control (LR after) improved significantly compared to both methods prior to training. Also, while in the initial session, one and three pins were dropped in total with CC and LR, respectively, after the home phase no pin was dropped

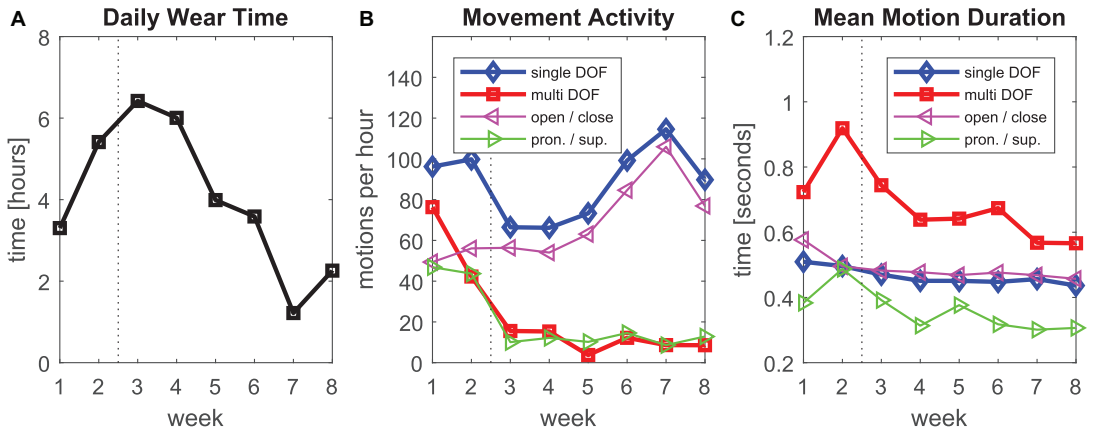

FIGURE 2 | Data log of the regression prosthesis during the home phase of the study. **(A)** Daily wear time, average per week. **(B)** Counts of single and multi-DOF motions per hour of wear time. **(C)** Average duration of each individual motion. In all plots, the dashed vertical line indicates the time, when final adjustments to the socket and the parameters were finalized.

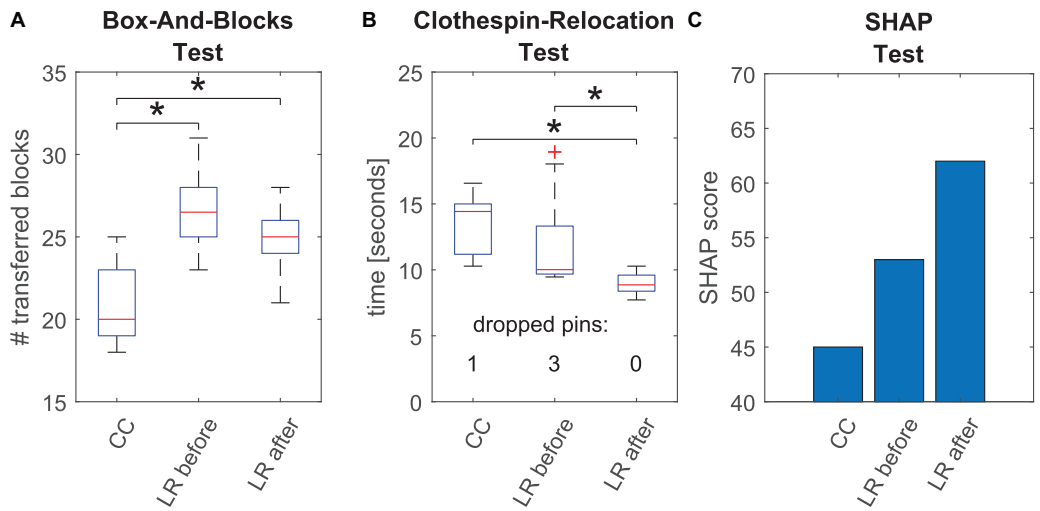

FIGURE 3 | Results of the functional tests. Box-And-Blocks Test **(A)**, Clothespin-Relocation Test **(B)**, and SHAP Test **(C)**. All tests were conducted with the conventionally controlled Michelangelo hand owned by the participant (CC) and the regression-based research prosthesis (LR before) in the beginning of the study. The regression control was evaluated a second time after the 8-week home phase (LR after). For Box-And-Blocks and Clothespin-Relocation Test 10 repetitions were conducted each time to apply intra-subject statistics. Statistically significant differences ($p < 0.05$) are marked with asterisks.

with LR. In the SHAP Test the participant reached higher SHAP score with the regression (score 53) with respect to CC (score 45) already at the beginning of the study and further improved after the home phase (score 62).

Subjective Assessment

At the beginning of the study, the participant graded the reliability of the regression control higher than the one of his own prosthesis (**Figure 4A**). In the end both prostheses got full scores. This evaluation followed the longitudinal experience and final adjustments of the socket and the threshold parameters in LR and the deactivation of the rotation function for the Michelangelo hand. The naturalness of the control and the perception of the prosthesis as own hand were rated with maximal scores in the beginning and the end for LR while CC got only moderate scores, slightly increasing in the end (**Figures 4B,C**). The frequency of dropped items during the home phase was rated higher for CC. This score further improved with LR at the end of the study (**Figure 4D**). The participant graded a moderate advantage of LR in comparison with CC, slightly increasing at the end (**Figure 4E**).

DISCUSSION

We evaluated a regression-based controller for simultaneous and proportional control of a 2-DOF prosthetic hand for 8 weeks in daily use. The regression model was trained with data recorded in less than 1 min and no retraining was required during the 2 months. In the first two weeks we encountered

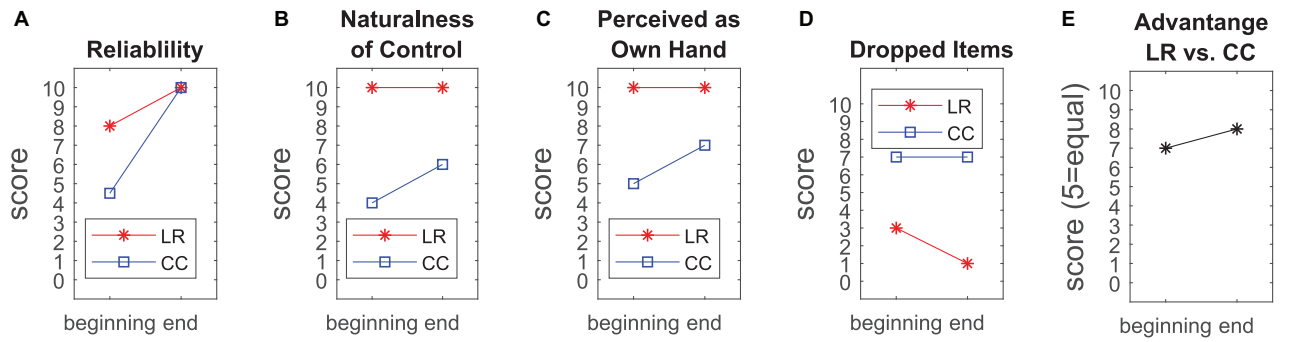

FIGURE 4 | Questionnaires. The participant graded for the first and last week of the home phase the reliability **(A)**, naturalness of control **(B)**, to which extent he perceived the prosthesis as his own hand **(C)**, and the frequency of dropped or unintendedly released items **(D)** for both prostheses. In these metrics, LR scored better than CC at each time point. He reported a moderate advantage of LR compared to CC **(E)**.

some reliability issues (mainly unintended rotations), that were fixed by modifications on the socket and final adjustments of the thresholds. The participant was then very satisfied with the control and did not report any further reliability issues. The strong decrease of rotation and multi-DOF motions after the adjustments in the second week (**Figure 2B**) could be an indication that many of these motions during the first two weeks were unintended activations.

As expected, the motion counts after week two revealed that the hand DOF (open/close) was more important than the wrist rotation for the participant. Hand use occurred 5 to 10 times more often than wrist rotation. Nevertheless, the participant reported to find the rotation useful, especially due to the simultaneous and intuitive control. The control of his own prostheses was in contrast perceived as so unphysiological and slow that he decided to remove the rotation there.

Multi-DOF motions were as frequent as rotations. This could be an indication for a physiological use of the hand, where in preparation of a grasp rotation is, e.g., combined with opening of the hand. In this light, the longer duration of multi-DOF motions could be explained by including the whole preparation movement in one Multi-DOF motion. Such more natural motions are not possible with current commercial control systems, where the user has to activate the individual functions sequentially. After the adjustment of the thresholds the participant reported that he did not notice any false activations of prosthesis functions in daily life. However, there is no final proof that all recorded multi-DOF motions were intended by the participant of the study.

The average daily wear time of the prosthesis decreased toward the end of the study, which could be a sign of dissatisfaction with the control. However, at the same time, the number of grasp motions per hour increased. Together, this could indicate that the participant used the prosthesis especially for physically active tasks and changed to his Michelangelo for less active phases, as he preferred its visual appearance and the more comfortable socket. The trend of decreased motion duration toward the end of the study could indicate an increased confidence, i.e., a more precise control of the velocity leading to a faster execution of the task. It would be interesting to record also the number motions per hour for CC and compare them with these of LR. However, this was technically not possible in this study and could be subject of future investigations.

It is not possible to conclude that the functional improvements of the regression-based control between the two assessments were only due to user learning (Hahne et al., 2017), as parameters were changed during the home phase of the study. However, we believe that progressive learning was indeed the main reason for improved performance, as the increase in threshold values that we have made would potentially, if at all, decrease the speed of the motions.

The subjectively reported larger frequency of dropped items in daily life with CC (**Figure 4D**) seems to be in contradiction to improved reliability rating and the higher number of dropped pins within the functional assessment of LR in the beginning. However, the participant explained that these item drops in daily life were not related to the control, but rather to the geometry of the lateral grip of the Michelangelo hand. The use of different prostheses to compare control algorithms is a limiting factor. On the other hand, we previously compared CC and LR with the same prosthetic hand in laboratory conditions (Hahne et al., 2018), and found a higher performance for LR. In the present work we decided to use the system the participant was wearing in daily life before the study as baseline to compare with the system he is most familiar with. Additionally, the maximal speed of the Michelangelo hand (325 mm/s for open/close, 25 rpm for rotation) is larger than the VariPlus Speed hand (300 mm/s, 17 rpm). So a potential bias due to the speed of the prosthesis would be in favor of CC. In the direct comparison (**Figure 4E**), the participant rated the advantage of the regression-controlled research prosthesis with 8 out of 10 points. This evaluation includes a combination of different aspects of the prosthesis, such as controllability, socket comfort, esthetic appearance of the prosthesis, that may confound each other. The research socket was constructed by a professional orthopedic technician with an inner socket of soft silicone, similar as the socket of the participant's own Michelangelo hand. However, the eight electrode modules for the research prosthesis had to be pressed against the skin with a certain pressure to ensure a good contact, which made the socket less comfortable. This is a clear

shortcoming of the study. A possible way to mediate this problem in future experiments may be to apply small conductive inserts (Hanson, 2008) that directly integrate into the inner socket or prosthesis liner to improve the comfort for control approaches that require a larger number of EMG-channels.

In (Kuiken et al., 2016) a classification-based approach was evaluated in three participants before and after home-use. While with their system a higher number of functions could be controlled, it required a frequent retraining during the home phase. Comparing the functional performance, our participant performed better than all three participants of the classification system in the SHAP, Box-And-Blocks, and Clothespin-Relocation Test already before the home phase. After the home phase the performance generally improved in both studies. Our participant using regression still outperformed all three participants of the classification-study in almost all metrics, emphasizing the daily-life suitability of our system.

In conclusion, this eight-week home trial demonstrates in a case study that a simultaneous and proportional control of two DOFs based on LR is reliably applicable in daily life. After final adjustments of the socket and parameters in week two, the control was robust and the participant was highly satisfied with the system. For this participant, the regression-controlled prosthesis outperformed the conventionally controlled one, which the participant used daily before this study in all functional metrics. The regression model was trained with data recorded in less than 1 min, with no retraining of the regression model being required over the entire study. This suggests a practical feasibility and potential clinical relevance of the presented approach, although tests with further prosthetic users are required to show whether a regression is useful for a broader range of users.

DATA AVAILABILITY STATEMENT

The datasets generated for this study are available on request to the corresponding author.

ETHICS STATEMENT

The studies involving human participants were reviewed and approved by Ethikkomission der Universitätsmedizin Göttingen. The patients/participants provided their written informed consent to participate in this study.

AUTHOR CONTRIBUTIONS

JH developed the controller, and the MATLAB framework, planned and executed the laboratory experiments, supervised the home phase, analyzed the data, and wrote the manuscript. MW, DF, and AS planned and supported the experiments, analyzed the data, and revised the manuscript. MK build and improved the socket and revised the manuscript.

FUNDING

This work was supported by the German Ministry for Education and Research (BMBF) under grant agreement number 16SV7657 (project INOPRO) and the European Union's Horizon 2020 research and innovation program under grant agreement number 687795 (project INPUT). This work was also partly supported by the European Research Council Synergy under the grant number 810346 (project Natural BionicS).

SUPPLEMENTARY MATERIAL

The Supplementary Material for this article can be found online at: https://www.frontiersin.org/articles/10.3389/fnins.2020.00600/full#supplementary-material

REFERENCES

Ameri, A., Kamavuako, E. N., Scheme, E. J., Englehart, K. B., and Parker, P. A. (2014). Support vector regression for improved real-time, simultaneous myoelectric control. *IEEE Trans. Neural Syst. Rehabil. Eng.* 22, 1198–1209. doi: 10.1109/TNSRE.2014.2323576

Amsuess, S., Goebel, P., Graimann, B., and Farina, D. (2014). Extending mode switching to multiple degrees of freedom in hand prosthesis control is not efficient. *Conf. Proc. IEEE Eng. Med. Biol. Soc.* 2014, 658–661. doi: 10.1109/EMBC.2014.6943677

Amsuss, S., Paredes, L. P., Rudigkeit, N., Graimann, B., Herrmann, M. J., and Farina, D. (2013). Long term stability of surface EMG pattern classification for prosthetic control. *Conf. Proc. IEEE Eng. Med. Biol. Soc.* 2013, 3622–3625. doi: 10.1109/EMBC.2013.6610327

Beaulieu, R. J., Masters, M. R., Betthauser, J., Smith, R. J., Kaliki, R., Thakor, N. V., et al. (2017). Multi-position training improves robustness of pattern recognition and reduces limb-position effect in prosthetic control. *J. Prosthetics Orthot.* 29, 54–62. doi: 10.1097/JPO.0000000000000121

Cipriani, C., Sassu, R., Controzzi, M., and Carrozza, M. C. (2011). "Influence of the weight actions of the hand prosthesis on the performance of pattern recognition based myoelectric control: preliminary study," in *Proceedings of the Annual International Conference of the IEEE Engineering in Medicine and Biology Society*, Boston, MA.

Coapt-LLC (2019). *Coapt - Complete Control*. Available online at: http://coaptengineering.com (accessed 8 Apr 2020).

Englehart, K., and Hudgins, B. (2003). A robust, real-time control scheme for multifunction myoelectric control. *Biomed. Eng. IEEE Trans.* 50, 848–854. doi: 10.1109/tbme.2003.813539

Fougner, A., Scheme, E., Chan, A. D. C., Englehart, K., Stavdahl, O., and Stavdahl, O. (2011). Resolving the limb position effect in myoelectric pattern recognition. *IEEE Trans. Neural Syst. Rehabil. Eng.* 19, 644–651. doi: 10.1109/TNSRE.2011.2163529

Gijsberts, A., Bohra, R., González, D. S., Werner, A., Nowak, M., Caputo, B., et al. (2014). Stable myoelectric control of a hand prosthesis using non-linear incremental learning. *Front. Neurorobot.* 8:8. doi: 10.3389/fnbot.2014.00008

Hahne, J. M., Biessmann, F., Jiang, N., Rehbaum, H., Farina, D., Meinecke, F. C., et al. (2014). Linear and nonlinear regression techniques for simultaneous and proportional myoelectric control. *IEEE Trans. Neural Syst. Rehabil. Eng.* 22, 269–279. doi: 10.1109/TNSRE.2014.2305520

Hahne, J. M., Graimann, B., and Muller, K.-R. (2012). Spatial filtering for robust myoelectric control. *IEEE Trans. Biomed. Eng.* 59, 1436–1443. doi: 10.1109/TBME.2012.2188799

Hahne, J. M., Markovic, M., and Farina, D. (2017). User adaptation in myoelectric man-machine interfaces. *Sci. Rep.* 7:4437. doi: 10.1038/s41598-017-04255-x

Hahne, J. M., Schweisfurth, M. A., Koppe, M., and Farina, D. (2018). Simultaneous control of multiple functions of bionic hand prostheses: Performance and robustness in end users. *Sci. Robot.* 3:eaat3630. doi: 10.1126/scirobotics.aat3630

Hanson, W. J. (2008). "Conductive inserts to acquire myoelectric signals through silicone liners," in *Proceedings of the MyoElectric Controls/Powered Prosthetics Symposium*, New Brunswick.

Hussaini, A., and Kyberd, P. (2017). Refined clothespin relocation test and assessment of motion. *Prosthet. Orthot. Int.* 41, 294–302. doi: 10.1177/0309364616660250

Hwang, H. J., Hahne, J. M., and Müller, K. R. (2017). Real-time robustness evaluation of regression based myoelectric control against arm position change and donning/doffing. *PLoS One* 12:e0186318. doi: 10.1371/journal.pone.0186318

Jiang, N., Dosen, S., Muller, K. R., and Farina, D. (2012). "Myoelectric control of artificial limbsis there a need to change focus?," in *Proceedings of the IEEE Signal Processing Magazine*, Piscataway, NJ, doi: 10.1109/MSP.2012.2203480

Jiang, N., Englehart, K. B., and Parker, P. A. (2009). Extracting simultaneous and proportional neural control information for multiple degree of freedom prostheses from the surface electromyographic signal. *Biomed. Eng. IEEE Trans.* 56, 1070–1080. doi: 10.1109/TBME.2008.2007967

Khushaba, R. N., Al-Timemy, A., Kodagoda, S., and Nazarpour, K. (2016). Combined influence of forearm orientation and muscular contraction on EMG pattern recognition. *Expert Syst. Appl.* 61, 154–161. doi: 10.1016/J.ESWA.2016.05.031

Kuiken, T., Miller, L., Turner, K., and Hargrove, L. (2016). A comparison of pattern recognition control and direct control of a multiple degree-of-freedom transradial prosthesis. *IEEE J. Transl. Eng. Heal. Med.* 4, 1–8. doi: 10.1109/JTEHM.2016.2616123

Kyberd, P. J., Murgia, A., Gasson, M., Tjerks, T., Metcalf, C., Chappell, P. H., et al. (2009). Case studies to demonstrate the range of applications of the southampton hand assessment procedure. *Br. J. Occup. Ther.* 72, 212–218. doi: 10.1177/030802260907200506

Light, C. M., Chappell, P. H., and Kyberd, P. J. (2002). Establishing a standardized clinical assessment tool of pathologic and prosthetic hand function: normative data, reliability, and validity. *Arch. Phys. Med. Rehabil.* 83, 776–783. doi: 10.1053/apmr.2002.32737

Mathiowetz, V., Volland, G., Kashman, N., and Weber, K. (1985). Adult norms for the box and block test of manual dexterity. *Am. J. Occup. Ther.* 39, 386–391. doi: 10.5014/ajot.39.6.386

Muzumdar, A. (2004). *Powered Upper Limb Prostheses: Control, Implementation And Clinical Application*. Berlin: Springer.

Oskoei, M. A., and Hu, H. (2007). Myoelectric control systems—a survey. *Biomed. Signal Process. Control* 2, 275–294. doi: 10.1016/j.bspc.2007.07.009

Ottobock (2019). *Ottobock*. Available online at: https://www.ottobock.com/en/press/press-releases/news-detail-page_24962.html (accessed February 28, 2019).

Peerdeman, B., Boere, D., Witteveen, H., Hermens, H., and Stramigioli, S. (2011). Myoelectric forearm prostheses: state of the art from a user-centered perspective. *J. Rehabil. Res. Dev.* 48:719. doi: 10.1682/JRRD.2010.08.0161

Scheme, E., and Englehart, K. (2011). Electromyogram pattern recognition for control of powered upper-limb prostheses: state of the art and challenges for clinical use. *J. Rehabil. Res. Dev.* 48, 643–659.

Vidovic, M. M. C., Hwang, H. J., Amsuss, S., Hahne, J. M., Farina, D., and Muller, K. R. (2016). Improving the robustness of myoelectric pattern recognition for upper limb prostheses by covariate shift adaptation. *IEEE Trans. Neural Syst. Rehabil. Eng.* 24, 961–970. doi: 10.1109/TNSRE.2015.2492619

Young, A. J., Hargrove, L. J., and Kuiken, T. A. (2011). The effects of electrode size and orientation on the sensitivity of myoelectric pattern recognition systems to electrode shift. *IEEE Trans. Biomed. Eng.* 58, 2537–2544. doi: 10.1109/TBME.2011.2159216

Conflict of Interest: MK was employed by company Ottobock SE & Co. KGaA.

The remaining authors declare that the research was conducted in the absence of any commercial or financial relationships that could be construed as a potential conflict of interest.

frontiers in Neuroscience

ORIGINAL RESEARCH
published: 07 July 2020
doi: 10.3389/fnins.2020.00663

Sensory Feedback in Hand Prostheses: A Prospective Study of Everyday Use

Ulrika Wijk[1,2], Ingela K. Carlsson[1,2], Christian Antfolk[3], Anders Björkman[1,2] and Birgitta Rosén[1,2]*

[1] Department of Translational Medicine, Faculty of Medicine, Lund University, Malmö, Sweden, [2] Skåne University Hospital, Lund, Sweden, [3] Department of Biomedical Engineering, Faculty of Engineering, Lund University, Lund, Sweden

OPEN ACCESS

Edited by:
Jacqueline S. Hebert, University of Alberta, Canada

Reviewed by:
Strahinja Dosen, Aalborg University, Denmark
Burak Güçlü, Boğaziçi University, Turkey

****Correspondence:***
Ulrika Wijk
ulrika.wijk@med.lu.se

Specialty section:
This article was submitted to Neuroprosthetics, a section of the journal Frontiers in Neuroscience

Received: *15 October 2019*
Accepted: *29 May 2020*
Published: *07 July 2020*

Citation:
Wijk U, Carlsson IK, Antfolk C, Björkman A and Rosén B (2020) Sensory Feedback in Hand Prostheses: A Prospective Study of Everyday Use. Front. Neurosci. 14:663. doi: 10.3389/fnins.2020.00663

Introduction: Sensory feedback in hand prostheses is lacking but wished for. Many amputees experience a phantom hand map on their residual forearm. When the phantom hand map is touched, it is experienced as touch on the amputated hand. A non-invasive sensory feedback system, applicable to existing hand prostheses, can transfer somatotopical sensory information via phantom hand map. The aim was to evaluate how forearm amputees experienced a non-invasive sensory feedback system used in daily life over a 4-week period.

Methods: This longitudinal cohort study included seven forearm amputees. A non-invasive sensory feedback system was used over 4 weeks. For analysis, a mixed method was used, including quantitative tests (ACMC, proprioceptive pointing task, questionnaire) and interviews. A directed content analysis with predefined categories *sensory feedback from the prosthesis, agency, body ownership, performance in activity,* and *suggestions for improvements* was applied.

Results: The results from interviews showed that sensory feedback was experienced as a feeling of touch which contributed to an experience of completeness. However, the results from the questionnaire showed that the sense of agency and performance remained unchanged or deteriorated. The ability to feel and manipulate small objects was difficult and a stronger feedback was wished for. Phantom pain was alleviated in four out of five patients.

Conclusion: This is the first time a non-invasive sensory feedback system for hand prostheses was implemented in the home environment. The qualitative and quantitative results diverged. The sensory feedback was experienced as a feeling of touch which contributed to a feeling of completeness, linked to body ownership. The qualitative result was not verified in the quantitative measurements.

Clinical Trial Registration: Name: Evaluation of a Non-invasive Sensory Feedback System in Hand Prostheses. Date of registration: March 15, 2019. Date the first participant was enrolled: April 1, 2015. ClinicalTrials.gov Identifier: NCT03876405.
ORCID ID: https://orcid.org/0000-0002-4140-7478.

Keywords: artificial arm, amputation, amputation stumps, sensory feedback, upper limb, traumatic amputation

INTRODUCTION

Amputation of a hand results in the loss of motor and sensory functions, but also changed body balance and self-esteem as well as a feeling of being mutilated (Murray and Forshaw, 2013). Impairments, activity limitations, and participation restrictions (World Health Organization, 2001) can all be consequences of the amputation. In the human hand there is a delicate interaction between motor and sensory functions which is important for good hand function and also for incorporating the hand in the body representation (Gardner and Johnson, 2013). Hand sensibility is crucial for motor performance and motor learning (Kandel et al., 2013). However, to execute a voluntary movement and to learn how to improve performance, several senses can be used. For example, amputees with myoelectric prostheses often use audio information from the motor of the prosthesis to help adjust the grip (Markovic et al., 2018b). Amputees also get some useful sensory information through vibrations in the socket when using the grip (Childress, 1980). An expected advantage of sensory feedback is to make the prosthesis easier to use and improve the body image and thus make social interaction easier (Ackerley and Kavounoudias, 2015). A concept of importance in prosthesis use is the sense of agency, which is the experience of causing a movement generated by motor commands. One way of documenting a sense of agency is by asking if the person had control over the movement (Kalckert and Ehrsson, 2012; Haggard, 2017). Today's prostheses allow the user to feel agency concerning the prosthesis, but the lack of sensory feedback seems to be an important factor limiting the experience of body ownership of the prosthesis (Wijk and Carlsson, 2015).

The need of sensory feedback in prostheses is debated, but several recent studies have found that it is something that prosthesis users desire in their hand prostheses (Pylatiuk et al., 2007; Wijk and Carlsson, 2015; Benz et al., 2016; Farina and Amsuss, 2016), in addition to comfort, function, appearance, and durability (Biddiss et al., 2007; Cordella et al., 2016). Even if the performance in grasping tasks already is good, feedback could be beneficial for complex tasks and for situations when visual feedback is constrained. Regardless of the possible improvement in performance, the subjective experience of embodiment tends to increase when feedback is added (Markovic et al., 2018a). In addition, some studies have reported reduced PLP when sensory feedback is added to a prosthetic hand (Dietrich et al., 2012; Page et al., 2018; Petrini et al., 2018). In recent years researchers have tried to provide sensory feedback in hand prostheses in different ways (Schofield et al., 2014; Svensson et al., 2017; Pasluosta et al., 2018; Stephens-Fripp et al., 2018), using invasive methods, using implanted neural interfaces (Ortiz-Catalan et al., 2014; Oddo et al., 2016; Schiefer et al., 2016; Graczyk et al., 2018; Petrini et al., 2019), and using non-invasive methods through vibrotactile or mechanotactile feedback methods (Hebert et al., 2014; Clemente et al., 2016; Raveh et al., 2018; Schoepp et al., 2018). Studies with sensory prosthetic hands in home use are infrequently presented, but a few case reports are published (Ortiz-Catalan et al., 2014; Clemente et al., 2016; Graczyk et al., 2018; Cuberovic et al., 2019).

Schofield et al. (2014) illustrate three aspects of sensory feedback in hand prostheses. Feedback can be *somatopically matched* (the feedback is perceived as originating from the "correct" body part), *modality matched* (the sub-modality is matched, e.g., pressure is pressure) and *sensory substitution* by input from another sense (e.g., vision, hearing, vibrotactile or electrotactile feedback).

The non-invasive method used here provides somatotopically matched sensory feedback by use of the areas of referred sensation on the residual arm, that is, the PHM. This map of the lost hand and fingers is evoked when touching specific areas of the skin of the residual arm (Ramachandran et al., 1992; Ramachandran and Hirstein, 1998) and in one study was found in a majority of participants with acquired hand amputation at the transradial level (Ehrsson et al., 2008). The PHM is highly individual; some have a very detailed map with several specific areas with referred sensation, while others have a smudged map or only experience few areas of the phantom hand (Bjorkman et al., 2016). When the PHM is stimulated with relevant feedback from the prosthesis, somatotopically matched information can be sent to the brain. Results from a fMRI study showed that stimulation of the finger areas in the PHM on the residual arm activated the same areas in the primary somatosensory cortex as stimulation of the fingers in an able-bodied control group (Bjorkman et al., 2012). Not all amputees experience a PHM (Ehrsson et al., 2008), but touch on predefined areas on the forearm can be learned to be associated to specific fingers (Wijk et al., 2019).

Antfolk et al. (2012, 2013a) have earlier presented a non-invasive sensory feedback concept utilizing the PHM that is also somatotopically matched as well as modality matched, regarding pressure (Antfolk et al., 2012, 2013a). Often prosthetic solutions are tested in a laboratory environment, but the need to evaluate sensory feedback in prostheses in real-life activities has been highlighted (Schofield et al., 2014). The aim of this study was to evaluate how forearm amputees experienced a non-invasive sensory feedback system used in daily life over a 4-week period.

Abbreviations: ACMC, The Assessment of Capacity for Myoelectric Control; EMG, electromyographic; PHM, phantom hand map; PLP, phantom limb pain.

MATERIALS AND METHODS

Sample

Inclusion criteria: acquired unilateral transradial amputation, experiencing a PHM (minimum three finger areas), experience using a myoelectric prosthesis and ability to understand and speak Swedish. Exclusion criteria: psychiatric or cognitive disorders. Seven regional prosthetic centers in Scandinavia were asked to be involved in the recruitment of subjects during 2014–2018, and three centers participated. Nine individuals that met the inclusion criteria were contacted and asked for participation, and of these seven agreed to participate.

Median age was 49 years (range 42–72 years, 3 women and 4 men). Five had an amputation of the dominant side. Time since amputation was at median 13 years (range 1–36 years). Five reported PLP. Five presently used a myoelectric prosthesis (4 myoelectric VariPlus Speed hand; OttoBock and 1 I-limb; Össur). One participant used an AxonHook, OttoBock but had used a myoelectric prosthesis earlier, and 1 had a passive aesthetic prosthesis but had also used a myoelectric prosthesis earlier. The normal prosthesis use was 6–16 h/day, with a median of 11 h/day.

Design

To achieve a broad understanding of the outcome of the intervention, several evaluation and analysis methods were used: qualitative deductive analyses of interviews as well as quantitative measures by use of a questionnaire and objective measurements (method triangulation) (Carter et al., 2014). A longitudinal design was used in a series of cases to illuminate subjective experience and illustrate objective changes over time from use of sensory feedback from a hand prosthesis in daily life.

Experimental Setup

A non-invasive air-mediated sensory feedback system (Antfolk et al., 2012, 2013b) was integrated in a prototype prosthesis glove. The sensory feedback system used was a simple non-invasive, non-electronic system based on air-mediated pressure, described by Antfolk et al. (2012). A silicone glove with bulbs (35 mm in length) volar in every fingertip was made and applied on a single degree-of-freedom prosthetic hand (VariPlus Speed hand, OttoBock), size 73/4. It had no wrist flexibility but manually adjustable wrist rotation. In **Figure 1**, the system is shown as integrated into a silicone glove. The sensing bulbs on the fingers were manually manufactured so there was some variation in their sizes due to manufacturing but also depending on in which finger they were positioned.

The stimulation given was mechanotactile and the pressure was transferred from the silicon bulbs in the fingertips of the prosthesis via plastic tubes that reached actuators (silicon bulbs 13 mm in diameter) inside the prosthetic socket. The pressure applied to the skin from the silicon bulbs depends on the force and speed at the fingertip level (Antfolk et al., 2012). The sensing bulb was roughly a half-cylinder with diameter 20 mm and length 35 mm. This gives a volume of roughly 5500 mm^3 or 5.5 ml. The tubes were pneumatic tubes from FESTO (PUN-3 × 0.5 SI, FESTO, Esslingen am Neckar, Germany) with an inner diameter of 2.1 mm. In our previous paper (Antfolk et al., 2012), we measured the pressure generated by the sensing bulb using a pressure sensor when a monofilament was pressed against the sensing bulb. For a 60 g monofilament a pressure of 1.2 kPa was recorded, for a 100 g monofilament 2.3 kPa, 180 g monofilament 4.3 kPa, 300 g monofilament 6.5 kPa. More details on the sensing bulbs can be found in Svensson et al. (2020).

Other factors of importance for receiving the pressure are the quality of the skin (e.g., scarring) and damaged skin was avoided. The actuators were applied to the skin corresponding with the PHM areas (**Figure 1**).

Thus, it was possible to transfer both a modality matched and somatotopically matched feedback.

At the first meeting a "mapping" of the areas of the referred sensations in the residual forearm was done. The participants were asked to touch the skin on the residual forearm and define the zones with referred sensation of the PHM (digit I–V). The PHM was then marked with a pen, and the participant confirmed the mapping by blindly responding to stimulation of the different areas by the experimenter.

A casting for the prosthetic socket was made and the marks of the PHM were transferred to the inside of the socket. A socket with the sensory feedback system embedded was then constructed. When the participants were equipped with the prosthesis they were asked to orally confirm that the pressure was perceived, and somatotopically matched the PHM.

This was made through pressing the fingertips of the prosthetic hand. No structured training of the prosthetic hand or the sensory feedback was given.

The participants were asked to use the prosthesis at home for at least 2 h/day, 5 days/week over 4 weeks.

Subjective Experiences From Questionnaire and Interviews

A questionnaire consisting of 21 statements concerning sensory feedback from the prosthesis, agency, body ownership, performance in activity, and PLP was developed by the first and last author. The questionnaire was based on the ones used in experiments of rubber hand illusion (Botvinick and Cohen, 1998; Ehrsson et al., 2008). In the questionnaire, the participants were asked to match each statement on a 7-level Likert scale from "Strongly disagree" (—) to "Strongly agree" (+++) (Botvinick and Cohen, 1998). Six control statements were included in the questionnaire, not related to the construct, aiming to capture suggestibility and task compliance.

After the test period, the first author carried out semi-structured interviews with open-ended questions. All participants were asked to describe the activities in which they used the prosthesis and how they experienced it, if and why they chose not to wear the prosthesis during some activities, the

FIGURE 1 | When the silicon bulbs in the fingertips were pressed, the air was transferred via plastic tubes that reached actuators inside the prosthetic socket and gave pressure (mechanotactile feedback) on the skin corresponding with the PHM zones.

experiences of the sensory feedback from the prosthesis, agency and body ownership, and their suggestions for improving the feedback or the design of the prosthesis.

During the test period the participants were asked to keep a diary where they documented the time, activity, and place of wearing the prosthesis.

Objective Outcome

Function/capacity was assessed with The Assessment of Capacity for Myoelectric Control (ACMC). This is a standardized observational assessment which rates the subjects' capacity of myoelectric control in a bimanual activity, either standardized (such as "packing a suitcase for overnight stay," "repotting a plant," or "setting a table for four persons") or self-chosen. The ACMC consists of 22 items and a 4-grade rating scale (0 = Not capable, 1 = Somewhat capable, 2 = Generally capable, 3 = Extremely capable). The ACMC units are calculated on the ACMC website, converted to interval-level linear measures by using the Rasch measurement analysis, and reported in a range of 0–100. The higher the score, the better the task performance[1] (Lindner et al., 2009, 2014). In this study, the activity "to make a sandwich with toppings" was chosen by the authors. Actions included in the task are to take a bun from a bag, split it in two halves, spread butter on both halves, put cheese and ham, from a closed package, on the bread. Thereafter slice a tomato and cucumber and put on top. Wrap the sandwich in paper and clean up the table. The scoring was made by an experienced external rater (occupational therapist, certified ACMC-rater). The ACMC was performed without sensory feedback in the pre-tests and with sensory feedback at the follow up.

Body ownership was assessed with the proprioceptive pointing task (Botvinick and Cohen, 1998; Rohde et al., 2011). The participants were asked to mark on a ruler (proximally to distally from their own body) with their index finger on the other hand and their eyes closed, where they estimated the location of the prosthetic index finger and where they experienced their phantom index finger (**Figure 2**).

The order in which the data collection was performed: Questionnaire, ACMC without feedback, proprioceptive pointing task, using the prosthesis with sensory feedback at home (4 weeks), questionnaire, ACMC with sensory feedback, proprioceptive pointing task, and interview. The tests were applied in one session before the test period and in one session for follow up, except for the interview that was only done at the follow up.

Analysis

The interviews were transcribed by the first author and analyzed independently by the first and second authors (investigator triangulation) in a directed qualitative content analysis (Patton, 1999; Hsieh and Shannon, 2005) and according to the procedure described by Graneheim and Lundman (2004). The text was read and reread in order to obtain a sense of the entire data. Meaning units, that is, words or sentences related to the aim of the study, were then identified and thereafter coded while still preserving the core meaning (**Table 1**). Codes were then grouped into categories according to predefined concepts. The categories were then discussed with the other authors and adjustments were made to reach consensus.

Regarding the authors' preunderstanding, the first and second authors are occupational therapists with previous experience in qualitative research (Carlsson et al., 2010; Wijk and Carlsson, 2015). The third author is a researcher in biomedical engineering at the Department of Biomedical Engineering and has a long experience of research in the field of prosthetic hands; the fourth author is a hand surgeon; and the last author an occupational therapist. All authors except the third work at the Hand Surgery Department in Malmö, Sweden, and have long clinical experience (Graneheim and Lundman, 2004).

The quantitative results were analyzed and presented descriptively, added with Wilcoxon signed rank test to compare differences in pretests and follow-up regarding Questionnaire, ACMC, and Proprioceptive Pointing task. Results from the questionnaire were analyzed in the categories to predefined concepts (**Table 2**: sensory feedback, agency, body ownership, performance in activity, phantom limb pain). Graphpad Prism version 8.2.1 was used for calculation.

RESULTS

The reported time the prosthesis with the sensory feedback system was used was 2–15 h/day. The wearing time for individual 1 to 7 was: 2–15 h, 2–3 h, 2 h, 2–5 h, 2 h, 2–4 h, 2–3 h, respectively. Since the wearing time were around 2–3 h for the majority of participants, no conclusions could be drawn regarding prosthesis use in relation to user experience or performance.

Subjective Experiences

Questionnaire

The responses in the questionnaire varied a lot among the participants, and also among the questions (**Figure 3**). Four out of seven participants experienced less agency compared to when using their normal prosthesis. There was a significant negative change regarding Agency [pre/post median 2 and 0 ($p = 0.023$)], and Performance in activity [pre/post median 1 and 0 ($p = 0.007$)], but there was a significant improvement regarding Sensory feedback (pre/post median −1 and 0 [$p = 0.031$]). Four of the five individuals with PLP reported a decrease of pain when using the sensory feedback prosthesis (pre/post median −2 and 0.5) but the change was not significant (**Figure 3**). One reported an increase of pain and associated it with the tight socket fit of the prosthesis. The six control questions were visually analyzed and all answers were on the far disagree-side of the scale, diverged from the rest of the answers, and filled their purpose and was removed prior analysis.

Directed Content Analysis

Sensory feedback from the prosthesis

The air-mediated system gave a sensory feedback when the fingertips of the prosthesis were compressed and at the same time the corresponding area of the PHM was stimulated by pressure. Someone described it as a tingling feeling. However, the feedback was experienced as too weak and it was difficult to feel small objects with the fingertips. A distinct change in the pressure, as when grasping or releasing, was needed for the user to notice the feedback. When using the prosthesis in heavy manual work, the experience from the feedback vanished, but when releasing the grip the change in pressure was noticed. The feedback seemed

[1] http://acmc.se/

FIGURE 2 | In the Proprioceptive pointing task the participants were asked, with their eyes closed, to mark on a ruler (proximally to distally from their own body) with their index finger on the sound hand, where they estimated the location of: (1) the prosthetic index finger and (2) where they experienced their phantom index finger.

TABLE 1 | Example from the condensation in the directed content analysis.

Meaning unit	Code	Category
"When you grasp with it and feel that you grasp. It's a fantastic feeling!"	Feel the grasp	Sensory feedback from the prosthesis

TABLE 2 | Individual questions included in questionnaire and grouped according to concept.

Sensory feedback (SF)	SF1: "When I grip something it feels like I grasp it with my real fingers." SF2: When I grip objects, I can feel the touch in the fingers of the prosthesis."
Agency (AG)	AG1: "It feels like I control the movement of the prosthesis." AG2: "The prosthesis moves like I want it to, like I am controlling it with my will."
Body ownership (BO)	BO1: "It feels like the prosthesis is my hand." BO2: "It feels like the prosthesis is a part of my body." BO3: "It feels like the phantom hand is inside the prosthetic hand."
Performance in activity (PIA)	PIA1: "I can use the prosthesis without looking." PIA2: "I can put away a plastic cup without looking." PIA3: "I can control the grip of the prosthesis." PIA4: "I even feel that I can hold a small child with the prosthesis." PIA5: "I feel that I can control how hard I hold something." PIA6: "The prosthesis feels like a tool."
Phantom limb pain (PLP)	PLP1: "I have phantom limb pain when wearing the prosthesis." PLP2: "I have phantom limb pain when not wearing the prosthesis."
Control questions	"It feels like the prosthesis controls my movements." "My (real) arm feels rubbery when I wear the prosthesis." "It feels like the prosthesis has its own will." "My (real) arm feels like a robot when I use the prosthesis." "Sometimes I perceive a feeling of touch somewhere outside the prosthesis." "When I grip objects with the prosthesis, it feels like the feeling of touch is projected toward my upper arm and/or chest."

to be dependent on which activity the prosthesis was used in, and the feedback could disappear due to other disturbing impressions that come with the use of a myoelectric prosthesis, and was easily disturbed by muscle activity. One of the participants found it hard to feel the feedback at all, possibly due to scarring on the stump. It was expressed that the more the prosthesis was used, the better the feedback. A nice feeling as "scratching" the fingers could be experienced when pressing the bubbles of the prosthesis fingers. The feedback was perceived as the pressure really stimulated the corresponding finger. The feedback was distinct when touching the prosthetic fingertips with the other fingers on their own hand, in contrast to when using the

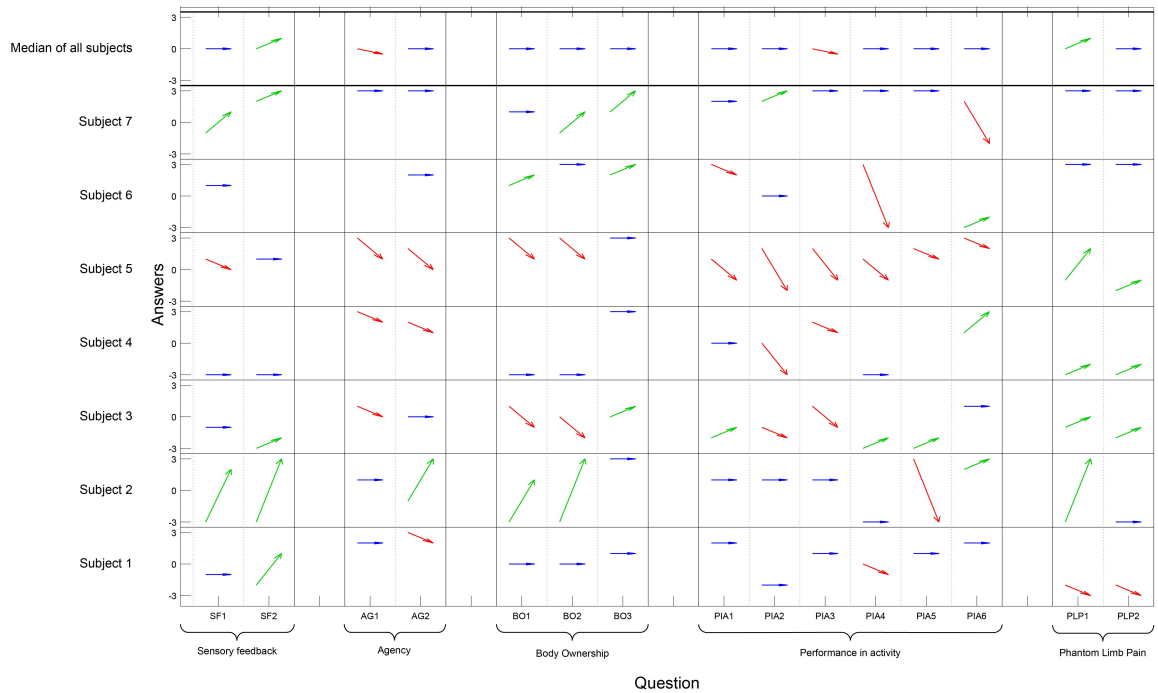

FIGURE 3 | On the *x*-axis each question has a column and the questions are grouped according to concept. The *y*-axis presents each participant and the Likert scale. The answers pre- and post- are illustrated with an arrow for each question and participant; an improvement is illustrated by a green arrow, an impairment by a red arrow, and if there was no change the arrow is blue (Question PLP1–PLP2 for homogeneity in the table, a high value [3] indicates less pain). The six control questions are not presented in the figure. Wilcoxon signed rank test showed a significant positive change regarding Sensory feedback ($p = 0.031$), a significant negative change regarding Agency ($p = 0.023$), and Performance in Activity ($p = 0.007$). No significant changes were seen in the other concept categories in the questionnaire.

prosthesis actively. A kind of feedback was experienced also in the regular prosthesis, e.g., vibrations in the socket when using the prosthesis. When comparing this to the sensory feedback in the test prosthesis it was described as a completely different feeling. The feedback from the test prosthesis was more like a real sensational experience which could be surprising. Even if the sensation was weak and not beneficial for practical use the experience of sensory feedback from the prosthesis was strongly expressed as feeling the touch in the prosthetic finger. They very much appreciated feeling the feedback, and it was also expressed that the experience of the sensory feedback was so good that it was desired in the regular prosthesis.

> *"When touching the bubbles (fingertips) I got full feedback from all of them, when I don't have any other load on the arm. When I sit in a relaxed position, then it is very distinct."* (Id 7)

> *"It is this. . .feeling, when I grasp something it really feels like I grasp it!"* (Id 2)

> *"I have really bad sensibility on the stump and a lot of scars, so it was difficult to feel the feedback."* (Id 4)

Agency

The feeling of agency was expressed in different terms. The participants expressed that even though they liked the sensory feedback, the feeling of agency did not change much; they controlled the prosthesis as they normally did. For better grip control a stronger feedback was desired. The experience of agency with the regular prosthesis was compared with wearing a thick oven glove, to be able to control the movement but lack the normal sensibility.

> *"I like the feeling. When there is a sensory response the movement is more natural."* (Id 3)

> *"If the feedback would have been stronger I may have had more utility regarding controlling the grip."* (Id 6)

Body ownership

It was expressed that the sensory feedback contributed to a strong feeling of completeness. The prosthesis felt like a part of them and this was a really pleasant feeling. It was described in quite an abstract way as if they could feel something that did not exist but which was still strongly linked to them. The prosthesis with feedback was used in situations when participants would not normally wear a prosthesis and when it was not used actively. To enjoy the feeling of touch from the prosthetic hand the participants touched the prosthesis with the other hand when relaxing, e.g., when watching TV. It was expressed that the connection to the test prosthesis became stronger because of the feeling of touch and that was a reason for wearing the prosthesis for a longer time than required.

> *"It is a big feeling. I feel complete!"* (Id 2)

". . .it feels more like a part of me. I don't know how to express it, but it feels good!" (Id 7)

Performance in activity

The participants reported that they used the prosthesis when performing normal tasks, e.g., at work, the gym, and at home. They did everything they usually did with their regular prosthesis, such as working at the computer, cooking, cleaning, shopping, gardening, driving, biking, etc. Someone mentioned that the prosthesis was removed in heavy activities due to the risk of damaging and puncturing the silicon bubbles, e.g., when carrying heavy things, or at the gym. In this prototype prosthesis, the design was a hinder in some situations, e.g., it was hard to handle small nuts and to hold cutlery because of the soft bubbles/sensors on the fingertips of the prosthesis.

"The sensory feedback has not helped me so much in the practical performance, so to speak, but I have a feeling. . ." (Id 6)

"I cannot feel small objects." (Id 1)

Suggestions for improvements

The participants felt that the sensory feedback needs to be improved. The feedback was not strong enough to be detected during muscle contractions when controlling the electrodes of the myoelectric function, and the feedback was too weak in active grips but sufficient when touching the fingers passively. The prototype prosthesis was experienced as clumsier than their normal prosthesis. Smaller bubbles on the fingertips were suggested, to give a more precise feedback when handling small objects, but also to enable a more distinct grip. The bubbles were considered too soft and it was hard to hold small objects and use force simultaneously. It was also noted that for the feeling of pleasantness from the touch of all fingers, the fingers should be represented separately. For grasping control the feedback areas might be larger. The appearance of the prototype prosthesis was not satisfactory. The bubbles/sensors on the fingertips looked oversized and the air-tubes were visual on the dorsal side of the prototype prosthetic hand. Some of the participants were not confident being around people with the prosthesis on and wore it only at home because of its appearance. An improvement of the aesthetics was therefore requested.

"I want a more defined pressure, not so fuzzy. It is a soft feeling and it is too slow. I want more of an impact, something more distinct." (Id 5)

"The air bulbs might be developed a bit, in terms of getting stronger feedback in the grip. (Id 6)

Objective Results

The objective outcomes were analyzed descriptively. The ACMC showed a median score of 65.8 (range 45.4 – 100) in pre-tests and 68.5 (range 38.1 – 100) at follow-up (**Figure 4**.). Three individuals showed no change (1, 2, 7); three individuals had a worsened performance (3, 5, 6); and only one individual showed an improved performance. The Proprioceptive pointing task (**Figure 2**) when the participants were asked to mark on a ruler where they estimate the prosthetic index finger was at median deviation of 1.5 cm (range −10 – 4) in pre-test and −2 (range −9.5 – 1) at follow-up. When marking where they experienced their phantom index finger the distance relative to the prosthetic index finger was −14 cm (range −20 – −5) proximal to the prosthetic index finger in pre-tests and −13.5 (range −17.5 – 3) proximal to the prosthetic index finger at follow-up. The Wilcoxon signed rank test showed no differences between pretests and follow-up (not significant) regarding ACMC and Proprioceptive pointing task.

DISCUSSION

The use of a non-invasive sensory feedback system in daily activities over 4 weeks resulted in positive subjective experiences linked to body ownership and experiences of sensory feedback from the prosthesis, but did not improve the performance with the prosthesis as rated by the ACMC and self-rated performance on the questionnaire. Three participants showed unchanged performance, three showed deteriorated performance, and one showed improved performance.

To achieve a broad understanding of the evaluation of the prosthesis with sensory feedback, multiple methods were used. Qualitative analyses of interviews were performed as well as quantitative measures by use of a questionnaire and objective measurements, so-called method triangulation. In the analysis and report of results, as in the conclusions drawn, equal focus was on both the quantitative and the qualitative results. In the interviews, it was expressed that the sensory feedback was experienced as real touch which contributed to a feeling of completeness, linked to body ownership of the prosthesis. However, the quantitative results did not verify the qualitative results regarding body ownership. Either there were no changes or the quantitative measurements were not responsive enough to measure change over time. Another explanation may be that when people express their thoughts more freely as in the interview situation, a subtler in-depth answer is achieved which can be difficult to capture in a questionnaire. We cannot say which of the quantitative or the qualitative results have the most impact (Murray, 2009). According to Patton (1999), it should be expected to come to assorted results when using method triangulation. Instead, when qualitative and quantitative measures are used together, it can emphasize the result from different perspectives.

The experience that our limbs actually are a part of our own body is a feeling that is generated by sensory and visual feedback (Tsakiris et al., 2007). The non-invasive sensory feedback could promote the integration of the hand prosthesis in the bodily self and enhance the acceptance of the prosthesis. When acceptance is high, this may also affect the performance in a positive way (D'Alonzo et al., 2015; Imaizumi et al., 2016; Beckerle et al., 2018). Markovic et al. (2018a) show that regardless of improvement in performance the participants reported a positive experience of the feedback and rated an increased embodiment of the prosthesis (Markovic et al., 2018a). In our study, it was expressed in the interviews that the prosthesis was worn also in situations when not using it in practice, as when watching a movie, just because of the pleasantness of experiencing the touch through

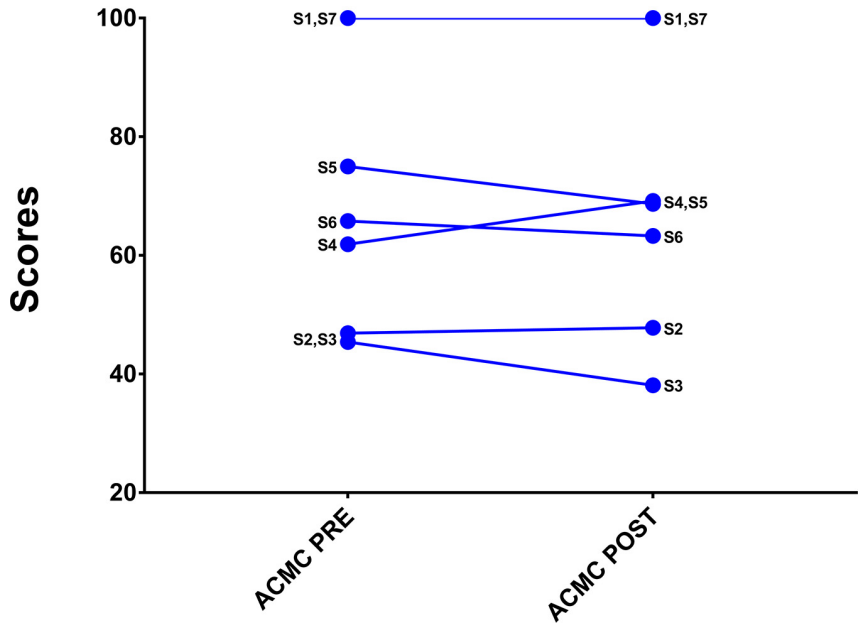

FIGURE 4 | The ACMC-scores for each participant at pre-tests and follow-up.

the prosthesis. If the prosthesis was used and experienced only as a tool one would assume that the prosthesis would be taken off in such situations. The qualitative positive experience of body ownership of the prosthesis due to the sensory feedback was the most important result. In previous studies using the rubber hand illusion experimental setup (Botvinick and Cohen, 1998), amputees experienced a hand prosthesis with a robotic appearance like a part of their own body (Ehrsson et al., 2008).

Phantom limb pain was alleviated in four of the five participants with PLP in our study, and reported that the sensory feedback affected PLP in a positive way in the questionnaire. Similar results have earlier been reported with significantly decreased PLP when sensory feedback is added to a prosthetic hand (Dietrich et al., 2012; Page et al., 2018; Petrini et al., 2018). Restored balance between afferent and efferent signaling, which is the case when sensory feedback is present in a hand prosthesis, can be one explanation (Flor et al., 2006; Vaso et al., 2014). However, the effect on PLP should be further investigated.

It has been suggested that sensory feedback could improve the functioning and performance with prostheses. This hypothesis is based on the knowledge of the importance of sensibility for motor function and the ability to use one's hands (Gardner and Johnson, 2013). However, the importance of sensory feedback in hand prostheses is debated. Some studies support the hypothesis and have shown improved control of grasping force when sensory feedback is added (Witteveen et al., 2015; Clemente et al., 2016). On the other hand, Markovic et al. (2018a) showed, in a recent study, that sensory feedback was beneficial only when it came to complex tasks such as relocating clothespins and turning blocks. In simpler tasks, such as the "Box and Block Task," the sensory feedback was not that important for performance. When naive prosthesis users (able-bodied) learned to control a myoelectric prosthesis, they showed relative good skills also without added feedback, just learning the muscle control needed for controlling the EMG-electrodes. However, when adding feedback sources, such as sound and vision, there was an improvement of the control (Markovic et al., 2018b). Similar results were shown in amputees, where task performance improved only by learning motor control. However, when vibrotactile feedback was added, task performance was further improved especially in complex tasks (Markovic et al., 2018a). Our results, however, suggest that sensory feedback does not improve the performance in the chosen activities. The worse performance that was experienced in some cases was probably due to changed socket fitting, the adjustment of the EMG electrodes, or bulky bulbs in the prosthetic fingertips. These changes may have altered the reliability of the prosthesis. The participants in our study were experienced prosthesis users, and they had over several years learned how to control their own prosthetic hand, probably relying on several sources of feedback such as vision, hearing, and proprioception (Wijk and Carlsson, 2015). Another possibility could be too weak feedback that was "masked" in muscle contractions.

The participants expressed that the best quality of the sensory feedback was achieved when they touched the prosthesis' fingers themselves. They thought it was pleasant, comfortable, or even fantastic to touch the prosthesis. They felt the touch as if it was their own fingers being touched, even if it was a single modality feedback. It was during these moments the feeling of ownership could occur or the attachment to the prosthesis became stronger.

Beckerle et al. (2018) discusses three aspects of touch: social, affective, and self-touch. They highlight the concept of self-touch because of its importance for both establishing representation of our bodies as infants and for maintaining this representation throughout life (Bremner and Spence, 2017). Self-touch is also significant for the experience of body ownership (Hara et al., 2015; Beckerle et al., 2018), and in our study the participants' expressions confirms that.

The sensory feedback system used in this study is a simple and low-tech concept, but still both modality and somatotopically matched. However, the prototype system has potential for improvement. The feedback should be stronger or adjustable for each individual, which could be possible if the system used electric pressure sensors and, for example, electric motors as feedback actuators, which means that the feedback can be adjusted individually. The benefit of our system is that it is integrated in the prosthesis glove and the socket, and that it is not dependent on the type of prosthesis. The location of sensors in the glove was individualized in our study based on which fingers were represented in the PHM. In future versions, the prosthesis glove can be further developed for each individual and with desired location of both sensors and actuators, by making the system flexible. It can be applied to different types of prostheses and since the system is air-mediated and not dependent on the prosthesis design it is also suitable for, for example, body-powered or cosmetic prostheses. In a myoelectric prosthesis, there may be advances regarding practical use and the feeling of grip control, but as our result shows the sensory feedback has importance in emotional dimensions, thus regardless of the type of prosthesis. Another point that needs to be taken into account in the development of hand prostheses is the robustness and reliability to the prosthesis. If a prosthetic hand often breaks, or needs frequent and extensive service, it may be considered too much bother and end in rejection.

Methodological Considerations

The system was integrated in a glove and a socket, not bigger than their respective size in a regular myoelectric hand prosthesis. Evaluation was made in everyday life with focus on activity in an environment that was relevant and meaningful for every participant. It includes complex tasks in an uncontrolled environment where the participant may not have complete focus on the prosthesis and the feedback. Most research in the area of sensory feedback is made in a laboratory environment, where tests and most evaluations are standardized into a few simple grip tests (Clemente et al., 2016; Schiefer et al., 2018; Mastinu et al., 2019). The prosthesis used in this study is still at a prototype stage, with cables on the outside, and because of that some participants experienced the prosthesis as less cosmetically appealing and chose to use it only at home. On the other hand, some of the seven participants used it full days, including at work, in sports activities, and domestics. We did not have control over the time when the prosthesis was used, or what the participants did when wearing the prosthesis; instead we had to rely on the information given. Maybe wearing the prosthesis 2 h/day, which was suggested as minimum, in the 4-week test period is not enough to change behavior and capacity in experienced users.

Minor discrepancies in the adjustment of the sensitivity of the EMG-electrodes in the new socket that was provided for the study could also affect the skillfulness. If the new socket of the test-prosthesis did not feel exactly like the regular one, this could be a disturbance in the use and performance with the prosthesis or even a pain trigger.

The studied group was small and heterogeneous. Almost all the participants were skilled prosthesis users, some of them for decades. If one has used a myoelectric prosthesis for several hours a day for many years, the capacity of controlling the grip and grasping of the prosthesis is very good. Markovic et al. (2018a) also claim that the feedback is not as important for experienced prosthesis users as for novel users. Regarding the qualitative analyses the low number of participants may also limit the possibility to achieve saturation of data. However, a low number of participants is a frequent problem in this research area, due to a low number of cases with transradial amputation and meeting the specific inclusion criteria.

All the interviews were carried out by the first author. Some of the participants had met the interviewer also at the clinic as a patient, which may have influenced the interview situation and affected the dependability of the results. It could be inhibitory for the respondents, but it may even deepen the interview and the narratives being shared.

To check for trustworthiness, specifically dependability, the first author and one co-author read and coded the interviews independently and by in-depth analysis and discussion interpreted the text together (investigator triangulation) (Patton, 1999; Carter et al., 2014). The trustworthiness was also achieved by including representative quotations from the participants, making the interpretation transparent for the reader. Constant confirming and clarifying information during the interviews assured confirmability. The focus was consistently on the text to reduce the risk of over-interpretation. Transferability is limited but a thorough description of the participants and the study context is presented (Graneheim and Lundman, 2004).

CONCLUSION

The participants expressed that this non-invasive, somatotopically and modality matched sensory feedback system has positive qualities regarding feeling of body ownership and experienced sensory feedback from the prosthesis. In addition, it may alleviate phantom pain. However, performance with the prosthesis was not improved. The positive experience of the sensory feedback was highly expressed, and the users felt complete while wearing the prosthesis. The technical solution presented here has to be seen as a prototype with potential for improvements. The aesthetics need to be better so it can be used without shyness in social contexts. The silicon bulbs (sensors) on the fingertips were quite large which made them bulky in fine manipulation. Participants wished for a stronger or more distinct pressure, which should be taken into account in further development of the actuators. The silicon bulbs were

also in some situations experienced as too soft, making it hard to hold small objects, or to get a distinct grip. It is of outmost importance to have close communication with the users in future developmental work.

IMPLICATIONS FOR REHABILITATION

1. The positive (qualitative) experience of body ownership of the prosthesis due to the sensory feedback was the most important result.
2. The participants expressed that the best quality of the sensory feedback was achieved when they touched the prosthesis' fingers themselves.
3. There is a need to evaluate different features of hand prosthesis, and it is of importance to do it close to the users in a meaningful environment.
4. The phantom hand map (PHM) offers a possibility to transfer sensory, non-invasively, information from the prosthesis to the user.

DATA AVAILABILITY STATEMENT

The datasets generated for this study are available on request to the corresponding author.

ETHICS STATEMENT

The studies involving human participants were reviewed and approved by Regional Ethics Review Board in Lund, Sweden. The patients/participants provided their written informed consent to participate in this study.

AUTHOR CONTRIBUTIONS

BR, UW, AB, and CA participated in the design of the study. UW conducted the interviews and the tests. UW and IC read and analyzed the data from the interviews. The content in the predefined categories were then confirmed by all co-authors. UW, CA, and BR analyzed the data from the self-report questionnaire and objective data. UW wrote the manuscript. IC, CA, AB, and BR revised and approved the manuscript. All authors contributed to the article and approved the submitted version.

FUNDING

This work was supported by grants from the County Council of Skåne and the Healthcare Academy at Skåne University Hospital, Sweden.

ACKNOWLEDGMENTS

The authors want to thank all participants that took part of the study and shared their experiences. They also wish to thank Anita Stockselius and Winnie Jensen for recruiting participants and to Lis Sjöberg for the ACMC-scoring. Thanks to Jan-Åke Nilsson for methodological and statistical discussions.

REFERENCES

Ackerley, R., and Kavounoudias, A. (2015). The role of tactile afference in shaping motor behaviour and implications for prosthetic innovation. *Neuropsychologia* 79(Pt B), 192–205. doi: 10.1016/j.neuropsychologia.2015.06.024

Antfolk, C., Bjorkman, A., Frank, S. O., Sebelius, F., Lundborg, G., and Rosen, B. (2012). Sensory feedback from a prosthetic hand based on air-mediated pressure from the hand to the forearm skin. *J. Rehabil. Med.* 44, 702–707.

Antfolk, C., Cipriani, C., Carrozza, M. C., Balkenius, C., Bjorkman, A., Lundborg, G., et al. (2013a). Transfer of tactile input from an artificial hand to the forearm: experiments in amputees and able-bodied volunteers. *Disabil. Rehabil. Assist. Technol.* 8, 249–254. doi: 10.3109/17483107.2012.713435

Antfolk, C., D'Alonzo, M., Controzzi, M., Lundborg, G., Rosen, B., Sebelius, F., et al. (2013b). Artificial redirection of sensation from prosthetic fingers to the phantom hand map on transradial amputees: vibrotactile versus mechanotactile sensory feedback. *IEEE Trans. Neural Syst. Rehabil. Eng.* 21, 112–120. doi: 10.1109/TNSRE.2012.2217989

Beckerle, P., Kõiva, R., Kirchner, E. A., Bekrater-Bodmann, R., Dosen, S., Christ, O., et al. (2018). Feel-good robotics: requirements on touch for embodiment in assistive robotics. *Front. Neurorobot.* 12:84. doi: 10.3389/fnbot.2018.00084

Benz, H. L., Jia, Y., Rose, L., Olgac, O., Kreutz, K., Saha, A., et al. (2016). Upper extremity prosthesis user perspectives on unmet needs and innovative technology. *Conf. Proc. IEEE Eng. Med. Biol. Soc.* 2016, 287–290. doi: 10.1109/embc.2016.7590696

Biddiss, E., Beaton, D., and Chau, T. (2007). Consumer design priorities for upper limb prosthetics. *Disabil. Rehabil. Assist. Technol.* 2, 346–357. doi: 10.1080/17483100701714733

Bjorkman, A., Weibull, A., Olsrud, J., Ehrsson, H. H., Rosen, B., and Bjorkman-Burtscher, I. M. (2012). Phantom digit somatotopy: a functional magnetic resonance imaging study in forearm amputees. *Eur. J. Neurosci.* 36, 2098–2106. doi: 10.1111/j.1460-9568.2012.08099.x

Bjorkman, A., Wijk, U., Antfolk, C., Bjorkman-Burtscher, I., and Rosen, B. (2016). Sensory qualities of the phantom hand map in the residual forearm of amputees. *J. Rehabil. Med.* 48, 365–370.

Botvinick, M., and Cohen, J. (1998). Rubber hands 'feel' touch that eyes see. *Nature* 391:756. doi: 10.1038/35784

Bremner, A. J., and Spence, C. (2017). The development of tactile perception. *Adv. Child Dev. Behav.* 52, 227–268. doi: 10.1016/bs.acdb.2016.12.002

Carlsson, I. K., Edberg, A. K., and Wann-Hansson, C. (2010). Hand-injured patients' experiences of cold sensitivity and the consequences and adaptation for daily life: a qualitative study. *J. Hand Ther.* 23, 53–61; quiz 62. doi: 10.1016/j.jht.2009.07.008

Carter, N., Bryant-Lukosius, D., DiCenso, A., Blythe, J., and Neville, A. J. (2014). The use of triangulation in qualitative research. *Oncol. Nurs. Forum* 41, 545–547.

Childress, D. S. (1980). Closed-loop control in prosthetic systems: historical perspective. *Ann. Biomed. Eng.* 8, 293–303.

Clemente, F., D'Alonzo, M., Controzzi, M., Edin, B. B., and Cipriani, C. (2016). Non-invasive, temporally discrete feedback of object contact and release improves grasp control of closed-loop myoelectric transradial prostheses. *IEEE Trans. Neural Syst. Rehabil. Eng.* 24, 1314–1322. doi: 10.1109/tnsre.2015.2500586

Cordella, F., Ciancio, A. L., Sacchetti, R., Davalli, A., Cutti, A. G., Guglielmelli, E., et al. (2016). Literature review on needs of upper limb prosthesis users. *Front. Neurosci.* 10:209. doi: 10.3389/fnins.2016.00209

Cuberovic, I., Gill, A., Resnik, L. J., Tyler, D. J., and Graczyk, E. L. (2019). Learning of artificial sensation through long-term home use of a sensory-enabled prosthesis. *Front. Neurosci.* 13:853. doi: 10.3389/fnins.2019.00853

D'Alonzo, M., Clemente, F., and Cipriani, C. (2015). Vibrotactile stimulation promotes embodiment of an alien hand in amputees with phantom sensations. *IEEE Trans. Neural Syst. Rehabil. Eng.* 23, 450–457. doi: 10.1109/tnsre.2014.2337952

Dietrich, C., Walter-Walsh, K., Preissler, S., Hofmann, G. O., Witte, O. W., Miltner, W. H., et al. (2012). Sensory feedback prosthesis reduces phantom limb pain: proof of a principle. *Neurosci. Lett.* 507, 97–100. doi: 10.1016/j.neulet.2011.10.068

Ehrsson, H. H., Rosen, B., Stockselius, A., Ragno, C., Kohler, P., and Lundborg, G. (2008). Upper limb amputees can be induced to experience a rubber hand as their own. *Brain* 131(Pt 12), 3443–3452. doi: 10.1093/brain/awn297

Farina, D., and Amsuss, S. (2016). Reflections on the present and future of upper limb prostheses. *Expert Rev. Med. Devices* 13, 321–324. doi: 10.1586/17434440.2016.1159511

Flor, H., Nikolajsen, L., and Staehelin Jensen, T. (2006). Phantom limb pain: a case of maladaptive CNS plasticity? *Nat. Rev. Neurosci.* 7, 873–881. doi: 10.1038/nrn1991

Gardner, E., and Johnson, K. (2013). "Touch," in *Principles of Neural Science*, 5th Edn, eds E. Kandel, S. JH, T. Jessel, S. Siegelbaum, and A. Hudspeth (New York, NY: McGraw Hill Medical), 498–529.

Graczyk, E. L., Resnik, L., Schiefer, M. A., Schmitt, M. S., and Tyler, D. J. (2018). Home use of a neural-connected sensory prosthesis provides the functional and psychosocial experience of having a hand again. *Sci. Rep.* 8:9866. doi: 10.1038/s41598-018-26952-x

Graneheim, U. H., and Lundman, B. (2004). Qualitative content analysis in nursing research: concepts, procedures and measures to achieve trustworthiness. *Nurse Educ. Today* 24, 105–112. doi: 10.1016/j.nedt.2003.10.001

Haggard, P. (2017). Sense of agency in the human brain. *Nat. Rev. Neurosci.* 18, 196–207. doi: 10.1038/nrn.2017.14

Hara, M., Pozeg, P., Rognini, G., Higuchi, T., Fukuhara, K., Yamamoto, A., et al. (2015). Voluntary self-touch increases body ownership. *Front. Psychol.* 6:1509. doi: 10.3389/fpsyg.2015.01509

Hebert, J. S., Olson, J. L., Morhart, M. J., Dawson, M. R., Marasco, P. D., Kuiken, T. A., et al. (2014). Novel targeted sensory reinnervation technique to restore functional hand sensation after transhumeral amputation. *IEEE Trans. Neural Syst. Rehabil. Eng.* 22, 765–773. doi: 10.1109/tnsre.2013.2294907

Hsieh, H., and Shannon, S. E. (2005). Three approaches to qualitative content analysis. *Qual. Health Res.* 15, 1277–1288.

Imaizumi, S., Asai, T., and Koyama, S. (2016). Embodied prosthetic arm stabilizes body posture, while unembodied one perturbs it. *Conscious. Cogn.* 45, 75–88. doi: 10.1016/j.concog.2016.08.019

Kalckert, A., and Ehrsson, H. H. (2012). Moving a rubber hand that feels like your own: a dissociation of ownership and agency. *Front. Hum. Neurosci.* 6:40. doi: 10.3389/fnhum.2012.00040

Kandel, E., Schwarz, J., Jessell, T., Siegelbaum, S., and Hudspeth, A. (2013). *Principles of Neural Science*. New York, NY: McGraw-Hill.

Lindner, H. Y., Langius-Eklof, A., and Hermansson, L. M. (2014). Test-retest reliability and rater agreements of assessment of capacity for myoelectric control version 2.0. *J. Rehabil. Res. Dev.* 51, 635–644. doi: 10.1682/jrrd.2013.09.0197

Lindner, H. Y., Linacre, J. M., and Norling Hermansson, L. M. (2009). Assessment of capacity for myoelectric control: evaluation of construct and rating scale. *J. Rehabil. Med.* 41, 467–474.

Markovic, M., Schweisfurth, M. A., Engels, L. F., Bentz, T., Wustefeld, D., Farina, D., et al. (2018a). The clinical relevance of advanced artificial feedback in the control of a multi-functional myoelectric prosthesis. *J. Neuroeng. Rehabil.* 15:28.

Markovic, M., Schweisfurth, M. A., Engels, L. F., Farina, D., and Dosen, S. (2018b). Myocontrol is closed-loop control: incidental feedback is sufficient for scaling the prosthesis force in routine grasping. *J. Neuroeng. Rehabil.* 15:81.

Mastinu, E., Clemente, F., Sassu, P., Aszmann, O., Branemark, R., Hakansson, B., et al. (2019). Grip control and motor coordination with implanted and surface electrodes while grasping with an osseointegrated prosthetic hand. *J. Neuroeng. Rehabil.* 16:49.

Murray, C. D. (2009). Being like everybody else: the personal meanings of being a prosthesis user. *Disabil. Rehabil.* 31, 573–581. doi: 10.1080/09638280802240290

Murray, C. D., and Forshaw, M. J. (2013). The experience of amputation and prosthesis use for adults: a metasynthesis. *Disabil. Rehabil.* 35, 1133–1142. doi: 10.3109/09638288.2012.723790

Oddo, C. M., Raspopovic, S., Artoni, F., Mazzoni, A., Spigler, G., Petrini, F., et al. (2016). Intraneural stimulation elicits discrimination of textural features by artificial fingertip in intact and amputee humans. *eLife* 5:e09148. doi: 10.7554/eLife.09148

Ortiz-Catalan, M., Hakansson, B., and Branemark, R. (2014). An osseointegrated human-machine gateway for long-term sensory feedback and motor control of artificial limbs. *Sci. Transl. Med.* 6:257re6. doi: 10.1126/scitranslmed.3008933

Page, D. M., George, J. A., Kluger, D. T., Duncan, C., Wendelken, S., Davis, T., et al. (2018). Motor control and sensory feedback enhance prosthesis embodiment and reduce phantom pain after long-term hand amputation. *Front. Hum. Neurosci.* 12:352. doi: 10.3389/fnhum.2018.00352

Pasluosta, C., Kiele, P., and Stieglitz, T. (2018). Paradigms for restoration of somatosensory feedback via stimulation of the peripheral nervous system. *Clin. Neurophysiol.* 129, 851–862. doi: 10.1016/j.clinph.2017.12.027

Patton, M. Q. (1999). Enhancing the quality and credibility of qualitative analysis. *Health Serv. Res.* 34(5 Pt 2), 1189–1208.

Petrini, F. M., Valle, G., Strauss, I., Granata, G., Di Iorio, R., D'Anna, E., et al. (2018). Six-month assessment of a hand prosthesis with intraneural tactile feedback. *Ann. Neurol.* 85, 137–154. doi: 10.1002/ana.25384

Petrini, F. M., Valle, G., Strauss, I., Granata, G., Di Iorio, R., D'Anna, E., et al. (2019). Six-month assessment of a hand prosthesis with intraneural tactile feedback. *Ann. Neurol.* 85, 137–154. doi: 10.1002/ana.25384

Pylatiuk, C., Schulz, S., and Doderlein, L. (2007). Results of an Internet survey of myoelectric prosthetic hand users. *Prosthet. Orthot. Int.* 31, 362–370. doi: 10.1080/03093640601061265

Ramachandran, V. S., and Hirstein, W. (1998). The perception of phantom limbs. The D. O. Hebb lecture. *Brain* 121(Pt 9), 1603–1630.

Ramachandran, V. S., Rogers-Ramachandran, D., and Stewart, M. (1992). Perceptual correlates of massive cortical reorganization. *Science* 258, 1159–1160.

Raveh, E., Portnoy, S., and Friedman, J. (2018). Adding vibrotactile feedback to a myoelectric-controlled hand improves performance when online visual feedback is disturbed. *Hum. Mov. Sci.* 58, 32–40. doi: 10.1016/j.humov.2018.01.008

Rohde, M., Di Luca, M., and Ernst, M. O. (2011). The rubber hand illusion: feeling of ownership and proprioceptive drift do not go hand in hand. *PLoS One* 6:e21659. doi: 10.1371/journal.pone.0021659

Schiefer, M., Tan, D., Sidek, S. M., and Tyler, D. J. (2016). Sensory feedback by peripheral nerve stimulation improves task performance in individuals with upper limb loss using a myoelectric prosthesis. *J. Neural Eng.* 13:016001. doi: 10.1088/1741-2560/13/1/016001

Schiefer, M. A., Graczyk, E. L., Sidik, S. M., Tan, D. W., and Tyler, D. J. (2018). Artificial tactile and proprioceptive feedback improves performance and confidence on object identification tasks. *PLoS One* 13:e0207659. doi: 10.1371/journal.pone.0207659

Schoepp, K. R., Dawson, M. R., Schofield, J. S., Carey, J. P., and Hebert, J. S. (2018). Design and integration of an inexpensive wearable mechanotactile feedback system for myoelectric prostheses. *IEEE J. Transl. Eng. Health Med.* 6:2100711. doi: 10.1109/jtehm.2018.2866105

Schofield, J. S., Evans, K. R., Carey, J. P., and Hebert, J. S. (2014). Applications of sensory feedback in motorized upper extremity prosthesis: a review. *Expert Rev. Med. Devices* 11, 499–511. doi: 10.1586/17434440.2014.929496

Stephens-Fripp, B., Alici, G., and Mutlu, R. (2018). A review of non-invasive sensory feedback methods for transradial prosthetic hands. *IEEE Access.* 6, 6878–6899. doi: 10.1109/ACCESS.2018.2791583

Svensson, P., Antfolk, C., Malesevic, N., and Sebelius, F. (2020). Characterization of pneumatic touch sensors for a prosthetic hand. *IEEE Sens. J.* 99:1. doi: 10.1109/JSEN.2020.2987054

Svensson, P., Wijk, U., Bjorkman, A., and Antfolk, C. (2017). A review of invasive and non-invasive sensory feedback in upper limb prostheses. *Expert Rev. Med. Devices* 14, 439–447. doi: 10.1080/17434440.2017.1332989

Tsakiris, M., Schutz-Bosbach, S., and Gallagher, S. (2007). On agency and body-ownership: phenomenological and neurocognitive reflections. *Conscious. Cogn.* 16, 645–660. doi: 10.1016/j.concog.2007.05.012

Vaso, A., Adahan, H. M., Gjika, A., Zahaj, S., Zhurda, T., Vyshka, G., et al. (2014). Peripheral nervous system origin of phantom limb pain. *Pain* 155, 1384–1391. doi: 10.1016/j.pain.2014.04.018

Wijk, U., and Carlsson, I. (2015). Forearm amputees' views of prosthesis use and sensory feedback. *J. Hand Ther.* 28, 269–277; quiz 278. doi: 10.1016/j.jht.2015.01.013

Wijk, U., Svensson, P., Antfolk, C., Carlsson, I. K., Bjorkman, A., and Rosen, B. (2019). Touch on predefined areas on the forearm can be associated with specific fingers: towards a new principle for sensory feedback in hand prostheses. *J. Rehabil. Med.* 51, 209–216.

Witteveen, H. J., Rietman, H. S., and Veltink, P. H. (2015). Vibrotactile grasping force and hand aperture feedback for myoelectric forearm prosthesis users. *Prosthet. Orthot. Int.* 39, 204–212. doi: 10.1177/0309364614522260

World Health Organization (2001). *International Classification of Functioning, Disability and Health (ICF)*. Geneva: World Health Organization.

Conflict of Interest: The authors declare that the research was conducted in the absence of any commercial or financial relationships that could be construed as a potential conflict of interest.

frontiers in Neuroscience

METHODS
published: 09 July 2020
doi: 10.3389/fnins.2020.00718

Functional Electrical Stimulation Therapy for Retraining Reaching and Grasping After Spinal Cord Injury and Stroke

Naaz Kapadia[1,2,3,4]*, *Bastien Moineau*[1,5,6] *and Milos R. Popovic*[2,3,4,5]

[1] Rehabilitation Engineering Laboratory, The KITE Research Institute, Toronto Rehabilitation Institute-University Health Network, Toronto, ON, Canada, [2] Rehabilitation Sciences Institute, University of Toronto, Toronto, ON, Canada, [3] CRANIA, University Health Network and University of Toronto, Toronto, ON, Canada, [4] The KITE Research Institute, Toronto Rehabilitation Institute-University Health Network, Toronto, ON, Canada, [5] Institute of Biomaterials and Biomedical Engineering, University of Toronto, Toronto, ON, Canada, [6] Myant Inc., Toronto, ON, Canada

Neurological conditions like hemiplegia following stroke or tetraplegia following spinal cord injury, result in a massive compromise in motor function. Each of the two conditions can leave individuals dependent on caregivers for the rest of their lives. Once medically stable, rehabilitation is the main stay of treatment. This article will address rehabilitation of upper extremity function. It is long known that moving the affected limb is crucial to recovery following any kind of injury. Overtime, it has also been established that just moving the affected extremities does not suffice, and that the movements have to involve patient's participation, be as close to physiologic movements as possible, and should ideally stimulate the entire neuromuscular circuitry involved in producing the desired movement. For over four decades now, functional electrical stimulation (FES) is being used to either replace or retrain function. The FES therapy discussed in this article has been used to retrain upper extremity function for over 15 years. Published data of pilot studies and randomized control trials show that FES therapy produces significant changes in arm and hand function. There are specific principles of the FES therapy as applied in our studies: (i) stimulation is applied using surface stimulation electrodes, (ii) there is minimum to virtually no pain during application, (iii) each session lasts no more than 45–60 min, (iv) the technology is quite robust and can make up for specificity to a certain extent, and (v) fine motor function like two finger precision grip can be trained (i.e., thumb and index finger tip to tip pinch). The FES therapy protocols can be successfully applied to individuals with paralysis resulting from stroke or spinal cord injury.

Keywords: functional electrical stimulation, spinal cord injury, stroke, rehabilitation, electrical stimulation, grasping, reaching, arm function

OPEN ACCESS

Edited by:
Reinhold Scherer,
University of Essex, United Kingdom

Reviewed by:
Jan Fridén,
Swiss Paraplegic Centre, Switzerland
Kevin Lloyd Kilgore,
The MetroHealth System,
United States

***Correspondence:**
Naaz Kapadia
naaz.desai@uhn.ca

Specialty section:
This article was submitted to Neuroprosthetics, a section of the journal Frontiers in Neuroscience

Received: *23 January 2020*
Accepted: *16 June 2020*
Published: *09 July 2020*

Citation:
Kapadia N, Moineau B and Popovic MR (2020) Functional Electrical Stimulation Therapy for Retraining Reaching and Grasping After Spinal Cord Injury and Stroke. Front. Neurosci. 14:718. doi: 10.3389/fnins.2020.00718

INTRODUCTION

Application of functional electrical stimulation (FES) for therapeutic purposes in rehabilitation settings dates back to the 1960's when Liberson et al. (1961) used an FES system to stimulate the peroneal nerve to correct foot drop by triggering a foot switch, a single-channel electrical stimulation device stimulated the common peroneal nerve via a surface electrode, producing ankle dorsiflexion during the swing phase of gait (Liberson et al., 1961). This led to the first commercially available FES system with surface stimulation electrodes. Since then FES technology has been

researched extensively to evaluate its benefits in diverse neurological conditions, and using an array of application techniques (Baldi et al., 1998; Field-Fote, 2001; Popovic et al., 2005, 2011, 2012, 2016; Yan et al., 2005; Frotzler et al., 2008; Griffin et al., 2009; Daly et al., 2011; Kapadia et al., 2011, 2013, 2014a; Giangregorio et al., 2012; Malešević et al., 2012; Martin et al., 2012; Kawashima et al., 2013; Lee et al., 2013; Sadowsky et al., 2013; Ho et al., 2014; Kapadia N. et al., 2014; Popović, 2014; Sharif et al., 2014; Bauer et al., 2015; Howlett et al., 2015; Vafadar et al., 2015; Buick et al., 2016; Cuesta-Gómez et al., 2017; Fu et al., 2019; Straudi et al., 2020). The two common uses of FES are to replace function (i.e., as an orthotic device) and to retrain function (i.e., as a therapeutic device). In this article we will limit ourselves to the therapeutic application of FES.

In the therapeutic application (FES therapy), FES is used as a short-term treatment modality. The expectation is that, after training with the FES system, the patients will be able to voluntarily perform the trained activities without FES (i.e., patients are expected to regain voluntary function). To date, a few high-quality randomized controlled trials have been performed, proving the efficacy of FES therapy over other rehabilitation techniques (Sharififar et al., 2018; Yen et al., 2019). This paucity in multicenter randomized controlled trials and the limited access to systems that can properly deliver FES therapy might have affected its uptake in clinical settings (Ho et al., 2014; Auchstaetter et al., 2016). Fortunately, both these issues are being addressed as new FES systems that are specifically developed for FES therapy are being introduced, as well as large scale multicenter randomized controlled trials are being planned to further confirm the efficacy of this rehabilitation modality. This article will provide readers with the details on how transcutaneous multichannel FES therapy for the upper extremity can be applied in clinical trials and as such the same methodology can be used in clinical practice by physiotherapists and occupational therapists.

The FES methodology discussed here has been developed with the intent to be user friendly, robust and to be able to produce better functional gains than the presently available best-practice rehabilitation techniques. The FES system used in our laboratory is a surface stimulation system with up to 4 stimulation channels that can produce gross motor function as well as precision grips such as two finger pinch grip. However, the methodology of FES application discussed here is pertinent to any multichannel transcutaneous FES device. We have used transcutaneous FES to retrain reaching and grasping in individuals with both spinal cord injury and stroke (Thrasher et al., 2008; Kapadia and Popovic, 2011; Kapadia et al., 2011, 2013; Popovic et al., 2012; Hebert et al., 2017). The results obtained in both patient populations indicate functional improvements after 8–14 weeks of therapy (20–48 h of stimulation). Patients showed reduced dependency on caregivers, and some even became independent in their activities of daily living.

This article will extensively detail how FES was applied in these previously successful clinical trials to retrain reaching and grasping functions in individuals who sustained a spinal cord injury or a stroke.

MATERIALS AND EQUIPMENT

The FES system we used was a four channel surface stimulation device consisting of a software, a portable stimulator with a programmed chip card, self-adhesive stimulation electrodes, and various man-machine interfaces, such as push buttons, sliding potentiometers (Mangold et al., 2005), accelerometers (Widjaja et al., 2011), EMG/biofeedback sensor, joysticks (Sayenko et al., 2013), foot switches (Popovic et al., 2001b), gait phase detection system (Pappas et al., 2004) and brain–machine interface (Márquez-Chin et al., 2009). This FES system has been extensively used in clinical trials by researchers both in North America and in Europe. Its unique capability is the ability to program stimulation protocols customized to a patient's needs in less than 10–15 min.

Software

The software of our FES system allows one to specify/alter all stimulation parameters: frequency, minimum and maximum intensity, pulse duration, ramp time, synchronization and order of stimulations, type of user interactions and number of repetitions. The sensory, motor, functional and maximum thresholds are set using the continuous stimulation mode where the stimulation frequency and pulse duration are pre-set to values of 40 Hz and 200 μs, respectively.

METHODS

Clinical Applications

To date, approximately 150 spinal cord injury and 50 stroke patients have been treated using transcutaneous FES in our facilities, ranging from pilot clinical trials to randomized controlled trials. The FES system has been primarily used as a therapeutic device for retraining reaching and grasping. More recently FES was successfully applied to an individual with cervical spondylotic myelopathy to retrain upper extremity function with very promising results (Popovic et al., 2016).

Neuroprosthesis for Grasping in Spinal Cord Injury Patients (University Health Network REB # 02-032, REB # 09-007, REB # 09-008)

In case of patients with spinal cord injury the upper extremity retraining program is designed based on the level and extent of injury. For example, in C1–C5 cervical incomplete injuries initially FES might be used to retrain proximal function and then once the patient is able to position their arm in the working space then distal function can be trained. The FES protocols for retraining proximal function in SCI remain the same as stroke (please refer to the next section on stroke for details). In patients with low cervical injury (C6 and below), proximal upper extremity function might be preserved, and FES might then be used to retrain distal function right from the beginning. Also, it is important to note that again based on level of injury patient with SCI may have difficulty with both hand closing and opening and will typically need to be trained for both.

Over the years, various grasping protocols have been identified and designed allowing for a wide variety of grasping patterns to be trained with a great deal of fidelity. Currently, the grasping patterns that can be successfully retrained using a transcutaneous multi -channel FES system are:

(1) Palmar Grasp (holding a ball)
(2) Lateral Grasp (holding a tray)
(3) Tripod grip (thumb, index, and middle finger: holding a pen)
(4) Two finger opposition (thumb and index finger: holding a peg)
(5) Lateral Pinch (thumb and index finger: holding a credit card)
(6) Two finger lateral pinch (index and middle finger: smoker's grip)
(7) Lumbrical grip (all four fingers with the thumb: holding a closed book).

It is important to mention that FES therapy has the capability to help stroke and spinal cord injury patients relearn how to voluntarily perform all of the above grasps bilaterally and simultaneously, using surface FES system.

We have conducted a number of clinical studies using this FES technology the most recent one being a randomized controlled trial in incomplete cervical SCI patients (Popovic et al., 2011). Individuals allocated to the intervention group in this trial received FES stimulation protocols specifically designed for their upper extremity functional deficits. Individualized stimulation sequences were developed for each patient. The commonly trained grasping patterns were power and precision grasp where power grasp was used mainly to grasp larger everyday objects and the precision grip was used mainly to manipulate smaller objects. Power grasp was generated by partly flexing the fingers and the thumb in flexion and slight opposition. Lateral pinch was generated by fully flexing the fingers followed by the thumb flexion. Muscles that were stimulated during therapy were the following:

- Wrist flexors: flexor carpi radialis and flexor carpi ulnaris;
- Wrist extensors: extensor carpi radialis (longus and brevis) and ulnaris;
- Finger flexors: flexor digitorum superficialis and flexor digitorum profundus;
- Finger extensors: extensor digitorum;
- Thumb abductors: median nerve, or abductor pollicis brevis and longus;
- Thumb flexors: flexor pollicis brevis and flexor pollicis longus;
- Thumb oppositors: opponens pollicis;
- Metacarpophalangeal flexors and interphalangeal joint extensors: lumbricals.

The FES protocol allowed for individuals with little to no voluntary movement at the wrist and fingers to be able to perform simple tasks while being stimulated with the FES. This is what differentiates FES from other therapies. In the early stages of FES therapy, all the movements were performed with the help of FES. The treatment plan and instruction to participants were as follows:

(1) "Imagine hand opening" (or any movement that the therapist would like to train).
(2) "Try to perform the movement using your own muscle strength."
(3) After trying for about 10 s: "Now, try to perform the movement with the help of FES."

Hence, emphasis was put on participants voluntarily attempting the movement while being stimulated with the FES. During therapy when the participants started showing an ability to voluntarily contract certain muscle groups FES for those muscle groups was reduced to a minimum and gradually withdrawn completely. The available channel was then used on other muscle groups that were still weak and needed to be trained. The order in which muscle groups were sequentially "reactivated" was subject-dependent. FES was always delivered while the participants were performing functional tasks, such as grasping a mug, pouring water, holding a pen, etc.

The distinctiveness of this intervention is that FES is not primarily intended for muscle strengthening. Instead, it is used to retrain the neuromuscular system to execute tasks that it is unable to carry out voluntarily. Movements were performed against gravity and sometimes against light manual resistance. The number of repetitions was determined based on individual participant's strength and endurance. In general, all participants spent 30–45 min out of 1-h session performing activities of daily living with FES. The stimulation parameters used were the following: (a) balanced, biphasic, current regulated electrical pulses; (b) pulse amplitude from 8 to 50 mA (typical values 15–30 mA); (c) pulse width 250 μs; and (d) pulse frequency 40 Hz (Popovic et al., 2011). During the intervention, the therapist, at their discretion, adjusted the placement of electrodes and guided the hand movements. The therapist ensured that the movements were functional. Occasionally FES would be combined with conventional rehabilitation strategies including strengthening exercises, stretching exercises, etc.

Neuroprosthesis for Grasping in Stroke Patients (University Health Network REB # 02-032).

The most important difference between FES training in spinal cord injury and stroke patients; is that stroke patients have difficulty opening their hand as they often exhibit flexor synergy and high levels of tone in the finger flexors. In stroke patients therefore, the focus of the therapy is on hand opening and relaxing the fingers. In spinal cord injury patient's the focus of the FES therapy is on finger flexion and grasping tasks as weakness of the finger flexors is a bigger problem. Below are the methods of FES application in clinical trials conducted in individuals who suffered a stroke (Popovic et al., 2005; Thrasher et al., 2008; Kapadia et al., 2013).

For individuals allocated to the FES therapy group, treatment began by proximal shoulder muscle training. The muscles that were stimulated were deltoid, biceps, and triceps. Typically, participants would recover proximal function first. As soon as they gained functional strength in the proximal muscles, FES

for those muscles would be discontinued and applied to distal muscles of the forearm and hand. The most difficult and time-consuming task was to train voluntary extension of the fingers. This is crucial to be able to get one's hand around the objects that need to be manipulated. Once the participants were able to successfully open their hand with FES assistance, low amplitude stimulation of the finger flexors was used to signal hand closing. Stimulation parameters used to stimulate the muscles and nerves were the same as used for individuals with spinal cord injury (See section on "Neuroprosthesis for Grasping in Spinal Cord Injury Patients).

In the early stages of the treatment, the arm/hand tasks were performed predominantly with the help of FES. As participants showed improvement stimulation was gradually reduced to a minimum and eventually phased out. Typical treatment session lasted for about 45 min, including the donning and doffing of electrodes. During all FES sessions the physiotherapist guided the movements and provided assistance as appropriate to carry out the intended movement in as close to physiological manner as possible.

Over the years the FES-reaching protocols have expanded to cover various functional reach patterns:

(1) Sideways reaching
(2) Sideways reaching with hand opening
(3) Forward reaching and retrieving
(4) Forward reaching and retrieving with hand opening
(5) Reaching over opposite shoulder
(6) Reaching over opposite shoulder to forward reaching to sideways reaching
(7) Reaching over opposite knee
(8) Hand to mouth

All of these protocols can easily be paired with the FES-grasping protocols for the spinal cord injury population to train reaching and grasping together.

Practical Considerations for Therapist

In most of the clinical trials, FES sessions of 45–60 min were delivered 3–5 days a week, for 8–16 weeks, for a total of about 40 sessions. In our clinical experience, we found that patients are able to tolerate a maximum of one 60 min session per day and within the session typically we are able to stimulate one movement pattern for approximately 10–15 repetitions before fatigue sets in, however, it is important to note that this frequency is individual based and may vary based on extent of injury, chronicity and status of neuro-muscular system. Self-adhesive surface stimulation electrodes were used during therapy. All the patients were treated by registered physiotherapists or occupational therapists. In all instances, each phase of the FES was triggered by the treating Physiotherapist or Occupational therapist using a push button. All FES sessions incorporated functional tasks during FES sessions. All FES training was in combination with conventional physiotherapy or occupational therapy techniques selected based on individual patient needs. Also, irrespective of the population, patients were required to concentrate and actively make an attempt to carry out the movement while being assisted by FES, as described above.

The stepwise directions to conduct an upper extremity FES training session with a transcutaneous multi-channel FES device are as follows:

(1) *Identify the functions to be trained* (reaching and/or grasping).
(2) *Select the order of the tasks to be re-trained:* typically, start with gross motor tasks (proximal muscles) in early stages of therapy followed by fine movement control (distal muscles).
(3) *For each task identify the muscles to be stimulated: at any given time either only simple* reaching or grasping tasks such as touching mouth or palmar grasp can be trained or more complex tasks such as reaching + grasping can be trained based on number of channels available for stimulation.
(4) *First identify the optimal electrodes positioning*: For a given function, find the motor point; the electrode position where a maximal contraction is obtained with minimum stimulation current delivered. We recommend finding the motor point using a smaller electrode, by trying several positions on the bulk of the muscles to be stimulated. This allows for finding an electrode position with minimal secondary and unintentional stimulation of other muscles and/or nerves. Once you find the optimal electrode position(s) for a muscle, mark it with a pen/marker, and identify position(s) for other muscles.
(5) *Apply self-adhesive electrodes over the motor points of the muscles identified.*
Note: In case one has a stimulator that has galvanically isolated stimulation channels, one can apply the following: all electrodes on one aspect of the forearm can be "grounded" using a single return/anode electrode, i.e., all muscles on the palmar aspect of the forearm can be grounded using one electrode just proximal to the ventral aspect of the wrist joint and similarly all electrodes on the dorsal aspect of the forearm can be grounded using one electrode over the dorsal aspect of the wrist. If the stimulator does not have galvanically isolated stimulation channels one should not use this "common ground" strategy.
If you use non-alternate and asymmetrical pulses waveform (with the negative depolarizing pulse always on the same electrode, and the positive balancing pulse at a lower amplitude), then you will have an "active" electrode to be positioned on the motor point, and a "passive" or return/anode electrode under which there is no effective stimulation (setting typically used for smaller muscles). If you use alternate and/or symmetrical pulse waveform, then both electrodes are "active" and will trigger contractions similarly (setting typically used for larger muscles). The choice between one or two active electrode(s) is based on the muscle size (one active electrode is preferable where there is no space on the bulk of the muscle to position two electrodes). Also, having a single "active" electrode ensures

greater specificity of the muscle and muscle volume that is stimulated.

(6) *Identify and record the different stimulation thresholds:* Identify sensory threshold (when the patient feels the current for the first time), motor threshold (when a palpable or a visible contraction is produced), functional threshold (when the desired functional movement is produced) and maximum threshold (beyond which the patient does not tolerate an increase in current amplitude). *Note:* It is important to define the thresholds with the same current characteristics (pulse width and frequency) as the one used during FES therapy, because it has an impact on the comfort and efficiency of the stimulation.

(7) *Explain to the patient what to expect when the FES in turned on*
Example: "First your hand will close and then it will open."

(8) *Turn on the stimulator and adjust the current intensities for all muscles to the levels determined previously* (intensity should not exceed the determined maximum threshold). Trigger the FES protocol a few times so the patient has a clear understanding of what to expect with each phase of FES. Once the patient has a clear understanding of the protocol, select the functional object to be used during training. If needed, assist the patient to bring their hand close to/around the object to be manipulated.

(9) *Instruct the patient that she/he has to make an active attempt to perform the intended movement.*
Example: For a grasp/release task, ask the patient to close the hand to grasp the object and, after the patient has attempted for about 5–10 s, assist with FES. Once the patient is able to grasp the object with assistance from FES, complete the functional task, for example transfer object from point A to point B. Following successful object transfer, instruct the patient to release the object and after about 5–10 s of the patient unsuccessfully attempting to release the object trigger the FES sequence for hand opening.

(10) *Repeat this protocol 10–15 times.* Then, select another protocol and perform the next task for 5–7 min or as appropriate for that task. Execute 3–6 different protocols in a 1-h session, with active stimulation for 30–40 min (depending on patient's fatigue and therapist's expertise with the system). The 1-h therapy duration includes positioning of the electrodes and all relevant preparations for therapy initiation and therapy completion.

(11) *Rest time should be given when the patient asks for it and/or when muscle fatigue sets in.*

(12) *When the therapy is completed, turn off the stimulator, remove the electrodes and inspect the skin underneath for any redness.*
Note: Occasionally redness may be present from the electrode sticking on the skin, but it should dissipate in less than 24 h. Ask patient to monitor area and re-inspect at the next session.

The selection of stimulation sequences is done based on clinical assessments which typically include use of standardized assessment tools like Graded Redefined Assessment of Strength, Sensibility and Prehension, Toronto Rehabilitation Institute-Hand Function Test and Spinal Cord Independence Measure Self-care Sub-scores in spinal cord injury (Popovic et al., 2011) and Action Research Arm Test and Fugl Meyer assessment – upper extremity scores in stroke (Hebert et al., 2017).

Limitations

There are certain limitations to this technology. The limb muscles that are intended for FES treatment have to be accessible for placement of the stimulation electrodes (Popovic et al., 2001a). There should not be a major degree of lower motor neuron injury or nerve-root damage of the stimulated muscle. In a number of patients with spinal cord injury, there may be a variable amount of peripheral nerve damage (Doherty et al., 2002) (motoneurons and nerve-roots) that restricts the application of FES. Also, the patient has to be cognitively able to follow the instructions and actively participate in the therapy process. The patient should not have any contraindications for FES application like metal implants at the site of stimulation, pace-maker, open wound or rash at the site of electrode placement, uncontrolled autonomic dysreflexia, etc.

Besides, with programmable surface stimulation devices, one would need an inter-professional team including bio medical engineers who are proficient in programming the stimulation protocols. This programming limitation may not apply to the more sophisticated newer FES systems. Presently there are commercially available FES systems that can deliver FES therapies discussed in this article. The reader is encouraged to find a device that delivers FES therapies and is approved by the local regulatory body. Systems that do not have neuroplasticity and neuromodulation in their indication for use defined by the regulatory body should be avoided, as these stimulators are for muscle strengthening and improving range of motion, and not for FES therapy discussed in this article.

RESULTS

To date, in our laboratory transcutaneous FES therapy has been successfully applied to over 200 patients with either stroke or spinal cord injury. Based on the outcomes of these studies, it can be said that short duration FES therapy combined with conventional occupational therapy and physiotherapy has the ability to produce positive changes in these patients (Popovic et al., 2005, 2011, 2016; Thrasher et al., 2008; Kapadia and Popovic, 2011; Kapadia et al., 2013). The underlying mechanism responsible for these changes include central modulation effects. Stimulation induces cortical plasticity by modulating the ascending pathways through the Ia muscle fiber afferents (Chipchase et al., 2011). Additionally, somatosensory inputs to the motor cortex are essential for motor learning and control, and play critical roles in the motor recovery process (Vidoni et al., 2010; Pan et al., 2018). Stimulation above the motor threshold increases excitability of corticomotor pathway by activating sensory axons and recruiting synaptic motoneurons and motor reflex (Chipchase et al., 2011). FES therapy in combination

with conventional PT and OT techniques harnesses the benefits of neuroplasticity thereby improving function and enhancing participant independence with activities of daily living.

In the randomized controlled trial carried out in individuals with subacute (<6 months post injury) incomplete traumatic C3–C7 spinal cord injury, it was found that the individuals who received 40 h of FES therapy had far greater improvements on the Self Care Sub-scores of the Functional Independence Measure and Spinal Cord Independence Measure as compared to individuals who received 40 h of conventional occupational therapy (Popovic et al., 2011). These gains were retained, or further improvement was observed, in the FES therapy group at the time of 6 months follow up assessment (Popovic et al., 2011). To date we have obtained similar results in all individuals with sub-acute incomplete spinal cord injury who received 40 h of FES therapy (**Figure 1**).

Similar results were obtained in the randomized controlled trial carried out in individuals with acute (2–7 weeks post) severe stroke with a total arm and hand score no more than 2 on the Chedoke McMaster Stages of Motor Recovery (less than 15 points on Fugl Meyer Assessment Upper Limb Sub-score) (Thrasher et al., 2008; Hebert et al., 2017; Marquez-Chin et al., 2017). The individuals who received 12–16 weeks of FES therapy for the arm and hand had statistically better improvement on the Self-care sub-score of the Functional Independence Measure (**Figure 2**), Fugl Meyer Assessment, Barthel Index, and Chedoke McMaster Stages of Motor Recovery as compared to individuals who received conventional

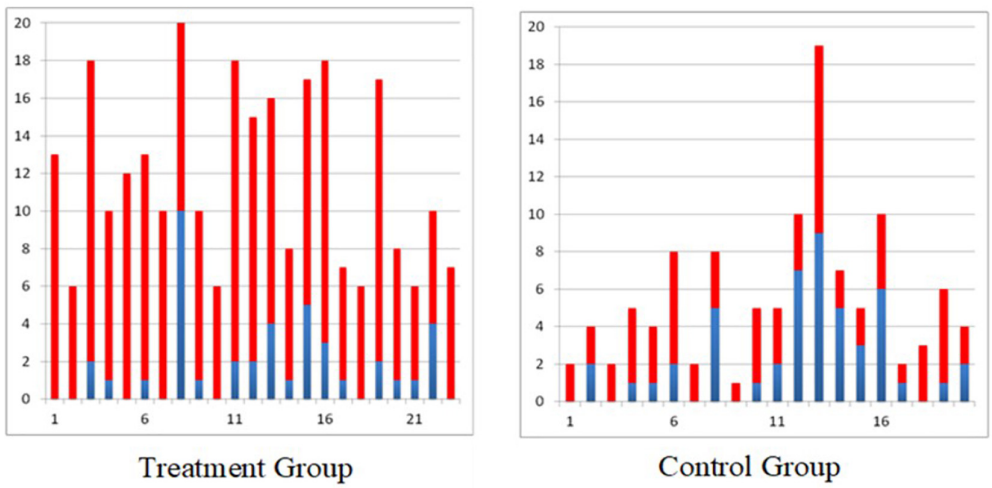

FIGURE 1 | Self-care Spinal Cord Independence Measure scores for all individuals with incomplete sub-acute spinal cord injury (blue bar indicates score at baseline and red bar indicates gain after 40 × 1 h therapy, treatment group received functional electrical stimulation and control group received conventional PT/OT).

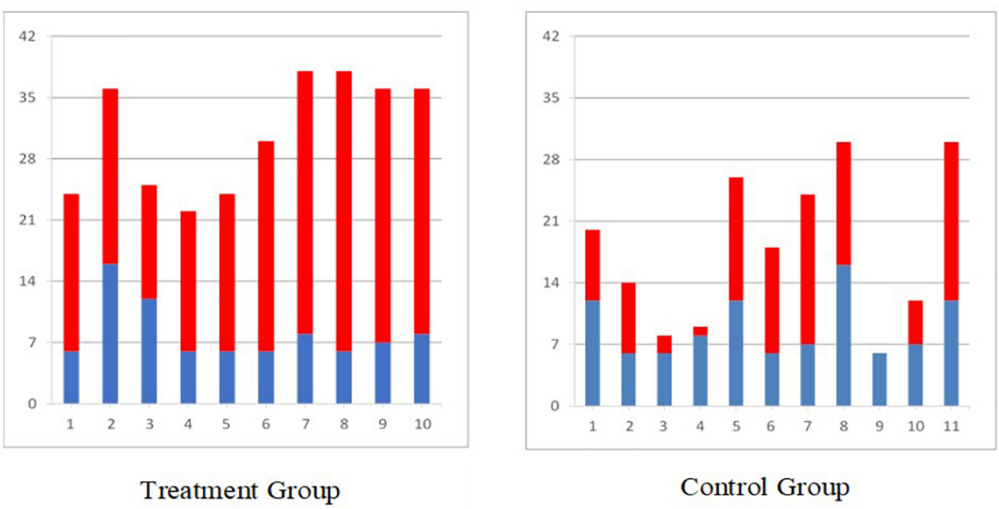

FIGURE 2 | Self-care Functional Independence Measure scores for all individuals with sub-acute stroke (blue bar indicates score at baseline and red bar indicates gain after 40 × 1 h therapy, treatment group received functional electrical stimulation and control group received conventional PT/OT).

occupational therapy and physiotherapy for the same duration. Detailed results of this study are published elsewhere.

In another clinical trial in chronic severe pediatric stroke population (Kapadia N. et al., 2014), where all four participants received a total of 48 h of FES therapy, statistically significant improvements were observed on the Quality of Upper Extremity Skills Test as well as on various sub components of the Rehabilitation Engineering Laboratory Hand Function Test (this is the Toronto Rehabilitation Institute- Hand Function Test with a scoring system adapted for stroke).

DISCUSSION

Short duration multichannel surface FES is a viable and safe treatment modality that can be successfully applied in patients with neurological conditions. It is important to note that we did not formally investigate safety and feasibility in our clinical trials mainly because transcutaneous FES has been applied in clinical trials for over 5 decades now without any reports of major adverse events. However, given that we have applied FES to over 200 patients over the past 15+ years we are able to confidently say that transcutaneous FES is both safe and feasible. Across all of our clinical trials we did not encounter any serious adverse events and we have been able to successfully retain our study participants for the duration of the research therapy. Discussed here is an in-depth application of transcutaneous multi-channel FES therapy of the upper extremity in spinal cord injury and stroke patients. In order to obtain maximum benefits of this therapy there are some general points to keep in mind.

The goal of this manuscript is not to explore the mechanism of improvement in individuals with stroke and spinal cord injury following FES as this is a methods paper and as such these mechanisms have been widely discussed in literature (Quandt and Hummel, 2014; Hara, 2015; Luo et al., 2020; Marquez-Chin and Popovic, 2020). We do, however, recommend some basic principles of FES application on the widely accepted belief that mechanism of improvement with this therapy is based on the principles of neuroplasticity (Nagai et al., 2016). First and foremost it is strongly recommended that therapy should be started as soon as the medical condition of the patient is stabilized, i.e., preferably in the acute or sub-acute phase post-injury. Secondly, active participation of the patient during treatment is critical. Along with the FES, patients have to make an active attempt to execute the target movement. Third, the movements carried out should be functional and should follow a physiological pattern as closely as possible (movements similar to those of able-bodied individuals). Fourth, therapy should be combined with conventional rehabilitation modalities (example: stretching and strengthening) to reap maximum benefits. Lastly, while no specific dosing study has been conducted, our group recommends delivering at least three 1 h sessions per week. However, our group does not recommend more than one session per day, as this often exhausts the patient and prevents them from actively participating in the second session. In total, at least 20 sessions are needed to obtain clinically relevant changes, however, it is often recommended that patients have 40 or more hours of therapy to maximize outcomes and experience greater gains in function.

It should be noted that, in certain very acute or chronic spinal cord injury cases, a strengthening phase is necessary prior to the functional training phase because the muscles are minimally responsive to stimulation at first (Popovic et al., 2002) due to initial spinal shock (Galeiras Vázquez et al., 2017) or due to long-term disuse (Popovic et al., 2002).

It is important to bear in mind that although FES therapy has not been extensively tested in individuals with cervical complete spinal cord injury, those that have been trained with the system have shown remarkable improvements that were much more profound than those produced with conventional therapy (Popovic et al., 2006). This evidence merits conducting more comprehensive clinical trials with FES therapy in cervical complete spinal cord injury patients.

In conclusion, the most attractive feature of multichannel surface stimulators is that they are non-invasive, often programmable and allow for various muscles/muscle groups to be stimulated simultaneously in physiological patterns. They have a high level of fidelity and are able to produce global upper-limb motions as well as fine finger movements like two pinch grip (thumb and index finger) and tripod grip (thumb, index, and middle finger) using surface stimulation electrodes.

The specific surface stimulator used in our clinical studies, is not widely available any longer, however, the methodological considerations discussed above remain the same irrespective of the type of stimulation device. Any stimulator that can produce protocols discussed in this article can be used for FES therapy. Although the new stimulators used for the FES therapy come with guidelines for locating motor points, therapists should be mindful that motor points can anatomically vary between individuals. If required, the first session should be dedicated to finding correct stimulation points, after which these can be marked down for future sessions.

As important as it is to assist weak muscles with FES during execution of functional tasks, it is equally important that once functional voluntary strength is recovered (at least 3/5 on Manual Muscle Testing), stimulation is withdrawn from those muscles and the patient is encouraged to voluntarily control the muscles themselves. The available FES channels can then be applied to other weaker muscle groups that still need retraining. In some cases, with severe spasticity, manual stretching of the tight muscles prior to stimulation may yield better results.

DATA AVAILABILITY STATEMENT

The datasets generated for this study are available on request to the corresponding author.

ETHICS STATEMENT

The studies involving human participants were reviewed and approved by Research Ethics Board, Toronto Rehabilitation Institute-University Health Network. The patients/participants provided their written informed consent to participate in this study.

AUTHOR CONTRIBUTIONS

NK, MP, and BM were responsible for the concept and writing of the manuscript and had read and approved the manuscript. All authors contributed to the article and approved the submitted version.

FUNDING

This project was supported by the Christopher & Dana Reeve Foundation (TA1-0706-2), Spinal Cord Injury Ontario, Rick Hansen Institute (SCISN grant 200936), Physician's Services Incorporated Foundation (PSI Grant #05-06), Ontario Neurotrauma Foundation, Toronto Rehab Foundation, and through generous donation of Dean Connor and Maris Uffelmann. During his postdoctoral position at Toronto Rehabilitation Institute, BM was supported by grants from Spinal Cord Injury Ontario and Age-Well. NK is a Ph.D. candidate at Rehabilitation Sciences Institute, University of Toronto and is supported by the CIHR - Frederick Banting and Charles Best Canada Graduate Scholarship – Doctoral Award.

REFERENCES

Auchstaetter, N., Luc, J., Lukye, S., Lynd, K., Schemenauer, S., Whittaker, M., et al. (2016). Physical Therapists' use of functional electrical stimulation for clients with stroke: frequency, barriers, and facilitators. *Phys. Ther.* 96, 995–1005. doi: 10.2522/ptj.20150464

Baldi, J. C., Jackson, R. D., Moraille, R., and Mysiw, W. J. (1998). Muscle atrophy is prevented in patients with acute spinal cord injury using functional electrical stimulation. *Spinal Cord* 36, 463–469. doi: 10.1038/sj.sc.3100679

Bauer, P., Krewer, C., Golaszewski, S., Koenig, E., and Müller, F. (2015). Functional electrical stimulation-assisted active cycling – therapeutic effects in patients with hemiparesis from 7 days to 6 months after stroke: a randomized controlled pilot study. *Arch. Phys. Med. Rehabil.* 96, 188–196. doi: 10.1016/j.apmr.2014.09.033

Buick, A. R., Kowalczewski, J., Carson, R. G., and Prochazka, A. (2016). Tele-supervised FES-assisted exercise for hemiplegic upper limb. *IEEE Trans. Neural Syst. Rehabil. Eng.* 24, 79–87. doi: 10.1109/tnsre.2015.2408453

Chipchase, L. S., Schabrun, S. M., and Hodges, P. W. (2011). Peripheral electrical stimulation to induce cortical plasticity: a systematic review of stimulus parameters. *Clin. Neurophysiol.* 122, 456–463. doi: 10.1016/j.clinph.2010.07.025

Cuesta-Gómez, A., Molina-Rueda, F., Carratala-Tejada, M., Imatz-Ojanguren, E., Torricelli, D., and Miangolarra-Page, J. C. (2017). The use of functional electrical stimulation on the upper limb and interscapular muscles of patients with stroke for the improvement of reaching movements: a feasibility study. *Front. Neurol.* 8:186. doi: 10.3389/fneur.2017.00186

Daly, J. J., Zimbelman, J., Roenigk, K. L., McCabe, J. P., Rogers, J. M., Butler, K., et al. (2011). Recovery of coordinated gait: randomized controlled stroke trial of functional electrical stimulation (FES) versus no FES, with weight-supported treadmill and over-ground training. *Neurorehabil. Neural Repair* 25, 588–596. doi: 10.1177/1545968311400092

Doherty, J. G., Burns, A. S., O'Ferrall, D. M., and Ditunno, J. F. Jr. (2002). Prevalence of upper motor neuron vs lower motor neuron lesions in complete lower thoracic and lumbar spinal cord injuries. *J. Spinal Cord Med.* 25, 289–292. doi: 10.1080/10790268.2002.11753630

Field-Fote, E. C. (2001). Combined use of body weight support, functional electric stimulation, and treadmill training to improve walking ability in individuals with chronic incomplete spinal cord injury. *Arch. Phys. Med. Rehabil.* 82, 818–824. doi: 10.1053/apmr.2001.23752

Frotzler, A., Coupaud, S., Perret, C., Kakebeeke, T. H., Hunt, K. J., Donaldson, N. N., et al. (2008). High-volume FES-cycling partially reverses bone loss in people with chronic spinal cord injury. *Bone* 43, 169–176. doi: 10.1016/j.bone.2008.03.004

Fu, M. J., Harley, M. Y., Hisel, T., Busch, R., Wilson, R., Chae, J., et al. (2019). Ability of people with post-stroke hemiplegia to self-administer FES-assisted hand therapy video games at home: an exploratory case series. *J. Rehabil. Assistive Technol. Eng.* 6:2055668319854000.

Galeiras Vázquez, R., Ferreiro Velasco, M. E., Mourelo Fariña, M., Montoto Marqués, A., and Salvador de la Barrera, S. (2017). Update on traumatic acute spinal cord injury. Part 1. *Med. Intensiva* 41, 237–247.

Giangregorio, L., Craven, C., Richards, K., Kapadia, N., Hitzig, S. L., Masani, K., et al. (2012). A randomized trial of functional electrical stimulation for walking in incomplete spinal cord injury: effects on body composition. *J. Spinal Cord Med.* 35, 351–360. doi: 10.1179/2045772312y.0000000041

Griffin, L., Decker, M. J., Hwang, J. Y., Wang, B., Kitchen, K., Ding, Z., et al. (2009). Functional electrical stimulation cycling improves body composition, metabolic and neural factors in persons with spinal cord injury. *J. Electromyogr. Kinesiol.* 19, 614–622. doi: 10.1016/j.jelekin.2008.03.002

Hara, Y. (2015). Brain plasticity and rehabilitation in stroke patients. *J. Nippon Med. School Nippon IKA Daigaku Zasshi* 82, 4–13. doi: 10.1272/jnms.82.4

Hebert, D. A., Bowen, J. M., Ho, C., Antunes, I., O'Reilly, D. J., and Bayley, M. (2017). Examining a new functional electrical stimulation therapy with people with severe upper extremity hemiparesis and chronic stroke: a feasibility study. *Br. J. Occup. Ther.* 80, 651–659. doi: 10.1177/0308022617719807

Ho, C. H., Triolo, R. J., Elias, A. L., Kilgore, K. L., DiMarco, A. F., and Bogie, K. (2014). Functional electrical stimulation and Spinal Cord Injury. *Phys. Med. Rehabil. Clin. N. Am.* 25:631–ix.

Howlett, O. A., Lannin, N. A., Ada, L., and Mckinstry, C. (2015). Functional electrical stimulation improves activity after stroke: a systematic review with meta-analysis. *Arch. Phys. Med. Rehabil.* 96, 934–943. doi: 10.1016/j.apmr.2015.01.013

Kapadia, N., Masani, K., Craven, B. C., Giangregorio, L. M., Hitzig, S. L., Richards, K., et al. (2014). A randomized trial of functional electrical stimulation for walking in incomplete spinal cord injury: effects on walking competency. *J. Spinal Cord Med.* 37, 511–524. doi: 10.1179/2045772314y.0000000263

Kapadia, N., Zivanovic, V., and Popovic, M. R. (2013). Restoring voluntary grasping function in individuals with incomplete chronic spinal cord injury: pilot study. *Top. Spinal Cord Injury Rehabil.* 19, 279–287. doi: 10.1310/sci1904-279

Kapadia, N. M., Bagher, S., and Popovic, M. R. (2014a). Influence of different rehabilitation therapy models on patient outcomes: hand function therapy in individuals with incomplete SCI. *J. Spinal Cord Med.* 37, 734–743. doi: 10.1179/2045772314y.0000000203

Kapadia, N. M., Nagai, M. K., Zivanovic, V., Bernstein, J., Woodhouse, J., Rumney, P., et al. (2014b). Functional electrical stimulation therapy for recovery of reaching and grasping in severe chronic pediatric stroke patients. *J. Child Neurol.* 29, 493–499. doi: 10.1177/0883073813484088

Kapadia, N. M., and Popovic, M. R. (2011). Functional electrical stimulation therapy for grasping in spinal cord injury: an overview. *Top. Spinal Cord Injury Rehabil.* 17, 70–76. doi: 10.1310/sci1701-70

Kapadia, N. M., Zivanovic, V., Furlan, J., Craven, B. C., Mcgillivray, C., and Popovic, M. R. (2011). Functional electrical stimulation therapy for grasping in traumatic incomplete spinal cord injury: randomized control trial. *Artif. Organs* 35, 212–216. doi: 10.1111/j.1525-1594.2011.01216.x

Kawashima, N., Popovic, M. R., and Zivanovic, V. (2013). Effect of intensive functional electrical stimulation therapy on the upper limb motor recovery after stroke: single case study of a chronic stroke patient, Stroke. *Physiother. Can.* 65, 20–28. doi: 10.3138/ptc.2011-36

Lee, S. Y., Kang, S. Y., Im, S. H., Kim, B. R., Kim, S. M., Yoon, H. M., et al. (2013). The effects of assisted ergometer training with a functional electrical stimulation on exercise capacity and functional ability in subacute stroke patients. *Ann. Rehabil. Med.* 37, 619–627.

Liberson, W. T., Holmquest, H. J., Scot, D., and Dow, M. (1961). Functional electrotherapy: stimulation of the peroneal nerve synchronized with the swing phase of the gait of hemiplegic patients. *Arch. Phys. Med. Rehabil.* 42, 101–105.

Luo, S., Xu, H., Zuo, Y., Liu, X., and All, A. H. (2020). A review of functional electrical stimulation treatment in spinal cord injury. *Neuromol. Med.* doi: 10.1007/s12017-019-08589-9 [Epub ahead of print].

Malešević, N. M., Maneski, L. Z. P., Iliæ, V., Jorgovanoviæ, N., Bijeliæ, G., Keller, T., et al. (2012). A multi-pad electrode based functional electrical stimulation system for restoration of grasp. *J. NeuroEng. Rehabil.* 9:66. doi: 10.1186/1743-0003-9-66

Mangold, S., Keller, T., Curt, A., and Dietz, V. (2005). Transcutaneous functional electrical stimulation for grasping in subjects with cervical spinal cord injury. *Spinal Cord* 43, 1–13. doi: 10.1038/sj.sc.3101644

Marquez-Chin, C., Bagher, S., Zivanovic, V., and Popovic, M. R. (2017). Functional electrical stimulation therapy for severe hemiplegia: randomized control trial revisited. *Can. J. Occup. Ther.* 84, 87–97. doi: 10.1177/0008417416668370

Marquez-Chin, C., and Popovic, M. R. (2020). Functional electrical stimulation therapy for restoration of motor function after spinal cord injury and stroke: a review. *Biomed. Eng. Online* 19:34.

Márquez-Chin, C., Popovic, M. R., Cameron, T., Lozano, A. M., and Chen, R. (2009). Control of a neuroprosthesis for grasping using off-line classification of electrocorticographic signals: case study. *Spinal Cord* 47, 802–808. doi: 10.1038/sc.2009.41

Martin, R., Sadowsky, C., Obst, K., Meyer, B., and McDonald, J. (2012). Functional electrical stimulation in spinal cord injury: from theory to practice. *Top. Spinal Cord Injury Rehabil.* 18, 28–33. doi: 10.1310/sci1801-28

Nagai, M. K., Marquez-Chin, C., and Popovic, M. R. (2016). "Why is functional electrical stimulation therapy capable of restoring motor function following severe injury to the central nervous system?," in *Translational Neuroscience: Fundamental Approaches for Neurological Disorders*, ed. M. Tuszynski (Boston, MA: Springer).

Pan, L. L. H., Yang, W. W., Kao, C. L., Tsai, M. W., Wei, S. H., Fregni, F., et al. (2018). Effects of 8-week sensory electrical stimulation combined with motor training on EEG-EMG coherence and motor function in individuals with stroke. *Sci. Rep.* 8:9217.

Pappas, I. P. I., Keller, T., Mangold, S., Popovic, M. R., Dietz, V., and Morari, M. (2004). A Reliable gyroscope-based gait-phase detection sensor embedded in a shoe insole. *IEEE Sensors J.* 4, 268–274. doi: 10.1109/jsen.2004.823671

Popoviæ, D. B. (2014). Advances in functional electrical stimulation (FES). *J. Electromyogr. Kinesiol.* 24, 795–802. doi: 10.1016/j.jelekin.2014.09.008

Popovic, M. R., Curt, A., Keller, T., and Dietz, V. (2001a). Functional electrical stimulation for grasping and walking: indications and limitations. *Spinal Cord* 39, 403–412. doi: 10.1038/sj.sc.3101191

Popovic, M. R., Kapadia, N., Zivanovic, V., Furlan, J. C., Craven, B. C., and McGillivray, C. (2011). Functional electrical stimulation therapy of voluntary grasping versus only conventional rehabilitation for patients with subacute incomplete tetraplegia: a randomized clinical trial. *Neurorehabil. Neural Repair* 25, 433–442. doi: 10.1177/1545968310392924

Popovic, M. R., Keller, T., Papas, I. P. I., Dietz, V., and Morari, M. (2001b). Surface-stimulation technology for grasping and walking neuroprostheses. *IEEE Eng. Med. Biol. Magazine* 20, 82–93. doi: 10.1109/51.897831

Popovic, M. R., Masani, K., and Micera, S. (2012). "Functional electrical stimulation therapy: recovery of function following spinal cord injury and stroke," in *Neurorehabilitation Technology*, eds D. Reinkensmeyer and V. Dietz (Cham: Springer).

Popovic, M. R., Popovic, D. B., and Keller, T. (2002). Neuroprostheses for grasping. *Neurol. Res.* 24, 443–452. doi: 10.1179/016164102101200311

Popovic, M. R., Thrasher, T. A., Adams, M. E., Takes, V., Zivanovic, V., and Tonack, M. I. (2006). Functional electrical therapy: retraining grasping in spinal cord injury. *Spinal Cord* 44, 143–151. doi: 10.1038/sj.sc.3101822

Popovic, M. R., Thrasher, T. A., Zivanovic, V., Takaki, J., and Hajek, V. (2005). Neuroprosthesis for retraining reaching and grasping functions in severe hemiplegic patients. *Neuromodulation* 8, 58–72. doi: 10.1111/j.1094-7159.2005.05221.x

Popovic, M. R., Zivanovic, V., and Valiante, T. A. (2016). Restoration of upper limb function in an individual with cervical spondylotic myelopathy using functional electrical stimulation therapy: a case study. *Front. Neurol.* 7:81. doi: 10.3389/fneur.2016.00081

Quandt, F., and Hummel, F. C. (2014). The influence of functional electrical stimulation on hand motor recovery in stroke patients: a review. *Exp. Transl. Stroke Med.* 6:9.

Sadowsky, C. L., Hammond, E. R., Strohl, A. B., Commean, P. K., Eby, S. A., Damiano, D. L., et al. (2013). Lower extremity functional electrical stimulation cycling promotes physical and functional recovery in chronic spinal cord injury. *J. Spinal Cord Med.* 36, 623–631. doi: 10.1179/2045772313y.0000000101

Sayenko, D. G., Robinson, M. F., Milosevic, M., Masani, K., and Popovic, M. R. (2013). Video game-based approach in calf muscle training: lessons from pilot study. *Clin. Res. Foot Ankle* 1:110.

Sharif, H., Gammage, K., Chun, S., and Ditor, D. (2014). Effects of FES-ambulation training on locomotor function and health-related quality of life in individuals with spinal cord injury. *Top. Spinal Cord Injury Rehabil.* 20, 58–69. doi: 10.1310/sci2001-58

Sharififar, S., Shuster, J. J., and Bishop, M. D. (2018). Adding electrical stimulation during standard rehabilitation after stroke to improve motor function. A systematic review and meta-analysis. *Ann. Phys. Rehabil. Med.* 61, 339–344. doi: 10.1016/j.rehab.2018.06.005

Straudi, S., Baroni, A., Mele, S., Craighero, L., Manfredini, F., Lamberti, N., et al. (2020). Effects of a robot-assisted arm training plus hand functional electrical stimulation on recovery after stroke: a randomized clinical trial. *Arch. Phys. Med. Rehabil.* 101, 309–316. doi: 10.1016/j.apmr.2019.09.016

Thrasher, T. A., Zivanovic, V., McIlroy, W., and Popovic, M. R. (2008). Rehabilitation of reaching and grasping function in severe hemiplegic patients using functional electrical stimulation therapy. *Neurorehabil. Neural Repair* 22, 706–714. doi: 10.1177/1545968308317436

Vafadar, A. K., Côté, J. N., and Archambault, P. S. (2015). Effectiveness of functional electrical stimulation in improving clinical outcomes in the upper arm following stroke: a systematic review and meta-analysis. *Biomed. Res. Int.* 2015:729768.

Vidoni, E. D., Acerra, N. E., Dao, E., Meehan, S. K., and Boyd, L. A. (2010). Role of the primary somatosensory cortex in motor learning: an rTMS study. *Neurobiol. Learn. Memory* 93, 532–539. doi: 10.1016/j.nlm.2010.01.011

Widjaja, F., Shee, C. Y., Au, W. L., Poignet, P., and Ang, W. T. (2011). "Using electromechanical delay for real-time anti-phase tremor attenuation system using functional electrical stimulation," in *Proceedings of the IEEE International Conference on Robotics and Automation, ICRA 2011*, Shanghai.

Yan, T., Hui-Chan, C. W. Y., and Li, L. S. W. (2005). Functional electrical stimulation improves motor recovery of the lower extremity and walking ability of subjects with first acute stroke: a randomized placebo-controlled trial. *Stroke* 36, 80–85. doi: 10.1161/01.str.0000149623.24906.63

Yen, H. C., Chen, W. S., Jeng, J. S., Luh, J. J., Lee, Y. Y., and Pan, G. S. (2019). Standard early rehabilitation and lower limb transcutaneous nerve or neuromuscular electrical stimulation in acute stroke patients: a randomized controlled pilot study. *Clin. Rehabil.* 33, 1344–1354. doi: 10.1177/0269215519841420

Conflict of Interest: MP is a shareholder in company MyndTec Inc. Technology and the results presented in the document, except for study "D. A. Hebert, J. M. Bowen, C. Ho, I. Antunes, D. J. O'Reilly, and M. Bayley," "Examining a new functional electrical stimulation therapy with people with severe upper extremity hemiparesis and chronic stroke: A feasibility study," "British Journal of Occupational Therapy, pp:1–10, 2017," have been produced before the company created its first product. MyndTec did not participate in any aspect of data generation, data acquisition, data processing, data interpretation, manuscript preparation and it did not financially support any aspect of this project or the studies that were discussed in this article. BM is affiliated with Myant Inc., a company that develops electrical stimulation garments. Myant Inc. was not involved in the preparation of this manuscript.

The remaining author declares that the research was conducted in the absence of any commercial or financial relationships that could be construed as a potential conflict of interest.

Advantages of publishing in Frontiers

OPEN ACCESS
Articles are free to read for greatest visibility and readership

FAST PUBLICATION
Around 90 days from submission to decision

HIGH QUALITY PEER-REVIEW
Rigorous, collaborative, and constructive peer-review

TRANSPARENT PEER-REVIEW
Editors and reviewers acknowledged by name on published articles

Frontiers
Avenue du Tribunal-Fédéral 34
1005 Lausanne | Switzerland

Visit us: www.frontiersin.org
Contact us: frontiersin.org/about/contact

REPRODUCIBILITY OF RESEARCH
Support open data and methods to enhance research reproducibility

DIGITAL PUBLISHING
Articles designed for optimal readership across devices

FOLLOW US
@frontiersin

IMPACT METRICS
Advanced article metrics track visibility across digital media

EXTENSIVE PROMOTION
Marketing and promotion of impactful research

LOOP RESEARCH NETWORK
Our network increases your article's readership